THE UNIVERSITY
of EDINBURGH

Hydrolytic Stability and Protodeboronation of Boronic Esters

THE UNIVERSITY *of* EDINBURGH

Hannah L. D. Hayes

Doctor of Philosophy

University of Edinburgh

2021

Declaration

I declare that the work presented in this thesis was completed and composed by myself, under the supervision of Professor Guy C. Lloyd-Jones FRS and is in accordance with the requirements of the University of Edinburgh. The research reported in this thesis is original, except where explicitly indicated by reference in the text, and has not been submitted for any other degree or professional qualification.

Collaboration

Computations which were used to support aspects of the experimental work presented in this thesis were performed by Dr Andrew Leach (The University of Manchester) and Michele Assante (Liverpool John Moores University). Stopped-flow experiments which were performed by Ran Wei are indicated by special reference in the text.

Publications

The work reported in this thesis is communicated:

Hannah L. D. Hayes, Ran Wei, Michele Assante, Katherine J. Geogheghan, Na Jin, Simone Tomasi, Gary Noonan, Andrew G. Leach, and Guy C. Lloyd-Jones. Protodeboronation of (Hetero)Arylboronic Esters: Direct versus Pre-hydrolytic Pathways and Self/Auto-Catalysis. *J. Am. Chem. Soc.* **2021**, *143*, 14814-14826.

Abstract

Boronic acids and esters are indispensable building blocks in modern synthetic chemistry. Furthermore, their usage is widespread, spanning a broad range of applications, and yet it is often hampered by the inescapable nature of these substrates to undergo decomposition, commonly by means of protodeboronation, involving formal protonation of the C-B bond. In different circumstances, the ability to effectively remove remaining boronic acid/ester starting material post process is highly desirable. Therefore, studying the kinetics and mechanism of protodeboronation is of importance to understand and modulate their reactivity as required. Whilst the protodeboronation of a diverse range of boronic acids has been extensively studied in the Lloyd-Jones group, revealing an assortment of behaviors for electron-rich, polyfluorinated examples and heteroaromatic systems, the pathway by which their boronic esters react is relatively unknown. Given the complexity of pH-rate profiles for the protodeboronation of boronic acids and the dependence upon the exact nature of the substrate, the prospect of direct protodeboronation of boronic esters or alternatively the potential for a hydrolysis-protodeboronation sequence presents a more difficult kinetic challenge.

This research has centred on discerning the various pathways by which boronic esters undergo protodeboronation, with the ultimate aim of understanding and controlling the efficient application of these substrates in modern synthetic chemistry. By exploiting the use of *in-situ* and stopped flow (^{19}F, ^{1}H and ^{11}B) NMR spectroscopy for reaction monitoring, the kinetics and mechanism of the base-catalysed hydrolysis and protodeboronation of a series of boronic esters, encompassing eight different polyols, and including ten polyfluoroaryl and heteroaryl moieties have been probed. These investigations were facilitated by pH-rate dependence studies, isotopic entrainment, ^{1}H/^{2}H KIEs and KS-DFT computations. The study reveals the phenomenological stability of boronic esters in basic 50% aq.-dioxane media, at 27 °C, to be highly nuanced (Scheme 1). Contrary to common assumption, esterification

does not necessarily impart greater stability compared to the corresponding boronic acid. In fact, protodeboronation by the pre-hydrolytic pathway dominates for most esters studied, and the rate of hydrolysis is augmented by self-, auto- and phenolic catalysis when the pH is close to the pK_a of the boronic acid/ester.

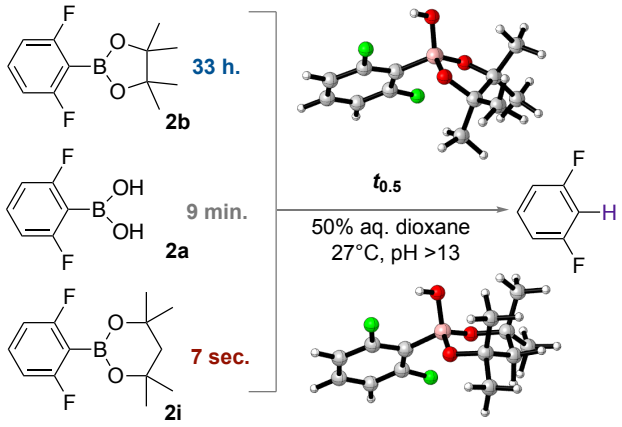

Scheme 1. Half-lives of protodeboronation for pinacol ester **2b** and its homologue **2i**, relative to the 2,6-difluorophenylboronic acid **2a** ($t_{0.5}$ = 33 h, 7 sec and 9 min respectively).

Lay Summary

Recognised in 2010 by the Nobel Prize awarded to Akira Suzuki for its discovery, the Suzuki-Miyaura reaction is considered to be one of the most important reactions in modern synthetic chemistry. This reaction is frequently incorporated as a key step towards the production of active ingredients for medicines and herbicides. However, one of the chemicals commonly used as starting material is susceptible to decomposition under the reaction conditions which can hinder its industrial application. This chemical is called a boronic ester and can decompose by means of a process called protodeboronation (Scheme 2). A richer understanding of the mechanism by which boronic esters decompose is crucial for ensuring the mitigation of this undesirable side reaction. Boronic esters can also breakdown into their free acid forms by reaction with water in a process called hydrolysis (Scheme 2). Until now, the hydrolysis of boronic esters has largely been studied within the context of carbohydrate sensing, and scant kinetic information is available relating to their hydrolysis at basic pH and at concentrations routinely used in synthesis.

In this research, a broad range of boronic esters which are unstable under basic conditions were studied. To reflect the conditions used in reactions which employ boronic esters, including the Suzuki-Miyaura reaction, experiments were performed in basic aqueous-organic media. The analytical technique of Nuclear Magnetic Resonance spectroscopy was employed to measure the rates of hydrolysis and protodeboronation of boronic esters. Reaction monitoring by NMR spectroscopy facilitated the detailed structural analysis and differentiation of the organic substances involved.

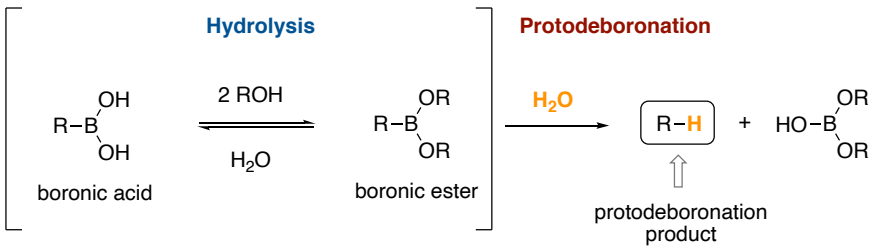

Scheme 2. Pathways for hydrolysis and protodeboronation of boronic esters.

Acknowledgements

I feel an overwhelming sense of fulfilment in writing this and am in debt to so many who have contributed to this chapter of my life in Edinburgh.

I can express with certainty that reaching this point would not have been realised without the steady guidance, generosity of support, and patience of Professor Guy Lloyd-Jones FRS. I thank Guy for many insightful discussions which ensued from his unfaltering curiosity and efforts to teach me a good grounding in kinetics...

I thank the EPSRC and AstraZeneca for funding this research and Dr Gary Noonan, for his enthusiasm, advice, and valuable contributions to my project. Thanks to Dr Andrew Leach and Michele Assante for their collaboration and computations which helped to bring all of this work together.

I couldn't have hoped for a more remarkable team of people to have worked with over the past four years and thank the GLJ group in its entirety for making my studies thoroughly enjoyable, despite it being testing at times. I thank Ran Wei for her unrelenting positivity, optimism, and efforts towards my project. A special thanks also to Alex Pagett for welcoming me to this wonderful city.

I will forever be thankful that I embarked on this journey with Harvey Dale, and I am honoured to have shared a lab and flat with him these past four years. Thanks to Maggie Knight for all of our baking banter and being a reliable source of motivation for home workouts when the pandemic hit hard. I am lucky to have found the best training buddy in Mike Mullins. I thank him for always being keen to get out climbing and for the countless pizza nights. I am glad for my friendship with Jack Turner and Zoë Petard, and I thank them for all our adventures. Thank you to the Eden Rock Edinburgh climbing community for the fun times and to all of the staff members who I worked with along the way.

I owe Harry Moloney my gratitude for his constant reassurance and belief in me when my own confidence was lacking, for his generosity and caring nature. But most importantly, for willing me to embark on my own journey despite the challenges of being apart. For this, I will be forever grateful.

To my whole family, my parents, Ian and Ally, my brothers, Ed and Seán, and my grandparents, Kath and Graham, I thank them for being there every step of the way as always. And especially to my Dad, for his unwavering belief in me to succeed and for being the perfect role model from day one. Therefore, it is him to whom I dedicate this thesis.

Contents

Abbreviations

Ac	acetyl
Approx.	approximately
AQ	acquisition
Aq.	aqueous
BA	boronic acid
BE	boronic ester
BINAP	2,2’-bis(diphenylphosphino)-1,1’-binaphthyl
Bu	butyl
cal	calorie
calc	calculated
CAT	catechol
conc.	concentrated
DFT	density functional theory
dppb	1,4-bis(diphenylphosphino)butane
ESI	electrospray ionisation
est	esterification
Et	ethyl
eq	equilibrium
equiv.	equivalents
HER2	human epidermal growth factor receptor 2
HR	hormone receptor
HRMS	high-resolution mass spectrometry
hyd	hydrolysis

IEF	integral equation formalism
IR	infrared
KIE	kinetic isotope effect
KS	Kohn-Sham
Me	methyl
MIDA	*N*-methyliminodiacetic acid
mp	melting point
NMR	Nuclear Magnetic Resonance
obs	observed
PCM	polarizable continuum model
PDB	protodeboronation
PIN	pinacol
Pr	propyl
PTFE	polytetrafluoroethylene
rel	relative
SF	stopped-flow
tet	tetrahedral
Tf	triflic
TFA	trifluoroacetic acid
TOT	total
trig	trigonal
Ts	toluenesulfonyl
TS	transition state
UV-Vis	ultraviolet-visible

Chapter 1

Introduction

1.1 Boronic acid derivatives

1.1.1 Structure and properties

Organoboron compounds are derivatives of BH_3 containing a carbon-boron bond, a simple example being a trialkyl borane, specifically triethyl borane.[1] Boronic acids and their ester derivatives belong to this family of compounds.[2] The generic structures of an organoborane and examples of oxygenated organoboron compounds are highlighted in Figure 1.

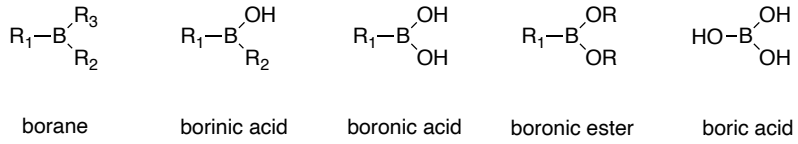

Figure 1. Organoboron compounds.

The organoboron compounds shown in Figure 1 adopt a trigonal planar geometry as a result of the bonding electrons located within the outer shell of the boron atom ($2s^2$, $2p^1$) which may participate in three sp^2-hybridised bonds.[3] These trivalent boron-containing organic compounds are highly electrophilic due to a vacant p-orbital which exists orthogonal to the plane (Figure 2). This non-bonding, empty p-orbital dictates both the physical characteristics and reactivity of the neutral boron species.[4]

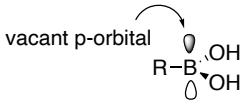

Figure 2. Trigonal planar geometry of a boronic acid.

1.1.2 Boronic acids

The Lewis acidity of boronic acids is attributed to the electron deficiency of the central boron atom.[5] Upon coordination with a Lewis base, anionic tetrahedral complexes are formed which are sp^3-hybridised. The term borate is associated with all derivatives of boric acid, and includes both trigonal BO_3 and tetrahedral

BO_4 species, the tetrahedral 'ate' complexes of organoboron species are more commonly referred to as boronates.[2] Water has an affinity for the vacant p-orbital, and hence aqueous solution of boronic acids become slightly acidic. Scheme 3 highlights the equilibrium of ionisation established between a boronic acid and the respective boronate anion, or conjugate base, formed in the presence of water.[6] K_a represents the association constant for the equilibrium of ionisation of water by a boronic acid in aqueous solution, and is described by equation (1). The assumption that water is in excess, and hence $[H_2O]$ is a constant, in aqueous solutions, accounts for its omission in the equilibrium equation (1). The equilibrium position can be modified by altering the pH of the solution.

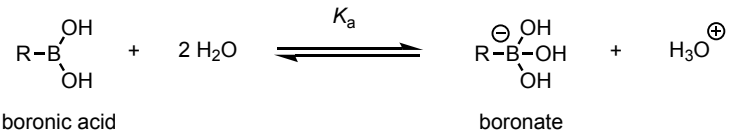

Scheme 3. Equilibrium of ionisation for a boronic acid in aqueous solution.

$$K_a = \frac{[RB(OH)_3]^-[H_3O]^+}{[RB(OH)_2]} \quad (1)$$

Substituents on the aromatic ring of phenylboronic acids exhibit a significant effect on the electron density of both the ring and boron atom, the extent of which is dependent on the nature and position of the substituent. In the case of ortho-substituents, steric interactions with the boronic acid group will be apparent. A review comparing the inductive and steric effects for *para*- and *ortho*-substituted phenylboronic acids was reported by Adamczyk-Woźniak *et al.* (Figure 3).[7]

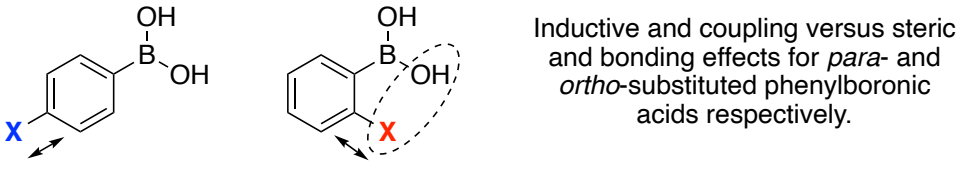

Figure 3. Influence of substituent position on the phenyl ring on the types of effects observed for phenylboronic acids.[7]

The nature of the substituents and substitution pattern on the phenyl ring affects the acidity of phenylboronic acids. Halogens, in particular fluorine, are electron withdrawing in an inductive capacity. The acidity constant (pK_a) was measured by Adamczyk-Woźniak *et al.*, utilising spectrophotometric and potentiometric techniques, for all isomers of polyfluorinated phenylboronic acid (F_1-F_5).[7] The *ortho*-fluoro derivative has a lower-than-expected pK_a when compared with other members of Table 1. This has been attributed to a stable 6-membered hydrogen-bonding arrangement between the fluorine atom and the neighbouring hydroxyl group. A correlation between increasing fluorination on the phenyl ring and increasing acidity of the derivatives was observed (Table 1). The presence of fluorine substituents, and their position on the ring of phenylboronic acids, has been shown to influence their susceptibility to undergo decomposition by protodeboronation, and this will be discussed further in section 1.3.[8]

Table 1. Acid dissociation constant, K_a measured by spectrophotometry at 25 °C for phenylboronic acid and fluorinated substrates prepared in aq. buffer solutions.[9]

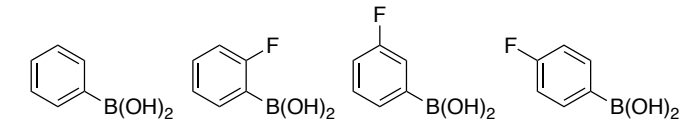

Phenylboronic acid 2-F 3-F 4-F

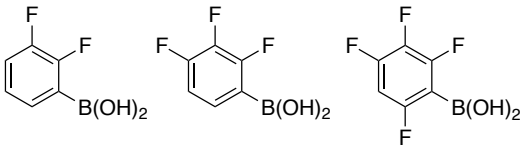

2,3-F_2 2,3,4-F_3 2,3,4,6-F_4

Phenylboronic acid derivative	K_a (in H_2O)
-	8.8
2-F	7.89 ± 0.01
3-F	8.09 ± 0.01
4-F	8.77 ± 0.01
2,3-F_2	6.99 ± 0.04
2,3,4-F_3	6.97 ± 0.01
2,3,4,6-F_4	6.17 ± 0.04

1.1.3 Boronic esters

Reaction of a boronic acid with an alcohol induces the replacement of both hydroxyl (-OH) groups with alkoxy groups (-OR) giving rise to boronic esters. This transformation results in a boronic ester being less polar relative to its corresponding boronic acid, due to the lack of hydrogen bonding facilitated by the hydroxyl groups present in boronic acids. There is little definitive kinetic evidence in the literature to support the speculation that boronic esters are generally more stable than boronic acids, due to the reduced Lewis acidity at the boron centre in the former.[3] Considering the relative inductive power of alkyl versus hydrogen, this improved stability is speculated to arise from the increased electron donating capacity of alkoxy groups compared to hydroxyl groups on boron. For example, RO-B where R = Me versus HO-B. This enables conjugation of the oxygen lone pairs into the electron-deficient boron centre to be more readily achieved.[3] In terms of Hammett sigma values, if σ_{meta} = 0 for H, a negative sigma value would be expected for Me or Et groups as electron-donating substituents, compared with a halogen or other electron-withdrawing substituents, which would have positive sigma values. The magnitude of σ_{meta} is dictated by electronic effects and depends on the relative inductive power of the substituents, determined by differences in electronegativity. It has been shown however, by Denmark and co-workers, that many arylboronic esters are more reactive to transmetallation than their corresponding arylboronic acids.[10] Catechol boronic esters are considered to be more Lewis acidic due to the presence of an aromatic ring and hence phenolic oxygens.[2] The catechol ester of 4-fluorophenylboronic acid was reported to undergo transmetallation approximately 4 times faster than the boronic acid.[10]

Some common boronic esters are shown in Figure 4 below, including catechol boronic ester in addition to five- and six-membered moieties.[2] Comparative studies for the stability of five- *versus* six-membered rings have been reported in the literature. Under neutral conditions, six-membered boronic esters were more stable towards hydrolysis than five-membered structures.[11] Bulky

boronic esters, for example pinacol and pinanediol boronic esters, were revealed to be more resistant towards hydrolysis than those less sterically hindered. It was concluded that increasing the number of methyl substituents on the ring resulted in more stable boronic esters. It has been postulated for 2-methyl-2,4-pentanediol esters, that the presence of 1,3-diaxial interactions between the methyl group and boron centre hinders the attack of water during hydrolysis, imparting greater stability in this instance (Figure 4).[2]

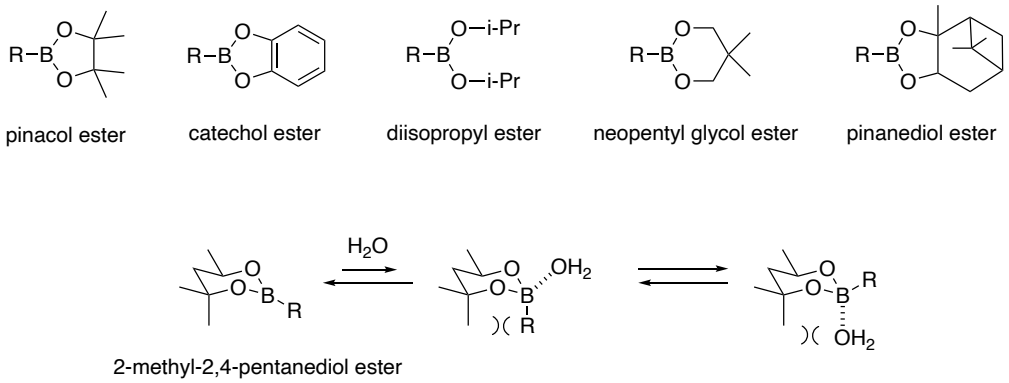

Figure 4. Six commonly encountered boronic esters; pinacol, catechol, diisopropyl, neopentyl glycol, pinanediol and 2-methyl-2,4-pentanediol esters. Stability towards hydrolysis, resultant from 1,3-diaxial interactions, for the latter ester is shown.[2]

Subsequently, a series of boronic esters were investigated to deduce their relative thermodynamic stabilities. The composition of products resultant at equilibrium, following the transesterification of 2-phenyl-1,3,2-dioxaborolane with a range of diols, was analysed by NMR spectroscopy in deuterated chloroform by Roy *et al*.[12-13] The trends observed included the increased stability of six-membered boronic esters in comparison to five-membered rings, and boronic esters formed from 1,2-diols possessing alkyl substituents on the α-carbon were found to be more stable, undergoing slower transesterification.

1.1.4 Utility

Synthesis

Boronic acids and boronic esters are indispensable building blocks in modern synthetic chemistry (Scheme 4).[2]

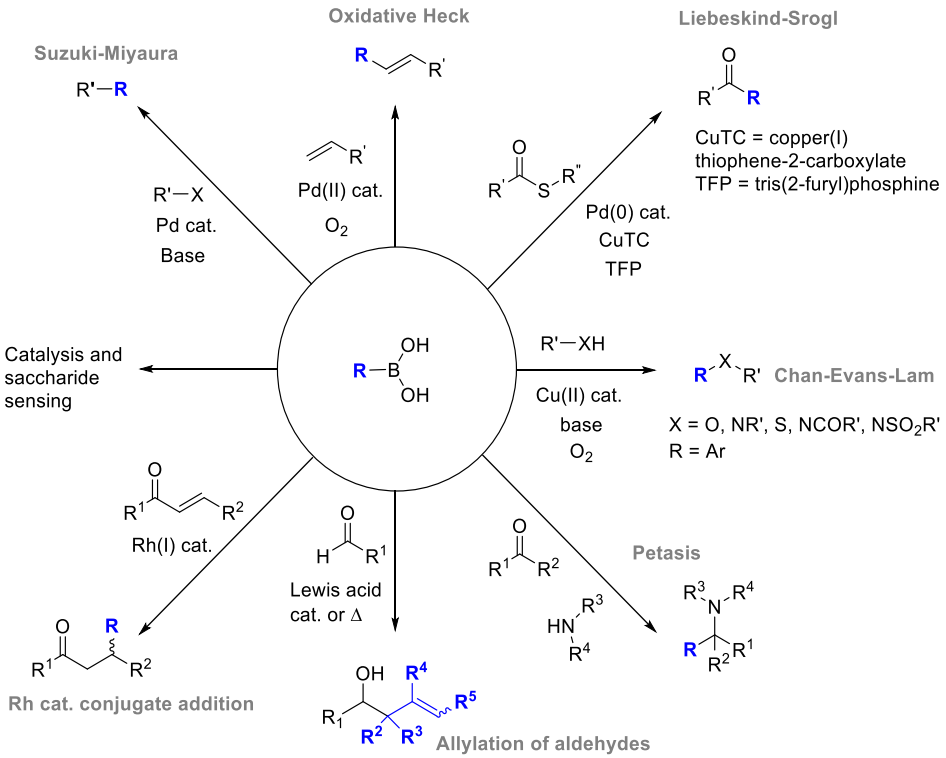

Scheme 4. Use of boronic acids in synthesis, catalysis, and saccharide sensing.

The synthetic utility of boronic acid and ester derivatives is widespread, spanning a broad range of applications, from cross-couplings to saccharide sensing and catalysis. Boronic acid catalysis has been leveraged in Diels-Alder reactions and amide formation. Organoboron compounds have been utilised to produce lead compounds in the manufacture of drugs and herbicides. Abemaciclib, a drug developed by Eli Lilly and Co. for the treatment of HR+, HER2- advanced and metastatic breast cancer, involves a Suzuki-Miyaura cross-coupling reaction between a pinacol boronic ester and chloro-pyrimidine, as a key step in the process (Scheme 5).[14] The 2,4,5-trisubstituted-3(2*H*)-pyridazinone is a common structural feature encountered in agrochemicals and pharmaceutics.[15] A synthetic procedure towards arylated 3(2*H*)-pyridazinones enabled by a Suzuki-Miyaura coupling reaction of arylboronic acids with chloro-3(2*H*)-pyridazinones has also been reported.[15]

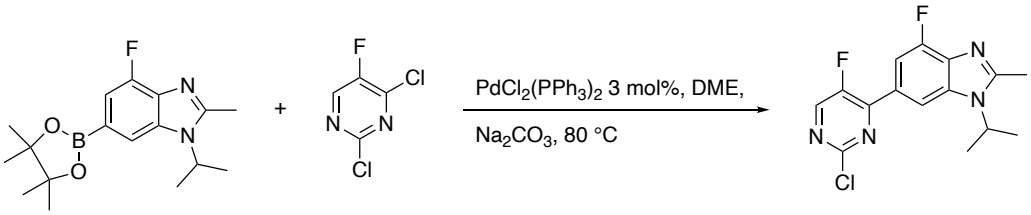

Scheme 5. Suzuki-Miyaura cross-coupling step in the synthesis of abemaciclib.

Reagents

Since the advent of the Suzuki-Miyaura cross-coupling reaction, first reported in the late 1970s, an insatiable demand amongst the synthetic community for a diverse range of boronic acids has ensued.[16-17] This reaction provides an elegant and efficient means of access to symmetrical and unsymmetrical biaryls, abundant in natural products.[2] Since the discovery of this reaction, significant advancements have been made and these improvements have allowed for its consideration as a viable option for use in the synthesis of complex molecules and the industrial manufacture of drugs. The initial requirement for high catalyst loadings has been overcome, the substrate scope has expanded, the boron reagent adapted, and the reaction may be conducted at significantly lower temperatures.[3] A general mechanism for Suzuki-Miyaura aryl-aryl coupling is shown in Scheme 6. This is a generic cycle of oxidative addition, transmetallation and reductive elimination steps.[18]

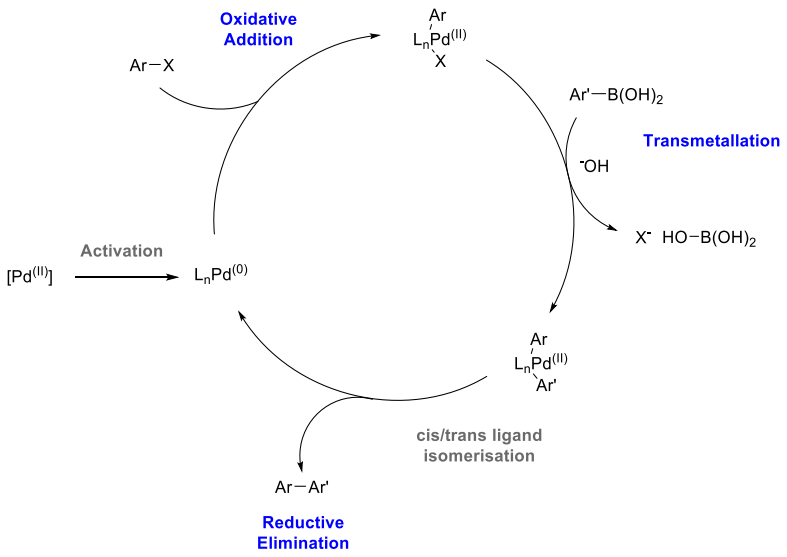

Scheme 6. General catalytic cycle for a biaryl Suzuki-Miyaura coupling.

A surge in the use of boronic esters, in particular the ubiquitous pinacol boronic ester, in Suzuki-Miyaura couplings as alternative reagents to boronic acids has necessitated research focused on their properties and role in such reactions. Denmark and co-workers recently reported a detailed mechanistic study in an effort to understand the participation of boronic esters in Suzuki-Miyaura reactions in context of the transmetallation step in the catalytic cycle.[10, 19] Pinacol boronic esters have been found to undergo transmetallation directly[10] in comparison to methyliminodiacetic acid (MIDA) boronates which must initially be subject to hydrolysis.[20] The previously discussed synthesis of abemaciclib employs an arylboronic acid pinacol ester as a key coupling reagent and is just one example of the use of boronic esters in Suzuki-Miyaura couplings in the industrial manufacture of drugs (Scheme 5).[14]

There are numerous other classic examples of cross-coupling reactions (Scheme 4)[2] which rely on the use boronic acids and boronic esters as key reagents, notably oxidative Heck,[21] Chan-Evans-Lam[22-24] and Liebeskind-Srogl couplings.[25] The oxidative boron Heck reaction emerged as an alternative to the traditional Mizoroki-Heck reaction. In contrast to the Pd(0)-catalysed Mizoroki-Heck reaction, oxidative Heck reactions are Pd(II)-catalysed. Where originally the first step of the catalytic cycle involved oxidative addition of Pd(0) into a halide or triflate, the oxidative Heck reaction utilises boronic acids which undergo transmetallation with the Pd(II) catalyst. Re-oxidation of Pd(0) to Pd(II) once the catalytic cycle is complete can be achieved through use of an oxidant like O_2, benzoquinone or $Cu(OAc)_2$.[26] Carbon-heteroatom bond formation can be accomplished by the copper-catalysed Chan-Evans-Lam reaction. This oxidative coupling of arylboronic acids with O-, N- and S-containing compounds including phenol, amines, amides, carbamates, thiols and sulfonamides is conducted in air and at room temperature.[2] Arylboronic acid pinacol esters are characteristically less reactive coupling reagents than their respective arylboronic acids in the Chan-Evans-Lam reaction.[27] Suspected catalyst inhibition of $Cu(OAc)_2$ by pinacol accounts for the lower reactivity of arylboronic acid pinacol esters as

substrates in this reaction.[28] Mechanistic insight by Watson *et al.* revealed that $B(OH)_3$ can be used to promote reactivity by acting a sequestering agent for free pinacol generated during the course of the reaction.[28] The Liebeskind-Srogl synthesis of ketones is a carbon-carbon bond-forming reaction between a boronic acid and thioester which proceeds under neutral conditions, catalysed by Pd(0) and mediated by stoichiometric Cu(I).[29-30]

Additional reactions utilising boronic acid derivatives include the Petasis reaction, the allylation of carbonyl compounds and rhodium-catalysed conjugate addition of organoboronic acids (Scheme 4).[2] The Petasis reaction, also known as the boronic acid Mannich reaction, allows for the synthesis of amines and α-amino acids, through a boronic acid mediated condensation of suitable carbonyl and amine compounds.[31-32] The efficient preparation of 1-amino-1*H*-indenes, enabled by a multistep synthesis involving both a Petasis reaction and a Suzuki-Miyaura reaction, was reported using 1,2-bis(boronates) as the starting material (Scheme 7).[33]

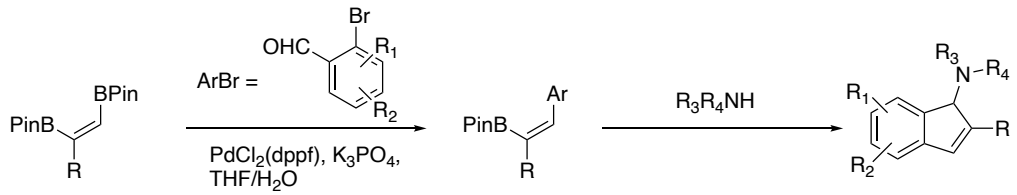

Scheme 7. Preparation of amino-1*H*-indenes.[33]

Acetate and propionate units are common in natural products and their stereoselective synthesis can be realised through the addition of allylboronates to aldehydes, a reaction which may be thermally or Lewis acid-catalysed.[34-35] Catalytic asymmetric allylation reactions between carbonyl compounds or imines with allylic boronic acids or boronic esters have also been realised.[36] The transition metal-catalysed conjugate addition of boronic acids to α,β-unsaturated compounds has been developed using rhodium catalysis.[37] This reaction has since been progressed to afford an asymmetric method by

replacing the original 1,4-bis(diphenylphosphino)butane, dppb ligand used with BINAP, a chiral phosphine ligand.[38]

Catalysis

Boronic acids and polyfluorinated arylboranes,[39] have found use as effective catalysts. They have been utilised to achieve the catalytic formation of amide bonds[40-46] and catalyse Diels-Alder reactions and cycloadditions.[40, 47-49] Synthetic methods enabling the efficient, direct condensation of an amine and carboxylic acid are desirable from an atom economy and green chemistry perspective.[50] Improved access to amide bond formation has been achieved by means of boronic acid and boronic ester catalysis (Scheme 8).[41, 45]

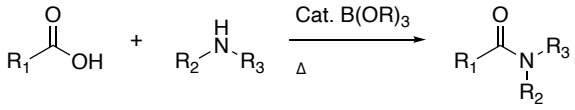

Scheme 8. Use of boronate esters as catalysts for amide formation

Boronic acid catalysis[51-52] has been applied by Hall and co-workers. for the activation of unsaturated carboxylic acids, specifically acrylic acid and 2-alkynoic acids, to participate as dienophiles in [4+2] cycloadditions with a variety of both cyclic and acyclic dienes (Scheme 9).[47]

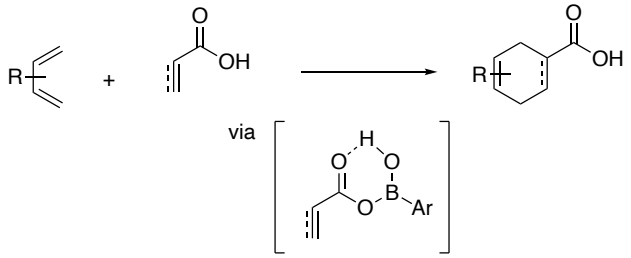

Scheme 9. Arylboronic acid-catalysed Diels-Alder [4+2] cycloaddition of a diene and unsaturated carboxylic acid (dienophile).

Carbohydrate recognition

Cyclic boronic esters are generated by reaction of a boronic acid and diol (Scheme 10).[53-54] Their formation is reversible under aqueous conditions, and this process, first studied by Lorand and Edwards,[55] has been exploited in sensing and the molecular recognition of saccharides.[56-57] The affinity of

boronic acids towards diols is influenced by pH and hence, design of boronic-acid based saccharide sensors necessitates consideration of the pH-dependence of boronic acid-diol interactions.[58-64]

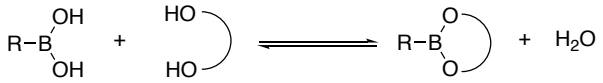

Scheme 10. Reaction of a generic boronic acid and a diol to form the respective cyclic boronic ester.

Other Uses

Boronic acid derivatives are vital in polymers,[65-72] as blocking and directing groups and as pharmacophores[73-75].

For example, there are currently several approved boronic acid and ester-based drugs (Figure 5).[75] The first to reach the market was Bortezomib (Velcade®), a proteasome inhibitor approved by the U.S. FDA in 2005 to treat myeloma, a form of bone marrow cancer. While Bortezomib is taken via weekly injection, Ixazomib (Ninlaro®) followed as a second-generation drug 10 years later, with the same mode of action but facilitating oral administration. 1 year prior to Ixazomib, Tavaborole (Kerydin®) was approved globally by the U.S. FDA for the treatment of onychomycosis, a fungal infection affecting finger and toenails. Another example of a boron-containing drug is Crisaborole (Eucrisa™), which was approved in 2016 to combat eczema.

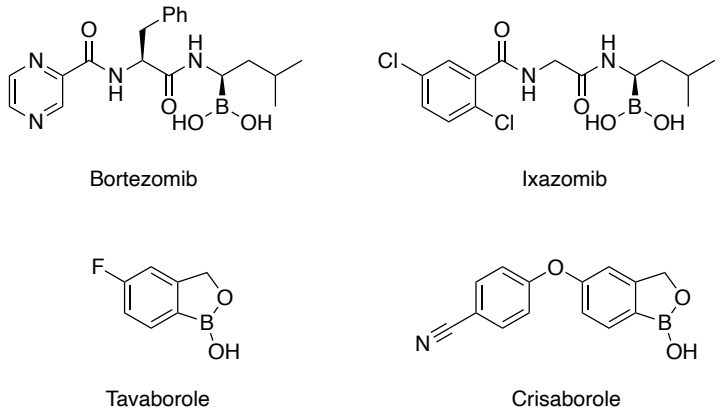

Figure 5. A selection of boron-containing drugs. Boronic acid-based include Bortezomib and Ixazomib and ester-based include Tavaborole and Crisaborole.[75]

One rationale for the incorporation of boron in drugs, in terms of drug design, is the capacity for boronic acids to act as bioisosteres, in particular for carboxylic acids. Both functional groups do not differ substantially in a structural sense but at physiological pH, approximately 7.4, the boronic acid remains unionised in contrast to a carboxylic acid moiety. The impact of boronic acid incorporation on both drug activity and bioavailability has been explored. The electrophilic character of boronic acids and hence, their ability to undergo reversible covalent binding, for example with a serine residue in an enzyme active site, underpins the mechanism of action of boronic acid-containing drugs as protease inhibitors.[75]

The boronic acid moiety has been employed as a blocking group enabling *ortho*-functionalisation of phenols and as a directing group for *meta*-functionalisation. Protodeboronation was utilised in this scenario for efficient removal of the boronic acid group revealing the desired products (Scheme 11).

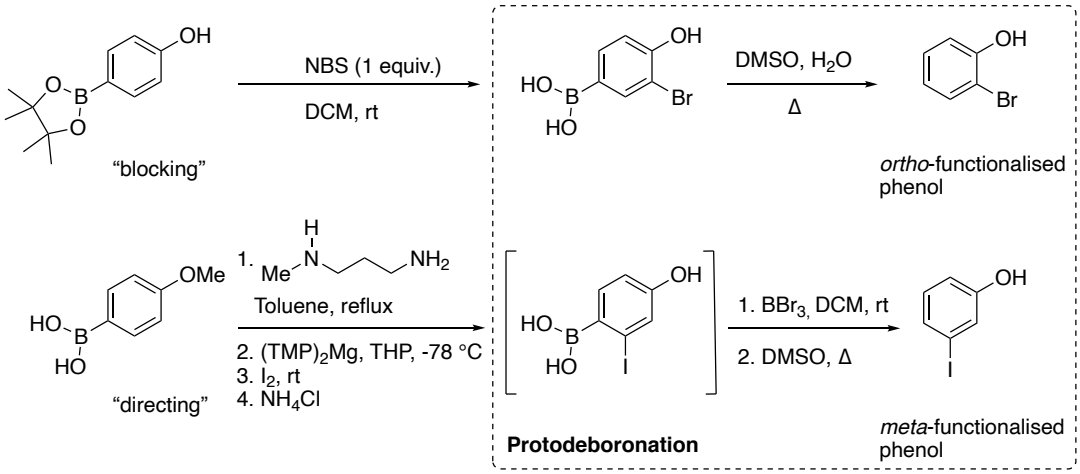

Scheme 11. *Ortho*- and *meta*-functionalisation of phenols.

1.2 Boronic acid-diol complexation

The factors which influence the equilibrium between boronic esters and their corresponding acids have been reported in considerable detail[53-55, 58, 60-63] and general processes for the pH-dependent hydrolysis of boronic esters have been elucidated by Pizer[76-78] and Ishihara.[79-82] However, the scope for such studies has largely been in context of carbohydrate recognition.[56-57, 59, 64] There is minimal kinetic information relating to the hydrolysis of boronic esters of simple diols e.g. pinacol,[58] at high pH and concentrations routinely employed in organic synthesis.

A reduced pK_a' is resultant for boronic esters, formed by the reaction of a boronic acid and *cis*-1,2-diol ($K_{eq\text{-}trig}$), in comparison to the corresponding boronic acid pK_a (Scheme 12).[82] One exception is for weakly binding diols.[54]

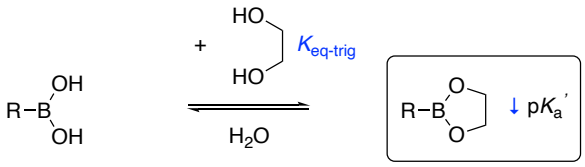

Scheme 12. Equilibrium ($K_{eq\text{-}trig}$) between boronic acid and ester in the presence of 1,2-ethanediol.

Given pK_a = -log$_{10}$(K_a), the association constant, K_a' is increased i.e. K_a' > K_a. At a given pH, the position of equilibrium will be shifted more towards the boronic ester favouring to exist in its "ate" form (Scheme 13), relative to the same process for boronic acids.

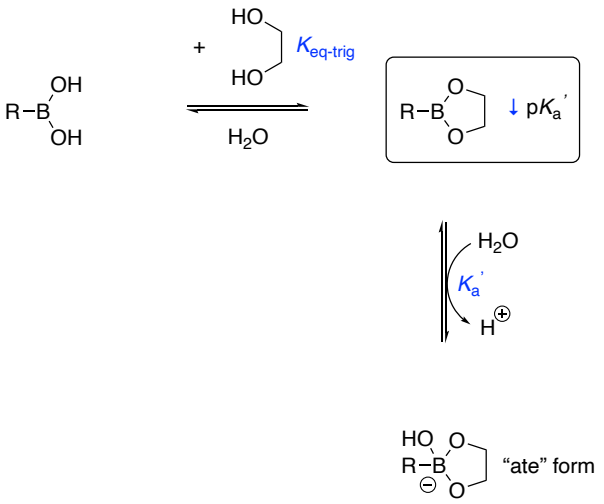

Scheme 13. Equilibrium between neutral, trigonal boronic ester and anionic, tetrahedral ester boronate (K_a').

At high pH, boronic acid boronate will be the dominant species present (Scheme 14) and diol binding and ester formation is favourable ($K_{eq\text{-}tet}$).[82] An increased binding constant (K_a) will result for boronic acids with a reduced pK_a.

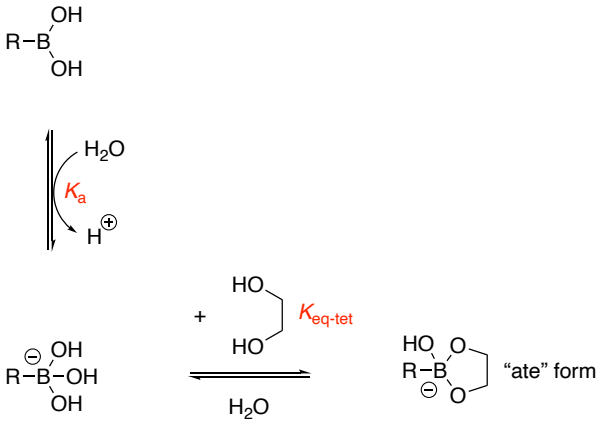

Scheme 14. Equilibrium between neutral, trigonal boronic acid and anionic, tetrahedral acid boronate (K_a) and equilibrium ($K_{eq\text{-}tet}$) between acid boronate and ester boronate in the presence of 1,2-ethanediol.

It can be inferred from $K_aK_{tet} = K_a'K_{trig}$, where $K_a' > K_a$, that formation of the anionic, tetrahedral boronic ester boronate, ($K_{eq\text{-}tet}$), is more favourable than the neutral, trigonal boronic ester ($K_{eq\text{-}trig}$) and so, $K_{eq\text{-}tet} > K_{eq\text{-}trig}$.[83] A complete picture for the two pathways possible for the equilibration of boronic acid and boronic ester in addition to acid boronate and ester boronate is represented schematically below (Scheme 15).

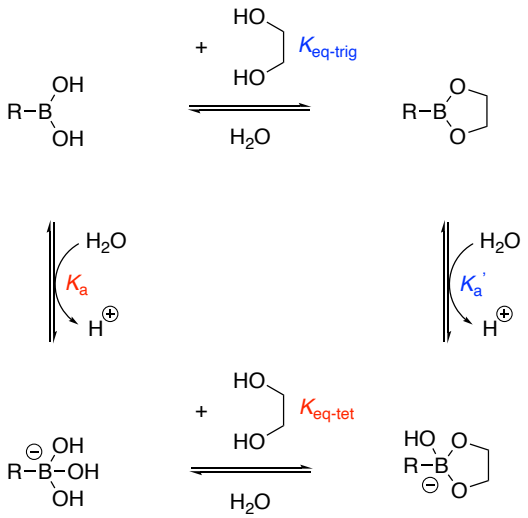

Scheme 15. Complexation pathways for the equilibration between boronic acid and ester species in their neutral and boronate forms.

The optimal pH for binding may not always be the most appropriate pH in context of saccharide sensor construction and the optimal pH for boronic acid-diol complexation is not always greater than the p*K*a of the boronic acid.[53] For example, with acidic ligands such as α-hydroxy carboxylic acids, the optimal pH for binding is lower than the pK_a of the boronic acid.[77] In addition to the impact of pH on the equilibrium of this system, the esterification is also pH-dependent. If the boronic acid is quite acidic (reduced pK_a), and hence its boronate form is weakly basic, faster complexation with diols will result for the neutral, trigonal species. For example, *m*-NO_2-PhB$(OH)_2$ will undergo complexation more rapidly than *m*-NO_2-PhB$(OH)_3^-$. In comparison, MeB$(OH)_2$ which will be subject to slower complexation than its respective boronate, MeB$(OH)_3^-$.[77] While this is a summary of some of the general trends observed in the literature, the process of boronic acid-diol complexation is seemingly case-dependent. Put rather succinctly by Pizer in 2017, “boron acid complexation reactions in alkaline media may proceed via either trigonal boron acids and/or their conjugate bases and the relative reactivity is a function of pK_a and pK_b values of the conjugate boron acid/borate base pair, respectively.”[77] Hence, the mechanistic understanding for hydrolysis of boronic esters and esterification of their corresponding acids, for both the neutral and boronate species, is far from fully substantiated.

1.3 Protodeboronation

1.3.1 Reaction background

Boronic acids are susceptible to undergo protonolysis by protodeboronation, a reaction also commonly referred to in the literature as protodeborylation (Scheme 16). Overall, cleavage of the carbon-boron bond and formation of a carbon-hydrogen bond gives the protodeboronation product and boric acid as a side product.[2]

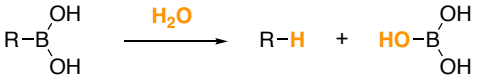

Scheme 16. Protodeboronation reaction of a boronic acid.

Protodeboronation is one of the major pathways by which boronic acids can decompose. The stability of boronic acids is variable, dependent on the structural differences between substrates and reaction conditions used. Early studies showed that protodeboronation could be catalysed by trace metal ions, for example by Hg(II) found in water.[2, 84] Ainley and Challenger subsequently reported the formation of benzene from phenylboronic acid and investigated the impact of varying the reaction conditions on the protodeboronation of phenylboronic acid.[2, 85] This included heating the substrate under acidic conditions (conc. HCl) and basic conditions (NaOH), with hot solutions of copper sulphate, cadmium bromide and zinc chloride and with water under pressure. Hammett plots were constructed to investigate the influence of pH and substituent effects for the metal-catalysed protodeboronation of arylboronic acids by Kuivila and co-workers.[86] Kinetic studies were performed for the reaction catalysed by cadmium ions and the pH-rate profile revealed catalysis between pH 3-6. An S_E2 mechanism was postulated for the reaction (Scheme 17). The impact of other metal ions on the rate of reaction was probed. Cu^{2+} ions were found to be the most effective at accelerating the rate of protodeboronation and Ni^{2+} ions the least.[86]

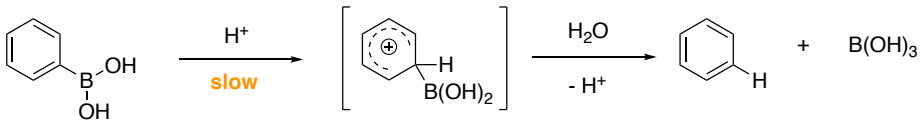

Scheme 17. Aromatic bimolecular electrophilic substitution (Ar-S_E2) for the protodeboronation of phenylboronic acid.

Further studies in the field of metal-catalysed protodeboronation were initiated by Liu *et al.* with the development of a Cu-cat. protodeboronation procedure, promoted by oxygen, for arylboronic acids in aq. ethanol.[87] Other protocols include the Ag-cat. protodeboronation of arylboronic acids and esters, promoted by base,[88] Au-cat. protodeboronation[89] and the Bi-cat protodeboronation of triborylated indole heterocycles.[90]

Some boronic acids and esters undergo rapid protodeboronation in aqueous media and under basic conditions, which is problematic in context of the Suzuki-Miyaura cross-coupling reaction. Significant yield losses in the synthesis of diflunisal were attributed to protodeboronation.[91] Sterically-hindered, electron-deficient boronic acids and esters, used in a Suzuki-Miyaura reaction by Cammidge and Crépy, proved to be challenging coupling partners due to their propensity to undergo protodeboronation under the reaction conditions.[92] Catalytic palladium was found to accelerate the protodeboronation of these substrates and formation of the boronate was postulated to be critical for decomposition by this pathway. The authors noted deceleration of the reaction rate when dry reagents and solvents were used. The susceptibility towards protodeboronation of sterically hindered boronic acids has also been reported by Watanabe and co-workers.[93]

Various strategies have been successfully implemented to suppress or bypass protodeboronation in cross-couplings,[94-95] a process which leads to undesired consumption of reagent or loss of function. These include direct transmetallation of boronic esters, [10, 19, 96-97] the 'slow-release' of boronic acids from trifluoroborates, MIDA boronates and esters (Figure 6),[98] and specialised catalysts.[99-100]

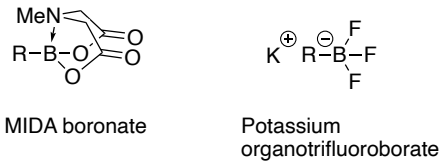

Figure 6. Boronic acids masked as MIDA boronates and organotrifluoroborates.

Carrow and co-workers reported the efficient Suzuki-Miyaura cross-coupling of polyfluorophenylboronic acids with a range of aryl halides (Scheme 18). The reaction was realised with minimal protodeboronation product formation using $Pd(PAd_3)(p\text{-}FC_6H_4)Br$, described in the report as an "on-cycle pre-catalyst".[99] The authors noted that while the improved stability of boronic esters compared to their respective boronic acids under anhydrous conditions was recognised,[95] the rate of protodeboronation of pentafluorophenylboronic acid pinacol ester in the presence of Et_3N was accelerated with increasing equivalents of water. Optimised coupling conditions were developed to include $Na_2SO_4.10H_2O$, allowing for the slow release of water during the reaction.

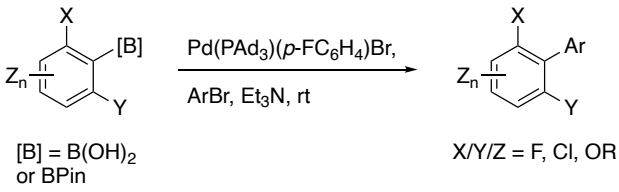

Scheme 18. Reaction conditions for Suzuki-Miyaura cross-couplings using an "on-cycle pre-catalyst".[99]

In some circumstances, protodeboronation is desirable, enabling the traceless rectification of overborylation[101] and, given that some arylboronic acids are suspected bacterial mutagens, the effective removal of remaining boronic acid reagent post process.[102]

1.3.2 Mechanistic studies

Until recently, despite the ubiquitous nature of boronic acids in organic synthesis, limited mechanistic information was available for the protodeboronation of these reagents under aqueous conditions. Kuivila and

co-workers pioneered the early mechanistic work behind the protodeboronation of arylboronic acids under aqueous conditions.[86, 103-106] UV-Visible spectroscopy enabled Kuivila to investigate the reaction kinetics for the protodeboronation of arylboronic acids in aqueous media, revealing acid and base-catalysed processes. Absorptions arising in the UV-Vis spectra due to boronic acid oxidation unfortunately prevented the authors from drawing conclusions about the mechanism under more basic conditions (pH > 7). These studies were conducted prior to the advent of the Suzuki-Miyaura cross-coupling reaction and the importance of understanding the mechanistic pathways for protodeboronation at high pH was yet unknown.

The protodeboronation of *p*-methoxyphenylboronic acid was investigated under acidic conditions using sulfuric acid, perchloric acid, formic acid and phosphoric acid. Hammett plots for aq. acids were compared at a range of temperatures (25 °C, 40 °C and 60 °C). The evidence presented by Kuivila was considered to be indicative of a general acid-catalysed process, supportive of a rate-determining proton transfer.[104] Based on subsequent solvent isotope effect studies,[105] the authors deemed an A-1 mechanism (Scheme 19) unlikely to be occurring.

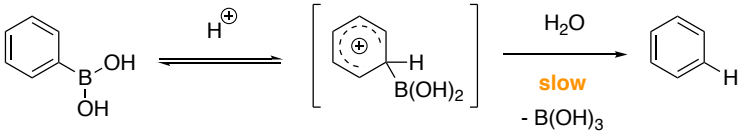

Scheme 19. A-1 mechanism for arylboronic acids, which was eliminated from consideration based on solvent KIEs.[104-105]

Instead, the pathway postulated for the acid-catalysed protodeboronation of arylboronic acids was instead an S_E2, with the mechanism involving a slow proton-transfer step prior to fast carbon-boron bond cleavage (Scheme 17).

Several years later, mechanistic investigations were reported by Kuivila and co-workers for base-catalysed protodeboronation between pH 2.0 and 6.7. (Scheme 20).[103] The pH-rate profile for 2,6-dimethoxyphenylboronic acid

revealed a change in mechanism, from general acid catalysis by an S_E2 process, at approximately pH 4.8. The impact of varying substituents on the phenyl ring was investigated and k_{obs} for the reaction was found to increase in all cases.[106] At pH 6.7, *ortho*-substitution of the phenyl ring resulted in an increased rate of protodeboronation for both electron-donating and electron-withdrawing groups. The rate increase was more substantial for the boronic acid with *ortho*-fluorine substitution in comparison to a methoxy group. Despite obtaining a ρ value of unusually small magnitude for an electrophilic aromatic substitution, – 2.3, this negative ρ value from the Hammett plot was still an indication of positive charge development in the transition state.

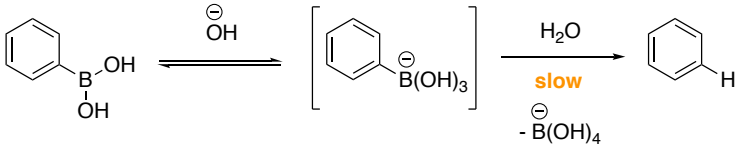

Scheme 20. Protodeboronation mechanism of arylboronic acids (pH 2.0 to 6.7).

In the early 2000s, Frohn *et al.* investigated the base-catalysed protodeboronation for a range of fluorinated boronic acids.[107] Boronic acid substrates possessing *ortho*-fluoro substitution were more reactive, with pentafluorophenylboronic acid giving the fastest rate of protodeboronation. An investigation was subsequently reported, by Perrin, examining the protodeboronation under basic conditions of (hetero)arylboronic acids and esters possessing 2,6-disubstitution, specifically electron-withdrawing groups (Scheme 21).[108] A range of electron-withdrawing groups including halogens (F, Cl, Br), -NO_2 and –CF_3 were tested and the substitution pattern on the phenyl ring was varied.

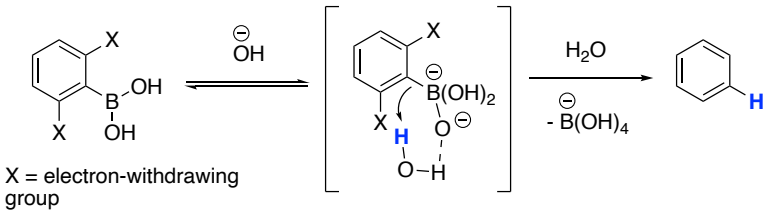

Scheme 21. Mechanism for the specific base-catalysed protodeboronation of electron-deficient, di-*ortho*-substituted arylboronic acids.

Recent work in the Lloyd-Jones group examined the protodeboronation reaction (between pH 1-13 in aqueous-organic media, specifically 1:1 1,4-dioxane/H_2O, at 70 °C) of a diverse range of arylboronic acids including polyfluorinated examples and heteroaromatic systems.[8, 109] The boronic acids studied could be categorised into different groups based on their reactivity; non-basic boronic acids, basic heteroaromatic boronic acids and polyfluorophenyl boronic acids. From profiles of pH versus log k_{obs} (Figure 7) the stability of the substrate of interest could be evaluated and potential mechanisms predicted for each category of boronic acid. These studies highlighted that for the reactive systems tested, the pH determines the boronic acid speciation between N-protonated, neutral and boronate. This governs which mechanistic pathways are viable and is hence responsible for determining the overall rate of protodeboronation.

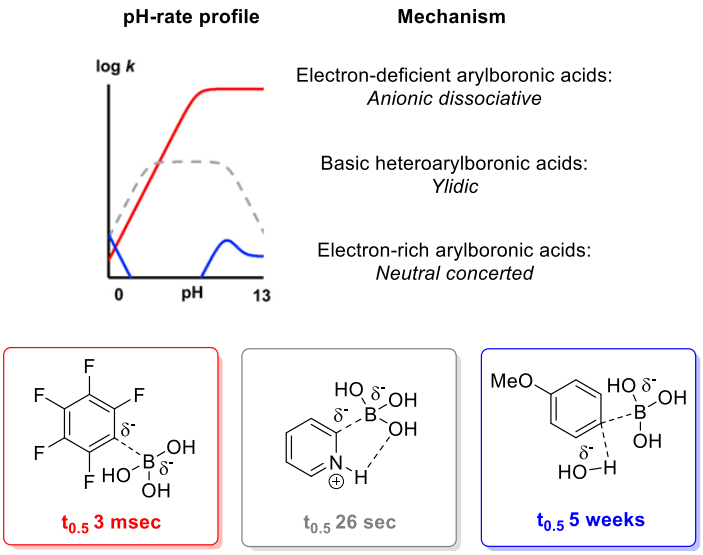

Figure 7. pH-rate profiles for polyfluorinated, heteroaromatic and electron-rich boronic acids.[8]

Initial studies aimed to classify the reactivity of 16 heterocyclic boronic acids across a wide pH range in order to establish the pH-stability regions for each substrate specifically and identify the contributing mechanistic pathways for protodeboronation. For the boronic acids studied, including cyclopropyl and vinyl boronic acids, the rates observed exhibited a pH-dependence, with rates

spanning 6 orders of magnitude. Kinetic analysis was facilitated by considering three different speciation states for the boronic acids studied; N-protonated (related to nitrogen-containing basic heterocycles), neutral and anionic, boronate forms.

Four non-basic heterocycles were studied, all of which were found to be most reactive at high pH. (Figure 8). Simulations for furyl and both thienyl boronic acids incorporated the mechanistic pathways established by Kuivila in addition to an autocatalytic process. Mechanistic analysis of pyrrolyl required inclusion of a water autoionization process between pH 3 and 6.

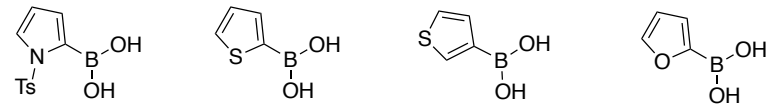

N-Ts-2-pyrrolyl boronic acid | 2-thienyl boronic acid | 3-thienyl boronic acid | furyl boronic acid

Figure 8. Non-basic heterocyclic boronic acids

Select examples of heteroaromatic boronic acids, for example the 2-pyridyl system, were found to be stabilised by base and most reactive at neutral pH (Figure 7). Other substrates within the class of basic heteroaromatics, for example 5-pyrazolyl and 5-thiazolyl, were found to be most reactive at high pH.

2-Pyridyl and 5-thiazolyl boronic acids underwent rapid protodeboronation via a fragmentation mechanism of zwitterionic intermediates ($t_{0.5}$ = 25 and 48 s respectively at pH 6.2 to 6.9, 70 °C). Lewis acid additives were found to either reduce or accelerate decomposition depending on the nature of the substrate (Figure 9). The decelerated protodeboronation rate for the 2-pyridyl system arises from complexation of metal (M = Cu or Zn) with nitrogen, thereby reducing the availability of zwitterion present to decompose by fragmentation. For the 5-thiazolyl boronic acid, the anti-bonding orbital S-C σ* acts as a proxy hydrogen-bond, thereby stabilising the $B(OH)_3$ leaving group. This effect is magnified through N-metal complexation, giving rise to an accelerated rate of

protodeboronation. Cyclopropyl, vinyl, 3- and 4-pyridyl boronic acids exhibited slower rates of protodeboronation, with half-lives of $t_{0.5}$ > 1 week under basic conditions (pH 12, 70 °C).

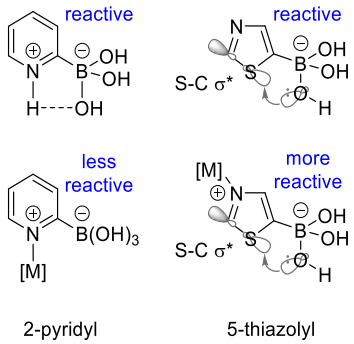

Figure 9. Effect of Lewis acid additives on the protodeboronation of 2-pyridal boronic acid and 5-thiazolyl boronic acid.[109]

Subsequent studies were focused on the protodeboronation of 30 polyfluorinated arylboronic acids at high pH. Under these conditions, the arylboronic acid exists exclusively as the anionic, boronate form. Polyfluorinated arylboronic acids with additional substituents including nitro, methoxy and trifluoromethyl groups were also tested. The range of half-lives observed in this study was vast, spanning nearly 10 orders of magnitude (Table 2) from $t_{0.5} \approx 7$ months for the 3-fluorophenylboronic acid to $t_{0.5} \approx 2.6$ ms for the pentafluorophenylboronic acid. *Ortho*-fluorinated arylboronic acids are subject to rapid protodeboronation with 2-fluorophenylboronic acid exhibiting $t_{0.5}$ ≈ 19 h and the 2,6-difluoro substrate $t_{0.5}$ ≈ 5 s. The acceleration in protodeboronation rate induced both by *ortho*-fluoro substitution and increasing number of fluorine atoms on the phenyl ring is consistent with observations by Frohn *et al.*[107]

Table 2. Impact of fluorination (number of fluorine atoms and substitution pattern) on the half-lives of protodeboronation for arylboronates (pH 13, 70 °C in 1:1 1,4-dioxane/H_2O).[8, 109]

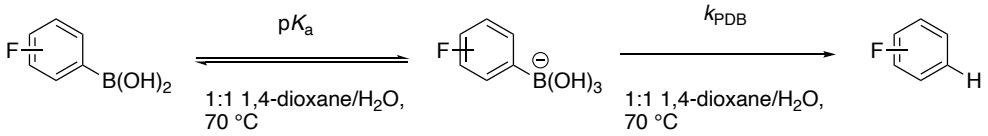

Boronic acid	~ $t_{0.5}$
3-F	7 months
H	6 months
4-F	4 months
3,4-F_2	3 months
3,4,5-F_3	7 weeks
2-F	19 h
2,3-F_2	2 h
2,3,5-F_3	10 min
2,3,4,5-F_4	3 min
2,6-F_2	5 s
2,3,4,6-F_4	66 ms
2,3,4,5,6-F_5	2.6 ms

Electron-deficient boronic acids with a Swain-Lupton parameter (σ_{SL}) of greater than 0.7 were most reactive under highly basic conditions. This substituent parameter is an extension of the Hammett value (σ) taking into consideration both resonance and field effects (R and F respectively). These substrates were proposed to undergo protodeboronation via a dissociative mechanism (Scheme 22). A modest PKIE, supportive of an early transition state, has been observed for “naked” aryl anions which undergo protonation in aqueous media.[110] The partitioning factor (Ar-H/Ar-D) observed for this class of substrates was on average 1.2 ± 0.05. The absence of a rate-determining proton transfer was indicated by k_H/k_D = 1.00. This mechanistic pathway is accompanied by the conversion in geometry at the boron centre from tetrahedral to trigonal.

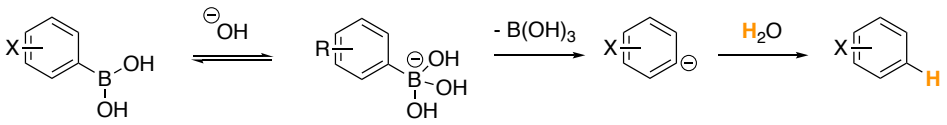

Scheme 22. Protodeboronation of electron-deficient arylboronic acids via an anionic dissociative mechanism.

In contrast, electron-rich boronic acids protodeboronate at a slower rate under basic conditions, likely via a concerted mechanism (Scheme 23). The boronic acids in this category are destabilised under acidic conditions and exhibit self/auto catalysis when the pH = p*K*a.

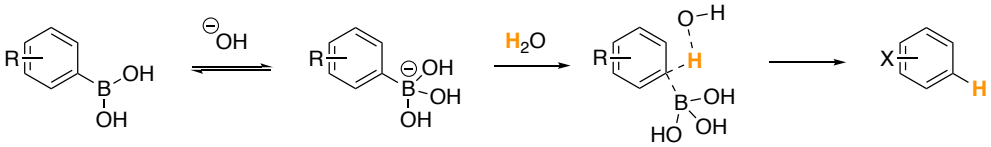

Scheme 23. Protodeboronation of electron-rich arylboronic acids via a neutral, concerted-type mechanism.

1.4 This work

Boronic esters are generally considered to be more stable towards protodeboronation than their corresponding boronic acids, and yet there is little kinetic data to corroborate or refute this assumption.[3, 18] The research presented herein was centred on discerning the various pathways by which a diverse range of (hetero)arylboronic esters undergo protodeboronation at high pH. This work was focused on the esterification of boronic acids which are especially susceptible to protodeboronation (Figure 10) and those which are most reactive under highly basic conditions, including polyfluorophenyl, thiazolyl and isoxazolyl systems.

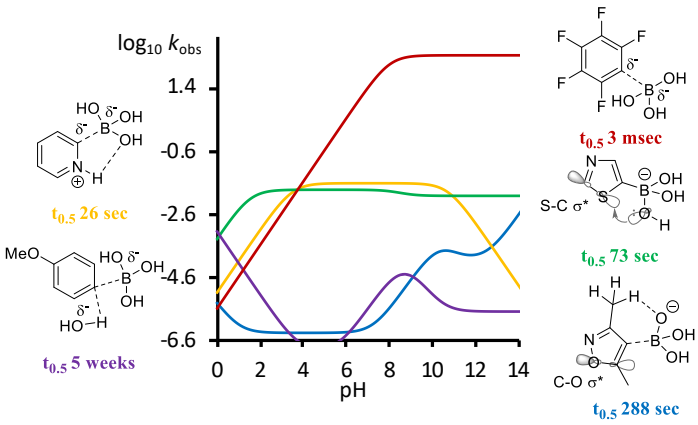

Figure 10. Selected pH-rate profiles for pentafluorophenylboronic acid (electron-deficient), 2-pyridyl, 5-thiazolyl and 3,5-dimethylisoxazolylboronic acids (heteroaromatic) and 4-methoxyboronic acid (electron-rich). Half-lives indicated are at 70 °C in 50% aq. 1,4-dioxane at pH 13 except for 2-pyridyl which is for the reaction at pH 7.[8, 109]

Initial studies concentrated on the protodeboronation of arylpinacolboronate esters, ubiquitous as reagents and intermediates in organic synthesis. The influence of modifying the ester component, using a series of simple diols and one triol, was subsequently probed using 2,6-difluorophenylboronic acid as a reference. The reaction to liberate the protodeboronation product for boronic esters was considered as a function of two separate, contributory pathways; *indirect* (pre-hydrolytic) versus *direct* protodeboronation.

In general, and unless specified otherwise, experiments were performed in 50% aqueous 1,4-dioxane, at 27 ºC and at pH >13. This solvent system was employed in order to corroborate with previous work,[8, 109] and proved to be an optimum medium for both boronic acid and potassium hydroxide solubility over a wide span of pH values. Trifluoroacetic acid (TFA or as its potassium salt under basic conditions) was utilised as an internal NMR reference standard for kinetic studies but also acted as a stabiliser for boronic acid/ester stock solutions.[8] Thereby the stock solutions were maintained under acidic conditions, necessary to avoid decomposition of boron reagent at higher pH. Reaction monitoring was facilitated by *in-situ* (^{19}F, ^{1}H and ^{11}B) NMR spectroscopy, with stopped-flow techniques harnessed for particularly rapid reactions.

Results and Discussion

2.1 Hydrolysis and protodeboronation of pinacol esters

2.1.1 *Direct* versus *indirect* protodeboronation of boronic esters

This thesis is centred on the esterification of boronic acids which are most reactive at high pH.[8] Boronic esters can undergo base-catalysed protodeboronation via two distinct pathways; *direct* (k_{BE}) and *indirect* pre-hydrolytic (k_{hyd}, k_{BA}) protodeboronation (Scheme 24). The *direct* process involves rate-limiting C-B bond cleavage of the boronic ester to liberate the corresponding protodeboronation product (Ar-H) and boric ester (Scheme 24, Path I). The alternative decomposition pathway for boronic esters occurs first via hydrolysis to afford the corresponding boronic acid and subsequent protodeboronation affords the product and boric acid (Scheme 24, Path II). The prospect of solely *direct* protodeboronation, a hydrolysis-protodeboronation sequence, or alternatively the potential for both pathways to be contributory under the same reaction conditions, presents an additional kinetic challenge. Deconvolution of the contribution of both routes for the protodeboronation of boronic esters is critical to understand the stabilising or destabilising influence of esterification of boronic acids (k_{BA}/k_{BE}).

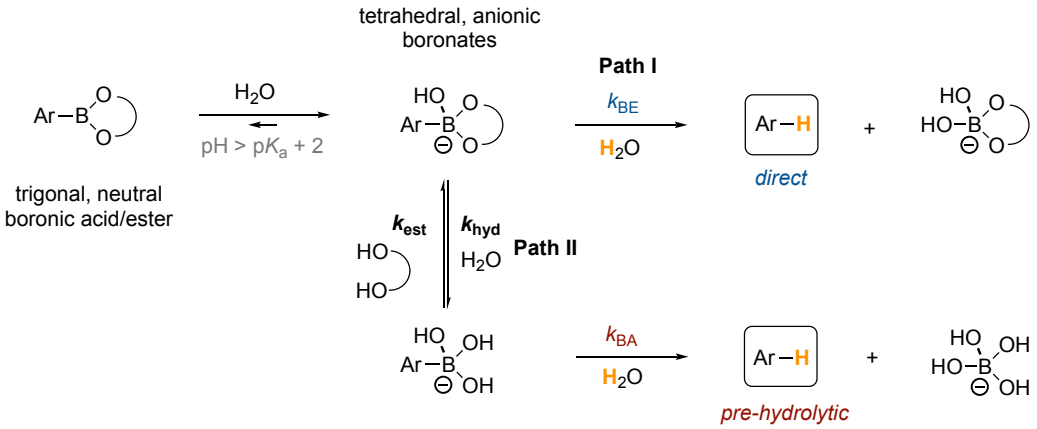

Scheme 24. Path I, *direct* (k_{BE}) and Path II, pre-hydrolytic *indirect* (k_{hyd}, k_{BA}) pathways for protodeboronation of arylboronate esters under basic conditions.

2.1.2 Hydrolysis and esterification of 2-fluorophenylboronic acid **1a** and its pinacol ester **1b**

The speciation of boronic acid/esters between the trigonal, neutral boron and the tetrahedral, anionic boronate forms is affected by pH (Scheme 25), and this influences the overall reactivity to hydrolysis and protodeboronation. A dynamic equilibrium is set up between boronic acid/ester and hydroxyboronate species upon addition of substoichiometric hydroxide base. Following the addition of excess hydroxide, exclusive and instantaneous conversion to the hydroxyboronate is achieved.

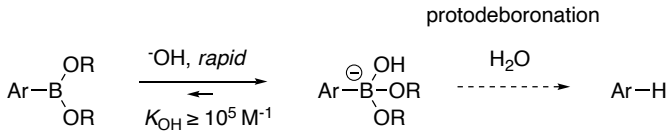

Scheme 25. Equilibrium between boronic acid/ester and respective hydroxyboronates in the presence of hydroxide, and subsequent protodeboronation reaction to liberate the protodeboronation product.

The Lewis acidity, K_a of $ArB(OR)_2$ towards H_2O is shown in equation (2) and the equilibrium constant for autoionization of water, to generate OH^- and H_3O^+, is represented by K_w, equation (3). The affinity of the boronic ester, $ArB(OR)_2$ for hydroxide, OH^- is represented by K_{OH}, which can be described by reference to both Ka and K_w, equation (4) and (5).

$$K_a = \frac{[ArB(OH)(OR)_2]^-[H_3O]^+}{[ArB(OR)_2]} \quad (2)$$

$$K_w = [OH]^-[H_3O]^+ \quad (3)$$

$$K_{OH} = \frac{K_a}{K_w} \quad (4)$$

$$K_{OH} = \frac{[ArB(OH)(OR)_2]^-}{[ArB(OR)_2][OH]^-} \quad (5)$$

The speciation of boronate, x_{BOH} is described by equation (6) and is pH-dependent, equation (7). From equation (7), the speciation of boronate can be determined at a given pH (see Appendix 6.1 for further detail). For example, at pH ≥2 units above the pK_a, speciation is x_B <0.01 (mol-fraction of neutral boron acid/ester) and x_{BOH} >0.99 (mol-fraction of boronate acid/ester).

$$x_{\mathrm{BOH}} = (1 - x_{\mathrm{B}}) = \frac{[\mathrm{ArB(OH)(OR)_2}]^-}{[\mathrm{ArB(OR)_2}] + [\mathrm{ArB(OH)(OR)_2}]^-} \quad (6)$$

$$x_{\mathrm{BOH}} = \frac{1}{1 + 10^{(\mathrm{p}K_\mathrm{a} - \mathrm{pH})}} \quad (7)$$

The effect of pH on the rates of hydrolysis (k_{hyd}) and esterification (k_{est}) for 2-fluorophenylboronic acid **1a** and its pinacol ester **1b** was investigated in 50% aq. dioxane at 300 K. Both substrates are subject to very slow protodeboronation under these conditions and across a wide pH range, enabling the pH-dependence of the hydrolysis/esterification pathways to be studied by ^{19}F NMR spectroscopy, without significant side reactions complicating the analysis. The esterification of **1a** was initiated by addition of 2 equivalents of pinacol **S1**, at the desired pH, and the kinetics of equilibrium of **1a** with pinacol ester **1b** was analysed by simulations of temporal-concentration profiles (Figure 11, B). Aqueous HCl or KOH was added to achieve acidic or basic reaction conditions, respectively. The pH-rate profiles were elucidated from either one or both of the time-averaged ^{19}F NMR signals for neutral, trigonal boronic acid/anionic, tetrahedral boronate [**1a**/**1a**$_{OH}$]$^-$ and pinacol ester/boronate [**1b**/**1b**$_{OH}$]$^-$ (Figure 11, C). The chemical shift for **1a** and **1b** is shifted upfield as the pH is increased, relative to the internal standard potassium trifluoroacetate (IS = KTFA). At pH >13, achieved by addition of excess KOH (>1 equiv.),[8] these species are quantitatively converted from their trigonal to tetrahedral form (**1a** and **1b**) and exist exclusively as boronates, [**1a**$_{OH}$]$^-$ and [**1b**$_{OH}$]$^-$ (Figure 11, D). The speciation of **1a** with [**1a**$_{OH}$]$^-$ and **1b** with [**1b**$_{OH}$]$^-$, described by equations (8) – (11), can be specifically calculated using equation (7).

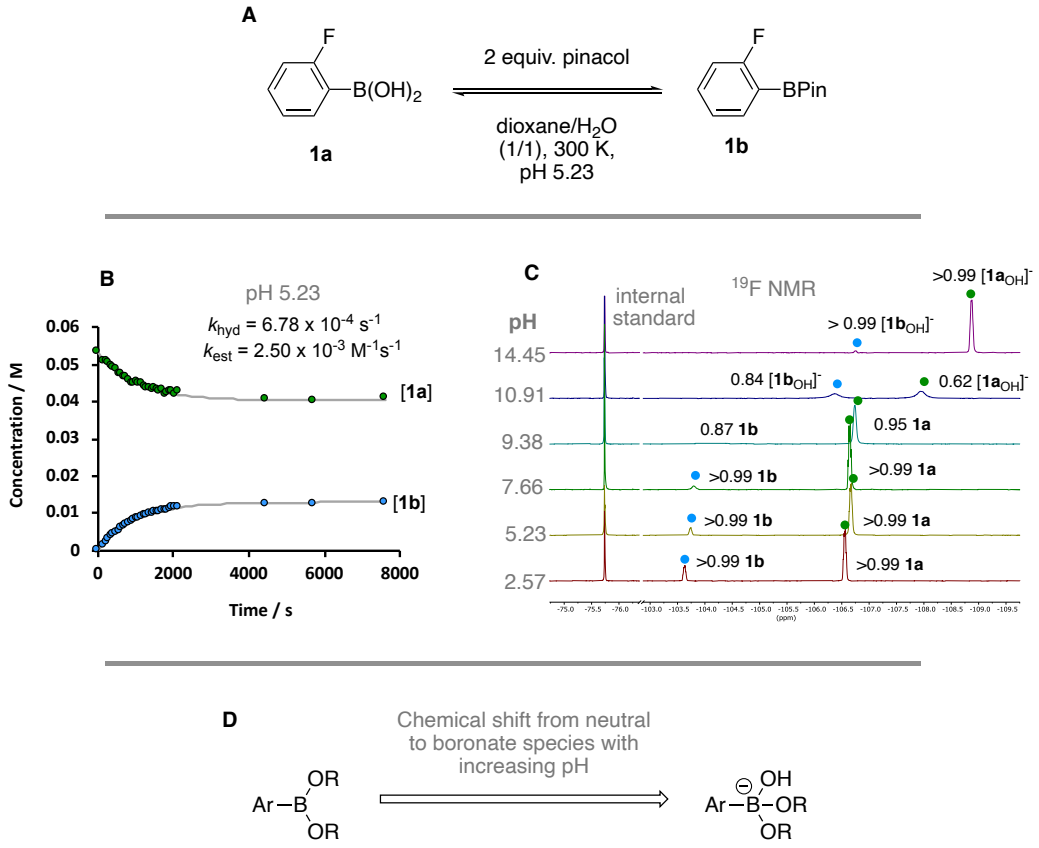

Figure 11. A) Reaction conditions and NMR tube set-up. Order of addition of reagents, in 1:1 1,4-dioxane/H_2O: 0.6 mL **1a**/IS, followed by HCl or KOH added to achieve desired pH. 0.4 mL pinacol added to initiate the reaction and pH measured. Internal standard (IS) = difluoroanisole, TFA or its potassium salt. B) graphical analysis for the esterification of **1a** by 2 equivalents pinacol at pH 5.23 to afford the corresponding pinacol ester **1b**. Rate coefficients k_{est} and k_{hyd} by kinetic modelling of temporal-concentration profiles, under conditions of varying pH (example at pH 5.23 in graph B of the time-averaged ^{19}F signals for **1a**/[**1a**$_{OH}$]$^-$ and **1b**/[**1b**$_{OH}$]$^-$). C) Stacked spectra of reactions, 4 mins after reaction initiation, across a wide pH range, including chemical shifts for KTFA, **1a**/[**1a**$_{OH}$]$^-$ and **1b**/[**1b**$_{OH}$]$^-$. D) Speciation between neutral boron and boronate forms for a generic aryl boronic acid/ester.

$$x_{\mathrm{BOH}\mathbf{1a}} = \frac{1}{1 + 10^{(\mathrm{p}K_{\mathrm{a}}\mathbf{1a} - \mathrm{pH})}} \quad (8)$$

$$x_{\mathrm{BOH}\mathbf{1b}} = \frac{1}{1 + 10^{(\mathrm{p}K_{\mathrm{a}}\mathbf{1b} - \mathrm{pH})}} \quad (9)$$

$$x_{\mathbf{B1a}} = (1 - x_{\mathrm{BOH}}\mathbf{1a}) = \frac{10^{(\mathrm{p}K_{\mathrm{a}}\mathbf{1a} - \mathrm{pH})}}{1 + 10^{(\mathrm{p}K_{\mathrm{a}}\mathbf{1a} - \mathrm{pH})}} \quad (10)$$

$$x_{\mathbf{B1b}} = (1 - x_{\mathrm{BOH}}\mathbf{1b}) = \frac{10^{(\mathrm{p}K_{\mathrm{a}}\mathbf{1b}-\mathrm{pH})}}{1 + 10^{(\mathrm{p}K_{\mathrm{a}}\mathbf{1b}-\mathrm{pH})}} \quad (11)$$

Following an extensive series of individual reactions, and subsequent kinetic modelling, a pH-rate profile, for the interconversion of [**1a**/**1a**$_{OH}$]$^-$ with [**1b**/**1b**$_{OH}$]$^-$ in the presence of pinacol, was generated (Figure 12).

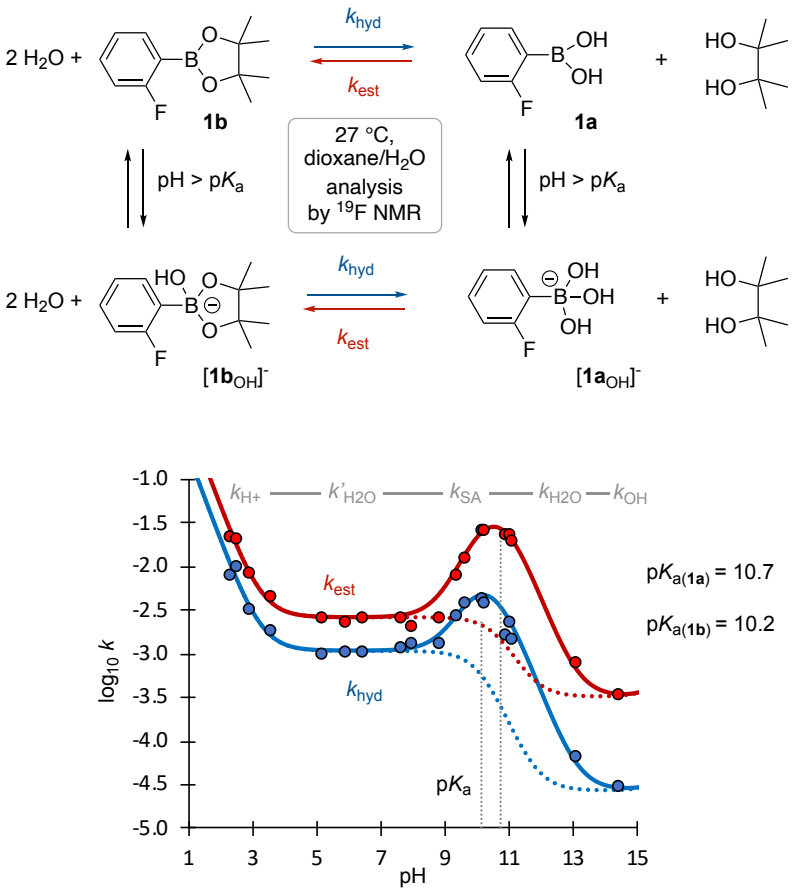

Figure 12. Pathways for hydrolysis (k_{hyd}) and esterification (k_{est}) of 2-fluorophenylboronic acid **1a**, in the presence of 2 equivalents pinacol, across a wide pH range, at 300 K, in 50% aq. dioxane and analysed by *in-situ* ^{19}F NMR spectroscopy. Rates of interconversion of acid **1a**/[**1a**$_{OH}$]$^-$ with ester **1b**/[**1b**$_{OH}$]$^-$. Data points (filled red/blue circles: $[B]_{TOT}$ = 50 mM, $[H_2O]$ = 27.75 M) plotted as $\log_{10}k$ versus pH. Kinetic model (solid red/blue lines: $k_{H+}[H^+] + k^{trig}_{H2O} + k_{H2O} + k_{SA} + K_{a(\mathbf{1a})} + K_{a(\mathbf{1b})}$, [ArOH] = 0 mM). For pinacol boronates, the impact of k_{OH} was found to be negligible. Dashed lines: $[B]_{TOT} \leq 5$ mM, and self/auto-catalysis (k_{SA}) is negligible.

The full profile was simulated using the following constants: k_{H+}, k^{trig}_{H2O}, k_{H2O}, k_{OH}, k_{SA}, $K_{a(\mathbf{1a})}$, $K_{a(\mathbf{1b})}$. For pinacol boronates, the impact of k_{OH} was found to be negligible. The summed processes for the hydrolysis and esterification rate

coefficients (k_{hyd} and k_{est}) are described below and individual simulated pH-rate profiles for the processes $k_{H+}[H^+] + k^{trigH}[H_2O] + k^{tetH}[H_2O]$ and $k_{OH}[OH]$ are shown in Figure 13.

Summed processes for hydrolysis and esterification rate coefficients, k_{hyd} and k_{est} respectively:

Rate = k_{hyd}[**1b**]; units for k_{hyd} s^{-1}

$k_{hyd} = x_{B\mathbf{1b}}(k^{H}{}_{H+}[H^+] + k^{trigH}{}_{H2O} + k^{H}{}_{SA}[\mathbf{1}_{OH}]) + x_{BOH\mathbf{1b}}(k^{H}{}_{H2O} + k^{H}{}_{OH}[OH])$

Rate = k_{est}[**1a**][pinacol]; units for k_{est} M^{-1} s^{-1}

$K_{est} = x_{B\mathbf{1a}}(k^{E}{}_{H+}[H^+] + k^{trigE}{}_{PIN} + k^{E}{}_{SA}[\mathbf{1}_{OH}]) + x_{BOH\mathbf{1a}}(k^{E}{}_{PIN} + k^{E}{}_{OH}[OH])$

$$\text{where } [\mathbf{1}_{OH}] \sim \frac{[\mathbf{1a}] + [\mathbf{1b}] + [\mathbf{1a}_{OH}]^- + [\mathbf{1b}_{OH}]^-}{1 + 10^{((0.5\ pK_a\mathbf{1a} + 0.5\ pK_a\mathbf{1b}) - pH)}} \quad (12)$$

$[H^+] = 10^{pH}$ and $[OH^-] = K^w/[H^+]$; pK^w set as 15.75 for 1:1 1,4-dioxane/H_2O.[8, 109]

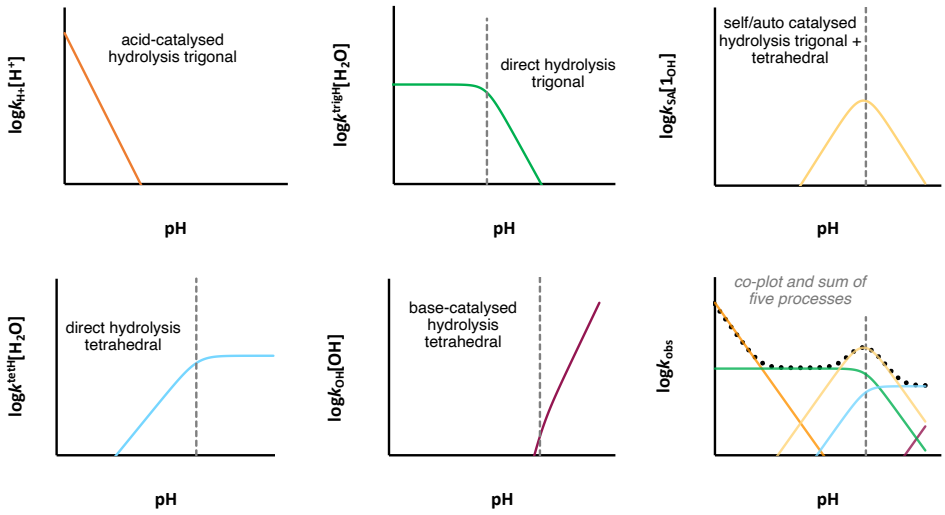

Figure 13. Individual simulated pH-rate profiles for the processes $k_{H+}[H^+] + k^{trigH}[H_2O] + k^{tetH}[H_2O]$, $k_{OH}[OH]$ and $k_{SA}[\mathbf{1}_{OH}]$. Co-plot of the five contributory processes with black dashed line representing the sum of these processes.

Acceleration of the rate of hydrolysis of **1b** at low pH, approx. pH 1-4, was evident from the pH-rate profile (Figure 12). The speciation between neutral boron and anionic boronate forms, at pH 2 for example, is x_B >0.99 and x_{BOH}

<0.01, where the pK_a of **1a** = 10.7. The potential for specific acid catalysis (k_{H+}), is supported by the negative slope (slope = -1) observed within this pH-range and is consistent with the acid-catalysed processes proposed by Pizer[76-78] and Ishihara.[79-82] Given the nature of the solvent blend, 50% aq. dioxane, the acceleration of the rate of reaction likely originates from catalysis specifically by protonated solvent, in this case H_3O^+, generated in the presence of strong acid, aq. HCl (kinetic model: $k_{H+}[H^+]$). Considering the rate enhancement observed under acidic conditions, for the acid-catalysed process (k_{H+}), protonation at the boronate oxygen, followed by attack of H_2O at the boron centre, can be envisaged to generate the mono-coordinate ester (Scheme 26).

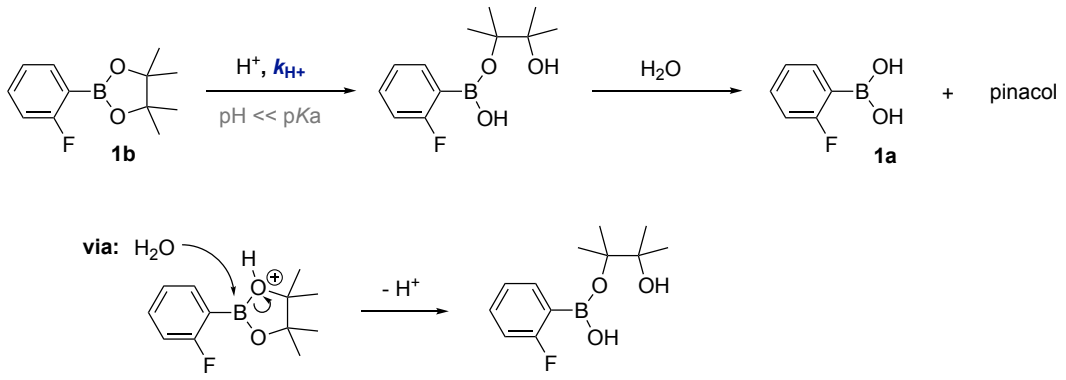

Scheme 26. Postulated pathway for the acid-catalysed hydrolysis (k_{H+}) of pinacol ester **1b** in 50% aq. dioxane (pH 1-4, pH << p*K*a) and postulated pathway.

A plateau in the rate of hydrolysis ($\log_{10}k$, slope = 0) was observed between pH 5-8 (Figure 12), indicative of the pH-independent hydrolysis of neutral, trigonal boronic ester **1b** within this pH range (kinetic model: k^{trig}_{H2O}). The speciation between neutral boron and anionic boronate forms, at pH 6 for example, is x_B >0.99 and x_{BOH} <0.01, where the pK_a of **1a** = 10.7. In this case, trigonal hydrolysis was postulated to proceed initially by attack of H_2O at the boron centre, followed by a subsequent proton transfer to afford the mono-ligated pinacol ester (Scheme 27).

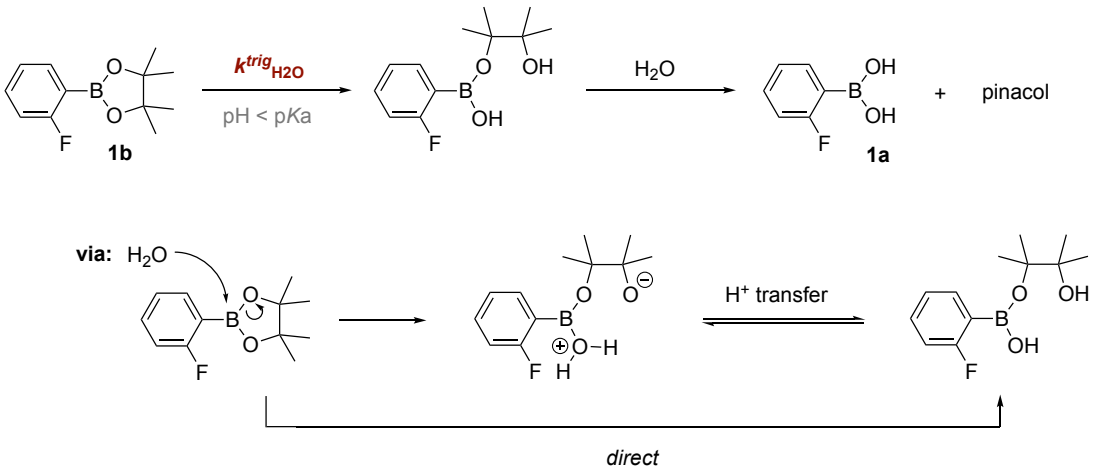

Scheme 27. The pH-independent hydrolysis (k^{trig}_{H20}) of neutral, trigonal pinacol ester **1b** in 50% aq. dioxane (pH 5-8, pH < pK_a).

At pH >13, **1b** undergoes conversion to the tetrahedral, anionic boronate and the rate of hydrolysis of [**1b**$_{OH}$]$^-$ was decelerated under basic conditions (Figure 12). Hence, base-catalysis (k_{OH}) of the pinacolate ester **1b** is negligible and at pH >13, the overall rate of hydrolysis is independent of the pH. A possible mechanism for this pathway is postulated and described in section 2.2.1 (Scheme 32).

2.1.3 Self/auto-catalysis

Dashed lines in the pH-rate profile indicate the predicted model in the absence of any catalysis between pH 9-11 (Figure 12). When [B]$_{tot}$ (= **1a** + **1b** + [**1a**$_{OH}$]$^-$ + [**1b**$_{OH}$]$^-$) is set to zero, the curved dashed lines are obtained. If no catalysis within this pH range was evident, a continuation of the plateau observed for the values of $\log_{10}k$ at neutral pH (k^{trig}_{H2O}) would be expected. This trend would then be followed by the reduction in the rate of hydrolysis observed as the pH rises, to approach pH >13, at which point k_{OH} is negligible. However, as the pH approaches the substrate pK_a (10.2 and 10.7 for **1b** and **1a** respectively), the rate of hydrolysis rises. The rate then decays as the pH values become greater than the pK_a (Figure 12, model: solid coloured lines). This feature of the pH-rate profile is suggestive of an self/auto-catalytic process (k_{SA}). When the pH = pK_a, equal and maximum concentrations of both boron/ate species exist in

solution (x_B =0.50 and x_{BOH} =0.50). Previously the potential for self/auto-catalysis, when the pH values are close to the pK_a, has not been identified for the hydrolysis of boronic esters. This is likely due to previous works employing UV-Vis spectroscopic analysis for studying the kinetics of hydrolysis of boronic esters, using dilute solutions in neutral or acidic media, and hence working at substantially lower substrate concentrations.[53-55, 58, 60-63, 76-82]

Since a self/auto-catalytic process is dependent on the total boron concentration, the correlation between the rate of esterification (k_{est}), of **1a** in the presence of pinacol, and concentration was independently probed at pH 10.8 and a linear correlation was confirmed (Figure 14). This supports a deceleration in the $\log_{10}k$ as the total boron concentration is reduced, at pH values close to the pK_a (Figure 12, dashed lines in kinetic model: $[B]_{TOT} \rightarrow 0$). When the total boron concentration is raised, an enhancement in the rate of hydrolysis of **1b** is observed when self/auto-catalysis dominates, within the limits of pH = pK_a ± 1.5 and $[\mathbf{1}]_{TOT} \geq 5$mM.

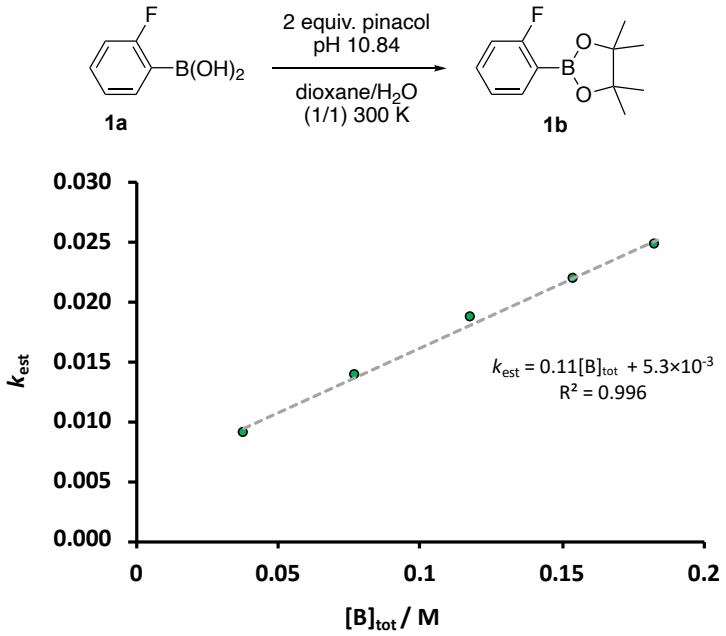

Figure 14. Graphical analysis of the linear dependence of rate of esterification (k_{est}) verus total boron concentration ([B_{TOT}] / M) at pH 10.8.

2.1.4 Phenolic catalysis

The presence of aerobically generated hydroperoxides in ethereal solvents can give rise to phenols from the corresponding arylboronates. The resulting 2-fluorophenol, produced from [**1b**$_{OH}$]$^-$ by an oxidative process, was found to accelerate the general-acid catalysed hydrolysis (k_{ArOH}) of pinacol ester boronate [**1b**$_{OH}$]$^-$ (Scheme 28).

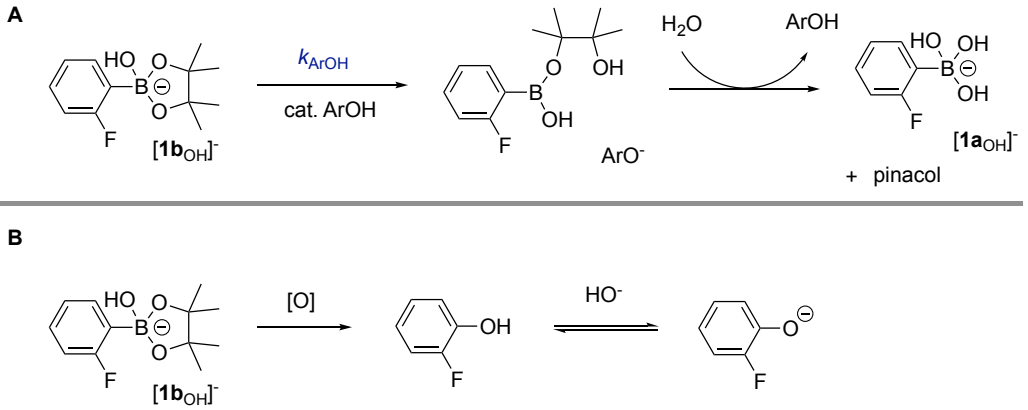

Scheme 28. A) General acid-catalysed hydrolysis of [**1b**$_{OH}$]$^-$ by the resulting 2-fluorophenol (k_{ArOH}) and B) generation of 2-fluorophenol by oxidation of [**1b**$_{OH}$]$^-$.

A linear correlation between the total rate of hydrolysis (k_{obs}, where $k_{obs} = k_{hyd} + k_{cat}$[ArOH]) and 2-F-phenol concentration was observed at pH 10.5 (Figure 15 A). Greater equivalents of phenol (0.2-0.9 equivalents) in the reaction lead to an increase in k_{obs} and decrease in pH of the solution (Figure 15 B). The extent of phenolic catalysis was explored for this system and revealed oxidative general-acid catalysis to prevail only at pH values close to the boronate pK_a. As per self/auto-catalysis (k_{SA}), phenolic catalysis (k_{ArOH}) was only contributory at total boron concentration > 5mM.

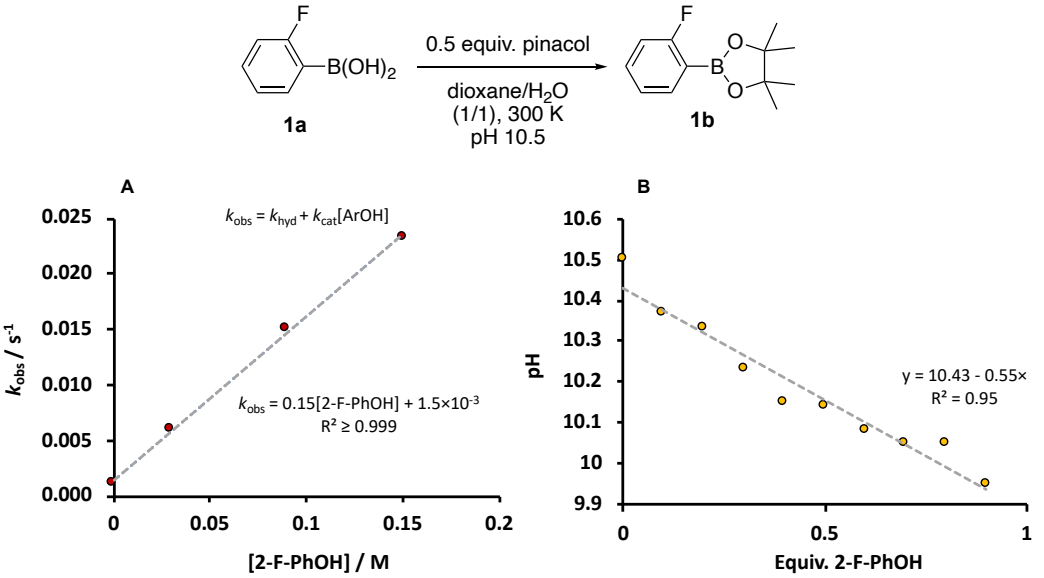

Figure 15. A) Graphical analysis at pH 10.5 of the linear dependence of k_{obs} versus 2-F-phenol concentration. B) pH change versus equivalents 2-F-phenol.

The pK_{aH} of 2-F-phenol was independently measured and estimated to be 10.0 (Figure 16). The pH of a solution of 2-F-phenol in 50% aq. dioxane was measured, using a pH probe, following each subsequent addition of potassium hydroxide, from 0.2 to 0.475 equivalents relative to 2-F-phenol.

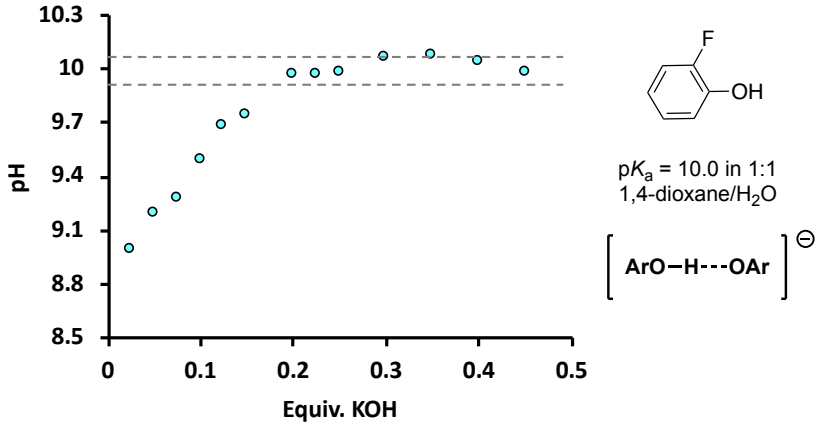

Figure 16. Plot of pH versus equivalents KOH. Taking the average pH across the plateau (0.2 to 0.475 equiv.) gives a pK_{aH} of 10.0 for 2-F-phenol.

2.1.5 Hydrolysis and esterification of 2,6-fluorophenylboronic acid **2a** and its pinacol ester **2b**, and pathways for protodeboronation

Since 2-fluorophenylboronic acid **1a** is subject to very slow protodeboronation at 27 °C in 50% aq. dioxane ($t_{0.5}$ = 19 h at 70 °C),[8] this substrate proved ideal for exclusively monitoring hydrolysis of the pinacol ester. In order to investigate the impact of esterification by pinacol on protodeboronation, the more reactive 2,6-difluorophenylboronic acid **2a** was selected. The presence of an additional *ortho*-fluorine on the phenyl ring is responsible for the greater reactivity of **2a** towards protodeboronation compared with **1a** (see 1.1.3 and 1.3 for details).[7-8, 107] Additionally, **2a** is most reactive under basic conditions when the boronate [**2a**$_{OH}$]$^-$ is dominant,[8] and therefore protodeboronation of the pinacolate ester [**2b**$_{OH}$]$^-$ was investigated at pH >13, at 27 °C in 50% aq. dioxane. The solvent blend, containing 500 g H_2O per litre ([H_2O] = 27.75 M), was optimised in earlier studies for adequate boronic acid solubility across pH 1-13, salt concentrations and boronic acid identities, and was retained in this study for facile comparisons with previous work.[8]

The addition of 2 equivalents pinacol to boronic acid **2a**, in 50% aq. dioxane, gave a final equilibrated mixture of 75:25 **2a**/**2b**. Conversion to the respective boronates [**2a**$_{OH}$]$^-$ and [**2b**$_{OH}$]$^-$ occurred after the addition of excess base (3 equivalents relative to [**2**]$_{TOT}$), and a temporal concentration profile of the base-catalysed protodeboronation of both species was elucidated. The stacked plot of ^{19}F spectra obtained for the reaction highlights the decay of the mixture of [**2a**$_{OH}$]$^-$ and [**2b**$_{OH}$]$^-$ and formation of the protodeboronation product over time. An upfield shift relative to boronic acid/ester **2a**/**2b**, following the addition of KOH, is experienced by boronates [**2a**$_{OH}$]$^-$/[**2b**$_{OH}$]$^-$ (Figure 17).

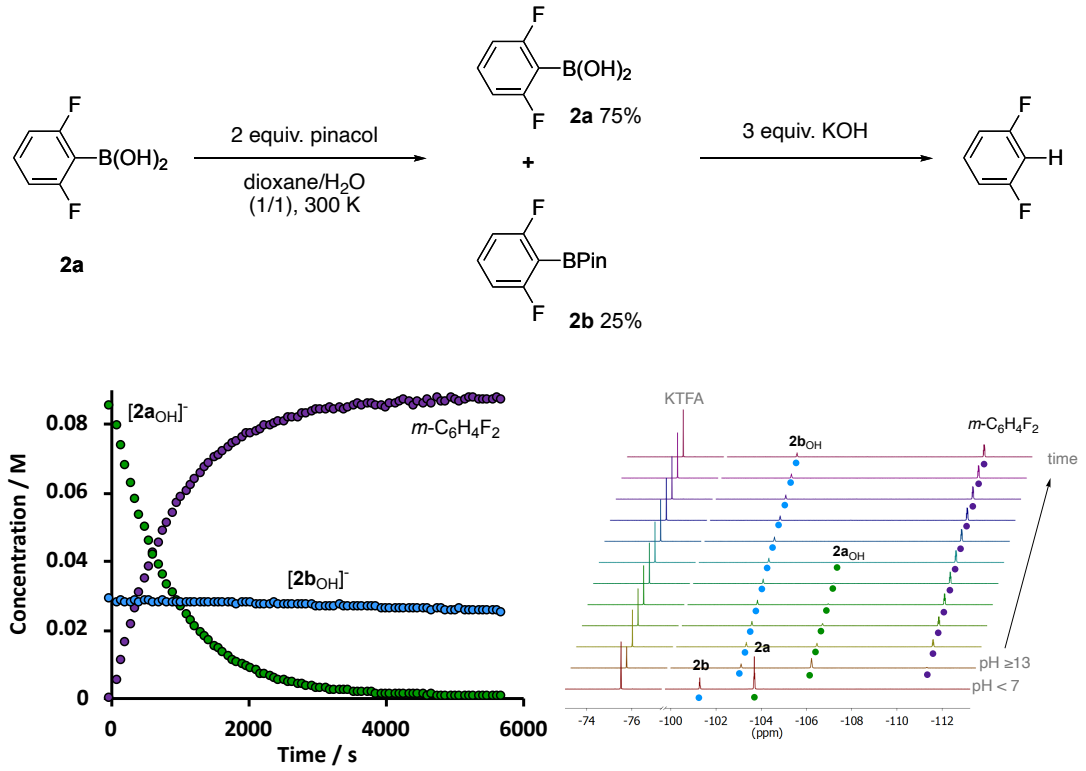

Figure 17. Reaction conditions, temporal-concentration profile and stacked plot of spectra for the protodeboronation, at pH > 13, of 2,6-difluorophenylboronic acid **2a** pre-equilibrated with pinacol.

Temporal concentration profiles differed for the addition of a KOH/pinacol mixture to boronic acid **2a** (Figure 18 A) compared with the addition of KOH to ester **2b** (Figure 18 B). The addition of excess base ensured almost instantaneous and complete conversion to the anionic, tetrahedral boronate species. Negligible (≤1%) [**2b**$_{OH}$]$^-$ or [**2a**$_{OH}$]$^-$ was detected in the respective scenarios, indicative of slow conversion between acid and ester boronates under basic conditions. This observation is in line with the behaviour of [**1b**$_{OH}$]$^-$ at high pH. Kinetic analysis of the pH-rate profile for [**1b**$_{OH}$]$^-$ revealed the absence of base-catalysed hydrolysis of the pinacolate for the 2-fluorophenylboronate system, and hence slow hydrolysis at pH >13. At pH >13, the rate of formation of protodeboronation product (*m*-$C_6H_4F_2$) from pinacolate ester [**2b**$_{OH}$]$^-$ was found to be approximately two orders of magnitude slower than from trihydroxyboronate [**2a**$_{OH}$]$^-$ ($\log_{10}$ k_{BA}/k_{BE} 2.3; $t_{0.5}$ 33 h and 9 min respectively). The rate of protodeboronation of [**2a**$_{OH}$]$^-$/[**2b**$_{OH}$]$^-$ in the presence of pinacol was unaffected by the rate of addition of base.

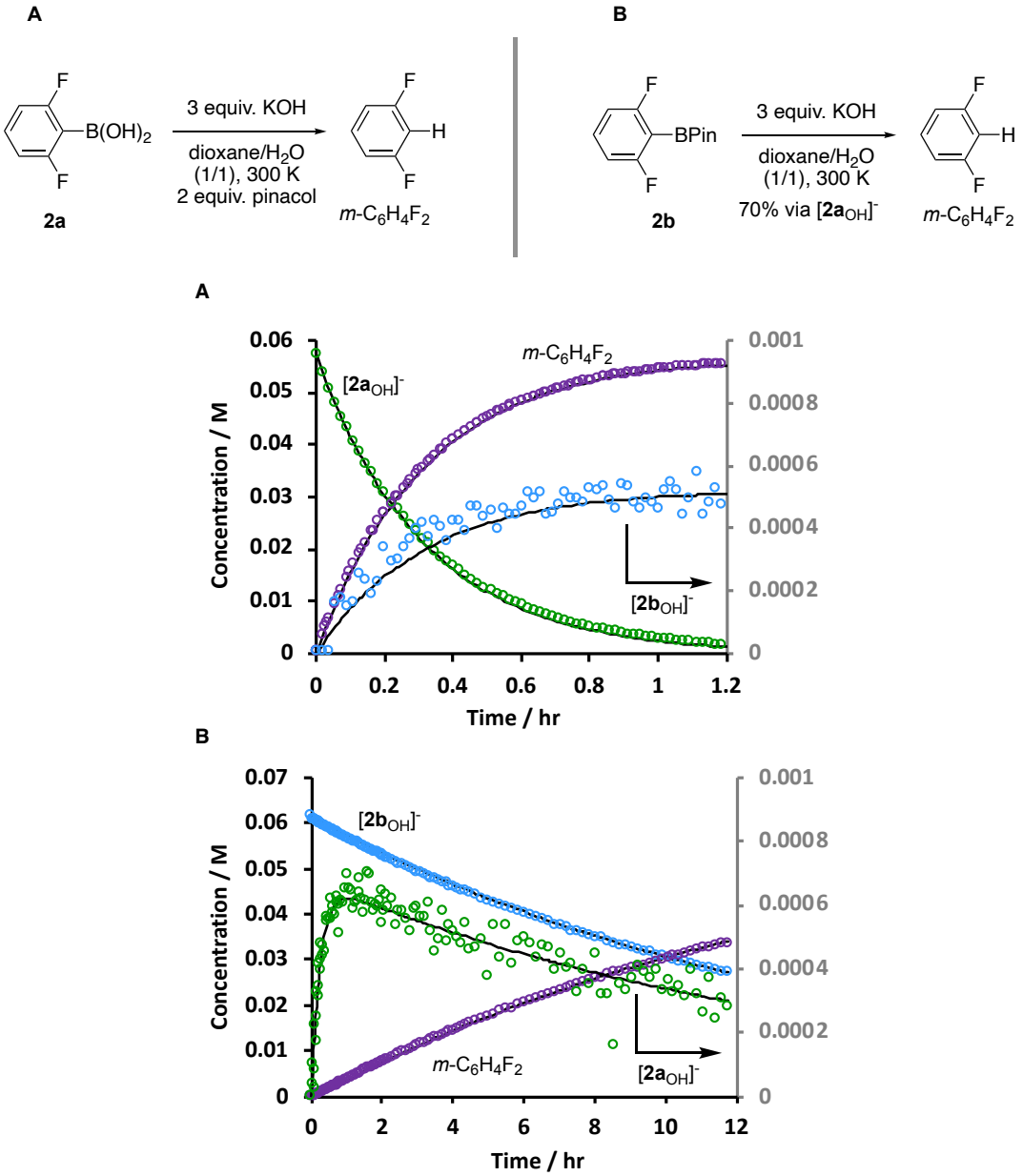

Figure 18. A) Base-catalysed protodeboronation of $[\mathbf{2a}_{OH}]^-$ in the presence of 2 equivalents pinacol and B) of $[\mathbf{2b}_{OH}]^-$, analysed by *in-situ* ^{19}F NMR spectroscopy (data points) and kinetic simulations (solid lines), at pH >13, 300K, in 50% aq. dioxane ($[H_2O]$ = 27.75 M). Arrows on profiles refer to $[\mathbf{2b}_{OH}]^-$ and $[\mathbf{2a}_{OH}]^-$ plotted on a secondary axis in A and B respectively.

At pH >13 (3 equiv. KOH), the rate of formation of product (*m*-$C_6H_4F_2$) for the protodeboronation of **2b** was insensitive to the addition of exogenous pinacol (Figure 19 A). However, when only 0.5 equivalents KOH were utilised, the rate of evolution of protodeboronation product decreased with increasing

equivalents pinacol (Figure 19 B). At this reduced pH, equilibration with [**2a**/**2a**$_{OH}$]$^-$ is faster and protodeboronation can proceed by the *indirect* pre-hydrolytic pathway (k_{BA}). The further addition of pinacol shifted the process in favour of protodeboronation by the *direct* pathway (k_{BE}) due to the greater presence of [**2b**/**2b**$_{OH}$]$^-$.

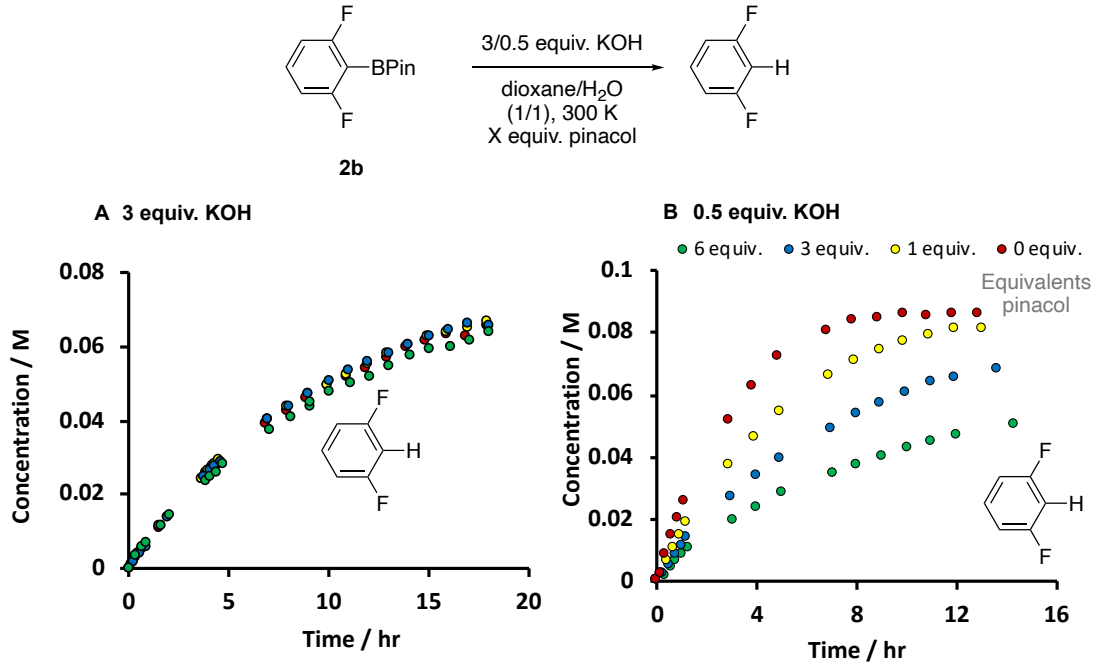

Figure 19. A) Plots of evolution of *m*-$C_6H_4F_2$ overtime for the protodeboronation of **2b**, in the presence of increasing pinacol (0, 1, 3 and 6 equivalents), at pH >13 (3 equiv. KOH) and B) reduced pH (0.5 equiv. KOH).

Kinetic simulations enabled extraction of the rates of the two competing protodeboronation processes for **2b**. At pH >13, arylboronate esters are subject to protodeboronation via two distinct pathways (Scheme 24). Hence, [**2b**$_{OH}$]$^-$ can undergo *direct* protodeboronation to generate product. Alternatively, hydrolysis of [**2b**$_{OH}$]$^-$ can occur and leads to *indirect* protodeboronation from [**2a**$_{OH}$]$^-$.

In order to confirm the relative contributions of both processes; *direct* (k_{BE}) and *indirect* pre-hydrolytic (k_{hyd}, k_{BA}) protodeboronation, an isotopic entrainment experiment[111-112] was performed. Isotopic entrainment involves the addition of

a small quantity of labelled species into a running reaction to induce the flux, in this case of [3,5-D_2-**2b**$_{OH}$]$^-$, through a reaction sequence involving unlabelled reactants. This experiment was used to probe the kinetic behaviour of [**2b**$_{OH}$]$^-$ and the reversibility of formation of species ([**2a**$_{OH}$]$^-$ and protodeboronation product *m*-$C_6H_4F_2$) in the overall process from [**2b**$_{OH}$]$^-$.

[3,5-D_2-**2b**], prepared in 5 steps from the 3,5-difluoroaniline[8] was spiked into an active reaction after 23% net fractional conversion to protodeboronation product *m*-$C_6H_4F_2$ (Figure 20). A rapid isotopic perturbation of the reaction was induced following the manual addition of [3,5-D_2-**2b**], which was immediately converted to the boronate [3,5-D_2-**2b**$_{OH}$]$^-$ *in-situ*.

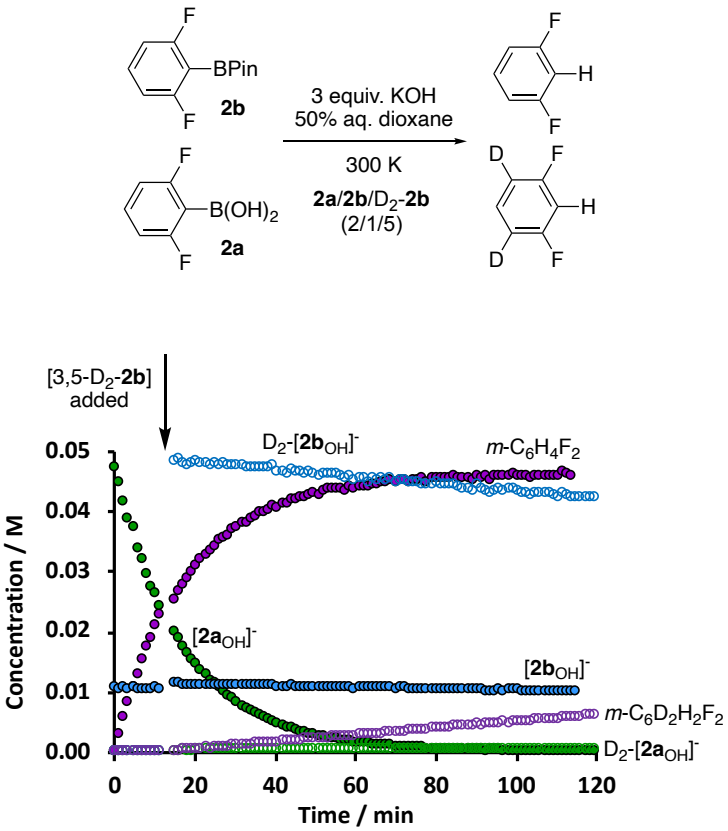

Figure 20. Reaction conditions and temporal concentration profile for isotopic entrainment experiment. Protodeboronation, at pH >13, of a mixture of [**2a**$_{OH}$]$^-$ and [**2b**$_{OH}$]$^-$ (25 mM and 11 mM at time of addition of 50 mM [3,5-D_2-**2b**$_{OH}$]$^-$).

Evolution of the deuterium-labelled species was monitored, taking advantage of the isotope effect on the ^{19}F chemical shift. In all cases, an approximately 0.5 ppm upfield shift was experienced by the deuterium-labelled species, with respect to their non-labelled analogues, in the ^{19}F NMR spectrum (Figure 21).

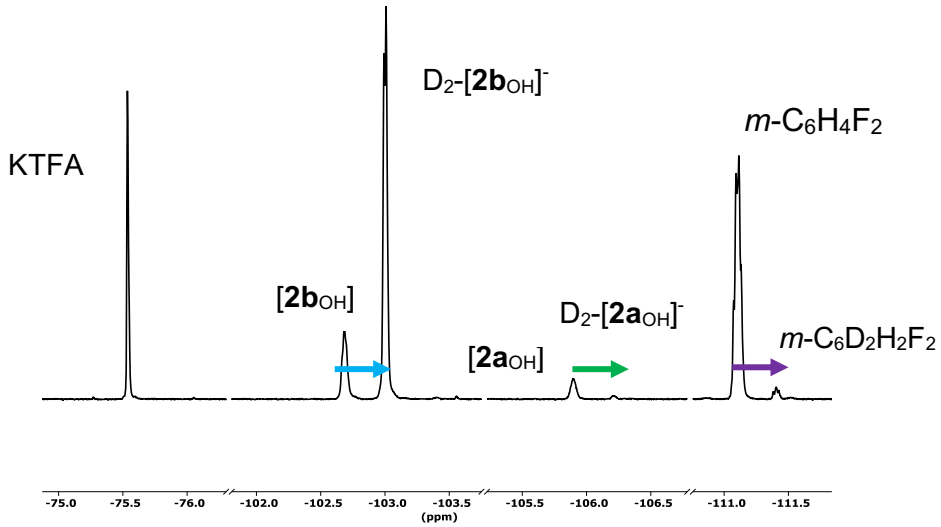

Figure 21. ^{19}F NMR spectrum from isotopic entrainment experiment at t = 46 min; -75.5 IS (KTFA), -102.6 ([**2b**$_{OH}$]$^-$), -102.9 (D$_2$-[**2b**$_{OH}$]$^-$), -105.8 ([**2a**$_{OH}$]$^-$), -106.2 (D$_2$-[**2a**$_{OH}$]$^-$), -111.0 (*m*-C$_6$H$_4$F$_2$) and -111.4 (4,6-D$_2$-*m*-C$_6$D$_2$H$_2$F$_2$).

Analysis of the isotope ratios as a function of reaction progress (indicated as % conversion of substrate), with the aid of kinetic simulations, enabled evaluation of the mechanistic pathway for the protodeboronation of [**2b**$_{OH}$]$^-$. The presence of [3,5-D$_2$-**2a**$_{OH}$]$^-$ and 4,6-D$_2$-*m*-C$_6$H$_4$F$_2$ were detected during the reaction by ^{19}F NMR spectroscopy, confirming the potential for a hydrolysis-protodeboronation sequence. Substantial accumulation of [3,5-D$_2$-**2a**$_{OH}$]$^-$ was not observed since [**2a**$_{OH}$]$^-$ is the significantly more reactive species towards protodeboronation. The rate of liberation of *m*-C$_6$H$_4$F$_2$ was previously established to be 50 times faster from trihydroxyboronate [**2a**$_{OH}$]$^-$ at pH >13, in 50% aq. dioxane, compared with the pinacolate ester [**2b**$_{OH}$]$^-$ (Figure 18).

Analysis of the deuterium fraction in each component by ^{19}F NMR spectroscopy revealed the dominant flux to be by the following sequence: [3,5-D$_2$-**2b**$_{OH}$]$^-$ → [3,5-D$_2$-**2a**$_{OH}$]$^-$ → 4,6-D$_2$-*m*-C$_6$H$_4$F$_2$ (Figure 22). 81% D$_2$-incorporation was retained by [**2b**$_{OH}$]$^-$ and approached by [**2a**$_{OH}$]$^-$. This

stipulated [**2a**$_{OH}$]$^-$ to be a genuinely productive intermediate from the pinacolate ester [**2b**$_{OH}$]$^-$ and is a result of negligible esterification (k_{est}) and rapid protodeboronation ($t_{0.5}$ = 9 min) of [**2a**$_{OH}$]$^-$. An increase in the deuterium content (%) in protodeboronation product *m*-$C_6H_4F_2$ was observed, but the rate of rise of isotope incorporation into the product was attenuated to some extent since it is dependent on the intermediate [**2a**$_{OH}$]$^-$. The kinetic model confirmed the potential for *indirect* protodeboronation of [**2b**$_{OH}$]$^-$ via a hydrolysis-protodeboronation sequence (k_{hyd}, k_{BA}) as the predominant pathway (70%). The pinacolate ester [**2b**$_{OH}$]$^-$ was shown to be two orders of magnitude more stable than the corresponding acid boronate [**2a**$_{OH}$]$^-$ at pH >13 ($\log_{10}$ $k_{rel\ PDB}$ 2.3). However, the potential for hydrolysis of [**2b**$_{OH}$]$^-$ (k_{hyd}) and the subsequent fast protodeboronation of [**2a**$_{OH}$]$^-$ (k_{BA}) leads to the *phenomenological* stability of [**2b**$_{OH}$]$^-$ being lessened relative to that predicted by k_{BE} only. The half-life for protodeboronation of [**2b**$_{OH}$]$^-$ at high pH, taking into consideration the hydrolytic equilibrium with [**2a**$_{OH}$]$^-$, is 10 h (k_{BE} and k_{hyd} combined).

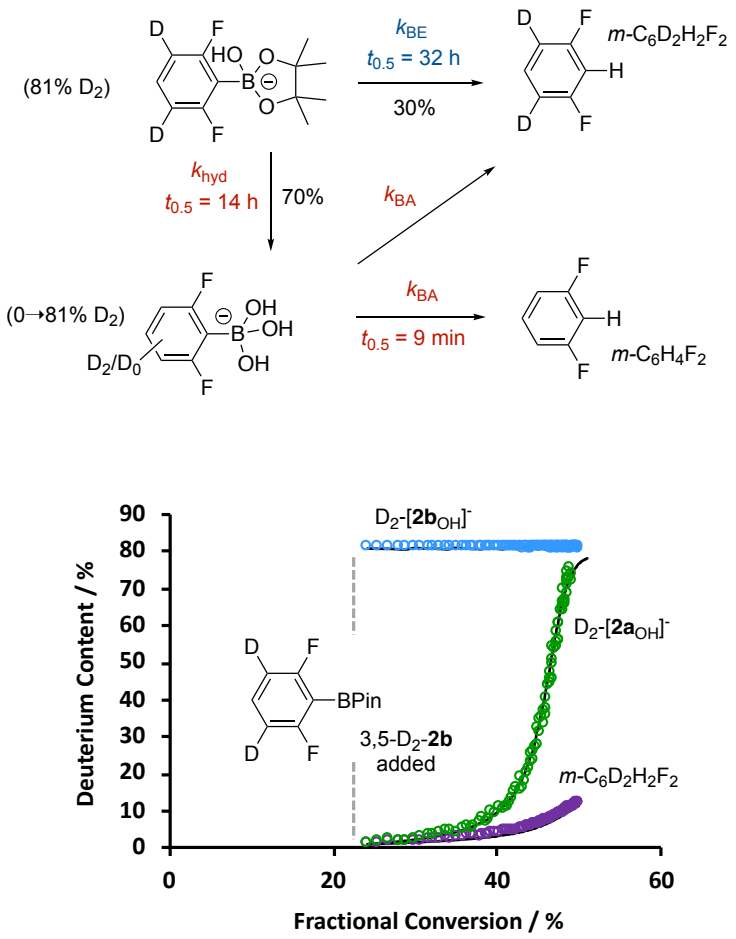

Figure 22. Pathways for protodeboronation of $[\mathbf{2b}_{OH}]^-$ evaluated by isotope entrainment. $[\mathbf{2a}_{OH}]^-_0$ 50 mM, $[pinacol]_0$ 99 mM, $[\mathbf{2b}_{OH}]^-_0$ 10 mM; then [3,5-D_2-**2b**] (50 mM) added after 23% net fractional conversion; simulation (solid lines through data) confirmed the dominant sequence to be [3,5-D_2-$\mathbf{2b}_{OH}$] → [3,5-D_2-$\mathbf{2a}_{OH}$] → 4,6-D_2-*m*-$C_6H_4F_2$. Approx. 5% of *m*-$C_6H_4F_2$ amd 4,6-D_2-*m*-$C_6D_2H_2F_2$ phase-separated from the 50% aq. dioxane during the reaction; product concentrations were corrected for this.

Computations were performed by collaborators Dr Andrew Leach and Michele Assante to probe the difference in behaviour between the 2,6-difluorophenyl and 2-fluorophenyl pinacol esters, in terms of hydrolysis versus protodeboronation. All calculations were performed at the M06L/6-311++** level in Gaussian09. A dissociative process for the hydrolysis (Scheme 29) revealed similar behaviour for both boronate ester systems **2b** and **1b**, despite gross differences in reactivity to protodeboronation. Transition states weren't identified for direct S_N2 or addition of water at the ester boronate center. The relative free energies in *k*cal/mol for the pinacol esters of 2,6-difluorophenylboronic acid and 2-fluorophenylboronic acid (**2b** and **1b**), for

water-mediated step 1 and 2 transition states were 27.6/28.0 (**2b**/**1b**), and 32.2/31.1 (**2b**/**1b**) for the respective steps.

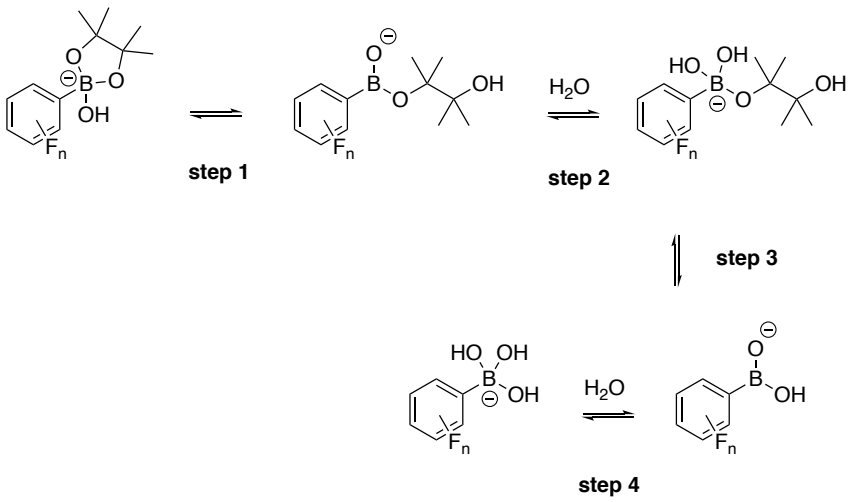

Scheme 29. Dissociative process for the hydrolysis of fluorinated pinacol boronate esters.

The identity, strength and concentration of the base employed in reactions involving aryl B-Pin reagents, conducted in basic *aq.*-organic media, for example the Suzuki-Miyaura cross-coupling,[18] can impact the behaviour of the boronate. Thus, the influence of both K_2CO_3 and NEt_3, compared with KOH, was explored for the protodeboronation of [**2b**$_{OH}$]$^-$. Conditions were as per Figure 18 A, and a mixture of base (3 equiv.)/pinacol was added to **2a** to initiate the reaction. At pH 11, when K_2CO_3 was utilised, equilibration of [**2a**$_{OH}$]$^-$ with [**2b**$_{OH}$]$^-$ was rapid (via k_{SA} and k_{H2O}) and overall protodeboronation proceeded with a half-life of 20 minutes (Figure 23 A). Contribution of self/auto-catalysis (k_{SA}) under these conditions is comparable with the significant acceleration of the hydrolysis of [**1b**/**1b**$_{OH}$]$^-$ evident from the pH-rate profile when the pH is close to the pK_a. At pH 10, when NEt_3 was utilised, rapid equilibration of [**2a**$_{OH}$]$^-$ with [**2b**$_{OH}$]$^-$ was also observed. The rate of protodeboronation was reduced ($t_{0.5}$ = 40 min) because the mol-fraction of boronate [**2a**$_{OH}$]$^-$ was lower at this pH (Figure 23 B).

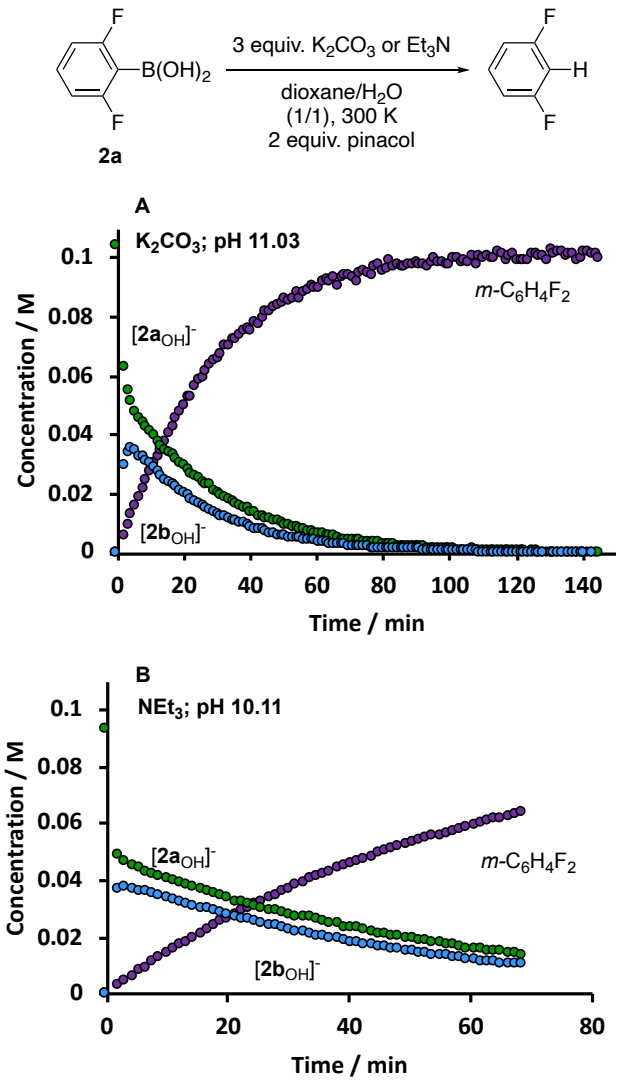

Figure 23. A) Base-catalysed protodeboronation of $[\mathbf{2a}_{OH}]^-$/$[\mathbf{2b}_{OH}]^-$ analysed by *in-situ* ^{19}F NMR spectroscopy, at pH 11.03, and B) pH 10.11, 300K, in 50% aq. dioxane ($[H_2O]$ = 27.75 M). Base was added as a pre-mixed solution with pinacol to intiate the reaction.

Previous work found the initial rates (k_{obs}/s^{-1}) of protodeboronation for 2,6-difluorophenylboronic acid **2a**, with varying equivalents of hydroxide, to reach saturation following the addition of 1 equivalent KOH.[8] The effect of increasing equivalents of hydroxide on the initial rates (s^{-1}) for the protodeboronation of **2a** in the presence of pinacol was probed. The same plateau in rate beyond 1 equivalent KOH was not observed in this case (Figure 24) due to the impact of hydrolysis of pinacol ester $[\mathbf{2b}_{OH}]^-$ catalysed by hydroxide, and subsequent protodeboronation of boronic acid $[\mathbf{2a}_{OH}]^-$.

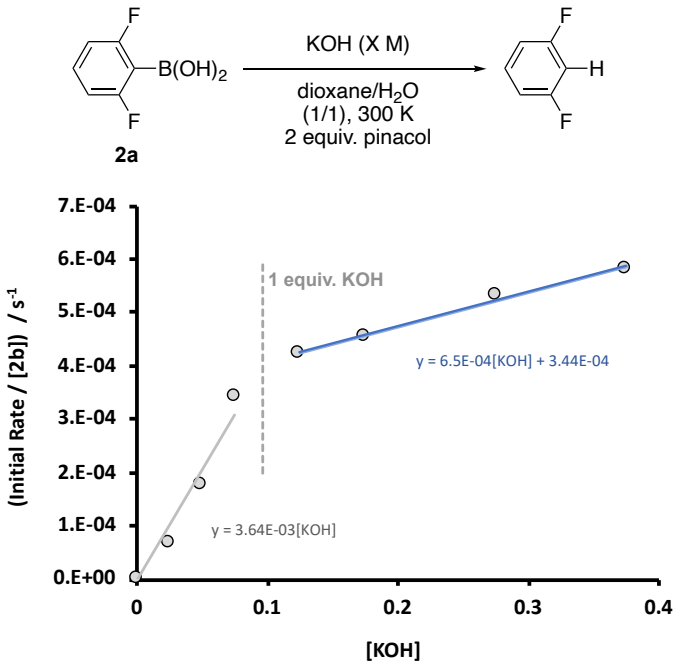

Figure 24. Reaction conditions for the protodeboronation of **2a** in the presence of pinacol and graphical analysis of initial rates (k_{obs}/s^{-1}) versus [KOH].

2.1.6 Summary and general trends for pinacol esters

Following the extensive mechanistic analysis of [**2b**$_{OH}$]$^-$, the impact of esterification by the ubiquitous pinacol moiety was further probed for a series of (hetero)aromatic systems **1a**-**9a** and **10a**. These included five polyfluorinated aryl examples and four heteroaromatic systems; thiazolyl, pyrazolyl, isoxazolyl and pyridyl (Table 3).

Table 3. Kinetics of overall protodeboronation (k_{BE} and k_{BA}) and hydrolysis (k_{hyd}) of (hetero)aryl pinacol ester boronates **1b**-**9b** at 300 K, in 50% aq. dioxane, at pH >13 and pinacol ester **10b** at pH 7.

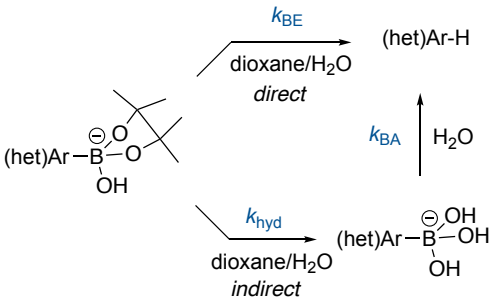

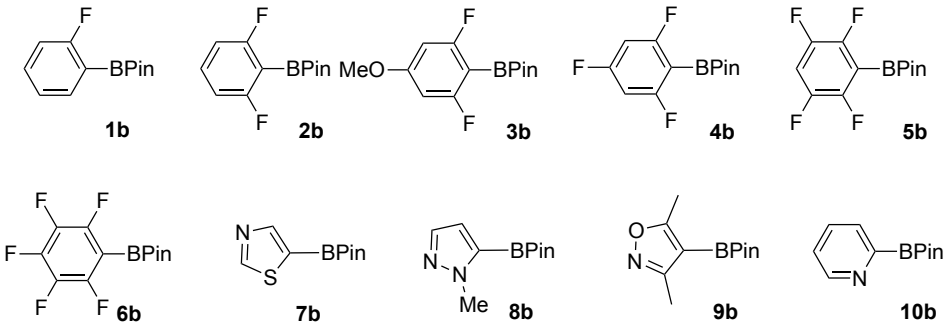

	Pinacol boronate	k_{BA} $t_{0.5}$	k_{BE} $t_{0.5}$	log k_{rel} PDB (k_{BA}/k_{BE})	k_{hyd} $t_{0.5}$	pK_{hyd}
1	2-Fluorophenyl[**1b**$_{OH}$]$^-$	--[a]	--[a]	--[a]	9.4 h	1.2
2	2,6-Difluorophenyl [**2b**$_{OH}$]$^-$	9.2 min	33.0 h	2.3	14.1 h	0.4
3	2,6-Difluoro-4-anisyl [**3b**$_{OH}$]$^-$	19.2 min	33.4 h	2.0	13.7 h	0.4
4	2,4,6-Trifluorophenyl [**4b**$_{OH}$]$^-$	3.9 min	5.5 h[b]	1.9	--[b]	--[b]
5	2,3,5,6-Tetrafluorophenyl [**5b**$_{OH}$]$^-$	1.1 s	2.3 min	2.1	--[c]	--[c]
6	2,3,4,5,6-Pentafluorophenyl [**6b**$_{OH}$]$^-$	0.1 s[d]	10.7 s	2.0	--[c]	--[c]
7	5-Thiazolyl [**7b**$_{OH}$]$^-$	4.6 h	7.3 d	1.6	3.6 d	≤2.5
8	1-Me-1H-5-pyrazolyl [**8b**$_{OH}$]$^-$	21.1 d	1.7 y	1.5	29.0 h	1.3
9	3,5-Dimethylisoxazolyl [**9b**$_{OH}$]$^-$	78.7 d	>5 y[e]	≥1.9[e]	8.0 h	1.4
10	2-Pyridyl [**10b**$_{H,OH}$]	2.4 h[f]	1.4 h[f]	–0.2[f]	3.9 min[f]	2.8[f]

[a]Protodeboronation product, C_6H_5F undetected. [b]*Direct* protodeboronation (k_{BE}) ≥98.5% and maximum 0.05% [**4a**$_{OH}$]$^-$ detected. [c]Rate of hydrolysis (k_{hyd}) and K_{hyd} not determined; k_{BE} > k_{hyd}. [d]Value previously determined and reported.[113] [e]Kinetic simulations utilised to estimate lower limits. [f]Rate coefficients for **10b** were determined at neutral pH. The dominant speciation, at neutral pH, is zwitterionic [**10**$_{H,OH}$] and at pH >13, k_{BA} [**10a**$_{OH}$]$^-$ $t_{0.5}$ = 35 h.

The rate of protodeboronation of each boronic acid was independently determined, i.e. in the absence of pinacol, at pH >13 for **1a**-**9a** and at neutral pH for **10a**. Reactions for **1a**-**9a** were initiated, in 50% aq. dioxane at 27 ºC, by the addition of excess base to ensure the instantaneous and quantitative conversion to the boronate form. The (pseudo) first order decay of boronic acid boronate (B_{OH}) is pH-dependent and the rate constant for protodeboronation (k_{BA}/s^{-1}) can be extracted by plotting $\ln([B_{OH}]_0/[B_{OH}]_t)$ versus time. Kinetic simulations of temporal concentration profiles for the protodeboronation at pH >13 of pinacolate esters **1b-9b** enabled extraction of rate coefficients, which were compared against the rate of protodeboronation (k_{BA}) for the corresponding trihydroxyboronates **1a-9a**. In the case of **10a** and **10b**, the addition of an acetic acid buffer ensured a neutral pH of approximately 7 was maintained over the course of the reaction. Half-lives ($t_{0.5}$), are based on protodeboronation proceeding exclusively by the *direct* pathway (k_{BE}), or by irreversible hydrolysis (k_{hyd}), reported in Table 3. However, the phenomenological stability of the boronic esters studied depends on the rate and equilibria (k_{hyd}, K_{hyd}) of *indirect* protodeboronation (k_{BA}).

Esterification by pinacol attenuated the rate of *direct* protodeboronation (k_{BE}) by approximately two orders of magnitude ($\log_{10}$ k_{BA}/k_{BE} 1.9 ±0.4) across all (hetero)aryl substrates studied at pH >13 (**2b-9b**). The stability imparted arises from the four methyl groups in pinacol which can sterically shield the O and B centres and therefore hinder the attack of water, but do not cause significant steric strain between the pinacol group and aryl ring. Compared to the span of rates observed for protodeboronation (k_{BA} and k_{BE}, Table 1), the rate of ester hydrolysis (k_{hyd}) proved relatively insensitive to the identity of the heteroaromatic and aromatic ring ($t_{0.5}$ = 8 h to 4 d), and stabilisation imparted by pinacol esterification was most pronounced in the reactive polyfluorophenyl systems (entries 4-6).

While the rate of *direct* protodeboronation (k_{BE}) and hydrolysis (k_{hyd}) for (hetero)aryl pinacol ester boronates **2b-9b** was probed at pH >13, the 2-pyridyl

pinacol ester was tested at pH 7. The protodeboronation of 2-pyridylboronic acid **10a** was monitored under neutral conditions as it has previously been reported to be most reactive when the zwitterionic boronate complex [$\mathbf{10}_{H,OH}$] is dominant at pH 7. This is in contrast to boronic acids **2a-9a**, including polyfluorophenyl and non-basic heteroaromatic substrates pyrazolyl, thiazolyl and isoxazolyl, which are most reactive under basic conditions.[8, 109] The half-life of protodeboronation for 2-pyridylboronic acid [$\mathbf{10a}_{OH}$]$^-$ was measured at pH >13 ($t_{0.5}$ = 35 h) by ^{1}H NMR spectroscopy.

At neutral pH, zwitterionic speciation is favourable for pinacol ester **10b** and neighbouring-group interaction arises between the 2-pyridinium proton and boronate oxygen. From DFT computations by collaborators Dr Andrew Leach and Michele Assante, this neighbouring-group participation by the 2-pyridinium proton is likely responsible for the accelerated rate of both hydrolysis (k_{hyd} $t_{0.5}$ = 4 min) and protodeboronation ($t_{0.5}$ = 1.4 h; $\log_{10}k_{rel\ PDB}$ (k_{BA}/k_{BE}) = -0.2) observed in contrast to the other (hetero)aryl pinacol esters studied (Figure 25).

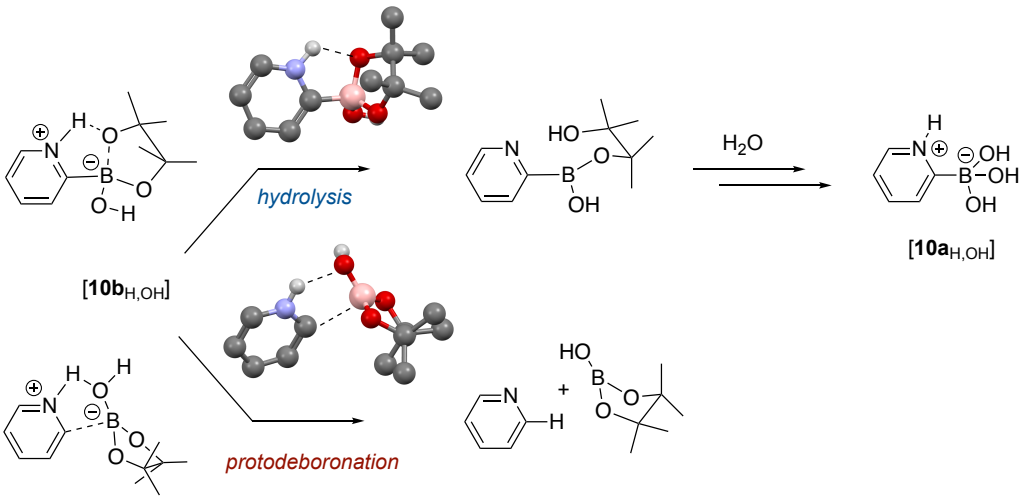

Figure 25. Hydrolysis and protodeboronation at neutral pH of zwitterionic [$\mathbf{10b}_{H,OH}$], with neighbouring-group participation by the 2-pyridinium proton. Transition state (TS) structures calculated by DFT (*k*cal mol^{-1}; M06L/6-311+G**).

2.2 Effect of ester identity

2.2.1 Summary and general trends for 2,6-difluorophenylboronic esters

Esterification by pinacol suppressed *direct* protodeboronation by approximately two orders of magnitude across the series of (hetero)aryl systems studied. Following on from these investigations, the kinetics and mechanism of base-catalysed protodeboronation for boronic esters, encompassing eight different polyols including simple diols and a triol, was probed. 2,6-Difluorophenylboronic acid **2a** proved to be an ideal system for these investigations and the series was explored by means of reaction monitoring utilising both *in-situ* and stopped-flow ^{19}F NMR spectroscopy. As per the pinacol esters, rate coefficients were extracted by kinetic simulations of concentration-time plots and half-lives ($t_{0.5}$) calculated were based on the *direct* protodeboronation (k_{BE}) of boronic esters and irreversible hydrolysis (k_{hyd}). The influence of an extensive range of polyols explored for **2a** revealed an unexpectedly expansive scale of overall rates, with half-lives spanning four orders of magnitude, for the protodeboronation of boronic esters at high pH (Table 4).

Table 4. Kinetics of overall protodeboronation (k_{BE} and k_{BA}) and hydrolysis (k_{hyd}) of 2,6-difluorophenylboronates **2a-2i** and **1i** at 300 K, in 50% aq. dioxane, at pH >13.

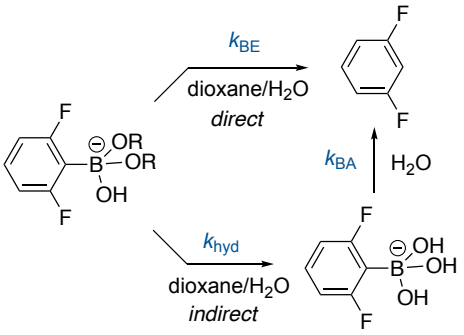

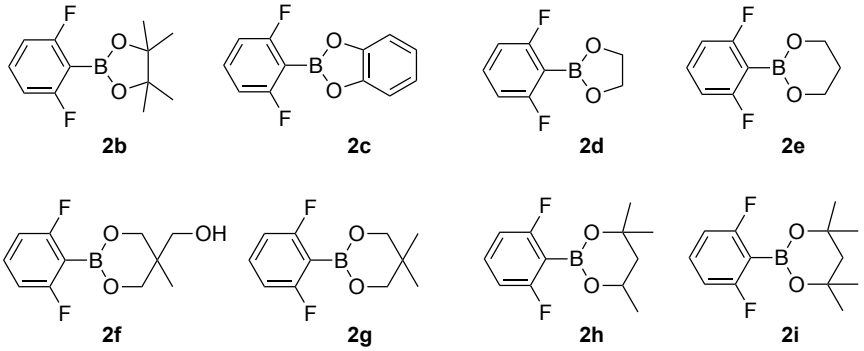

	Acid / Ester boronate	k_{PDB} $t_{0.5}$	$\log_{10} k_{rel}^{PDB}$ (k_{BA}/k_{BE})	k_{hyd} $t_{0.5}$	pK_{hyd}
1	Trihydroxyboronate [**2a**$_{OH}$]$^-$	9.2 min	--	--	
2	Pinacol ester [**2b**$_{OH}$]$^-$	33.0 h.	2.3	14.1 h	0.4
3	Catechol ester [**2c**$_{OH}$]$^-$	30.1 h[a]	2.3	≤1 s[b]	1.5
4	Ethylene glycol ester [**2d**$_{OH}$]$^-$	≥3.9 h	≥1.4	11 s	0.7
5	1,3-Propanediol ester [**2e**$_{OH}$]$^-$	15.0 min	0.2	4.4 s	0.4
6[c]	2-Hydroxymethyl-2-methyl-1,3-propanediol ester [**2f**$_{OH}$]$^-$	12.6 min	0.1	51.3 s	1.4
7	Neopentylglycol ester [**2g**$_{OH}$]$^-$	2.4 min	–0.6	12.9 s	0.3
8[d]	2-Methylpentan-2,4-diol ester [**2h**$_{OH}$]$^-$	23.1 s	–1.4	8.6 s	--[f]
9	2,4-Dimethylpentan-2,4-diol ester [**2i**$_{OH}$]$^-$	7.7 s	–1.9	3.4 min	--[f]
10[f]	2,4-Dimethylpentan-2,4-diol ester[d] [**1i**$_{OH}$]$^-$	--[g]	--[g]	2.5 min	−0.7

[a]Determined in the presence of 1.3 equiv. KOH and excess catechol to reduce excess hydroxide. The $t_{0.5}$ may be underestimated due to the impact of k_{OH} on k_{hyd}. [b]Determined at pH >13 where k_{OH} dominates k_{hyd}. [c][**2f**$_{OH}$]$^-$ is present as an equilibrium mixture of diastereoisomers (relative abundance (%): 45/25/35). [d][**2h**$_{OH}$]$^-$ is present as an equilibrium mixture of diastereoisomers (relative abundance (%): 81/19). [f]K_{hyd} not determined. [g][**1i**$_{OH}$]$^-$ is the mono *ortho*-fluoro isomer of [**2i**$_{OH}$]$^-$. Protodeboronation product, $C_6H_5F_1$ undetected.

Contrary to common assumption, greater stability is not necessarily imparted by esterification of boronic acids. Both pinacol [**2b**$_{OH}$]$^-$ and catechol [**2c**$_{OH}$]$^-$ esters exhibited rates of *direct* protodeboronation approximately two orders of magnitude slower than the corresponding trihydroxyboronate [**2a**$_{OH}$]$^-$ compared with the 2,4-dimethylpentan-2,4-diol ester [**2i**$_{OH}$]$^-$ which underwent *direct* protodeboronation at a rate approximately two orders of magnitude faster. The half-life for protodeboronation ($t_{0.5}$) can be considered on a scale relative to that of 9 minutes for [**2a**$_{OH}$]$^-$, with a substantially longer half-life for [**2b**$_{OH}$]$^-$ and [**2c**$_{OH}$]$^-$ ($t_{0.5}$ = 33.0 h and ≥30.1 h respectively) and only 7.7 seconds for [**2i**$_{OH}$]$^-$.

Influence of counter-cation (M^+) identity

Previous studies on the kinetics of protodeboronation of arylboronic acids in 50% aq. dioxane at 70 ºC, found the identity of the counter-cation (M^+) to influence the rate of protodeboronation only slightly.[8] The counter-cations investigated included Li^+, K^+ and Bu_4N^+ for boronate [**2a**$_{OH}$]$^-$. The impact of the same counter-cations on the rate of protodeboronation was probed at 27 ºC in this study, revealing analogous trends for [**2a**$_{OH}$]$^-M^+$ (k_{BA}) and for the *direct* protodeboronation of 2,4-dimethyl-2,4-pentandiol ester boronate [**2i**$_{OH}$]$^-M^+$ (k_{BE}). The rates of hydrolysis for [**2i**$_{OH}$]$^-M^+$ (k'_{hyd}) were measured and found to be accelerated for M^+ = Li^+, Bu_4N^+ relative to K^+, albeit only slightly (Table 5).

Table 5. Relative rates of prodeboronation for [**2a**$_{OH}$]$^-M^+$ (k_{BA}; previous work at 70 ºC and current study at 27 ºC) and [**2i**$_{OH}$]$^-M^+$ (k_{BE}), and hydrolysis (k_{hyd}) for [**2i**$_{OH}$]$^-M^+$.

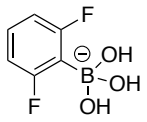

[**2a**$_{OH}$]$^-$

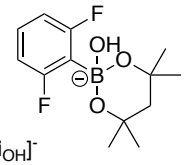

[**2i**$_{OH}$]$^-$

M^+	[**2a**$_{OH}$]$^-M^+$		[**2i**$_{OH}$]$^-M^+$	
	k_{BA} (70 ºC[8])	k_{BA} (27 ºC)	k_{BE} (27 ºC)	k'_{hyd} (27 ºC)
Li^+	0.66	0.44	0.50	1.7
K^+	1.0	1.0	1.0	1.0
Bu_4N^+	0.98	0.82	0.84	1.1

Hydrolysis of boronic esters: Ring size and degree of substitution

The susceptibility of boronic esters **2b-2i** towards hydrolysis (k_{hyd}) impacted the kinetics of overall protodeboronation which includes the *indirect* pre-hydrolytic (k_{hyd}, k_{BA}) pathway in addition to *direct* protodeboronation (k_{BE}). The ring size, degree of substitution and steric impact influences the extent of hydrolysis experienced by **2b-2i**.

A range of both 5- and 6-membered ring boronic esters, including the (hetero)aryl pinacol boronates, were studied which exhibit half-lives for hydrolysis spanning 1 seconds to 3.7 days at high pH. For similarly simple ring systems, Musgrave and Bowie found 5-membered ring esters to hydrolyse more rapidly than their 6-membered homologues, under neutral conditions.[11] Greater angle strain is experienced by 5-membered ring systems, and this accounts for the increased rate of attack by water at the trigonal boron centre during hydrolysis. This general trend, established in the 1960s, was shown in this work to be reversed at high pH. The 6-membered ring esters, studied in this body of work, were found to undergo hydrolysis under basic conditions more quickly than the 5-membered ring esters. The relative rates of hydrolysis (k_{hyd}) and protodeboronation (k_{BE}) for 5- versus 6-membered ring esters under neutral and basic conditions are highlighted in Scheme 30.

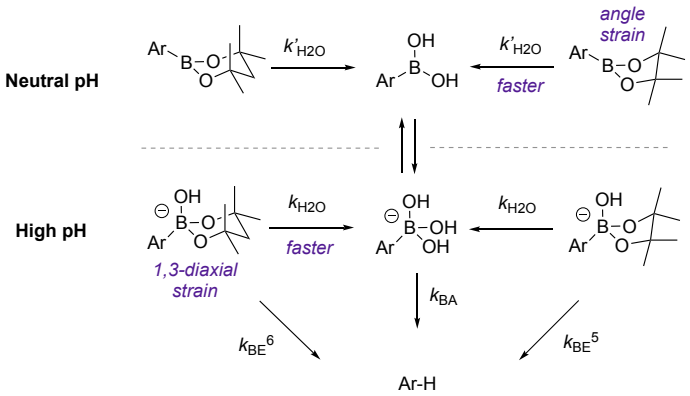

Scheme 30. Relative rates of hydrolysis (k_{hyd}) and protodeboronation (k_{BE}) under neutral and basic conditions for for 6-membered ring, 2,4-dimethylpentan-2,4-diol arylboronate esters versus 5-membered ring, pinacol arylboronate esters.

For example, the hydrolysis of 1,3-propanediol ester $[\mathbf{2g}_{OH}]^-$ proceeds with a half-life of 4.4 seconds in contrast to ethylene glycol ester $[\mathbf{2d}_{OH}]^-$ which undergoes hydrolysis slower ($t_{0.5}$ = 11 s). The angle strain experienced by 5-membered rings in the neutral, trigonal form is relieved upon conversion to the boronate. This, in addition to 1,3-diaxial strain experienced by 6-membered rings in the anionic, tetrahedral form, is reflected in the quicker hydrolysis of 6-membered ring esters at high pH.

The temporal concentration profile elucidated by ^{19}F stopped-flow NMR spectroscopy, in addition to kinetic simulations (Figure 26), revealed the 6-membered ring ester $[\mathbf{2g}_{OH}]^-$ to exhibit rapid hydrolysis (k_{hyd} = 12.9 s) at high pH. The neopentyl glycol ester was found to be more reactive towards protodeboronation than the corresponding trihydroxyboronate $[\mathbf{2a}_{OH}]^-$ ($t_{0.5}$ = 2.4 min versus 9 min respectively).

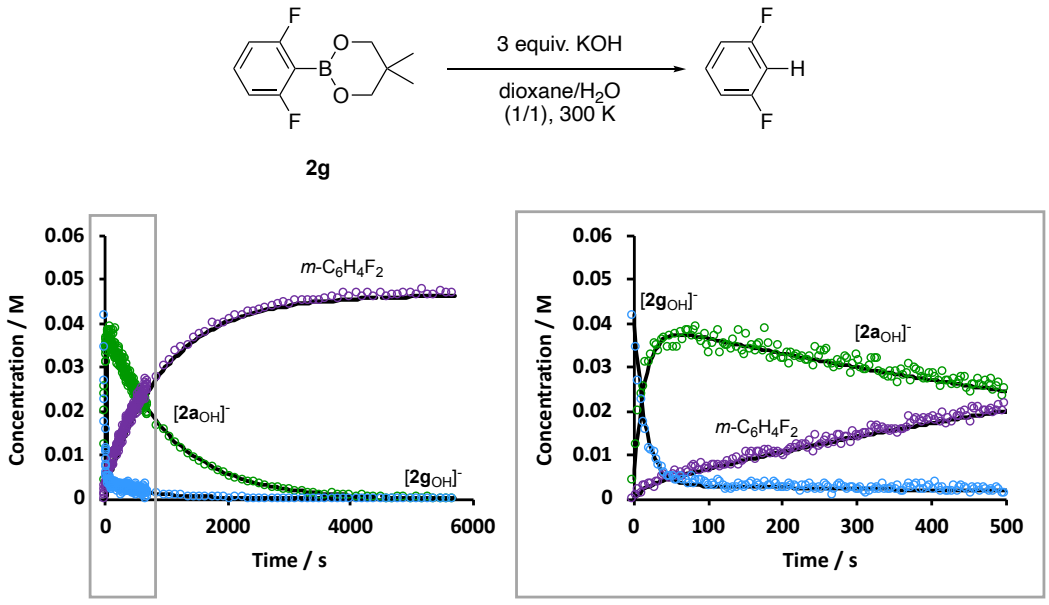

Figure 26. Kinetic analysis for the hydrolysis and protodeboronation of $[\mathbf{2g}_{OH}]^-$ at high pH.

With increasing substitution on the ring, formed by chelation of the boron centre by the diolate, the rate of hydrolysis (k_{hyd}) is attenuated in both 5- and 6-membered ring esters, while the rate of *direct* protodeboronation (k_{BE}) rises for the 6-membered ring systems. The influence of increasing substitution on

5-membered ring systems was probed by comparing the half-lives for hydrolysis of ethylene glycol ester $[\mathbf{2d}_{OH}]^-$ versus pinacol ester $[\mathbf{2b}_{OH}]^-$ ($t_{0.5}$ = 11 s and 14.1 h respectively). The 6-membered, 2-methylpentan-2,4-diol ester $[\mathbf{2h}_{OH}]^-$ is differentiated from 2,4-dimethylpentan-2,4-diol ester $[\mathbf{2i}_{OH}]^-$ by one additional methyl group on the ring of the latter ester ($t_{0.5}$ = 8.6 s and 3.4 min respectively). This increased steric crowding for $[\mathbf{2i}_{OH}]^-$ hinders the attack of water during hydrolysis to a greater degree than for $[\mathbf{2h}_{OH}]^-$. The difference in the degree of substitution between these substrates results in $k_{BE} > k_{hyd}$ for $[\mathbf{2i}_{OH}]^-$ in comparison with $k_{hyd} > k_{BE}$ for $[\mathbf{2h}_{OH}]^-$ (Figure 27).

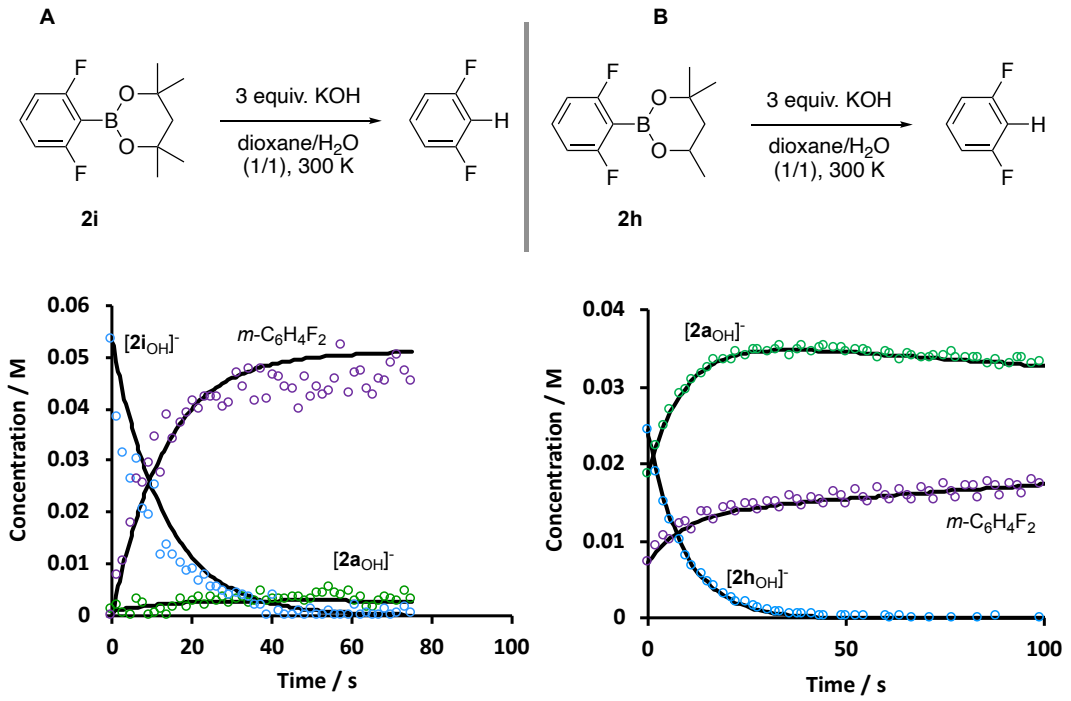

Figure 27. A) Kinetic analysis for the hydrolysis and protodeboronation of $[\mathbf{2i}_{OH}]^-$ compared with B) $[\mathbf{2h}_{OH}]^-$ at high pH.

Catechol ester 2e

The overall protodeboronation reaction for catechol ester $[\mathbf{2c}_{OH}]^-$ can be considered, as per the other esters studied, a function of two distinct, contributary pathways; *direct* (k_{BE}) and *indirect* pre-hydrolytic (k_{BA}) protodeboronation (Scheme 31). $[\mathbf{2c}_{OH}]^-$ undergoes very slow *direct* protodeboronation (k_{BE}), approximately two orders of magnitude slower than

the corresponding boronic acid [**2a**$_{OH}$]$^-$. Acceleration of the overall rate of protodeboronation is dictated by the liberation of [**2a**$_{OH}$]$^-$, and the rate of ester hydrolysis is dependent on the availability of hydroxide (k_{OH} versus k_{H2O}). Deconvolution of both *direct* and *indirect* processes in addition to probing the pH-dependent, pre-hydrolytic pathway was key to understanding the influence of esterification by catechol.

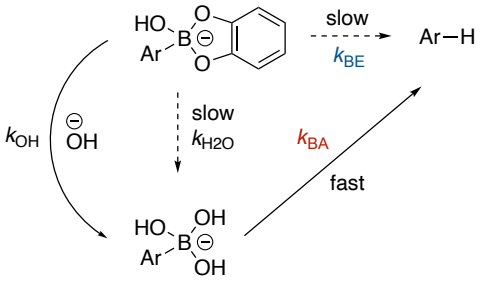

Scheme 31. *Direct* (k_{BE}) and *indirect* pre-hydrolytic (k_{BA}) protodeboronation of a catechol ester.

In the absence of excess hydroxide, [**2c**$_{OH}$]$^-$ undergoes very slow hydrolysis (k_{H2O}; $t_{0.5}$ ≥ 30 h). However, as the pH is raised and in contrast to the other esters studied, the catecholate ester becomes subject to substantial specific base-catalysis by hydroxide (k_{OH}) (Scheme 32). At pH >13, where k_{OH} dominates k_{H2O}, $t_{0.5}$ ≤ 1 s. The formation of a semi-liberated phenolate anion (partially attached by a single B-O bond), and subsequent liberation of a stable, free phenolate, acts as the thermodynamic driving force and facilitates the base-catalysed dissociative hydrolysis of [**2c**$_{OH}$]$^-$. The catechol boronate [**2c**$_{OH}$]$^-$ is therefore an exception to the general trends observed for the hydrolysis of esters of 2,6-difluorophenylboronic acid (Scheme 29).

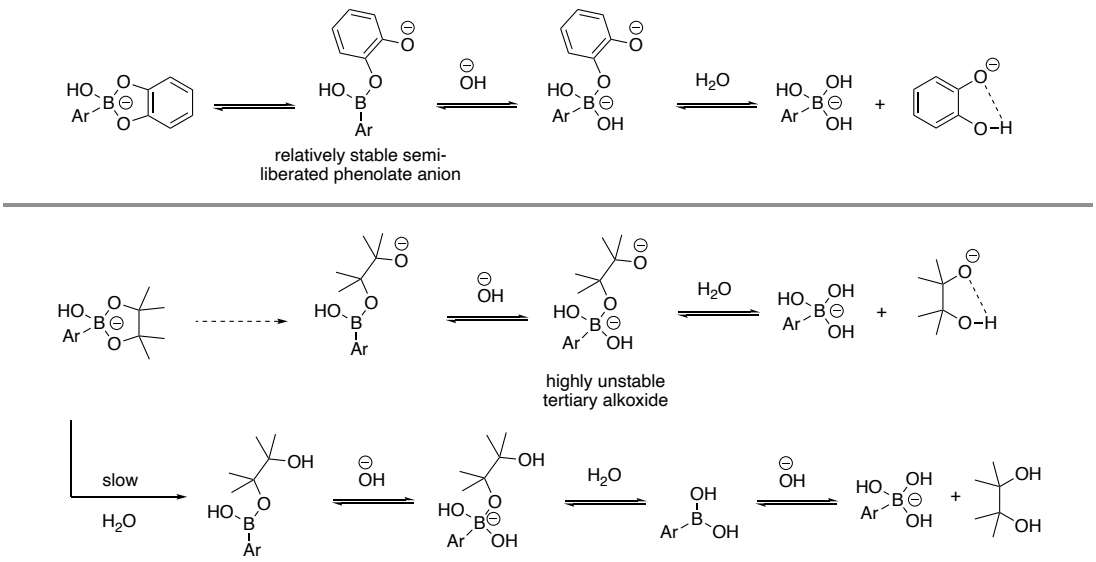

Scheme 32. Dissociative hydrolysis of catechol versus pinacol esters at high pH.

The availability of hydroxide has a considerable impact on the overall rate of protodeboronation of $[\mathbf{2c}_{OH}]^-$. At pH 13, hydrolytic equilibrium of catechol ester $[\mathbf{2c}_{OH}]^-$ with the trihydroxyboronate $[\mathbf{2a}_{OH}]^-$ is achieved in less than 2 seconds and protodeboronation proceeds near exclusively via species $[\mathbf{2a}_{OH}]^-$, with an overall half-life for the reaction of 20 min (Figure 28).

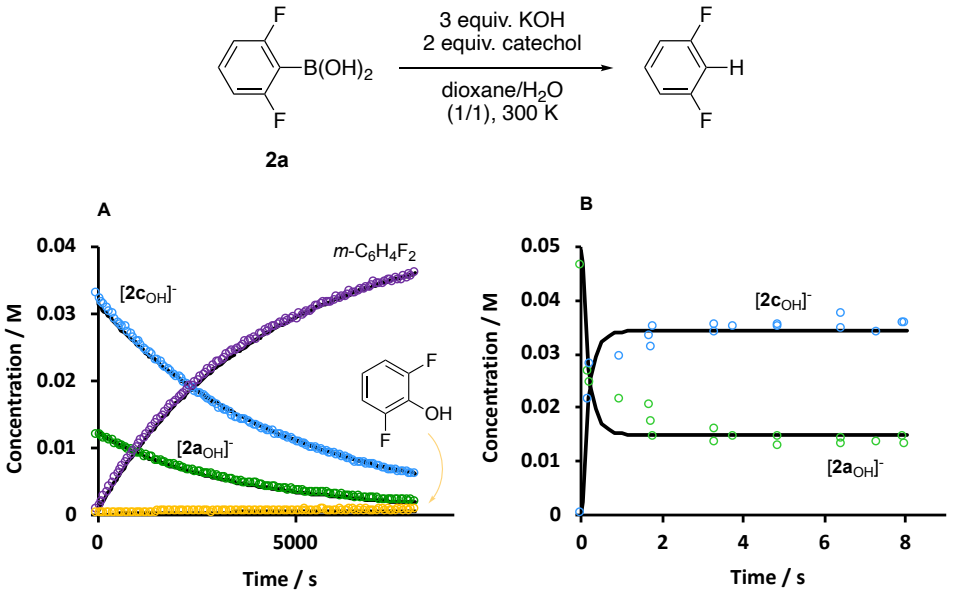

Figure 28. A) Reaction profile and kinetic simulation for the protodeboronation of $[\mathbf{2a}_{OH}]^-$, pre-equilibrated with catechol, and initiated with excess KOH. B) Reaction profile and kinetic simulation for the base-catalysed protodeboronation of $[\mathbf{2a}_{OH}]^-$, in the presence of catechol.

Following the addition of excess catechol to a running reaction of [**2a**$_{OH}$]$^-$ at high pH, a substantially reduced overall rate of protodeboronation was attained (Figure 29). Excess catechol in the reaction is capable of sequestering excess hydroxide, thereby lowering the pH of the reaction. Under these conditions, [**2c**$_{OH}$]$^-$ is subject to slow hydrolysis, and *direct* protodeboronation is slow (k_{BE}).

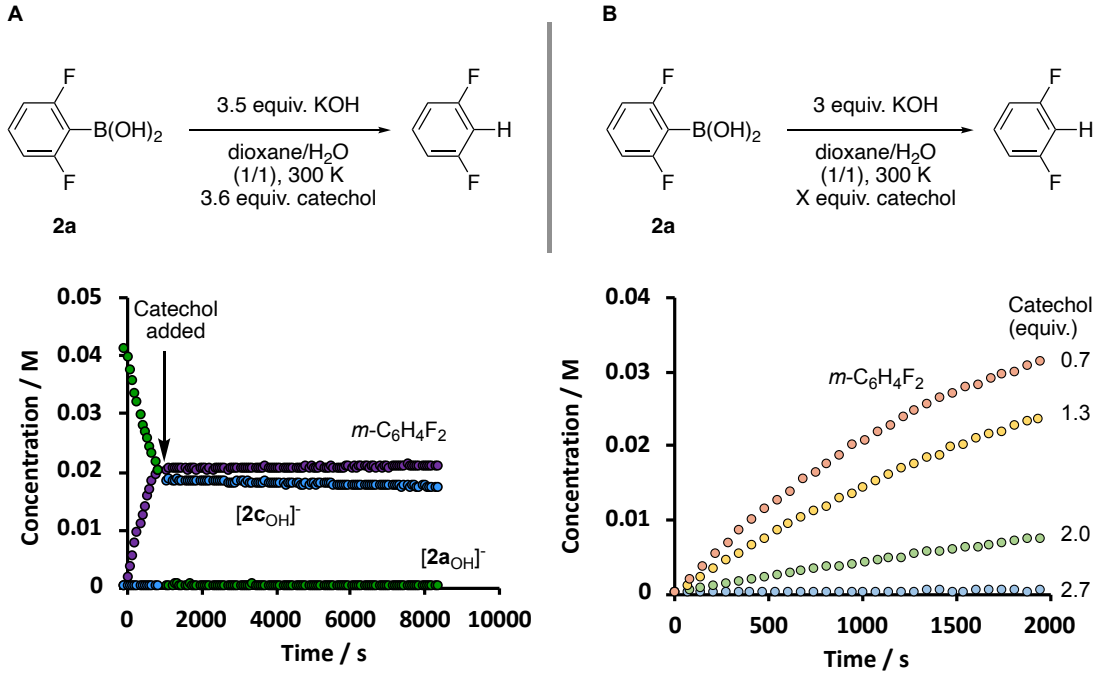

Figure 29. A) Reaction conditions and profile for the addition of excess catechol into a running reaction of [**2a**$_{OH}$]$^-$ at pH >13. B) Reactions conditions and kinetic analysis for the rate of formation of protodeboronation product formation in the presence of excess base with increasing equivalents catechol.

2.3 Protodeboronation mechanisms of boronic esters

Electron-deficient, polyfluorinated boronic acids have previously been shown to undergo protodeboronation, in basic aqueous-organic media, via an anionic dissociative mechanism (Scheme 33), involving proton-transfer to an aryl anionoid which arises from rate-limiting C-B bond cleavage.[8] The protodeboronation of two boronate esters was analysed, by determination of the $^{1}H/^{2}H$ product KIEs, for the 2,6-difluorophenylboronate complexes [**2b**$_{OH}$]$^{-}$ and [**2i**$_{OH}$]$^{-}$, relative to the trihydroxyboronate [**2a**$_{OH}$]$^{-}$. A low partitioning factor (Ar_H/Ar_D) distinguishes the anionic dissociative mechanistic pathway from a process involving rate-limiting protonatation, dominant for less-reactive and electron-rich aryl trihydroxyboronates like 4-anisyl trihydroxyboronate, which produces a substantial KIE.[8]

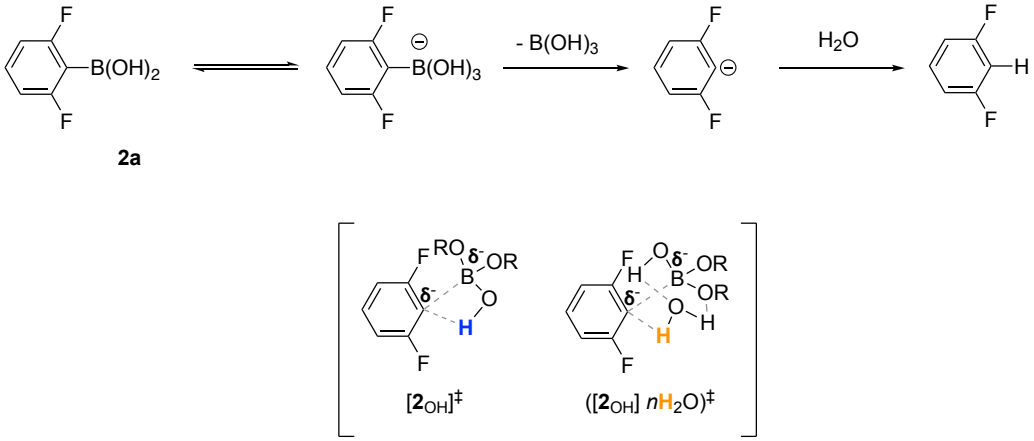

Scheme 33. Pathway for protodeboronation of 2,6-difluorophenylboronic acid **2a**, by anionic dissociation, involving the generation of an aryl anion and subsequent fast trapping by water to afford protodeboronation product.

The partitioning factors measured were small in magnitude (Ar_H/Ar_D = 1.26 ± 0.05), and the absence of a substantial solvent isotope effect (k_H/k_D = 1.12, Figure 30) supported protodeboronation via an early transition state and protonation of a developing anionoid.[110]

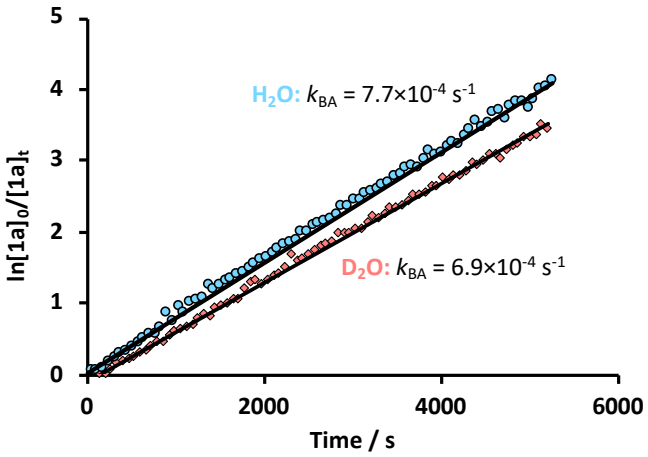

Figure 30. Rate analysis of protodeboronation of boronic acid **2a** in 1:1 1,4-dioxane/H_2O and 1,4-dioxane/D_2O. Net solvent KIE on absolute rate (k_H/k_D) = 7.7/6.9 = 1.12.

The small magnitude of the $^1H/^2H$ product KIEs (Ar_H/Ar_D = 1.19–1.27, k_{BE}), obtained in 1:1 dioxane/(50:50 H_2O/D_2O), for [**2a**$_{OH}$]$^-$, [**2b**$_{OH}$]$^-$ and [**2i**$_{OH}$]$^-$ was indicative of protodeboronation via an anionic dissociative pathway by both esters as per the corresponding boronic acid (Table 6). The KIE values determined supported the delivery of a proton to the anionoid from a hydroxyl group on the departing boronic acid, which can act as a Brønsted-acid, or alternatively the direct protonation via a network of water (Scheme 33). The fractionation of protodeboronation for the pinacolate boronate [**2b**$_{OH}$]$^-$, between the *direct* (0.3k_{BE}) and *indirect* (0.7k_{BA}) pathways (see Section 2.2), dictated the final calculated value for net H/D partitioning in the product (Ar_H/Ar_D = 1.23, k_{BE}).

Table 6. Experimental values for relative rates ($k_{rel\ (PDB)}$), half-lives of protodeboronation ($t_{0.5}$) and partitioning factors (Ar_H/Ar_D; 1:1 dioxane/L_2O, where **L** = H/D). The individual $^1H/^2H$ product KIEs were averaged from 3-6 reactions and ratios determined by ^{19}F NMR spectroscopy. ^{19}F NMR spectra of $^1H/^2H$ protodeboronation products after the reaction of $[\mathbf{2i}_{OH}]^-$ in 1:1 1,4-dioxane/(50:50 H_2O/D_2O) at pH >13.

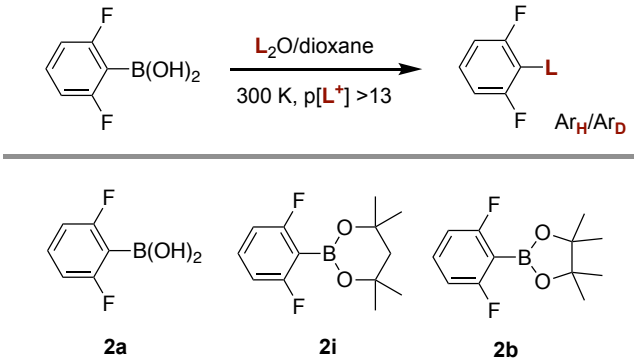

	2a	2i	2b
$t_{0.5}$	9 min	7 sec	33 h
$k_{rel\ (PDB)}$	2.1 $\times 10^2$	1.7 $\times 10^4$	1
Ar_H/Ar_D	1.26 $\pm$ 0.01	1.20 $\pm$ 0.01	1.25 $\pm$ 0.01

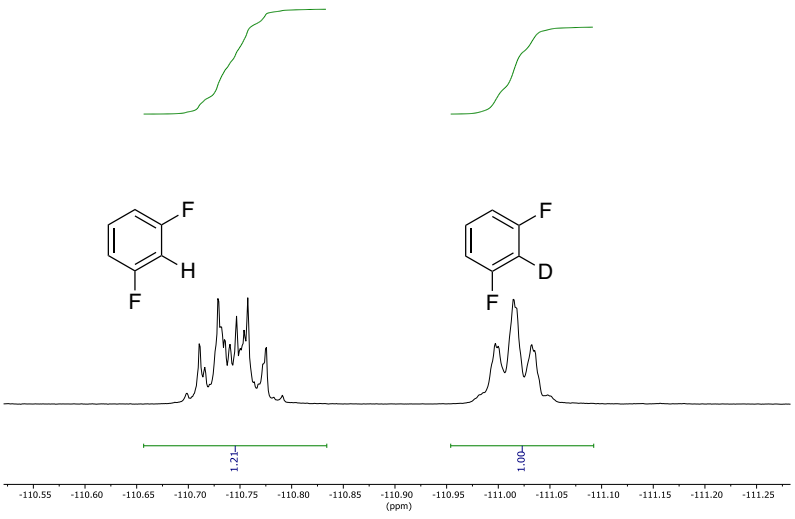

While the partitioning factors obtained for the three esters differed only slightly, the values for each were reproducible. A reaction was initiated from a 50:50 mixture of **2a** and **2i** in 1:1 dioxane/(50:50 H_2O/D_2O), at pH 13, and monitored by ^{19}F NMR spectroscopy. The boronate ester $[\mathbf{2i}_{OH}]^-$ is subject to faster protodeboronation than the corresponding trihydroxyboronate $[\mathbf{2a}_{OH}]^-$, and this

was reflected in the $^{1}H/^{2}H$ product KIEs (Ar_H/Ar_D ~ 1.20) observed at 50% conversion (see Table 6 for individual $^{1}H/^{2}H$ product KIEs and $k_{rel\ (PDB)}$). As the reaction progressed to 100% conversion, a rise in the Ar_H/Ar_D value was observed, as a result of the contribution of protodeboronation from $[\mathbf{2a}_{OH}]^-$. The shape of the experimental data obtained supports the differences apparent, albeit small in magnitude, in the individual partitioning factors for boronic esters **2a** and **2i** (Figure 31).

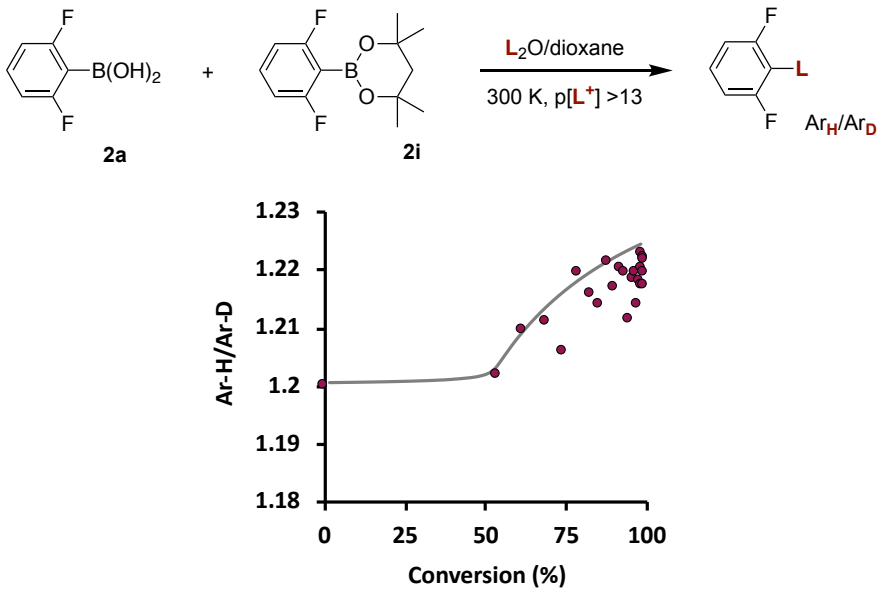

Figure 31. Analysis of conversion/% versus Ar-H/Ar-D for the protodeboronation of a 50:50 mixture of boronic acid $[\mathbf{2a}_{OH}]^-$ and boronic ester $[\mathbf{2i}_{OH}]^-$ at high pH.

Computations were performed for the protodeboronation at high pH of pinacol ester **2b** and 2,4-dimethylpentan-2,4-diol ester **2i**, by collaborators Dr Andrew Leach and Michele Assante (Figure 32). The free energies (*k*cal/mol) for the ground state and transition state (TS) structures were calculated using the M06L functional and 6-311+G** basis set (M06L/6-311+G**). Solvation was included in the calculations using IEFPCM ε = 60 (single point) in addition to explicit aqueous solvation by one or more water molecules. The placement and number of explicit solvent molecules is commonly selected based on chemical intuition. In this work, the placement of explicit water molecules was guided based on a novel approach, analogous to a method employed by Hunter and co-workers,[114] considering the electrostatic potential surfaces of

the solutes. The option to use explicit solvation, 'taking' a water molecule from the bulk medium, and thereby inducing hydrogen bonding interactions with the solute, was considered favourable only when the enthalpy (ΔH_{solv}) of addition of a H_2O exceeded an optimum cut-off of 9.7 *k*cal/mol.[115-116] Explicit solvation was included while the enthalpy gain, resultant from each addition of a single H_2O, outweighed the loss in entropy (ΔS_{solv}) due to the increased order and associative interactions between the solute and explicit water.

Computations supported the differences in reactivity found experimentally between the boronic esters **2b** and **2i**. The difference in reactivity between the pinacolate ester [**2b**$_{OH}$]$^-$ and its ring homologue [**2i**$_{OH}$]$^-$ can be attributed to two factors; (1) faster hydrolysis of 6-membered diol ring esters relative to the 5-membered ring systems at high pH. As previously discussed in Section 2.1.5, rapid hydrolysis is proposed to be due to the 1,3-diaxial strain which arises upon conversion of the neutral, trigonal ester **2i** to the anionic, tetrahedral boronate of the 6-membered ring [**2i**$_{OH}$]$^-$, and (2) 5-membered diol ring esters, in this case **2b**, are less stable in their neutral, trigonal form due to angle strain. This is relieved upon conversion to the boronate, increasing the stability and resulting in the decelerated hydrolysis, at high pH, of [**2b**$_{OH}$]$^-$.

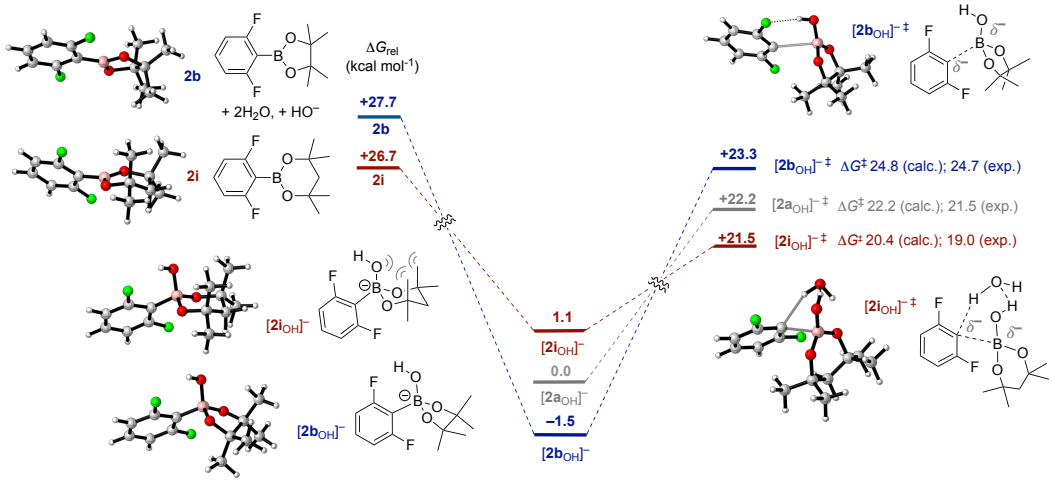

Figure 32. Computational analysis of the protodeboronation at high pH of pinacol ester **2b** and 2,4-dimethylpentan-2,4-diol ester **2i**. The 1,3-diaxial strain, responsible for the instability of the boronate ester [**2i**$_{OH}$]$^-$, is highlighted in addition to the relief of angle strain following the conversion of **2b** to [**2b**$_{OH}$]$^-$.

Thus, the origin of the substantial differences observed for varying k_{BE}, at high pH, between pinacol **2b** and 2,4-dimethylpentan2,4-diol **2i** 2,6-difluorophenylboronic esters (33 h versus 7 s respectively), was attributed to their relative stabilities in the boronate form (described by [**2b**$_{OH}$]$^-$ and [**2i**$_{OH}$]$^-$) respectively). The relief of substantial angle strain in [**2b**$_{OH}$]$^-$ under basic conditions accounts for its increased stability towards protodeboronation via C-B bond cleavage. The increased stability in the boronate form of the pinacol ester, [**2b**$_{OH}$]$^-$ is in stark contrast with ester [**2i**$_{OH}$]$^-$, which experiences 1,3-diaxial strain in this form, between axial methyl groups and axial aryl or hydroxyl groups on boron. The 1,3-dixial strain which arises upon conversion of neutral, trigonal **2i** to anionic, tetrahedral [**2i**$_{OH}$]$^-$ is the basis for the instability of [**2i**$_{OH}$]$^-$ towards dissociation and subsequent generation of a naked aryl anion.

The experimentally-determined half-lives for *direct* protodeboronation of bononate esters ($t_{0.5}$) were compared against calculated barriers for the transition state for protodeboronation ($\Delta G^{‡}_{calc}$), by Dr Andrew Leach and Michele Assante (Figure 33). Mechanistic coherency, for the full series of pinacolate esters [**2b-9b**$_{OH}$]$^-$ and [**10b**$_{H,OH}$], and their corresponding trihydroxyboronates [**2a-9a**$_{OH}$]$^-$ and [**10a**$_{H,OH}$] (Table 3) in addition to the (hetero)arylboronates [**2c-2i**$_{OH}$]$^-$ (Table 4), was confirmed by comparison of computations with experimentally-determined data.

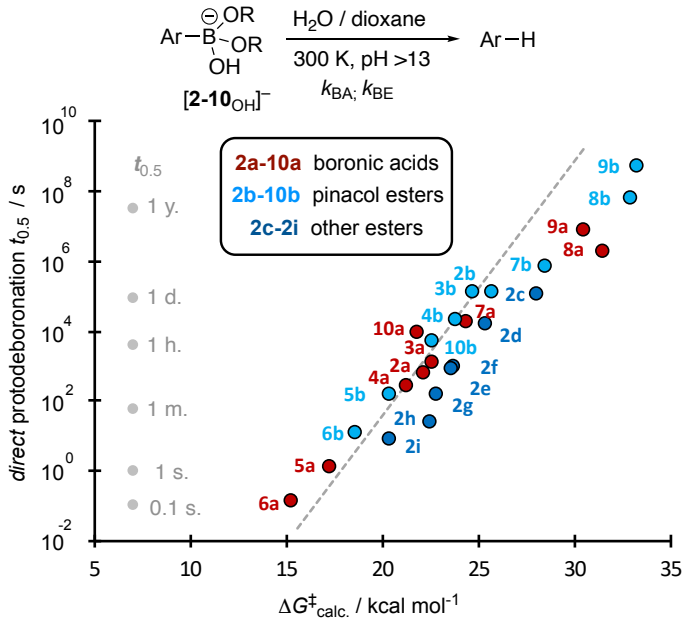

Figure 33. Half-lives ($t_{0.5}$) for *direct* protodeboronation of boronate esters versus computed transition state (TS) barriers. The dashed grey line shows the theoretical half-life based on the calculated TS barriers for protodeboronation.

Free energy barriers were calculated in *k*cal/mol for the protodeboronation of the boronic acids and esters which were investigated experimentally to probe the contribution of sequential versus concerted protonolysis (Table 7). Computations found sequential protonolysis (fragmentation) to be the dominant pathway in the more stabilised (hetero)aryl anionoids, for example in the penta and tetrafluorophenyl systems, [**5**$_{OH}$]$^-$ and [**6**$_{OH}$]$^-$ respectively. The fragmentation mechanism involves the formation of an aryl anionoid which is stabilised by electron-withdrawing fluorine groups on the phenyl ring. These electron-withdrawing groups can interact with the boric acid group and the hydrogen of a water molecule, and this complex will be more favourable at lower temperatures (27 ºC versus 70 ºC).[8] The entropic cost (ΔS) of having three molecules come together will be lower at reduced temperatures. The free energy barriers calculated for the alternative esters **2e**-**2f** of 2,6-difluorophenylboronic acid (Table 7) are lower for protodeboronation by the concerted pathway compared with fragmentation. In addition to steric effects, the computed barriers are closely linked to the structure geometries and interaction of water molecules with the solute.

Table 7. Computed free energy barriers for the protodeboronation of acid and ester boronates.

	Fragmentation	**Concerted proton transfer**
Free energy barriers (*k*cal/mol): Boronic acids		
2,3,4,5,6-F_5 [**6a**$_{OH}$]$^-$	15.4	15.3
2,3,5,6-F_4 [**5a**$_{OH}$]$^-$	17.6	17.3
2,4,6-F_3 [**4a**$_{OH}$]$^-$	21.3	21.3
2,6-F_2 [**2a**$_{OH}$]$^-$	22.4	22.2
2,6-F_2, 4-OMe [**3a**$_{OH}$]$^-$	23.8	22.6
2-F_1 [**1a**$_{OH}$]$^-$	32.3	29.0
5-thiazolyl [**7a**$_{OH}$]$^-$	27.3	24.4
Pyrazolyl [**8a**$_{OH}$]$^-$	35.4	31.5
Isoxazolyl [**9a**$_{OH}$]$^-$	34.7	30.5
Free energy barriers (*k*cal/mol): Pinacol esters		
2,3,4,5,6-F_5 [**6b**$_{OH}$]$^-$	18.7	19.5
2,3,5,6-F_4 [**5b**$_{OH}$]$^-$	20.4	21.1
2,4,6-F_3 [**4b**$_{OH}$]$^-$	23.9	24.5
2,6-F_2 [**2b**$_{OH}$]$^-$	24.8	25.6
2,6-F_2, 4-OMe [**3b**$_{OH}$]$^-$	25.8	25.7
2-F_1 [**1b**$_{OH}$]$^-$	34.1	32.5
5-thiazolyl [**7b**$_{OH}$]$^-$	29.5	28.5
Pyrazolyl [**8b**$_{OH}$]$^-$	35.5	33.0
Isoxazolyl [**9b**$_{OH}$]$^-$	36.1	33.3
Free energy barriers (*k*cal/mol): 2-Pyridyl (zwitterionic)		
2-pyridyl BA [**10a**$_{H,OH}$]	23.1	21.9
2-pyridyl BE [**10b**$_{H,OH}$]	22.7	24.0

Table 7 continued. Computed free energy barriers for the protodeboronation of acid and ester boronates.

	Fragmentation	**Concerted proton transfer**
Free energy barriers (*k*cal/mol): Alternative esters (2,6-difluorophenyl)		
2,6-F_2 boronic acid [**2a**$_{OH}$]$^-$	22.4	22.2
Pinacol [**2b**$_{OH}$]$^-$	24.8	25.6
Catechol [**2c**$_{OH}$]$^-$	Not found	28.1
Ethylene glycol [**2d**$_{OH}$]$^-$	Not found	25.4
1,3-propane diol [**2e**$_{OH}$]$^-$	25.8	23.7
Neopentyl glycol [**2g**$_{OH}$]$^-$	28.0	22.9
2-Hydroxymethyl-2-methyl-1,3-propanediol [**2f**$_{OH}$]$^-$	24.4	23.6
2,4-Dimethylpentan-2,4-diol [**2i**$_{OH}$]$^-$	23.4	20.4
2-Methylpentan-2,4-diol [**2h**$_{OH}$]$^-$	23.5	22.5

Chapter 3

Conclusions and Future Work

3.1 Conclusions

This research has focused on discerning the various pathways by which boronic esters undergo protodeboronation and understanding the factors which influence these processes. This will aid in optimising conditions and designing boronic ester substrates for efficient use in modern synthetic chemistry. The kinetics and mechanism for a diverse range of (hetero)arylboronic esters, comprising a series of diols, have been investigated by *in-situ* and stopped-flow NMR spectroscopy (^{1}H, ^{19}F and ^{11}B), supported by kinetic simulations, pH-rate dependence, isotopic entrainment, ^{2}H KIEs and KS-DFT computations. The work revealed boronic esters to be highly nuanced in their behaviour and highlights the prospect for controlling the overall rate of protodeboronation by means of varying the pH and polyol component.

Base-catalysed protodeboronation was shown to proceed via an analogous mechanism for the boronic esters and their corresponding acids. This pathway involves the generation of an aryl anionoid via rate-limiting C-B bond cleavage followed by sequential or concerted protonation. The speciation of boronic acid and ester between their neutral, trigonal boron form and anionic, tetrahedral boronate form is pH dependent. Almost exclusive and quantitative conversion to the boronic acid and ester boronates is instantaneously achieved after the addition of excess base. At pH ≥2 units above the pK_a, speciation is >99% boronate. The net rates of protodeboronation for (hetero)arylboronic esters are dictated by two competitive processes; *direct* protodeboronation or *indirect* pre-hydrolytic protodeboronation. The coexistence and extent of these two reaction pathways has been deconvoluted using kinetic simulations. In general, for the pinacol esters studied, and with the exception of the tri, tetra and pentafluorophenyl systems, protodeboronation by the pre-hydrolytic pathway was predominant under basic conditions.

By investigating the effect of diol structure, this work revealed that esterification does not necessarily confer greater stability to the corresponding boronic acid or attenuate the overall rate of protodeboronation. The impact of esterification

of 2,6-difluorophenylboronic acid by eight different polyols, including simple diols and a triol, was probed, revealing a substantial span of overall rates of protodeboronation at pH >13. Under basic conditions, the half-life for protodeboronation of the pinacol ester was longer ($t_{0.5}$ = 33 h) compared with that of the free acid ($t_{0.5}$ = 9 min). In contrast, esterification by 2,4-dimethylpentan-2,4-diol shortened its half-life to just 7 seconds.

The impact of esterification by the ubiquitous pinacol moiety was investigated for a range of (hetero)aromatic systems. The aryl B-Pin esters exhibit unique stability at high pH compared with other commonly used esters, arising from the reduction in angle strain on conversion of the neutral, trigonal ester to the anionic, tetrahedral boronate. Esterification by pinacol attenuated the rate of *direct* protodeboronation by approximately two orders of magnitude across all (hetero)aryl substrates studied at pH >13. The increased stability imparted by pinacol esterification was most apparent in the reactive polyfluorophenyl systems. The four methyl groups in pinacol sterically shield the O and B centres and hinder the attack of water but do not induce significant steric strain between the pinacol group and aryl ring. The potential for ester hydrolysis and the subsequent rapid protodeboronation from the corresponding trihydroxyboronate at high pH, results in the reduced *phenomenological* stability of pinacolate esters, compared to that indicated by the *direct* protodeboronation only.

Boronic ester hydrolysis rates were also nuanced due to the variation in diol structure, and the behaviour of 5- and 6-membered ring boronic esters is pH-dependent. A range of both 5- and 6-membered ring boronic esters were studied exhibiting half-lives for hydrolysis across a wide scale, spanning 1 second to 3.7 days at high pH. As reported by Musgrave and Bowie, at neutral pH, 5-membered cyclic boronic esters are subject to more rapid hydrolysis than 6-membered systems. In this work, the trend was shown to be inverted at high pH, and 6-membered cyclic boronic esters undergo hydrolysis quicker than their 5-membered homologues. There are two exceptions to this

observation including the catecholate ester and the 2-pyridyl system, both of which hydrolyse rapidly by alternative pathways. The diol acidity, ring size and degree of substitution impacts the susceptibility to hydrolysis of boronic esters.

An enhancement in the rate of hydrolysis of aryl B-Pin esters occurs when self/auto-catalysis dominates and this process is evident when the pH is close to the substrate pK_a. Self/auto-catalysis is suppressed at 2 pH units greater or less than the pK_a of the aryl B-Pin ester. Aerobically generated hydroperoxides present in ethereal solvents can oxidise arylboronates to their corresponding phenols. The phenol formed can catalyse the hydrolysis of aryl B-Pin esters when the pH is close to the substrate pK_a. Self/auto and phenolic catalysis becomes more rapid with increasing initial pinacol ester concentration. When the pH is 2 or more units greater than the pK_a of the aryl B-Pin ester, >99% speciation as the boronate is achieved. The rate of hydrolysis to the corresponding acid boronate is attenuated significantly under these conditions relative to hydrolysis of the neutral, trigonal ester.

The identity, strength, and concentration of the base, employed in cross-coupling reactions which utilise aryl B-Pin ester reagents, and are conducted in basic aqueous-organic media, can impact the boronate speciation and behaviour. The half-life for protodeboronation of the 2,6-difluorophenyl pinacol ester was 20 minutes, 40 minutes and >10 hours at pH 10, 11 and >13, achieved using bases NEt_3, K_2CO_3 and KOH. When the pH is 2 or more units greater than the pK_a of the aryl B-Pin ester, >99% speciation as the boronate is achieved. The rate of hydrolysis to the corresponding acid boronate is attenuated significantly under these conditions, which is in contrast to the rapid equilibration of acid boronate with ester boronate at reduced pH.

In summary, the pH is a critical factor in governing the susceptibility of (hetero)arylboronic esters towards hydrolysis. However, both the nature of the polyol and boronic acid moiety influence the extent of protodeboronation both via hydrolysis and the *direct* pathway.

3.2 Future work

3.2.1 Phenolic catalysis

In-situ oxidation of [**1b**$_{OH}$]$^-$, by aerobically-generated hydroperoxides in the solvent blend 50% aq. dioxane, afforded the 2-fluorophenol. This phenol was found to accelerate the rate of hydrolysis (k_{ArOH}) of pinacolate ester [**1b**$_{OH}$]$^-$ when the pH was close to the pK_a. In certain circumstances, when the deprotection of boronic esters by hydrolysis is desirable, acceleration of the process would be beneficial. Hence, future investigations would involve probing the scope of phenols, varying in acidity, steric hindrance, and chelating ability, which accelerate the general acid-catalysed hydrolysis of [**1b**$_{OH}$]$^-$ (examples in Figure 34).

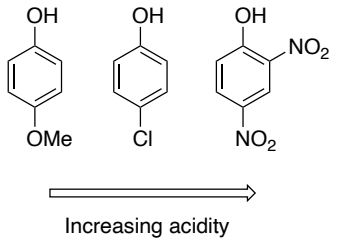

Figure 34. Examples of phenols (of increasing acidity from left to right) to test.

3.2.2 Substrate scope

The kinetics and mechanism of hydrolysis and protodeboronation for a broad range of pinacol esters (**1b-10b**) and 2,6-difluorophenylboronic esters (**2a-2i**), encompassing eight polyols, was investigated in this work. The scope of polyfluorinated pinacol esters and in particular heteroaryl pinacol esters studied could be expanded, to include several non-basic heterocycles; thienyl, furyl and pyrrol (Figure 35) given the importance of heterocyclic moieties as scaffolds in synthetic organic chemistry.

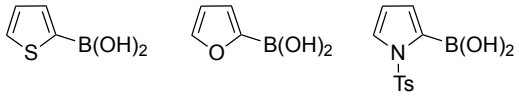

Figure 35. Non-basic heteroarylboronic acids including thienyl, furyl and pyrrol (left to right).

The impact of esterification by pinacol on cyclopropyl and vinyl boronic acids could also be probed.[109] A greater scope of diols used for the esterification of 2,6-difluorophenylboronic acid could be employed to further probe the impact of ring size and degree of substitution on the rate of hydrolysis of boronic esters. Due to the increasingly frequent incorporation of diethanolamine (DEA) boronic esters in organic synthesis within the pharmaceutical industry, this study could be expanded to include a DEA esters of 2,6-difluorophenylboronic acid and other (hetero)aryl boronic acids (Scheme 34).[117]

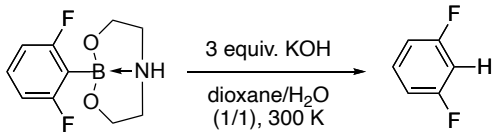

Diethanolamine (DEA) boronic ester

Scheme 34. Base-catalysed protodeboronation of a 2,6-difluorophenyl DEA ester.

3.2.3 Hydrolysis and esterification of 2-fluorophenylboronic acid **1a** and its catechol ester

It was found that the rate of ester hydrolysis for $[\mathbf{2c}_{OH}]^-$ is dependent on the availability of hydroxide (k_{OH} versus k_{H2O}). In the absence of excess hydroxide, $[\mathbf{2c}_{OH}]^-$ hydrolyses slowly (k_{H2O}; $t_{0.5} \geq 30$ h) but, as the pH is increased the catecholate ester becomes subject to base-catalysis (k_{OH}). At pH >13, where k_{OH} dominates k_{H2O}, $t_{0.5} \leq 1$ s. Catechol is unique due to its acidity relative to the other diols studied in this work. Exploring the hydrolysis and esterification of 2-fluorophenylboronic acid **1a** and its catechol ester, by constructing a detailed pH-rate profile across a wide pH range, would prove insightful.

3.2.4 Metal-catalysed protodeboronation and application in Suzuki-Miyaura cross-couplings

Esterification of boronic acids can promote rapid protodeboronation or attenuate the process. Thus, the potential for efficient removal of remaining starting material when required or mitigation of undesirable protodeboronation in cross-couplings could be exploited by the research presented in this study. Notably, this research should provide valuable guidance to support the usage of unstable (hetero)arylboronic esters in aqueous basic media, conditions commonly employed in the Suzuki-Miyaura reaction. Direct application of the findings herein would further aid the synthetic community, in particular relating to the appropriate selection of boronic esters for cross-couplings. Initial investigations probing the impact of catalytic palladium on the protodeboronation of the pinacolate ester **2b** at pH >13, by comparing the absolute rates of protodeboronation with and without the presence of a Pd metal catalyst, would likely prove insightful (Scheme 35). These studies could include Pd(II) species which are reduced *in-situ*, for example Pd(dppf)Cl_2, and Pd$(OAc)_2$, or Pd(0) species added directly to the reaction, for example Pd$(PPh_3)_4$. These studies could be expanded to explore other metal catalysts commonly used in Suzkui-Miyaura and analogous cross-couplings, for example nickel. The base could be varied and both KOH and K_2CO_3 tested. Subsequent studies could incorporate a coupling parter into the reaction, for example an aryl halide or triflate, and employing literature Suzuki-Miyarua reaction conditions with a range of (hetero)arylboronic esters.

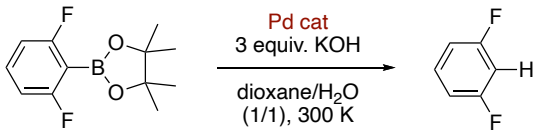

2b **S11**

Scheme 35. Protodeboronation of pinacolate ester **2b** at pH >13 and in the presence of catalytic palladium.

Chapter 4

Experimental

4.1 General information

4.1.1 NMR spectroscopy

Unless stated otherwise, all ^{1}H, $^{13}C\{^{1}H\}$, ^{10}B, ^{11}B and ^{19}F NMR spectra were acquired on a Bruker Ascend 400 MHz spectrometer at 300 K (27 °C) (^{1}H 400 MHz, $^{13}C\{^{1}H\}$ 101 MHz, ^{11}B (128 MHz) and ^{19}F (377 MHz). MestReNova versions 10.0 and 11.0 were used for processing all NMR spectra acquired. All chemical shifts for ^{1}H NMR spectra are reported in parts per million (ppm) relative to the solvent residual signals; DMSO-*d*$_5$ (δ_H = 2.50 ppm) and $CHCl_3$ (δ_H = 7.26 ppm). All chemical shifts for ^{13}C NMR spectra are reported in parts per million (ppm) relative to the solvent peak; DMSO-*d*$_6$ (δ_C = 39.5 ppm) and $CDCl_3$ (δ_C = 77.2 ppm). Coupling constants, J, are quoted in Hz and multiplicities as s (singlet), d (doublet), t (triplet), q (quartet), m (multiplet) and multiples of these (e.g. dd, doublet of doublets). NMR tubes made from borosilicate glass were used to record NMR spectra except for ^{10}B and ^{11}B NMR spectra when quartz NMR tubes were used. ^{19}F NMR spectra recorded are reported in ppm. ^{11}B and ^{19}F NMR chemical shifts are externally referenced to $BF_3.OEt_2$ = 0 ppm.

4.1.2 Infrared (IR) spectroscopy

A Bruker ALPHA^{TM} ATR-FTIR spectrometer was used to record IR spectra for all compounds. IR spectra were acquired over a range of 400-4000 cm^{-1} and peaks are reported in cm^{-1}.

4.1.3 Mass spectrometry

A Bruker ESI Micro-Tof mass spectrometer was used to record all electrospray ionisation (ESI^+) spectra. Data acquired is reported as m/z.

4.1.4 Melting points

A Griffin capillary apparatus and glass capillary tubes were used to determine the melting point (m.p.) of compounds. The melting points acquired were reported in degrees Celcius (°C).

4.1.5 Reagents and solvents

Reagents were obtained from commercial sources (Sigma Aldrich, Alfa Aesar, Fischer Scientific, Acros Organics and Fluorochem) and used without further purification unless otherwise specified. The reagent catechol was purified prior to use by recrystallization in toluene or hexane according to literature procedure.[118] 2-pyridyl boronic acid MIDA ester was purified prior to use by flash column chromatography in MeCN.[109] Anhydrous solvents were obtained from a Solvent Purification System (SPS). NMR solvents ($CDCl_3$ and DMSO-d_6) were dried over activated 3 Å molecular sieves prior to use. Deionised water was used unless otherwise specified.

4.2 Synthetic procedures

4.2.1 2,6-Difluorophenylboronic acid pinacol ester, **2b**[119]

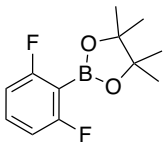

2b was prepared by modification of a reported procedure.[119] To a 100 mL round-bottomed flask, equipped with a stir bar was added pinacol (4.55 mmol, 0.54 g) in 10 mL MeCN and 2,6-difluorophenylboronic acid (4.14 mmol, 0.65 g) in 10 mL MeCN. The reaction mixture was allowed to stir at room temperature overnight (16 h). The reaction was washed with 10 mL deionised water and 2 x 20 mL extractions with diethyl ether were performed. The combined organic layers were dried over sodium sulfate, filtered and concentrated under reduced pressure to give a white crystalline solid. The product was subsequently dried on a high vacuum line (0.79 g, 79% yield). Spectroscopic data consistent with that reported.[119, 120] **^{1}H NMR** (400 MHz, $CDCl_3$) δ = 7.39-7.31 (m, 1H), δ = 6.81-6.87 (m, 2H), δ = 1.38 (s, 12H). **^{19}F NMR** (377 MHz, $CDCl_3$) δ = −100.7 (m). **^{11}B NMR** (128 MHz, $CDCl_3$) δ = 29.8. **^{13}C NMR** (101 MHz, $CDCl_3$) δ = 166.6 (dd, J = 250.5 Hz, 12.8 Hz), δ = 133.1 (t, J = 10.7 Hz), δ = 110.9-111.2 (m), 84.2 (s), 24.8 (s). The carbon attached to boron was not detected. **M.p.**= 48-51 °C.

4.2.2 3,5-Dideutero-2,6-difluorophenylboronic acid, 3,5-D_2-**2a**[8]

3,5-D_2-**2a** was prepared following the previously reported procedure.[8]

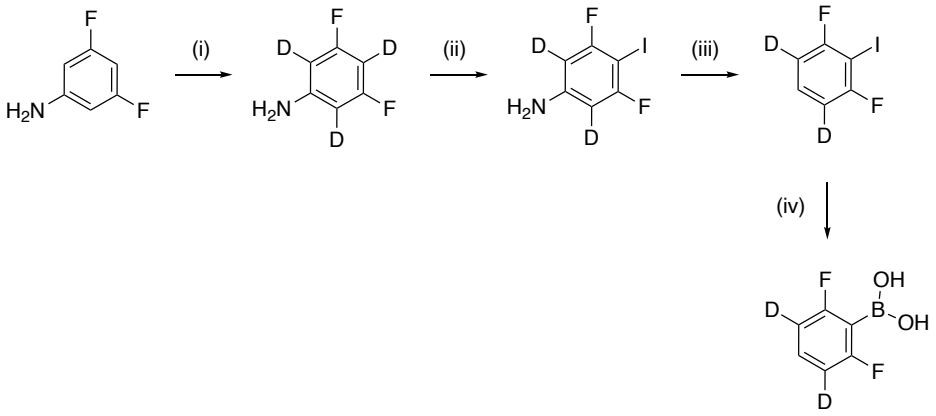

(i) Two subjections of D_2O, TfOH (0.4 equiv), 120 °C for 16 hrs. 49% yield, **m.p.**(°C) = 38 - 39.

(ii) I_2, $NaHCO_3$, D_2O, 0 °C to rt, 19 hrs. 66% yield, **m.p.**(°C) = 104 – 150.

(iii) ^{t}BuONO, DMF, 60 °C, 1 hr. 59% yield.

(iv) (a) ^{n}BuLi (1.4 M in hexane), Et_2O, -78 °C; (b) $B(O^{i}Pr)_3$, -78 °C to -10 °C, 1 hr; (c) 5 % DCl in D_2O. 30% yield, **m.p.**(°C) = 148 – 150 °C.

4.2.3 3,5-Dideutero-2,6-difluorophenylboronic acid pinacol ester, 3,5-D_2-**2b**

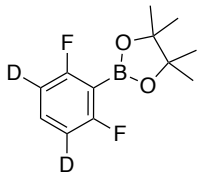

3,5-dideutero-2,6-difluorophenylboronic acid (0.63 mmol, 0.10 g) and pinacol (0.70 mmol, 0.08 g) were added to a 10 mL RBF equipped with a stir bar in 4 mL MeCN. The reaction mixture was allowed to stir at room temperature for 17 hours. The solvent was removed *in-vacuo* and after drying on a high vacuum line, a light brown crystalline solid was obtained (79 % yield). **^{1}H NMR**

(400 MHz, $CDCl_3$) δ = 7.35 (1H, tt, J = 6.6 Hz, 1.2 Hz), δ = 1.39 (s, 12H). **^{13}C NMR** (101 MHz, $CDCl_3$) δ = 166.6 (dd, J = 250.7 Hz, 12.7 Hz), 132.9 (t, J = 10.6 Hz), 110.8 (q, J = 25.6 Hz), 84.2 (s), 24.8 (s). The carbon attached to boron was not detected. **^{19}F NMR** (377 MHz, $CDCl_3$) δ = - 100.98 (d, J = 6.7 Hz). **^{11}B NMR** (128 MHz, $CDCl_3$) δ = 29.8. **M.p.**(°C) = 58 – 60. **V_{max} (neat)/cm^{-1}** 2978, 2941, 1614, 1562, 1417, 1323, 1203, 1136, 1054, 976, 844. **HRMS (ESI)** *m/z* calc. for [M^+] $C_{12}H_{13}D_2O_2{}^{11}BF_2$: 242.12439, found: 242.12532.

4.2.4 2,6-Difluoro-4-anisylboronic acid pinacol ester, **3b**[95]

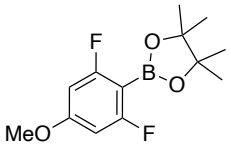

Following an alternate synthetic procedure, 2,6-difluoro-4-anisylboronic acid pinacol ester was prepared. To a 25 mL round-bottomed flask, equipped with a stir bar, was added boronic acid (3.14 mmol, 0.590 g) and pinacol (1 equiv., 3.13 mmol, 0.370 g) in 14 mL MeCN. The reaction mixture was allowed stir overnight with 3 A° molecular sieves. The solution was filtered and concentrated *in-vacuo* to give a light brown oil in 20% yield. Spectroscopic data consistent with that reported.[95] **^{1}H NMR** (400 MHz, $CDCl_3$) δ = 6.36 (2H, d), 3.79 (3H, s), 1.36 (12H, s). **^{13}C NMR** (101 MHz, $CDCl_3$) δ = 167.8 (dd, J = 249.9, 16.6 Hz), 163.9 (t, J = 14.8 Hz), 97.8 (m), 83.8 (m), 55.76 (s), 24.7 (s). The carbon attached to boron was not detected. **^{19}F NMR** (377 MHz, $CDCl_3$) δ = -99.03. **^{11}B NMR** (128 MHz, $CDCl_3$) δ = 29.5.

4.2.5 2,4,6-Trifluorophenylboronic acid pinacol ester, **4b**[121]

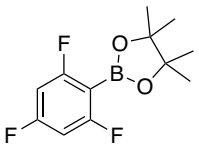

Following an alternate synthetic procedure, 2,4,6-trifluorophenylboronic acid pinacol ester was prepared. To a 25 mL round-bottomed flask, equipped with a stir bar, was added boronic acid (5.68 mmol, 1.003 g) and pinacol (1 equiv., 5.76 mmol, 0.681 g) in 14 mL MeCN. The reaction mixture was allowed stir overnight with 3 A° molecular sieves. The solution was filtered and concentrated *in-vacuo* to give an off-white crystalline solid in 56% yield. Spectroscopic data consistent with that reported.[121, 122] **^{1}H NMR** (400 MHz, $CDCl_3$) δ = 6.60 (2H, m), 1.37 (12H, s). **^{13}C NMR** (101 MHz, $CDCl_3$) δ = 168.6 (t), 166.2 (dt, J = 34.0 Hz, 15.8 Hz), 163.9 (t, J = 16.0 Hz), 100.1 (m), 84.3 (s), 24.7 (s). The carbon attached to boron was not detected. **^{19}F NMR** (377 MHz, $CDCl_3$) δ = -103.92 (1F), -97.24 (2F). **^{11}B NMR** (128 MHz, $CDCl_3$) δ = 29.4. **M.p.**(°C) = 38 – 41 °C.

4.2.6 2,3,5,6-Tetrafluorophenylboronic acid pinacol ester, **5b**[121]

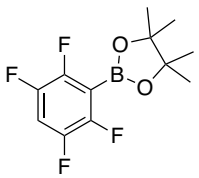

Following an alternate synthetic procedure, 2,3,5,6-tetrafluorophenylboronic acid pinacol ester was prepared. To a 25 mL round-bottomed flask, equipped with a stir bar, was added boronic acid (2.60 mmol, 0.505 g) and pinacol (1 equiv., 2.60 mmol, 0.306 g) in 8 mL MeCN. The reaction mixture was allowed to stir overnight with 3 A° molecular sieves. The solution was filtered and

concentrated *in-vacuo* to give a white crystalline solid in 33% yield. Spectroscopic data consistent with that reported.[121] **^{1}H NMR** (400 MHz, $CDCl_3$) δ = 7.10 (1H, ddd, J = 9.5 Hz, 7.4 Hz, 2.1 Hz), 1.38 (12H, s). **^{13}C NMR** (101 MHz, $CDCl_3$) δ = 148.7 (dddd, J = 249.1 Hz, 13.6 Hz, 10.4 Hz, 3.6 Hz), 145.7 (dddd, J = 248.8 Hz, 16.2 Hz, 8.8 Hz, 3.9 Hz), 108.6 (tt, J = 22.3 Hz, 1.7 Hz), 84.9 (s), 24.6 (d, J = 15.6 Hz). The carbon attached to boron was not detected. **^{19}F NMR** (377 MHz, $CDCl_3$) δ = -139.33, -131.00. **^{11}B NMR** (128 MHz, $CDCl_3$) δ = 29.2. **M.p.**(°C) = 41 – 43 °C.

4.2.7 2,3,4,5,6-Pentafluorophenylboronic acid pinacol ester, **6b**[122]

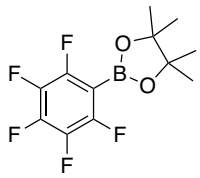

Following an alternate synthetic procedure, 2,3,4,5,6-pentafluorophenylboronic acid pinacol ester was prepared. To a round-bottomed flask equipped with a stir bar and Dean-Stark setup, was added boronic acid (7.57 mmol, 1.605 g) and pinacol (1 equiv. 7.65 mmol, 0.904 g) in 8 mL toluene. The reaction mixture was refluxed and once cooled to room temperature, concentrated *in-vacuo.* The resultant oil was purified using a silica plug with DCM as the eluent. A white crystalline solid was obtained and dried under high vacuum (70% yield). Spectroscopic data consistent with that reported.[122] **^{1}H NMR** (400 MHz, $CDCl_3$) δ = 1.37 (s). **^{13}C NMR** (101 MHz, $CDCl_3$) δ = 149.4 (m), 142.8 (m), 137.3 (m), 84.9 (s), 24.7 (s). The carbon attached to boron was not detected. **^{19}F NMR** (377 MHz, $CDCl_3$) δ = -129.52 (2F), -149.81 (1F), -161.97 (2F). **^{11}B NMR** (128 MHz, $CDCl_3$) δ = 29.0. **M.p.**(°C) = 34 – 36 °C.

4.2.8 5-Thiazolyl boronic acid pinacol ester, **7b**[123]

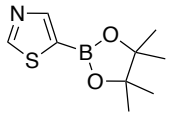

n-BuLi (1.2 equiv., 2.5 M in hexane, 1.6 mL) was added to a stirred solution of 2-trimethylsilylthiazole (3.38 mmol, 0.541 mL) in dry THF cooled to -78 °C under nitrogen over a period of 20 min. Triisopropyl borate (1.2 equiv., 4.06 mmol, 0.94 mL) was added after 15 min of stirring at -78 °C. The mixture was allowed to stir for 1.5 h at this temperature before warming to room temperature over the course of 45 min followed by 30 min stirring at room temperature. A solution of pinacol (1 equiv., 3.38 mmol, 0.40 g) in THF was added and after 10 min, glacial acetic acid was added dropwise until the pH reached 5. The mixture was diluted with ether and filtered. The filtrate was concentrated to 1/3 of its volume and diluted with cyclohexane and concentrated under vacuum three times. The resulting residue was triturated with n-hexane and filtered to afford the crude product. ^{1}H NMR spectrum obtained showed AcOH impurity in the crude product. After purification with saturated sodium bicarbonate solution, the product was isolated as off-white powder (0.12 g, 17%). Spectroscopic data consistent with that reported.[123] **^{1}H NMR** (400 MHz, $CDCl_3$) δ = 9.01 (s, 1H), 8.35 (s, 1H), 1.36 (s, 12H). **^{13}C NMR** (101 MHz, $CDCl_3$) δ = 158.7 (s), 152.7 (s), 84.6 (s), 24.8 (s). The quaternary carbon for the heteroaryl C-B bond was not detected. **^{11}B NMR** (128 MHz, $CDCl_3$) δ = 29.1. **M.p .**(°C) = 93 – 95 °C.

4.2.9 3,5-Dimethyl isoxazolyl boronic acid pinacol ester, **9b**[124]

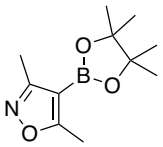

To a 25 mL round-bottomed flask, equipped with a stir bar, was added boronic acid (2.27 mmol, 0.320 g) and pinacol (1 equiv., 2.29 mmol 0.271 g) in 8 mL DCM. The reaction mixture was allowed to stir at room temperature for 4 hours with 4 A° molecular sieves. The solution was filtered and concentrated *in-vacuo* to yield a white crystalline solid which was dried on a high vacuum line (0.26 g, 51% yield). Spectroscopic data consistent with that reported.[124] **^{1}H NMR** (400 MHz, DMSO-d_6) δ = 2.46 (3H, s), 2.22 (3H, s), 1.27 (12H, s). **^{13}C NMR** (101 MHz, DMSO-d_6) δ = 178.0 (s), 163.2 (s), 83.7 (s), 25.1 (s), 12.9 (s), 11.8 (s). The quaternary carbon for the heteroaryl C-B bond was not detected. **^{11}B NMR** (128 MHz, DMSO-d_6) δ = 29.3. **M.p.**(°C) = 86 – 89 °C.

4.2.10 2,6-Difluorophenylboronic acid catechol ester, **2c**[125]

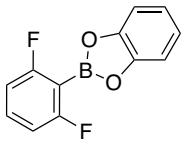

Following a modified procedure, 2,6-difluorophenylboronic acid catechol ester was prepared. To a 25 mL round-bottomed flask equipped with a stir bar and 4 Å molecular sieves was added 2,6-difluorophenylboronic acid (0.684 mmol, 0.11 g) and 1.1 equivalents catechol (0.752 mmol, 0.08 g) in 10 mL CH_2Cl_2. The reaction mixture was allowed to stir at room temperature for 5 hours. The solution was filtered to remove the molecular sieves and concentrated down on the rotary evaporator. A white crystalline solid was obtained (0.14 g, 87 % yield). **M.p.**(°C) = 123 – 126. Spectroscopic data for the DMSO adduct. **^{1}H**

NMR (400 MHz, DMSO-d_6) δ = 7.26 (tt, J = 8.2 Hz, 6.7 Hz, 1H), δ = 6.83 (ddd, J = 8.3 Hz, 6.8 Hz, 1.6 Hz, 2H), 6.71 (dd, J = 5.6 Hz, 3.3 Hz, 2H), 6.60 (dd, J = 5.6 Hz, 3.4 Hz, 2H). **^{13}C NMR** (101 MHz, DMSO-d_6) δ = 165.0 (dd), 150.9 (s), 129.5 (t), 118.4 (s), 110.6 (m), 108.7 (s). The carbon attached to boron was not detected. **^{19}F NMR** (377 MHz, DMSO-d_6) δ = - 102.61 (ddd, J = 11.2 Hz, 5.6 Hz, 2.4 Hz). **^{11}B NMR** (128 MHz, DMSO-d_6) δ = 10.4.

4.2.11 2,6-Difluorophenylboronic acid propanediol ester, **2e**

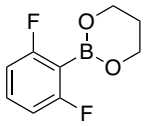

To a 100 mL round-bottomed flask, equipped with a stir bar, was added 2,6-difluorophenylboronic acid (8 mmol, 1.262 g) and 1,3-propanediol (1.1 equiv., 8.8 mmol, 0.6 mL) in 40 mL diethyl ether. The reaction mixture was allowed stir overnight with 4 A° molecular sieves. The solution was filtered and concentrated *in-vacuo* to yield a white solid in 48% yield. **M.p.**(°C) = 32 – 34 °C. **V_{max} (neat)/cm^{-1}** 3000, 1620, 1570, 1482, 1455, 1423, 1328, 1276, 1144, 1122, 985, 925, 847, 786, 763, 715, 652, 573, 547, 508, 486, 451. **^{1}H NMR** (400 MHz, $CDCl_3$) δ = 7.25 (1H, m), 6.79 (2H, m), 4.17 (4H, m), 2.08 (2 H, m). **^{13}C NMR** (101 MHz, $CDCl_3$) δ = 167.2 (d, J = 13.4), 164.7 (d, J = 13.3), 131.9 (s), 111.0 (m), 62.4 (s), 27.3 (s). The carbon attached to boron was not detected. **^{19}F NMR** (377 MHz, $CDCl_3$) δ = - 102.93. **^{11}B NMR** (128 MHz, $CDCl_3$) δ = 26.6. **HRMS (ESI)** *m/z* calc. for [MH^+] $C_9H_9O_2{}^{11}B_1F_2$: 198.06566, found: 198.06582.

4.2.12 2,6-Difluorophenylboronic acid neopentyl glycol ester, **2g**[126]

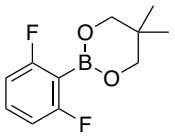

Following a modified procedure, 2,6-difluorophenylboronic acid neopentyl glycol ester was prepared. To a 100 mL round-bottomed flask, equipped with a stir bar was added 2,6-difluorophenylboronic acid (6.58 mmol, 1.04 g), 2,2-dimethyl-1,3-propanediol (7.2 mmol, 0.75 g) in 40 mL diethyl ether. Magnesium sulfate (6.23 mmol, 0.75 g) was added and the reaction mixture was allowed to stir at room temperature overnight (24 h). The reaction was filtered through a plug of cotton wool and a layer of Kieselgur (washed with acid), washed with diethyl ether and concentrated down under reduced pressure. A white crystalline solid was obtained and dried on a high vacuum line (95% yield). Spectroscopic data consistent with that reported.[127] **^{1}H NMR** (400 MHz, $CDCl_3$) δ = 7.27-7.35 (m, 1H), δ = 6.84 (t, 2H), δ = 3.83 (s, 4H), δ = 1.10 (s, 6H). **^{19}F NMR** (377 MHz, $CDCl_3$) δ = −102.9 (m). **^{11}B NMR** (128 MHz, $CDCl_3$) δ = 26.4. **^{13}C NMR** (101 MHz, $CDCl_3$) δ = 165.8 (dd, J = 247.5 Hz, 13.5 Hz), δ = 131.8 (t, J = 10.5 Hz), δ = 110.7-111.0 (m), δ = 72.6 (s), δ = 31.8 (s), δ = 21.7 (s). The carbon attached to boron was not detected. **M.p.**= 40-42 °C.

4.2.13 2,6-Difluorophenylboronic acid 2-methyl-2,4-pentanediol ester, **2h**

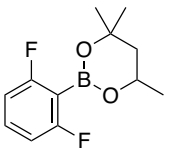

To a 50 mL round-bottomed flask equipped with a stir bar, was added 2,6-difluorophenyl boronic acid (2.09 mmol, 0.33 g) which was then dissolved in 10 mL Et_2O, followed by the addition of hexylene glycol (1 equiv., 2.09 mmol, 0.27 mL). The reaction mixture was allowed to stir at room temperature

overnight with 4 Å molecular sieves. The mixture was filtered and concentrated on a rotary evaporator to give a white crystalline solid. The product was dried under high vacuum (51% yield). **^{1}H NMR** (400 MHz, DMSO) δ = 7.42 (tt, J = 8.4 Hz, 6.9 Hz, 1H), 7.01 – 6.90 (m, 2H), 4.41 (dqd, J = 11.6 Hz, 6.2 Hz, 3.0 Hz, 1H), 2.01 (dd, J = 14.0 Hz, 3.1 Hz, 1H), 1.55 (ddd, J = 14.1 Hz, 11.6 Hz, 0.8 Hz, 1H), 1.33 (s, 3H), 1.28 (s, 3H), 1.23 (d, J = 6.2 Hz, 3H). **^{19}F NMR** (377 MHz, DMSO) δ = -103.22. **^{11}B NMR** (128 MHz, DMSO) δ = 26.3. **^{13}C NMR** (101 MHz, DMSO) δ = 165.1 (dd, J = 244.6 Hz, 13.9 Hz), 132.7 (t, J = 10.3 Hz), 111.5 (m), 72.7 (s), 66.1 (s), 45.6 (s), 31.1 (s), 28.7 (s), 23.1 (s). The carbon attached to boron was not detected. **M.p.** (°C) = 52 – 56. **Vmax (neat)/cm^{-1}** 2975, 2919, 1618, 1574, 1450, 1399, 1383, 1369, 1346, 1328, 1316, 1292, 1274, 1219, 1205, 1159, 1137, 1106, 1057, 1040, 979, 906, 876, 837, 794, 765, 734, 680, 662, 652, 566, 548, 514, 454, 437, 419. **HRMS (ESI)** *m/z* calc. for [MH^{+}] $C_{12}H_{16}O_2{}^{11}BF_2$: 241.11830, found: 241.12059.

4.2.14 2,6-Difluorophenylboronic acid 2,4-dimethyl-2,4-pentanediol ester, **2i**

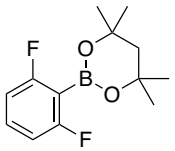

2,6-difluorophenylboronic acid (1.98 mmol, 0.31 g) was added to a 25 mL RBF equipped with a stir bar. To this was added 10 mL diethyl ether, followed by 2,4-dimethyl-2,4-pentanediol (1.94 mmol, 0.28 mL). The reaction mixture was allowed to stir at room temperature overnight with 4 Å molecular sieves. The reaction was filtered and concentrated *in-vacuo* to give a white crystalline solid. The product was dried under high vacuum (0.26 g, 52% yield).**^{1}H NMR** (400 MHz, DMSO-*d$_6$*) δ = 7.43 (m, 1H), δ = 6.96 (m, 2H), δ = 1.99 (s, 2H), δ = 1.37 (s, 12H). **^{13}C NMR** (101 MHz, DMSO-*d$_6$*) δ = 164.5 (dd, J = 244.4 Hz, 14.2 Hz), δ = 132.1 (t, J = 10.3 Hz), δ = 110.9 (m), δ = 72.0 (s), δ = 48.0 (s), δ = 31.2 (s). The carbon attached to boron was not detected. **^{19}F NMR** (377 MHz, DMSO-*d$_6$*) δ = - 98.87 (m). **^{10}B NMR** (128 MHz, DMSO-*d$_6$*) δ = 30.8. **^{11}B NMR** (128

MHz, DMSO-d_6) δ = 30.78. **M.p.**(°C) = 91 – 93. **V_{max} (neat)/cm^{-1}** 2983, 1617, 1570, 1447, 1371, 1328, 1296, 1192, 1141, 1105, 980, 800, 767, 660, 536, 514. **HRMS (ESI)** *m/z* calc. for [MH$^+$] $C_{12}H_{18}O_2{}^{11}BF_2$: 255.13840, found: 255.13624.

4.2.15 2,6-Difluorophenylboronic acid 2,4-dimethyl-2,4-hexanediol ester, **2j**

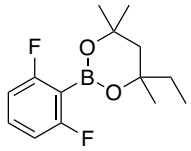

To a 50 mL round-bottomed flask equipped with a stir bar, was added 2,6-difluorophenyl boronic acid (1 equiv., 3.80 mmol, 0.60 g) which was then dissolved in 26 mL Et_2O, followed by the addition of 2,4-dimethyl-2,4-hexanediol (3.81 mmol, 0.56 g).[128] The reaction mixture was allowed to stir at room temperature overnight with 4 Å molecular sieves. The mixture was filtered and concentrated on rotary evaporator to give a white crystalline solid. The product was dried under high vacuum (0.58 g, 71%). **^{1}H NMR** (400 MHz, DMSO-d^6) δ = 7.43 (tt, J = 8.3 Hz, 7.0 Hz, 1H), 7.02 – 6.91 (m, 2H), 1.92 (m, 2H), 1.61 (qd, J = 7.5 Hz, 4.3 Hz, 2H), 1.41 (s, 3H), 1.34 (s, 6H), 0.90 (t, J = 7.5 Hz, 3H). **^{19}F NMR** (377 MHz, DMSO-d^6) δ = -103.52. **^{11}B NMR** (128 MHz, DMSO-d^6) δ = 26.3. **^{13}C NMR** (101 MHz, DMSO-d^6) δ = 165.1 (dd, J = 244.6 Hz, 14.1 Hz), 132.6 (t, J = 10.3 Hz), 111.5 (m), 74.7 (s), 72.3 (s), 45.8 (s), 36.9 (s), 32.2 (s), 31.4 (s), 28.3 (s), 8.4 (s). The carbon attached to boron was not detected. **M.p.** (°C) = 35 – 38. **V_{max} (neat)/cm^{-1}** 2971, 2919, 1619, 1576, 1450, 1424, 1381, 1329, 1296, 1218, 1183, 1134, 1106, 1056, 1005, 980, 865, 808, 796, 765, 722, 681, 662, 624, 590, 580, 545, 522, 512, 463, 455, 441, 427, 418. **HRMS (ESI)** *m/z* calc. for [MH$^+$] $C_{14}H_{20}O_2{}^{11}BF_2$: 269.15170, found: 269.15189.

4.2.16 2-Fluorophenylboronic acid 2,4-dimethyl-2,4-pentanediol ester, **2k**

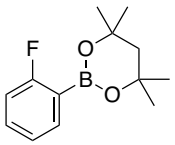

2-fluorophenylboronic acid (2.12 mmol, 0.29 g) was added to a 25 mL RBF equipped with a stir bar. To this was added 10 mL diethyl ether, followed by 2,4-dimethyl-2,4-pentanediol (2.08 mmol, 0.3 mL). The reaction mixture was allowed to stir at room temperature overnight with 4 Å molecular sieves. The reaction was filtered and concentrated *in-vacuo* to give a colourless-white crystalline solid. The product was dried under high vacuum (0.26 g, 53% yield). **^{1}H NMR** (400 MHz, DMSO-d_6) δ = 7.60 (m, 1H), 7.44 (m, 1H), 7.14 (m, 1H), 7.04 (m, 1H), 1.95 (s, 2H), 1.37 (s, 12H). **^{13}C NMR** (101 MHz, DMSO-d_6) δ = 167.1 (s), δ = 164.6 (s), 135.6 (d), 132.2 (d), 123.3 (d), 114.8 (d), 70.9 (s), 47.7 (s), 31.2 (s). The carbon attached to boron was not detected. **^{19}F NMR** (377 MHz, DMSO-d_6) δ = - 99.03 (m). **^{10}B NMR** (128 MHz, DMSO-d_6) δ = 31.1. **^{11}B NMR** (128 MHz, DMSO-d_6) δ = 30.96. **M.p.**(°C) = 44 – 46. **V_{max} (neat)/cm^{-1}** 2982, 1609, 1441, 1370, 1303, 1192, 1118, 1078, 820, 767, 658, 527. **HRMS (ESI)** *m/z* calc. for [MH$^+$] $C_{12}H_{19}O_2{}^{11}BF$: 237.14540, found: 237.14567.

4.2.17 3,5-Dimethyl isoxazolyl boronic acid 2,4-dimethyl-2,4-pentanediol ester, **9i**

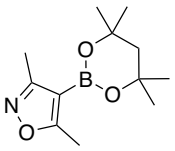

To a 25 mL round-bottomed flask, equipped with a stir bar, was added boronic acid (1.99 mmol, 0.281 g) and pinacol (1 equiv., 2.08 mmol 0.276 g) in 8 mL DCM. The reaction mixture was allowed to stir at room temperature for 4 hours with 4 A° molecular sieves. The solution was filtered and concentrated *in-*

vacuo to yield a white crystalline solid which was dried on a high vacuum line. Product yield was 38%. **^{1}H NMR** (400 MHz, DMSO-d^{6}) δ = 2.43 (3H, s), 2.21 (3H, s), 1.93 (2H s), 1.35 (12H, s). **^{13}C NMR** (101 MHz, DMSO-d^{6}) δ = 176.4 (s), 163.2 (s), 71.4 (s), 48.3 (s), 31.9 (s), 12.8 (s), 12.0 (s). The quaternary carbon for the heteroaryl C-B bond was not detected. **^{11}B NMR** (128 MHz, DMSO-d^{6}) δ = 25.7. **M.p.**(°C) = 72 – 74 °C. **V_{max} (neat)/cm^{-1}** 2970, 2927, 1604, 1419, 1350, 1314, 1200, 1100, 884, 774, 711, 623, 423. **HRMS (ESI)** *m/z* calc. for [MH^{+}] $C_{12}H_{20}O_3N_1{}^{11}B_1$: 237.15438, found: 237.15308.

4.3 *In-situ* reaction monitoring by ^{19}F NMR spectroscopy

4.3.1 General considerations

All *in-situ* reaction monitoring was performed on a Bruker Ascend 400 MHz spectrometer at 300 K (27 °C). A typical ^{19}F NMR monitoring experiment used a zg30 pulse sequence, an acquisition time of 1.468 seconds (4 scans) and a relaxation delay of 6 seconds. MestReNova versions 10.0 and 11.0 were used for processing all NMR spectra acquired.

The solvent system used for kinetics experiments was 1:1 1,4-dioxane/H_2O. 1 L of this solvent blend was made by adding 500 mL deionised H_2O to a 1 L volumetric flask and making up to the mark with 1,4-dioxane. The volumetric flask was then inverted ten times to mix. Unless otherwise stated, for reaction monitoring of the protodeboronation of boronic esters, boronic esters were prepared as stock solutions in 1,4-dioxane and the base in H_2O. In certain circumstances during reaction set-up, when equal volumes of 1,4-dioxane and H_2O were employed e.g., for Stopped-flow reaction monitoring by NMR spectroscopy of particular boronic esters, a solution of reagent in 1,4-dioxane was fired from syringe A to mix with a solution of reagent in H_2O fired from syringe B in a shot ratio of 0.5:0.5.

A high precision analytical balance (0.01 mg resolution) was used to weigh solid compounds and liquids were dispensed with gas-tight syringes and micro syringes.

Trifluoroacetic acid, or its potassium salt, was used as an internal standard for reaction monitoring by ^{19}F NMR spectroscopy, unless otherwise specified.

A Hanna instrument pH/ORP/ISE HI98191 pH meter was used with a Sigma-Aldrich micro pH combination, glass body electrode (Z113441, BNC connector, electrode L = 183 mm, Stem O.D. 3.5 mm) for pH measurements. Hanna instrument buffer solutions were used for calibration (pH 4.01, 7.01 and

10.01). The HI70300 storage solution for pH and ORP electrodes and HI7061 electrode cleaning solution for general use or 3.8 M KCl solution were utilised for care of the pH probe.

4.3.2 General procedures

General procedure A – Multi-point kinetics (*in-situ*) for polyfluorinated phenylboronic acids **2a**-**4a**.

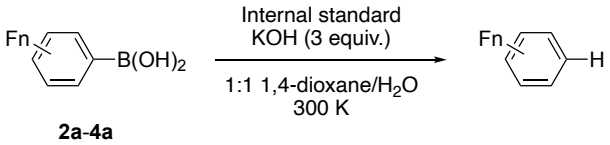

2a-**4a**

Scheme 36. Reaction conditions for the protodeboronation of boronic acids **2a**-**4a** at pH >13.

A stock solution of internal standard was prepared in 1:1 1,4-dioxane/H_2O. Internal standard was added by micro syringe directly to the volumetric flask. The stock solution of internal standard in 1:1 1,4-dioxane/H_2O was used to prepare a separate stock solution with boronic acid. A stock solution of KOH in 1:1 1,4-dioxane/H_2O was prepared in a volumetric flask.

Reaction monitoring by *in-situ* NMR spectroscopy was performed in a 5 mm borosilicate glass NMR tube. Reagent solution of boronic acid with internal standard was added to the NMR tube, which was capped, mixed by inversion and wiped clean. The sample was loaded into the NMR spectrometer with a probe temperature of 300 K. The command 'lock off' was applied since the sample was prepared in protic solvent, followed by tuning, shimming and spectrum acquisition to afford a ^1H t_0 spectrum. Prior to ejecting the sample, a ^{19}F NMR spectrum was also acquired.

Reagent solution of KOH was added to the NMR tube. The tube was capped immediately, and then to ensure sufficient mixing, the solution was shaken vigorously by inverting both horizontally and vertically for 10 seconds. The

NMR tube was inserted into the spectrometer and reaction monitoring was initiated. A stopwatch was used to record the 'dead time' between the addition of base and the first ^{19}F spectrum acquired.

General procedure B – Multi-point kinetics (stopped-flow) for polyfluorinated phenylboronic acids **5a**-**6a**.

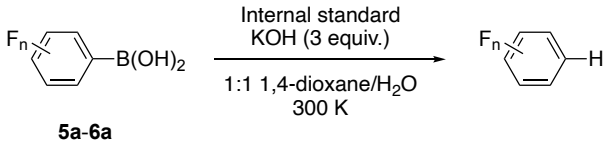

5a-**6a**

Scheme 37. Reaction conditions for the protodeboronation of boronic acids **5a**-**6a** at pH >13.

Stock solutions of boronic acid with TFA internal standard, and KOH were prepared separately in 1:1 1,4-dioxane/H_2O in volumetric flasks. The stock solutions were transferred to Schott reagent bottles equipped with 3-valve caps with threaded ports (Diba Labware: QSeries cap, GL32, 3 ports + valves), and connected to stopped-flow syringes respectively. On each reagent bottle, 1 valve was opened for venting purposes. The stopped-flow system was washed prior to running kinetic experiments with a solution of 1:1 1,4-dioxane/H_2O which was prepared in a reservoir bottle.

The waste line from the syringe drive was inserted into a waste solvent bottle in the fumehood and clamped in place. The thermostating unit was set to 27 °C, the umbilical inserted into the NMR spectrometer and the trigger output connected to the Bruker Prodigy 400 spectrometer console unit. Kinetic experiments were initiated using a pseudo-2D triggered pulse programme. The reactions were carried out at 300 K by performing a shot of a total volume of 600 µL, by injecting 300 µL boronic acid with TFA and 300 µL KOH at a flow rate of 1 mL s^{-1} (transport deadtime = 0.15 s).

For details of the SF-NMR system see references.[129, 113]

General procedure C – Multi-point kinetics (*in-situ*) for pinacol esters **2b**-**5b** and boronic esters **2c**, **2h** and **2j**.

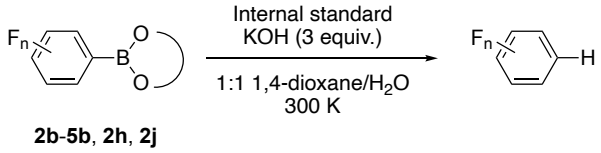

2b-**5b**, **2h**, **2j**

Scheme 38. Reaction conditions for the protodeboronation of pinacol esters **2b**-**5b** and boronic esters **2c**, **2h** and **2j**, at pH >13.

A stock solution of internal standard was prepared in 1,4-dioxane. Internal standard was added by micro syringe directly to the volumetric flask. The stock solution of internal standard in 1,4-dioxane was used to prepare a separate stock solution with boronic ester. A stock solution of KOH in H_2O was prepared in a volumetric flask.

Reaction monitoring was performed as per general procedure A. Equal volumes of boronic ester/internal standard in 1,4-dioxane and KOH in H_2O were added to the NMR tube to achive 1:1 ratio of 1,4-dioxane/H_2O in the final reaction mixture, the latter added to initiate the protodeboronation reaction.

General procedure D – Multi-point kinetics (stopped-flow) for polyfluorinated phenyl pinacol ester **6b** and boronic esters **2e**, **2g**-**2i**, **1i**.

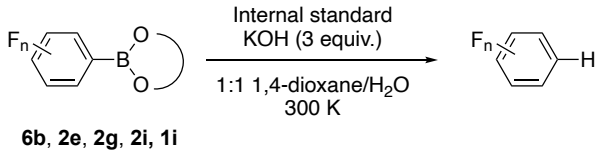

6b, **2e**, **2g**, **2i, 1i**

Scheme 39. Reaction conditions for the protodeboronation of pinacol ester **6b** and boronic esters **2e, 2g-2i, 1i** at pH >13.

Stock solutions of boronic ester with TFA internal standard, and KOH were prepared separately in volumetric flasks, in 1,4-dioxane and H_2O respectively. The stock solutions were transferred to Schott reagent bottles equipped with 3-valve caps with threaded ports (Diba Labware: QSeries cap, GL32, 3 ports

+ valves), and connected to stopped-flow syringes respectively. On each reagent bottle, 1 valve was opened for venting purposes. The stopped-flow system was washed prior to running kinetic experiments with a solution of 1:1 1,4-dioxane/H_2O which was prepared in a reservoir bottle. The reagent line with boronic ester/internal standard was washed with a solution of 1,4-dioxane.

Stopped-flow NMR spectroscopy was performed as per general procedure B.

General procedure E – Multi-point kinetics (*in-situ* and stopped-flow) for the base-catalysed protodeboronation of 2,6-difluorophenylboronic acid **2a** in the presence of diol.

1. *Addition of base to boronic acid **2a** pre-equilibrated with diol (in-situ reaction monitoring):*

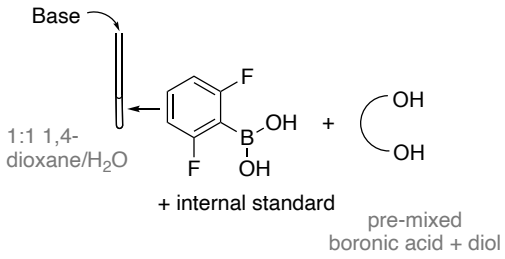

Scheme 40. Addition of base to a pre-equilibrated mixture of boronic acid/internal standard and diol.

A stock solution of internal standard was prepared in 1:1 1,4-dioxane/H_2O. Internal standard was added by micro syringe directly to the volumetric flask. The stock solution of internal standard in 1:1 1,4-dioxane/H_2O was used to prepare a separate stock solution with boronic acid. A stock solution of base in 1:1 1,4-dioxane/H_2O was prepared in a volumetric flask. A stock solution of diol in 1:1 1,4-dioxane/H_2O was prepared in a volumetric flask.

Reagent solution of boronic acid with internal standard (0.4 mL) and diol solution (0.2 mL) was added to the NMR tube (total volume = 0.6 mL), which

was capped, mixed by inversion, and wiped clean. The sample was loaded into the NMR spectrometer with a probe temperature of 300 K. The command 'lock off' was applied since the sample was prepared in protic solvent, followed by tuning, shimming and spectrum acquisition to afford a ^{1}H t_0 spectrum. Prior to ejecting the sample, a ^{19}F NMR spectrum was also acquired.

Reagent solution of base was added to the NMR tube (0.2 mL). The tube was capped immediately, and then to ensure sufficient mixing, the solution was shaken vigorously by inverting both horizontally and vertically for 10 seconds. The NMR tube was inserted into the spectrometer and reaction monitoring was initiated. A stopwatch was used to record the 'dead time' between the addition of base and the first ^{19}F spectrum acquired.

2. *Addition of pre-mixed base and diol to boronic acid* ***2a*** *(in-situ reaction monitoring):*

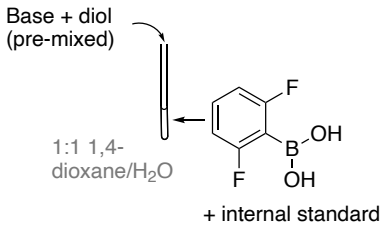

Scheme 41. Addition of a pre-mixed solution of base and diol to a solution of boronic acid/internal standard.

A stock solution of internal standard was prepared in 1:1 1,4-dioxane/H_2O. Internal standard was added by micro syringe directly to the volumetric flask. The stock solution of internal standard in 1:1 1,4-dioxane/H_2O was used to prepare a separate stock solution with boronic acid. A stock solution of KOH in 1:1 1,4-dioxane/H_2O was prepared in a volumetric flask. A stock solution of diol in 1:1 1,4-dioxane/H_2O was prepared in a volumetric flask.

Reagent solution of boronic acid with internal standard (0.6 mL) was added to the NMR tube, which was capped, mixed by inversion and wiped clean. The sample was loaded into the NMR spectrometer with a probe temperature of 300 K. The command 'lock off' was applied since the sample was prepared in protic solvent, followed by tuning, shimming and spectrum acquisition to afford a ^{1}H t_0 spectrum. Prior to ejecting the sample, a ^{19}F NMR spectrum was also acquired.

Reagent solution of base pre-mixed with diol solution was added to the NMR tube (0.2 mL, total reaction volume = 0.8 mL). The tube was capped immediately, and then to ensure sufficient mixing, the solution was shaken vigorously by inverting both horizontally and vertically for 10 seconds. The NMR tube was inserted into the spectrometer and reaction monitoring was initiated. A stopwatch was used to record the 'dead time' between the addition of base and the first ^{19}F spectrum acquired.

3. *Addition of base to boronic acid **2a** pre-equilibrated with diol (stopped-flow):*

In volumetric flasks, a stock solution of boronic acid with TFA internal standard and 2-hydroxymethyl-2-methyl-1,3-propanediol was prepared and a separate stock solution of KOH, in 1:1 1,4-dioxane/H_2O. The stock solutions were transferred to Schott reagent bottles equipped with 3-valve caps with threaded ports (Diba Labware: QSeries cap, GL32, 3 ports + valves), and connected to stopped-flow syringes respectively. On each reagent bottle, 1 valve was opened for venting purposes. The stopped-flow system was washed prior to running kinetic experiments with a solution of 1:1 1,4-dioxane/H_2O which was prepared in a reservoir bottle.

Stopped-flow NMR spectroscopy was performed as per **general procedure B**.

4.3.3 Temporal-concentration profiles and kinetic simulations

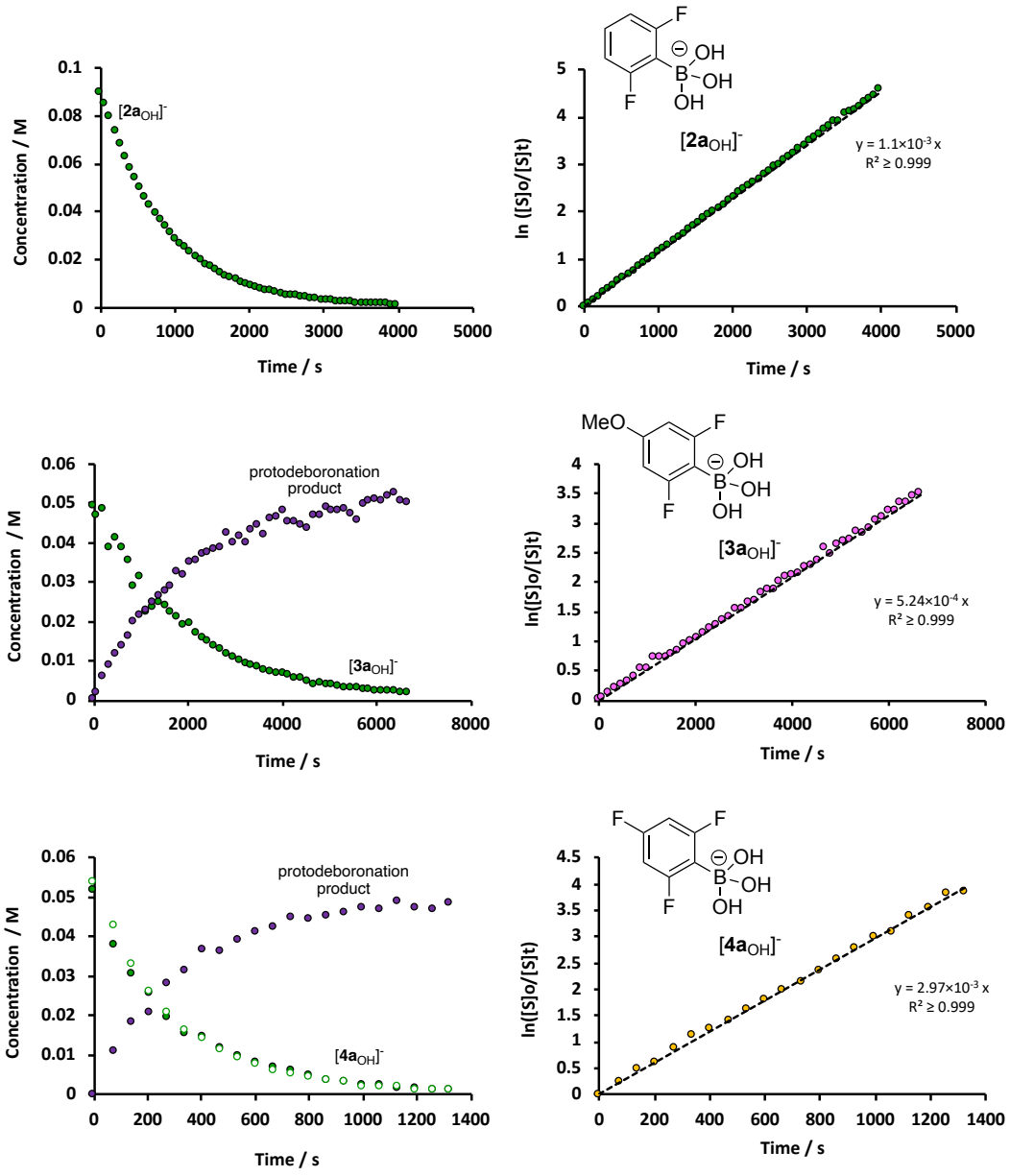

Figure 36. Reaction profiles and first order decay plots for the protodeboronation of boronic acids **2a**-**4a** at pH >13, in 1:1 1,4-dioxane/H_2O at 300 K (according to **general procedure A**).

Table 8. Reaction conditions and setup for the protodeboronation of $[\mathbf{2a}_{OH}]^-$ at pH > 13.

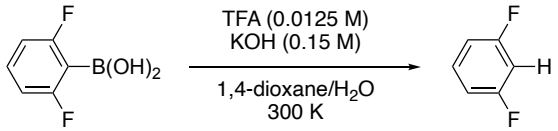

2a 0.05 M

Reagent	Conc. in stock solution (M)	Conc. in reaction (M)	Vol. of stock (mL)	Solvent	Syringe
2a/TFA	0.10/0.024	0.05/0.012	20	dioxane/H_2O	A2
2a/TFA	0.10/0.024	0.05/0.012	7.5	dioxane	A1
KOH	0.3	0.15	20	dioxane/H_2O	B
H_2O					C

% H_2O	Conc. H_2O (M)	A1	B	C	A2	B	C
30	16.7	0.5	0.4	0.1			
25	19.4	0.5	0.3	0.2			
40	22.2	0.5	0.2	0.3			
45	24.9	0.5	0.1	0.4			
50	27.8				0.5	0.5	0
55	30.6				0.5	0.4	0.1
60	33.3				0.5	0.3	0.2
65	36.1				0.5	0.2	0.3
70	38.8				0.5	0.1	0.4

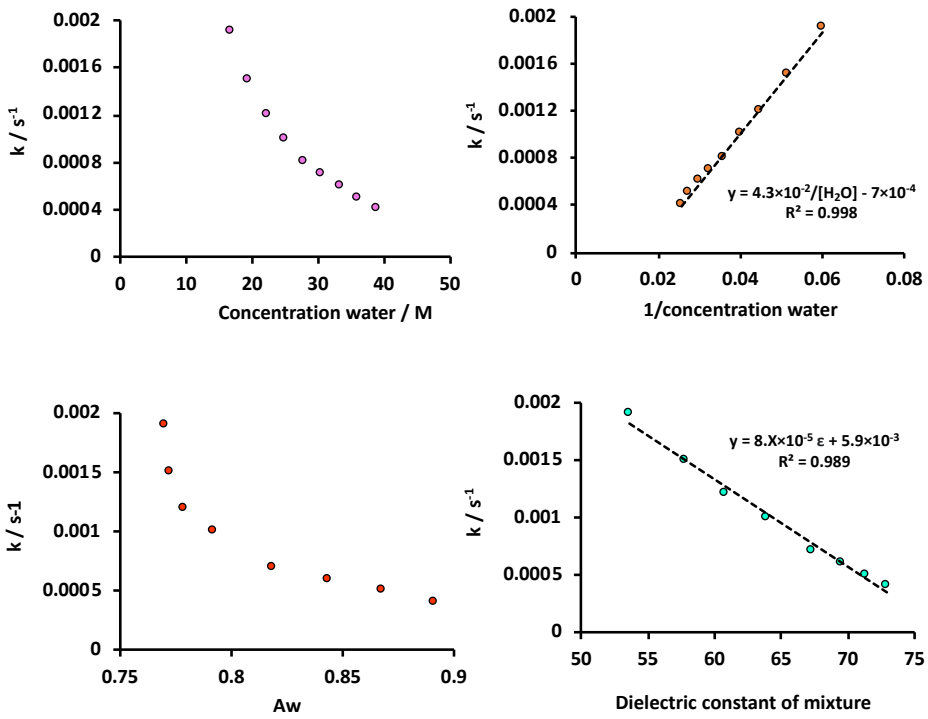

Figure 37. Graphical analysis for the protodeboronation of $[\mathbf{2a}_{OH}]^-$ at pH > 13 monitored by ^{19}F NMR spectroscopy using Stopped-flow (flow rate = 1 mL/s, t_{AQ} (acquisition time) = 0.5 s, d_{20} (trigger delay) = 0.04 s, d_1 (relaxation delay) = 3 s and flip angle = 90°), varying the % H_2O (H_2O 55.4 M and 1:1 1,4-dioxane/H_2O: 27.8 M H_2O).

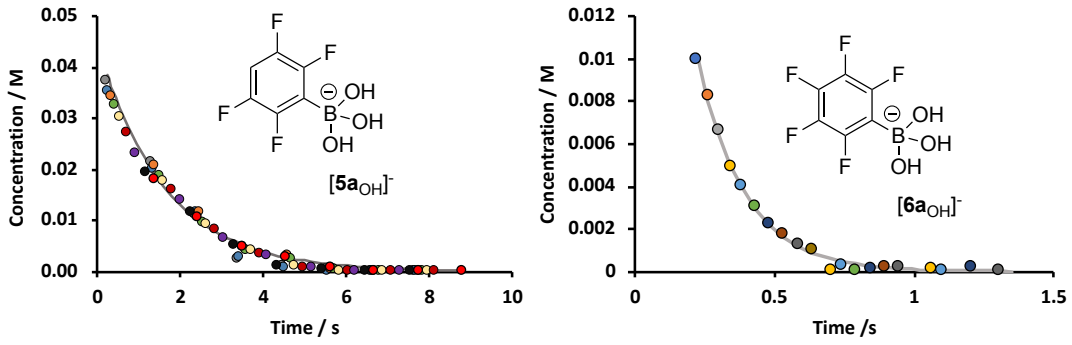

Figure 38. Reaction profiles for the protodeboronation of **5a**-**6a** at pH >13, in 1:1 1,4-dioxane/H_2O at 300 K (according to **general procedure B**). **5a**) Different coloured data represents interleaved experiments with incremented d_{20} (trigger delay), d_1 = 0.2 s, t_{AQ} = 0.8 s, flip angle = 45°. Grey line represents the fitted data to obtain a rate constant of 0.61 s^{-1}. **6a**) Different coloured data represents interleaved experiments with incremented d_{20} (trigger delay), d_1 = 0 s, t_{AQ} = 0.3 s, flip angle = 60°. Grey line represents the fitted data to obtain a rate constant of 5.93 s^{-1}. Stopped-flow ^{19}F NMR spectroscopy performed by Ran Wei.[113]

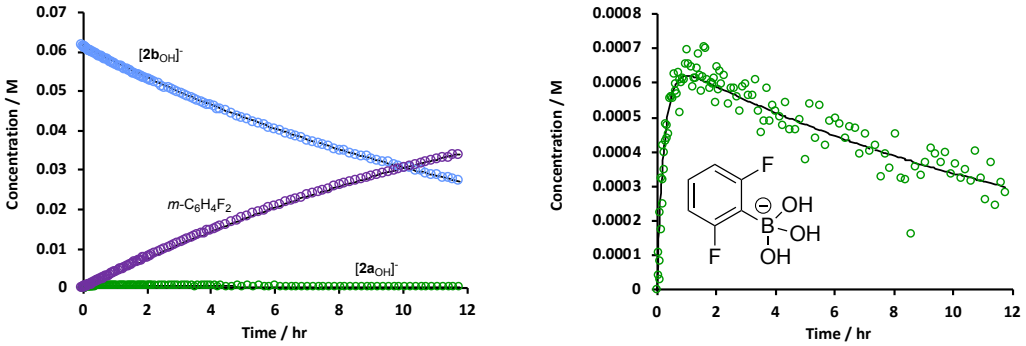

Reaction process	Rate constant (*k*)	Unit
[**2a**$_{OH}$]$^-$ > *m*-$C_6H_4F_2$ + **2a**	1.25 x 10^{-3}	1/s
[**2b**$_{OH}$]$^-$ > *m*-$C_6H_4F_2$ + **2b**	5.83 x 10^{-6}	1/s
[**2b**$_{OH}$]$^-$ > [**2a**$_{OH}$]$^-$ + PIN	1.37 x 10^{-5}	1/s
[**2a**$_{OH}$]$^-$ + PIN > [**2b**$_{OH}$]$^-$	3.60 x 10^{-5}	L/mol.s

Figure 39. Temporal-concentration profile (including inset, right) and kinetic simulations for the protodeboronation of [**2b**$_{OH}$]$^-$ at pH > 13, in 1:1 1,4-dioxane/H_2O at 300 K (according to **general procedure C**).

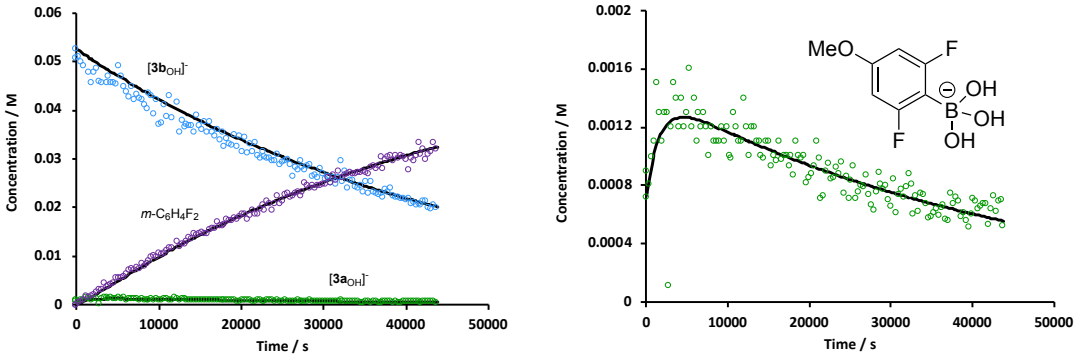

Reaction process	Rate constant (*k*)	Unit
[**3b**$_{OH}$]$^-$ > protodeboronation product	5.78 x 10^{-6}	1/s
[**3a**$_{OH}$]$^-$ > protodeboronation product	6.03 x 10^{-4}	1/s
[**3b**$_{OH}$]$^-$ > [**3a**$_{OH}$]$^-$ + PIN	1.61 x 10^{-5}	1/s
[**3a**$_{OH}$]$^-$ + PIN > [**3b**$_{OH}$]$^-$	3.60 x 10^{-5}	L/mol.s

Figure 40. Temporal-concentration profile (including inset, right) and kinetic simulations for the protodeboronation of [**3b**$_{OH}$]$^-$ at pH > 13, in 1:1 1,4-dioxane/H_2O at 300 K (according to **general procedure C**).

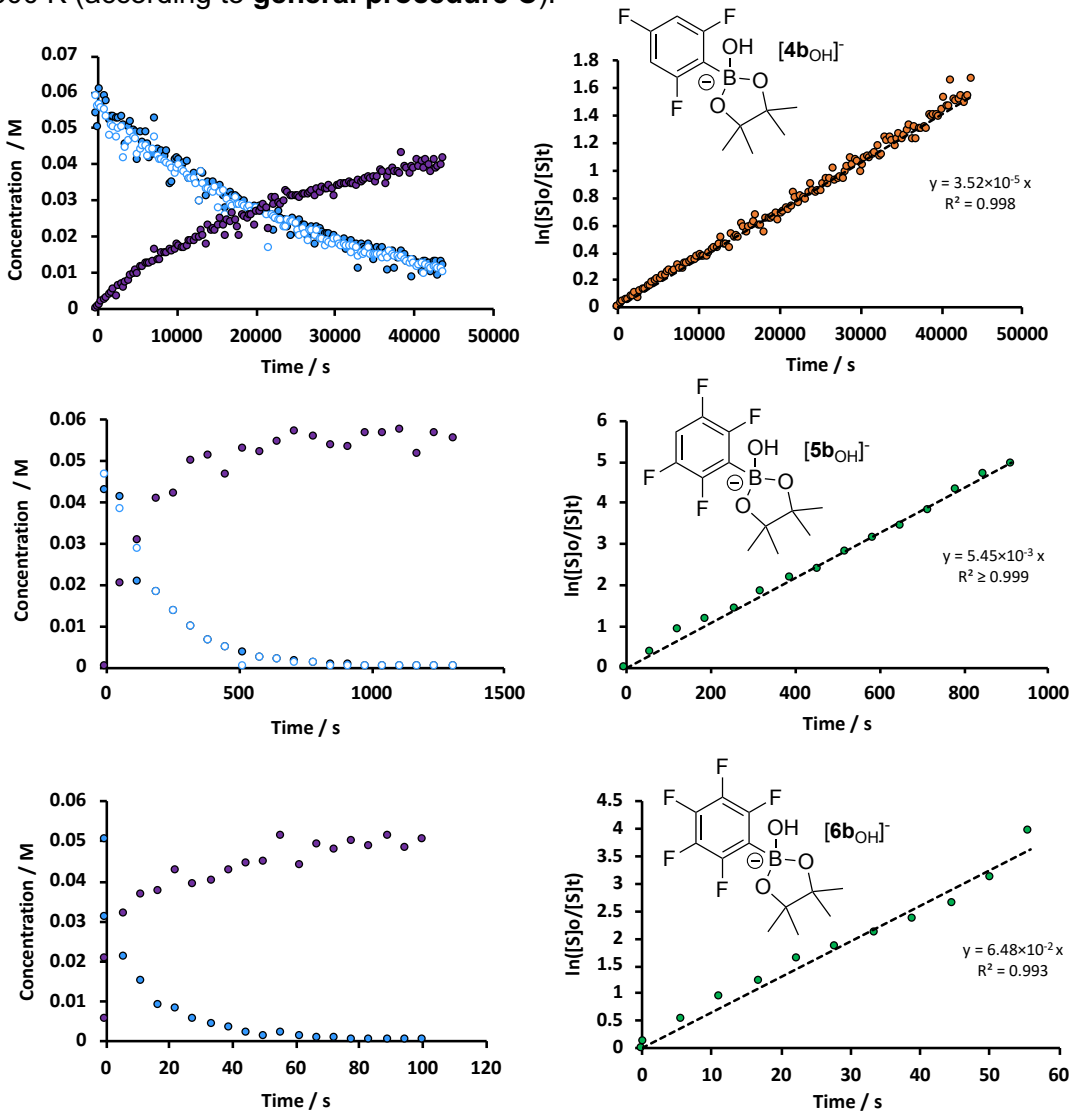

Figure 41. Reaction profiles and first order decay plots for the protodeboronation of pinacol esters **4b**-**6b** at pH >13, in 1:1 1,4-dioxane/H_2O at 300 K (according to **general procedure C** for **4b** and **5b** and **general procedure D** for **6b**). Stopped-flow conditions for **6b**: flow rate = 1 mL/s, t_{AQ} = 1 s, d_{20} (trigger delay) = 0.04 s, d_1 (relaxation delay) = 5 s and flip angle = 90°.

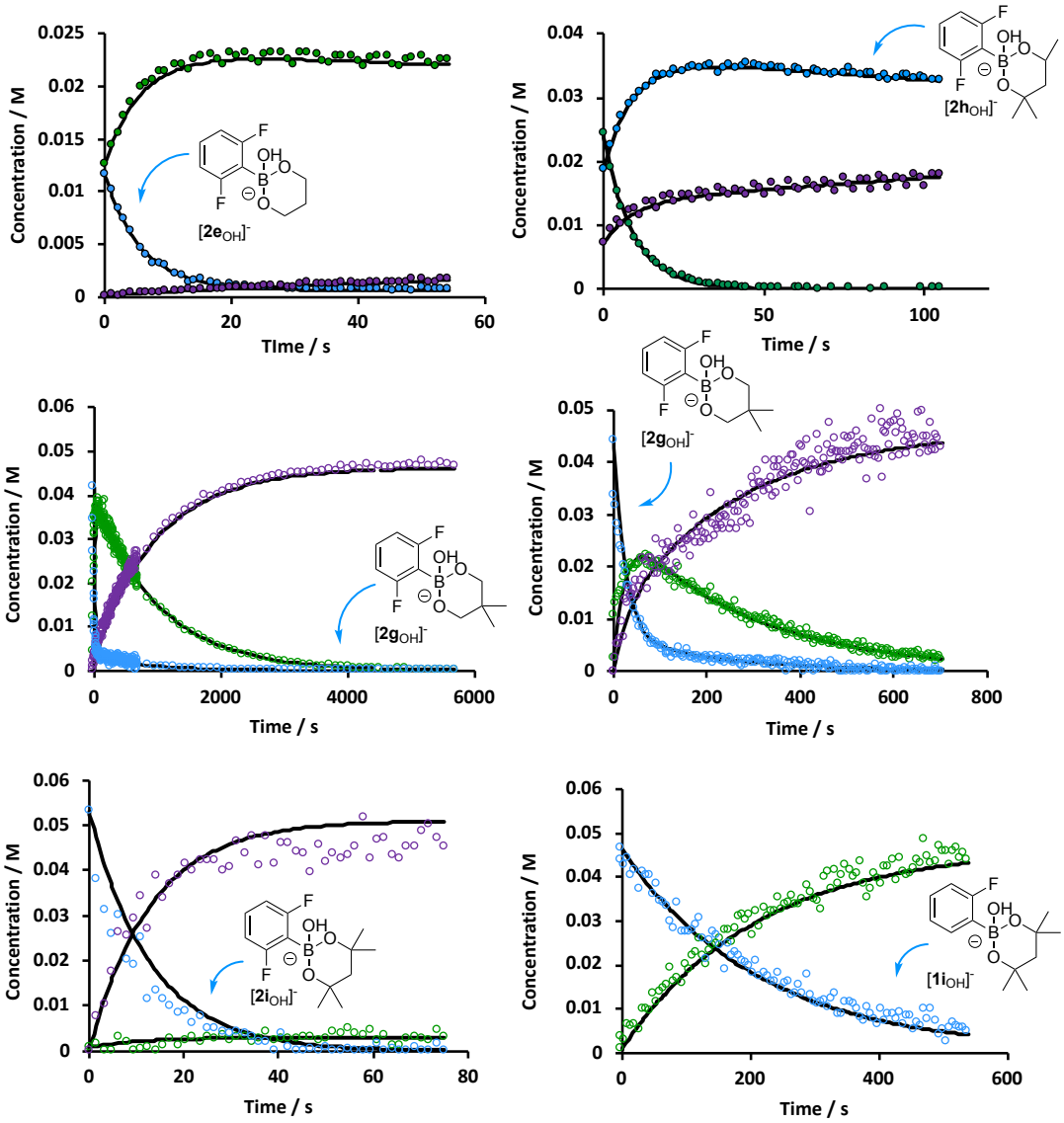

Figure 42. Temporal-concentration profiles for the protodeboronation of boronic esters **2e, 2g, 2i, 1i** at pH >13, in 1:1 1,4-dioxane/H_2O at 300 K (according to **general procedure D**). For **2e**: profile obtained by interleaving multiple data sets. For **2h**: stopped-flow ^{19}F NMR spectroscopy – flow rate = 1 mL/s, t_{AQ} = 1 s, flip angle = 45°. Profile generated using an interleaving technique from three stopped-flow runs varying the delay times. Experiment 1 (d_{20} 0.04 s, d_1 5 s), experiment 2 (d_{20} 2.4 s, d_1 5 s) and experiment 3 (d_{20} 4.4 s, d_1 5 s). [**2h**$_{OH}$]$^-$ exists as a mixture (4.2/1 ratio) of rapidly equilibrating diastereomers but modelled as a single species. For **2g** (left profile): stopped-flow ^{19}F NMR spectroscopy – flow rate = 1 mL/s, t_{AQ} = 0.5 s, d_{20} (trigger delay) = 0.04 s, d_1 (relaxation delay) = 3 s and flip angle = 90°. For **2g** (right profile): Reaction in 75:25 1,4-dioxane/H_2O and stopped-flow ^{19}F NMR spectroscopy – flow rate = 1 mL/s, t_{AQ} = 0.5 s, d_{20} (trigger delay) = 0.04 s, d_1 (relaxation delay) = 3 s and flip angle = 90°. For **2i**: stopped-flow – flow rate = 1 mL/s, t_{AQ} = 0.5 s, d_{20} (trigger delay) = 0.1 s, d_1 (relaxation delay) = 1 s and flip angle = 90°. For **1i**: stopped-flow – flow rate = 1 mL/s, t_{AQ} = 0.5 s, d_{20} (trigger delay) = 0.04 s, d_1 (relaxation delay) = 5 s and flip angle = 90°.

Table 9. Rate coefficients for kinetic simulations for protodeboronation of 1,3-propanediol boronic ester **2e** at pH >13.

Reaction process	Rate constant (*k*)	Unit
$[\mathbf{2e}_{OH}]^-$ > protodeboronation product	4.09×10^{-3}	1/s
$[\mathbf{2a}_{OH}]^-$ > protodeboronation product	9.73×10^{-4}	1/s
$[\mathbf{2e}_{OH}]^-$ > $[\mathbf{2a}_{OH}]$- + 1,3-propanediol	1.56×10^{-1}	1/s
$[\mathbf{2a}_{OH}]^-$ + 1,3-propanediol > $[\mathbf{2e}_{OH}]^-$	4.19×10^{-1}	L/mol.s

Table 10. Rate coefficients for kinetic simulations for the hydrolysis of 2-methyl-2,4-pentanediol boronic ester **2h** at pH >13.

Reaction process	Rate constant (*k*)	Unit
$[\mathbf{2h}_{OH}]^-$ > protodeboronation product	3.00×10^{-2}	1/s
$[\mathbf{2a}_{OH}]^-$ > protodeboronation product	1.10×10^{-3}	1/s
$[\mathbf{2h}_{OH}]^-$ > $[\mathbf{2a}_{OH}]^-$ + 2-methyl-2,4-pentanediol	8.08×10^{-2}	1/s
$[\mathbf{2a}_{OH}]^-$ + 2-methyl-2,4-pentanediol > $[\mathbf{2h}_{OH}]^-$	$0.00 \times 10^{+0}$	L/mol.s

Table 11. Rate coefficients for kinetic simulations for protodeboronation of neopentyl glycol (NPG) boronic ester **2g** at pH >13 (left profile in **Figure 42**.

Reaction process	Rate constant (*k*)	Unit
$[\mathbf{2g}_{OH}]^-$ > protodeboronation product + B(OH)(NPG)	4.99×10^{-3}	1/s
$[\mathbf{2a}_{OH}]^-$ > protodeboronation product + $B(OH)_4$	7.15×10^{-4}	1/s
$[\mathbf{2g}_{OH}]^-$ > $[\mathbf{2a}_{OH}]^-$ + NPG	5.39×10^{-2}	1/s
$[\mathbf{2a}_{OH}]^-$ + NPG > $[\mathbf{2g}_{OH}]^-$	1.19×10^{-1}	L/mol.s

Table 12. Rate coefficients for kinetic simulations for protodeboronation of neopentyl glycol (NPG) boronic ester **2g** at pH >13 (right profile in **Figure 42**).

Reaction process	Rate constant (*k*)	Unit
$[\mathbf{2g}_{OH}]^-$ > protodeboronation product	1.16×10^{-2}	1/s
$[\mathbf{2a}_{OH}]^-$ > protodeboronation product	2.30×10^{-5}	1/s
$[\mathbf{2g}_{OH}]^-$ > $[\mathbf{2a}_{OH}]^-$ + NPG	2.20×10^{-2}	1/s
$[\mathbf{2a}_{OH}]^-$ + NPG > $[\mathbf{2g}_{OH}]^-$	2.83×10^{-1}	L/mol.s

Table 13. Rate coefficients for kinetic simulations for protodeboronation of 2,4-dimethyl-2,4-pentanediol boronic ester **2i** at pH >13.

Reaction process	Rate constant (*k*)	Unit
$[\mathbf{2i}_{OH}]^-$ > protodeboronation product	9.73×10^{-2}	1/s
$[\mathbf{2a}_{OH}]^-$ > protodeboronation product	1.10×10^{-3}	1/s
$[\mathbf{2i}_{OH}]^-$ > $[\mathbf{2a}_{OH}]^-$ + 2,4-dimethyl-2,4-pentanediol	3.58×10^{-3}	1/s

Table 14. Rate coefficients for kinetic simulations for the hydrolysis of 2,4-dimethyl-2,4-pentanediol boronic ester **1i** at pH >13.

Reaction process	Rate constant (*k*)	Unit
$[\mathbf{1i}_{OH}]^-$ > $[\mathbf{2a}_{OH}]^-$ + 2,4-dimethyl-2,4-pentanediol	4.65×10^{-3}	1/s
$[\mathbf{2a}_{OH}]^-$ + 2,4-dimethyl-2,4-pentanediol > $[\mathbf{1i}_{OH}]^-$	8.91×10^{-4}	L/mol.s

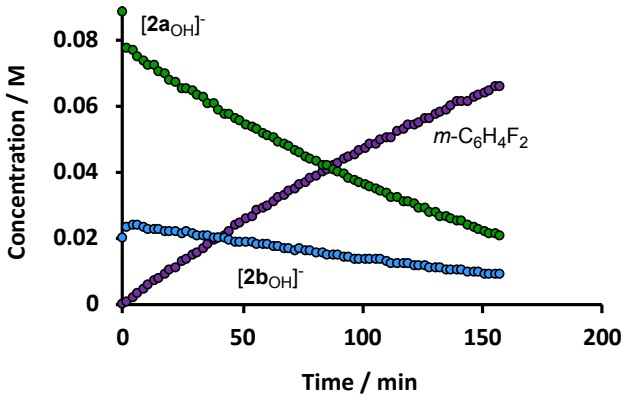

Figure 43. Temporal-concentration profile for the protodeboronation of **2a** pre-equilibrated with 2 equiv. pinacol (according to **general procedure E-1**, using 0.5 equiv. KOH).

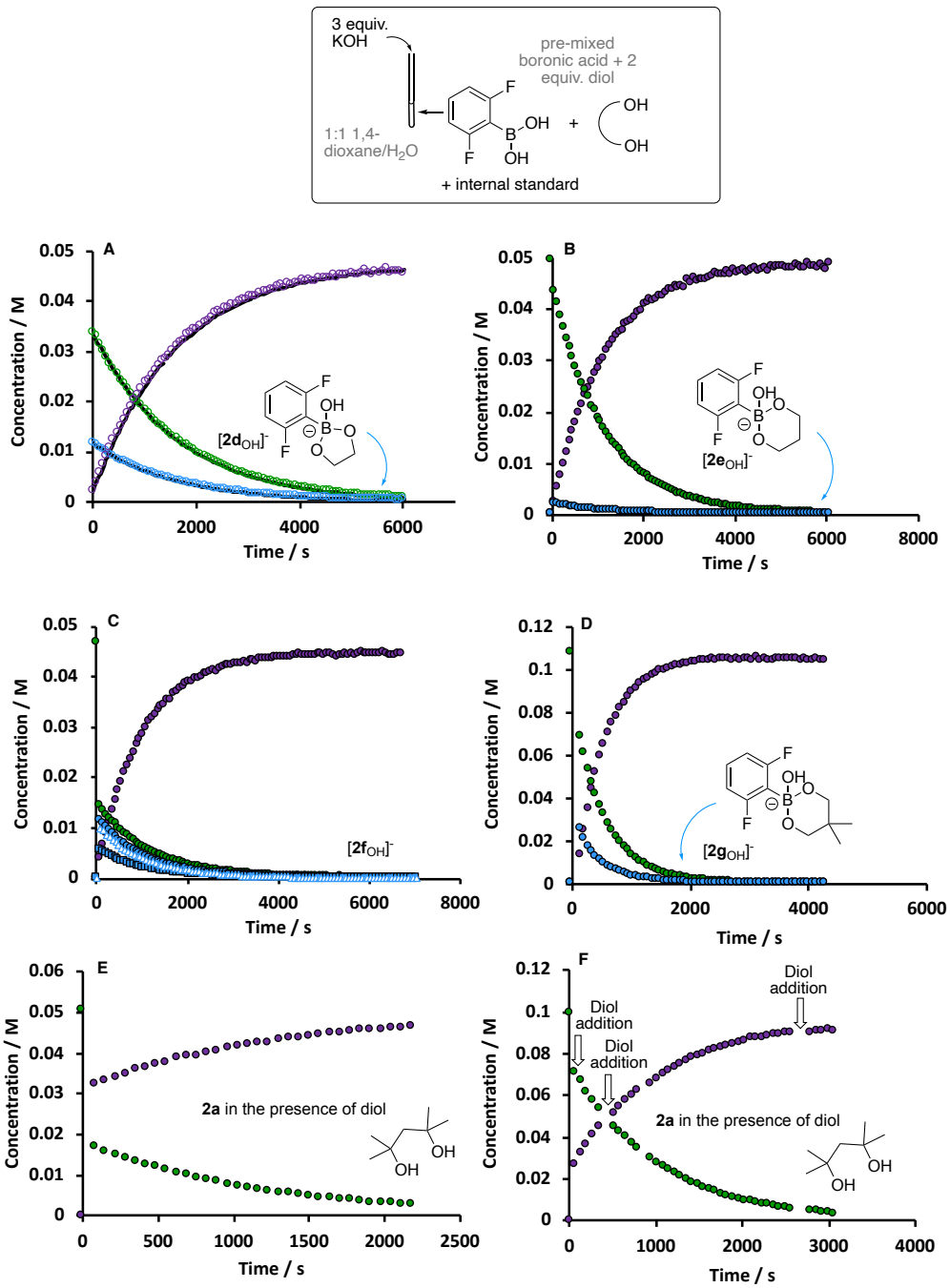

Figure 44. Temporal-concentration profiles for the protodeboronation of 2,6-difluorophenylboronic acid **2a** in the presence of diols, at pH >13, in 1:1 1,4-dioxane/H_2O at 300 K (according to **general procedure E-1**, involving the addition of KOH to a pre-equilibrated mixture of boronic acid/internal standard and diol). For **2f**: blue circles, triangles and squares correspond to 3 boronic ester isomers. F) 2a pre-equilibrated with 35% 2,4-dimethyl-2,4-pentanediol (0.028 mmol) and 3 equivalents KOH added. Subsequent additions of 35% 2,4-dimethyl-2,4-pentanediol added over the course of the reaction, after 340 seconds, 790 seconds and 2569 seconds.

Table 15. Rate coefficients from kinetic simulations for the protodeboronation, at pH > 13, of **2a** pre-equilibrated with ethylene glycol.

Reaction process	Rate constant (*k*)	Unit
$[\mathbf{2d}_{OH}]^-$ > protodeboronation product	1.00 x 10^{-5}	1/s
$[\mathbf{2a}_{OH}]^-$ > protodeboronation product	8.32 x 10^{-4}	1/s
$[\mathbf{2d}_{OH}]^-$ > $[\mathbf{2a}_{OH}]^-$ + ethylene glycol	6.32 x 10^{-4}	1/s
$[\mathbf{2a}_{OH}]^-$ + ethylene glycol > $[\mathbf{2d}_{OH}]^-$	1.14 x 10^{-6}	L/mol.s

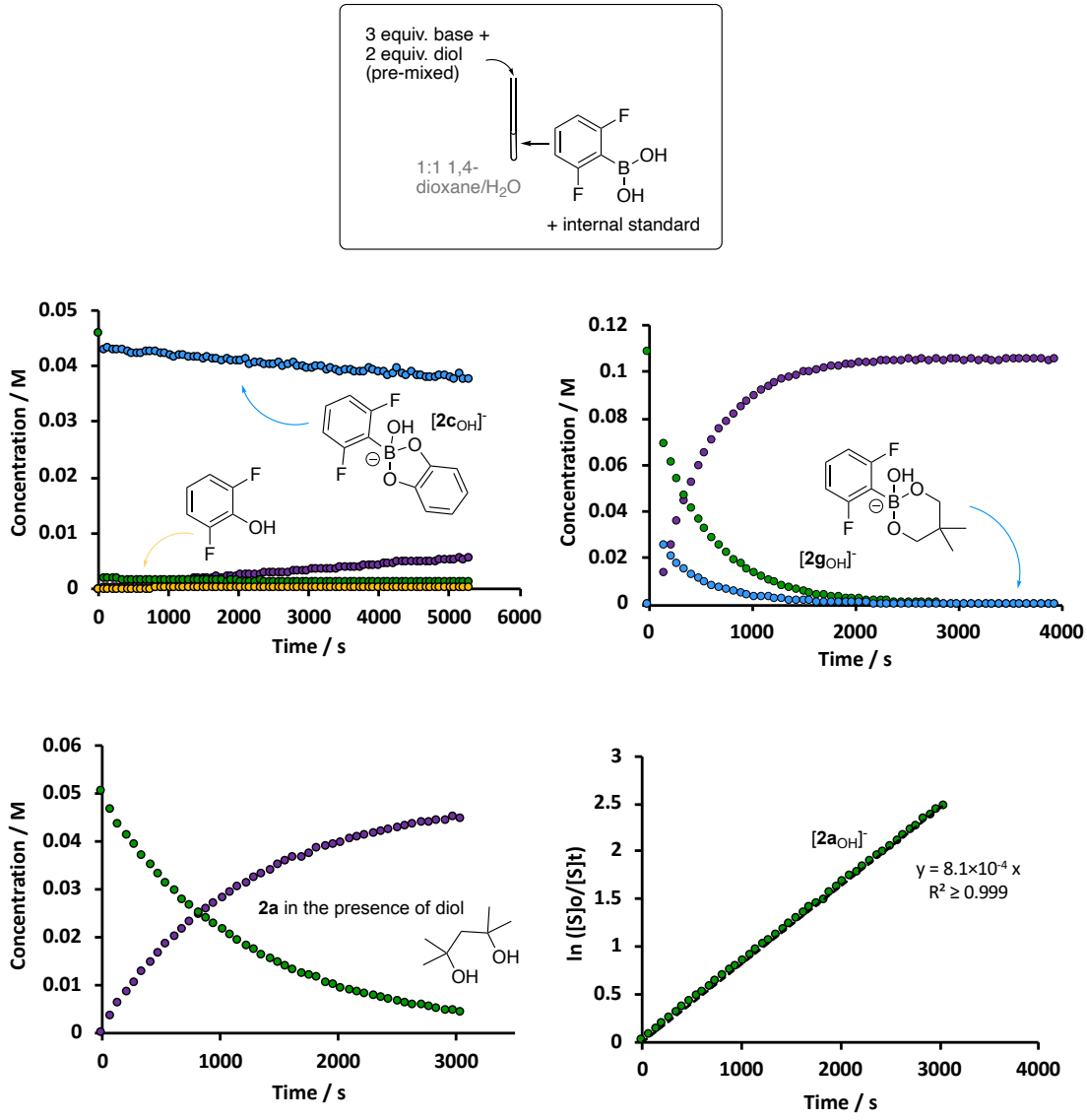

Figure 45. Temporal-concentration profiles for the protodeboronation of 2,6-difluorophenylboronic acid **2a** in the presence of diols, at pH >13, in 1:1 1,4-dioxane/H_2O at 300 K (according to **general procedure E-2**, involving the addition of 3-equivalents pre-mixed base and 2 equivalents diol to boronic acid **2a**).

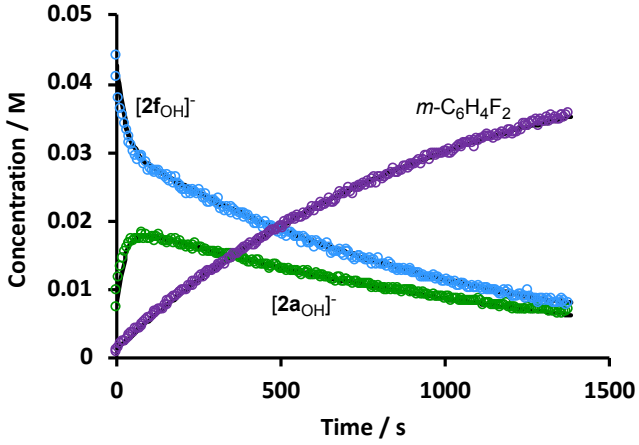

Reaction process	Rate constant (k)	Unit
[**2f**$_{OH}$]$^-$ > protodeboronation product	9.20 x 10^{-4}	1/s
[**2a**$_{OH}$]$^-$ > protodeboronation product	9.00 x 10^{-4}	1/s
[**2f**$_{OH}$]$^-$ > [**2a**$_{OH}$]$^-$ + triol	1.35 x 10^{-2}	1/s
[**2a**$_{OH}$]$^-$ + triol > [**2f**$_{OH}$]$^-$	3.20 x 10^{-1}	L/mol.s
B(OH)$_4$ + triol > B(OH)(triol)	2.88 x 10^{+8}	L/mol.s
B(OH)(triol) > B(OH)$_4$ + triol	1.00 x 10^{+2}	1/s
Protodeboronation product > phase	7.00 x 10^{-5}	1/s

Figure 46. Temporal-concentration profile and kinetic simulations for the protodeboronation of [**2a**$_{OH}$]$^-$ at pH > 13 in the presence of 2 equivalents 2-hydroxymethyl-2-methyl-1,3-propanediol (according to **general procedure E-3**). Reaction monitoring by stopped-flow ^{19}F NMR spectroscopy (flow rate = 1 mL/s, t_{AQ} = 1 s, d_{20} (trigger delay) = 0.04 s, d_1 (relaxation delay) = 5 s and flip angle = 45°). Boronic ester **2f** was treated as a single species for the purpose of kinetic modelling but was detected by ^{19}F NMR spectroscopy as 3 rapidly interconverting isomers. The structure/confirmation of each isomer was not elucidated.

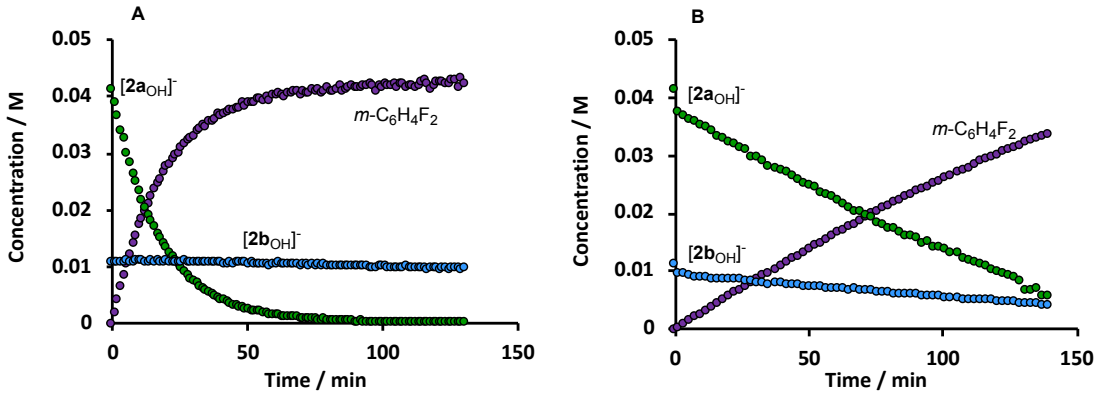

Figure 47. Temporal-concentration profiles for the protodeboronation of **2a** (according to **general procedure E-1**) pre-equilibrated with 2 equiv. pinacol (3:1 **2a**/**2b**) using tetrabutylammonium hydroxide (A) 3 versus B) 0.5 equiv.) as the base.

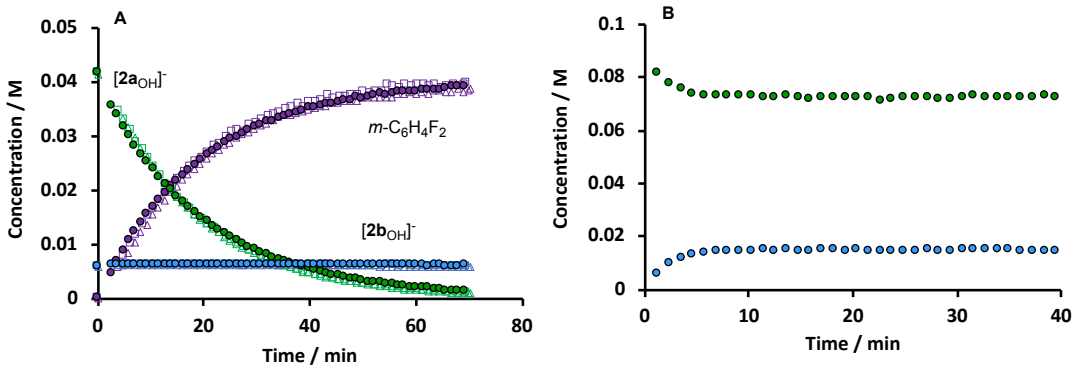

Figure 48. A) Reaction profiles overlayed for the protodeboronation of **2a** pre-equilibrated with pinacol (2 equiv.) at pH > 13 (according to **general procedure E-1**, using 3 equiv. KOH), varying the rate of addition of base (triangles: 49 seconds, squares: 13 seconds and circles: one shot, approx. 1 second). B) Graphical analysis for the esterification of **2a** with 2 equiv. pinacol to form the respective pinacol boronic ester **2b** (internal standard = F-naphthalene).

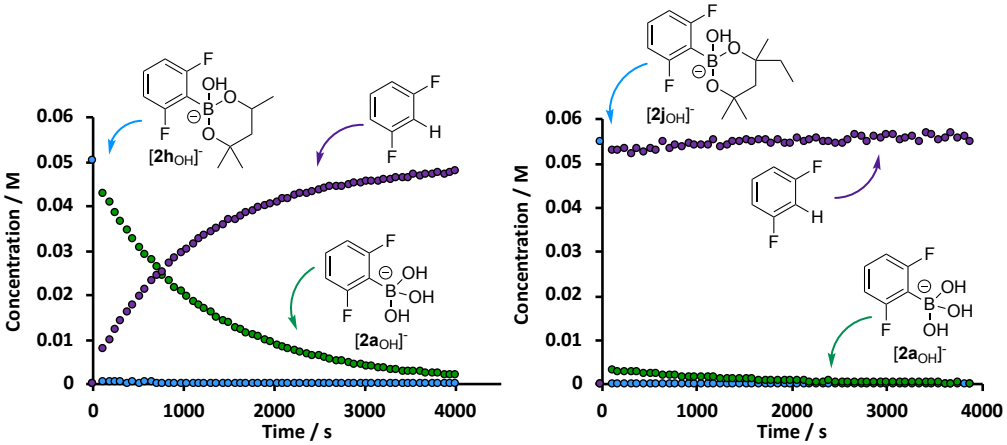

Figure 49. Reaction profiles for the protodeboronation of boronic esters **2h** and **2j** at pH >13, in 1:1 1,4-dioxane/H_2O at 300 K (according to **general procedure C**).

4.3.4 Experiments with catechol

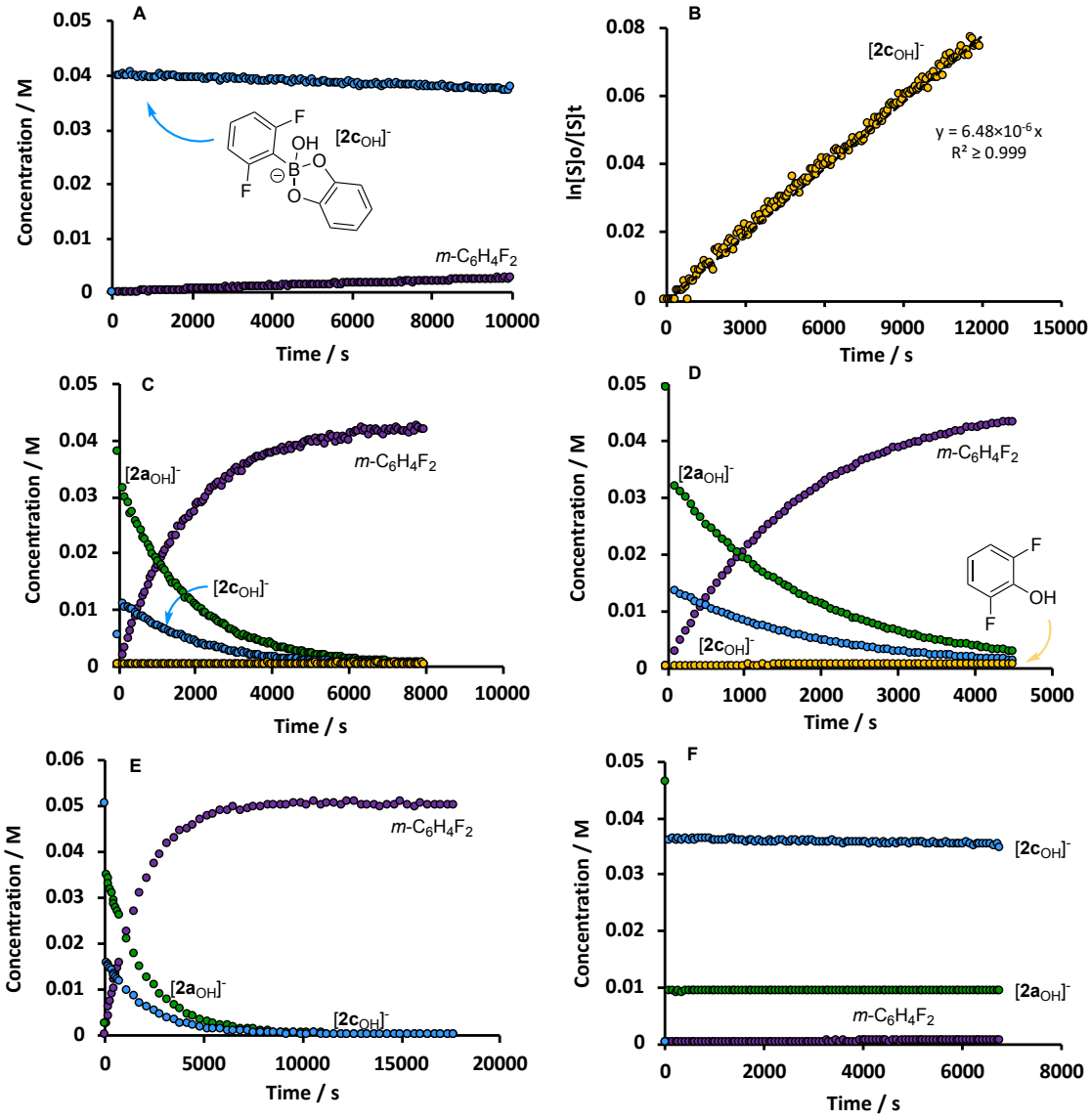

Figure 50.

A) Temporal-concentration profile and **B)** plot of first order decay for for the protodeboronation of 2,6-difluorophenylboronic acid **2a** (0.04 M) in the presence of catechol (0.05 M), at pH >13, in 1:1 1,4-dioxane/H_2O at 300 K (according to **general procedure E-1**, involving the addition of KOH (0.054 M) to a pre-equilibrated mixture of boronic acid/internal standard and catechol added neat – 4.85 mg, 0.044 mmol).

C) Temporal-concentration profile for the protodeboronation of 2,6-difluorophenylboronic acid **2a** pre-equilibrated with 1 equiv. catechol (according to **general procedure E-1**, involving the addition of 3 equiv. tertbutylammonium hydroxide).

D) Temporal-concentration profile for the protodeboronation of 2,6-difluorophenylboronic acid **2a** pre-equilibrated with 1 equiv. catechol (according to **general procedure E-1**, involving the addition of 3 equiv. KOH).

E) Reaction profile for the protodeboronation of boronic ester **2c** at pH >13, in 1:1 1,4-dioxane/H_2O at 300 K (according to **general procedure C**).

F) Temporal-concentration profile for the protodeboronation of 2,6-difluorophenylboronic acid **2a** pre-equilibrated with 2 equiv. catechol (according to **general procedure E-1**, involving the addition of 0.5 equiv. KOH).

Table 16. Rate coefficients from kinetic simulations for **Figure 28**. Stopped-flow ^{19}F NMR spectroscopy: flow rate = 1 mL/s, t_{AQ} = 0.5 s, flip angle = 90°. Profile generated using an interleaving technique from three stopped-flow runs varying the delay times. Experiment 1 (d_{20} 0.04 s, d_1 3 s), experiment 2 (d_{20} 0.04 s, d_1 1 s) and experiment 3 (d_{20} 0.01 s, d_1 1 s).

Reaction process	Rate constant (*k*)	Unit
$[\mathbf{2c}_{OH}]^-$ > protodeboronation product	6.40×10^{-6}	1/s
$[\mathbf{2a}_{OH}]^-$ > protodeboronation product	8.43×10^{-4}	1/s
$[\mathbf{2c}_{OH}]^-$ > $[\mathbf{2a}_{OH}]^-$ + CAT	$1.38 \times 10^{+0}$	1/s
$[\mathbf{2a}_{OH}]^-$ + CAT > $[\mathbf{2c}_{OH}]^-$	$4.81 \times 10^{+1}$	L/mol.s
$[\mathbf{2a}_{OH}]^-$ > phenol	1.14×10^{-6}	1/s

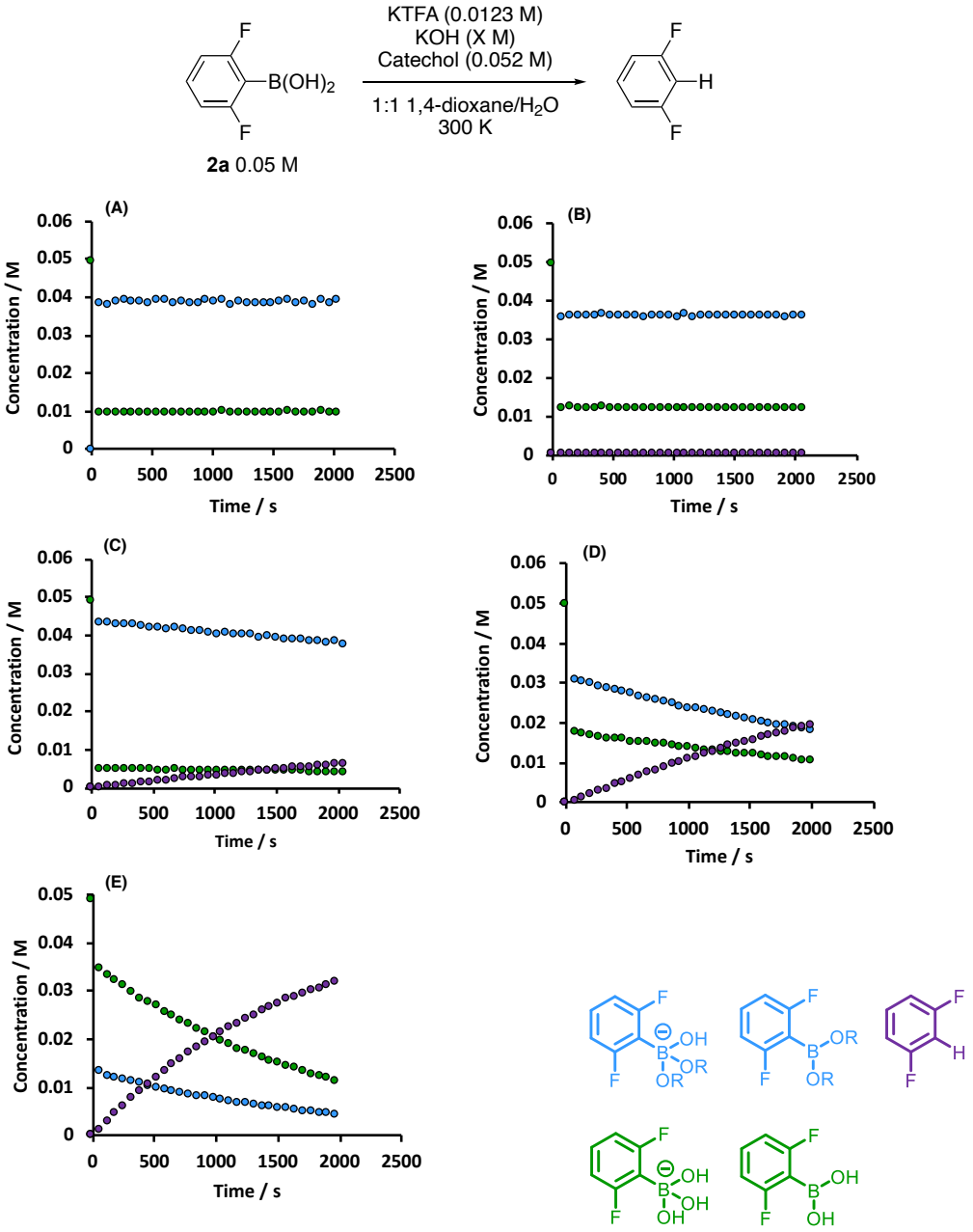

Figure 51. Reaction conditions for the protodeboronation of **2a** in the presence of catechol varying the equivalents of base. Base was added to a pre-equilibrated mixture of **2a** and catechol to initiate the reaction (according to **general procedure E-1**). A 0.65 M master stock solution of KOH in 1:1 1,4-dioxane/H_2O was prepared to achieve a concentration of 0.15 M (3 equivalents) during the reaction when 0.2 mL KOH solution was added to the NMR tube. Serial dilutions were performed to prepare stock solutions to achieve 2.2, 1.5, 1 and 0.5 equivalents in the reaction. Reaction profiles: (A) 0.5 equiv. KOH (0.025 M), (B) 1 equiv. KOH (0.050 M), (C) 1.5 equiv. KOH (0.075 M), (D) 2.2 equiv. KOH (0.109 M) and (E) 3 equiv. KOH (0.150 M). Initial concentration of 0.05 M **2a** prior to addition of base. Structures indicate anionic boronic acid $[\mathbf{2a}_{OH}]^-$ and ester $[\mathbf{2c}_{OH}]^-$ boronate species in addition to neutral boronic acid **2a** and ester **2c** species which under certain conditions (lower equivalents of base added) will also be present in solution.

4.3.5 Varying the cation

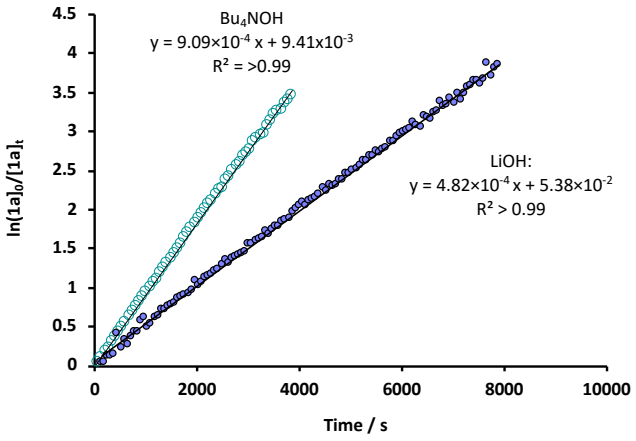

Figure 52. Rate analysis for the protodeboronation of $[\mathbf{2a}_{OH}]^-$ monitored by ^{19}F NMR spectroscopy, using bases LiOH versus Bu_4NOH. k_{rel} K^+, Bu_4N^+, Li^+ = 1: 0.82: 0.44.

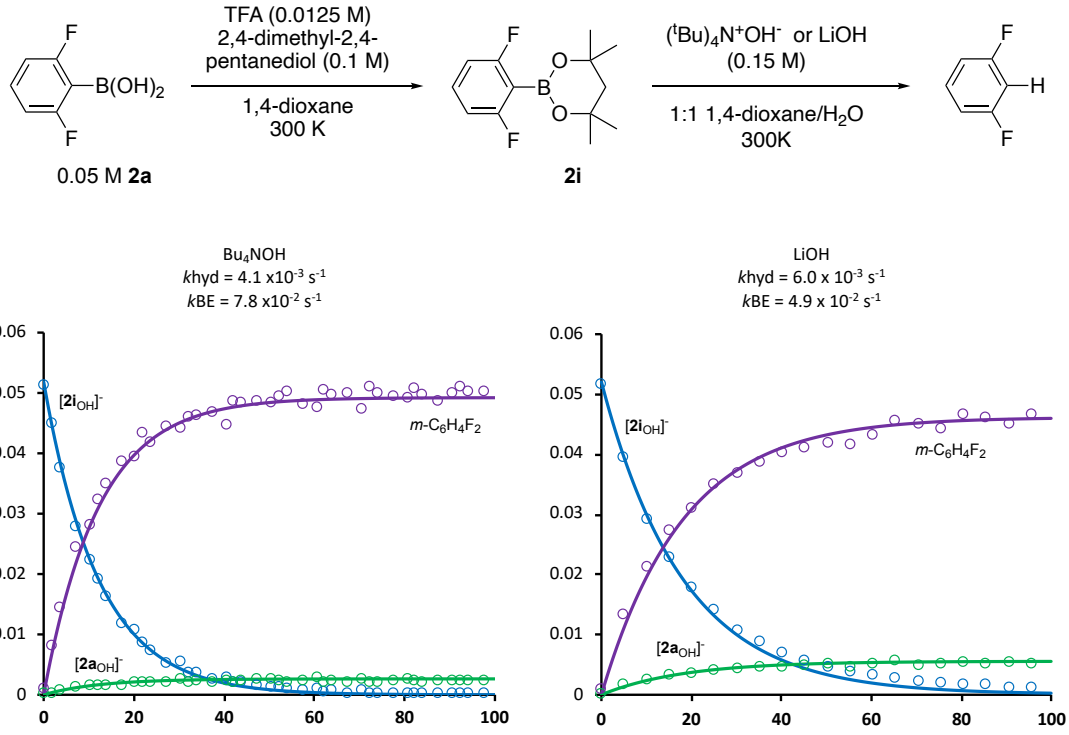

Figure 53. Reaction conditions, profiles and kinetic simulations for the protodeboronation, at pH >13, of $[\mathbf{2i}_{OH}]^-$ monitored by ^{19}F NMR spectroscopy using stopped-flow (flow rate = 1 mL/s, t_{AQ} = 0.5 s, d_{20} (trigger delay) = 0.1 s, d_1 (relaxation delay) = 1 s and flip angle = 90°). k_{rel} K^+, Bu_4N^+, Li^+ = 1.00 : 0.84 : 0.50 (protodeboronation) and 1.0 : 1.1 : 1.7 (hydrolysis).

4.3.6 Isotopic entrainment

Table 17. Rate coefficients for kinetic simulations of isotope entrainment experiment in **Figure** 20.

Reaction process	Rate constant (k)	Unit	K_{eq} (mol/L)
D-[**2a**$_{OH}$]$^-$ > *m*-$C_6H_4F_2$ + D-**2a**	1.25 x 10^{-3}	1/s	
D-[**2b**$_{OH}$]$^-$ > *m*-$C_6H_4F_2$ + D-**2b**	5.83 x 10^{-6}	1/s	
D-[**2b**$_{OH}$]$^-$ > D-[**2a**$_{OH}$]$^-$ + PIN	1.37 x 10^{-5}	1/s	3.80 x 10^{-1}

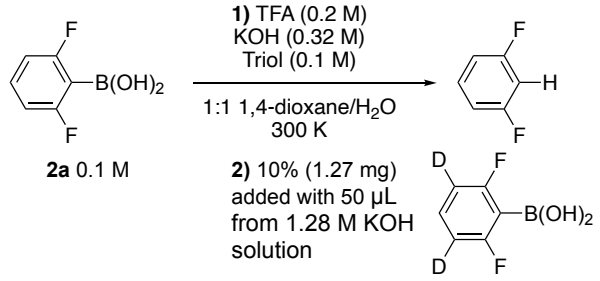

^{19}F NMR signals for three isomers of boronate [**2f**$_{OH}$]$^-$ and respective D_2-labelled species (~ 0.5 ppm upfield of each signal, as indicated with horizontal arrows).

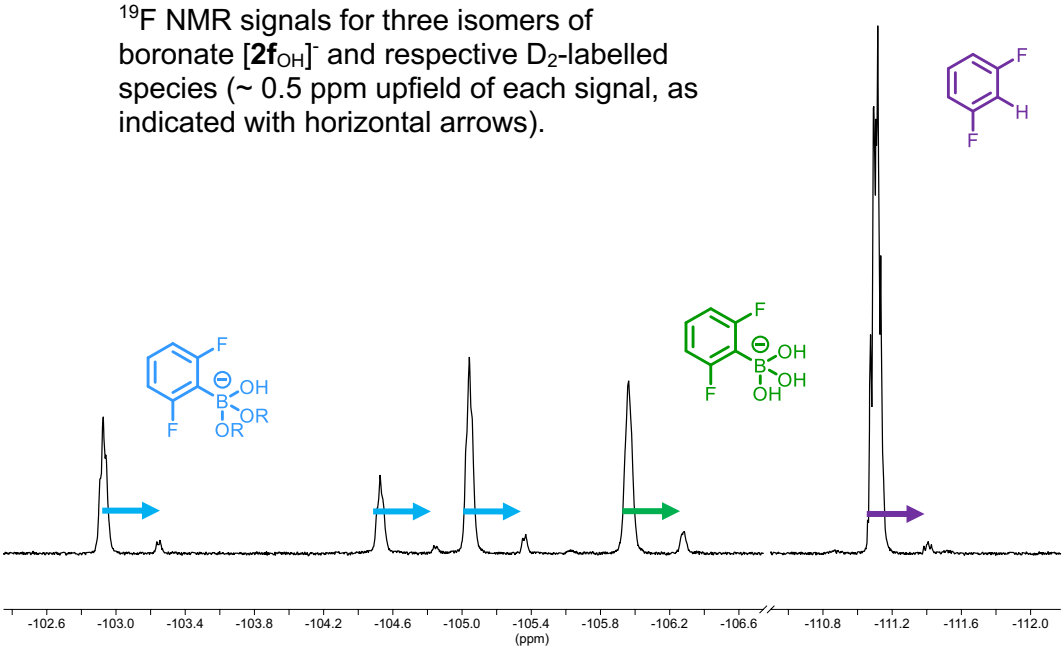

Figure 54. Reaction conditions for the protodeboronation of [**2a**$_{OH}$]$^-$ at pH >13 pre-equilibrated with 2-hydroxymethyl-2-methyl-1,3-propanediol (according to **general procedure E-1**) with 10% D2-**2a** entrained into the reaction with 50 µL KOH. ^{19}F NMR spectrum after entrainment of D2-labelled **2a** into the reaction of **2a** in the presence of 2-hydroxymethyl-2-methyl-1,3-propanediol at pH > 13. Signals for the respective D2-labelled species appear approximately 0.5 ppm upfield of each signal.

4.3.7 Experiments with 2-fluorophenylboronic acid, **1a**

Fitted values for pH-rate profile:

k^{H}_{H+} = 1.4 $M^{-1}s^{-1}$; k^{E}_{H+} = 4.8 $M^{-1}s^{-1}$
k^{trigH}_{H2O} = 0.73 x 10^{-4} s^{-1}; k^{trigE}_{H2O} = 2.6 x 10^{-3} s^{-1}
k^{H}_{SA} = 0.16 $M^{-1}s^{-1}$; k^{E}_{SA} = 0.8 $M^{-1}s^{-1}$
k^{H}_{H2O} = 1.8 x 10^{-5} s^{-1}; k^{E}_{H2O} = 3.2 x 10^{-4} s^{-1}
k^{H}_{OH} = 1 x 10^{-5} $M^{-1}s^{-1}$, k^{E}_{OH} = 2 x 10^{-4} $M^{-1}s^{-1}$
p$K_{a(\mathbf{1b})}$ = 10.15; p$K_{a(\mathbf{1a})}$ = 10.70

Table 18. Rate coefficients, k_{est} and k_{hyd} by kinetic modelling of temporal concentration profiles of the time-averaged ^{19}F NMR signals for **1a**/[**1a**$_{OH}$]$^-$ and **1b**/[**1b**$_{OH}$]$^-$.

pH	k_{est} / $M^{-1}s^{-1}$	k_{hyd} / s^{-1}
2.33	2.12 x 10^{-2}	5.33 x 10^{-3}
2.57	2.11 x 10^{-2}	6.47 x 10^{-3}
2.93	8.43 x 10^{-3}	2.16 x 10^{-3}
3.60	4.40 x 10^{-3}	1.26 x 10^{-3}
5.23	2.50 x 10^{-3}	6.78 x 10^{-4}
5.96	2.28 x 10^{-3}	7.09 x 10^{-4}
6.49	2.55 x 10^{-3}	6.99 x 10^{-4}
7.66	2.60 x 10^{-3}	7.66 x 10^{-4}
8.02	2.10 x 10^{-3}	8.85 x 10^{-4}
8.87	2.60 x 10^{-3}	8.90 x 10^{-4}
9.38	8.07 x 10^{-3}	1.83 x 10^{-3}
9.66	1.27 x 10^{-2}	2.54 x 10^{-3}
10.17	2.60 x 10^{-2}	2.85 x 10^{-3}
10.29	2.60 x 10^{-2}	2.51 x 10^{-3}
10.91	2.25 x 10^{-2}	1.07 x 10^{-3}
11.05	2.24 x 10^{-2}	1.54 x 10^{-3}
11.12	1.99 x 10^{-2}	9.68 x 10^{-4}
13.11	8.06 x 10^{-4}	4.40 x 10^{-4}
14.45	3.39 x 10^{-4}	2.04 x 10^{-5}

Table 19. Reaction conditions for the esterification of **1a** in the presence of pinacol at pH 10.84 (Figure 14) by stopped flow ^{19}F NMR spectroscopy (flow rate = 1 mL/s, t_{AQ} = 1 s, flip angle = 90°, d_{20} (trigger delay) = 0.04 s, d_1 (relaxation delay) = 10 s).

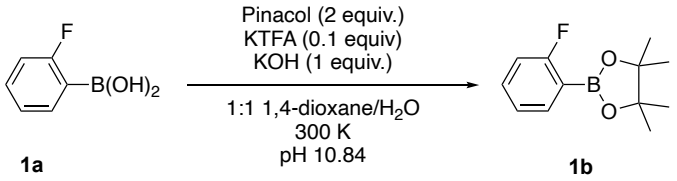

1a **1b**

Syringe A: **1a**/KOH/KTFA (volume ratio)	Conc. 0.39 M/0.40 M/ 0.04 M	Syringe B: 1:1 1,4-dioxane/H_2O (volume ratio)	Syringe C: Pinacol (0.20 M) (volume ratio)	Equiv. pinacol
0.45	0.18 M **1a**	0.5	0.5	0.57
0.40	0.16 M	0.1	0.5	0.64
0.30	0.12M	0.2	0.5	0.85
0.20	0.08 M	0.3	0.5	1.28
0.10	0.04 M	0.4	0.5	2.55

Table 20. Reaction conditions for the esterification of **1a** in the presence of pinacol at pH 10.54, with varying equivalents ArOH added, by stopped-flow ^{19}F NMR spectroscopy (Figure 14 A).

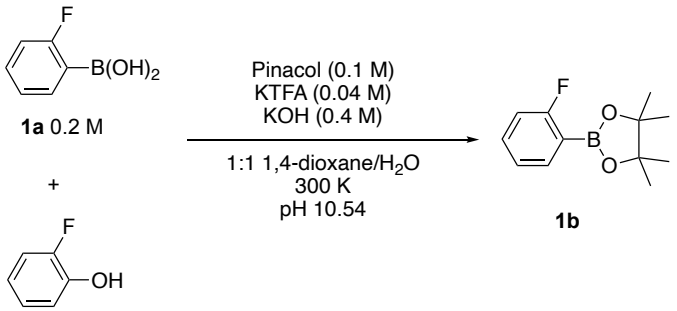

1b

Syringe A: **1a**/KOH/KTFA (volume ratio)	Conc. **1a** (M):	Syringe B: **1a**/KOH/KTFA + ArOH (volume ratio)	Conc. **1a** (M):	Conc. ArOH (M)	Syringe C: Pinacol (0.20 M) (volume ratio)
0.4	0.16	0.1	0.04	0.03	0.5
0.2	0.08	0.3	0.12	0.09	0.5
0.0	0.00	0.5	0.20	0.15	0.5

4.4 *In-situ* reaction monitoring by ^{1}H NMR spectroscopy

4.4.1 General considerations

All *in-situ* reaction monitoring was performed on a Bruker Ascend 400 MHz spectrometer at 300 K (27 °C). A typical ^{1}H NMR monitoring experiment used a zg30 pulse sequence, an acquisition time of 3.9 seconds (8 scans) and a relaxation delay of 1 seconds. MestReNova versions 10.0 and 11.0 were used for processing all NMR spectra acquired.

The solvent system used for kinetics experiments was 1:1 1,4-dioxane/H_2O. 1 L of this solvent blend was made by adding 500 mL deionised H_2O to a 1 L volumetric flask and making up to the mark with 1,4-dioxane. The volumetric flask was then inverted three times to mix.

A high precision analytical balance (0.01 mg resolution) was used to weigh solid compounds and liquids were dispensed with gas-tight syringes and micro syringes.
For reactions occurring over a longer time period (days or weeks), NMR tubes were kept in a water bath maintained at the desired temperature of 27 °C. The tubes were sealed with PTFE tape and capped to minimise solvent evaporation. The NMR tubes were additionally wrapped in parafilm whilst in the water bath.

4.4.2 Heteroaromatic boronic acids

5-Thiazolyl boronic acid, 7a

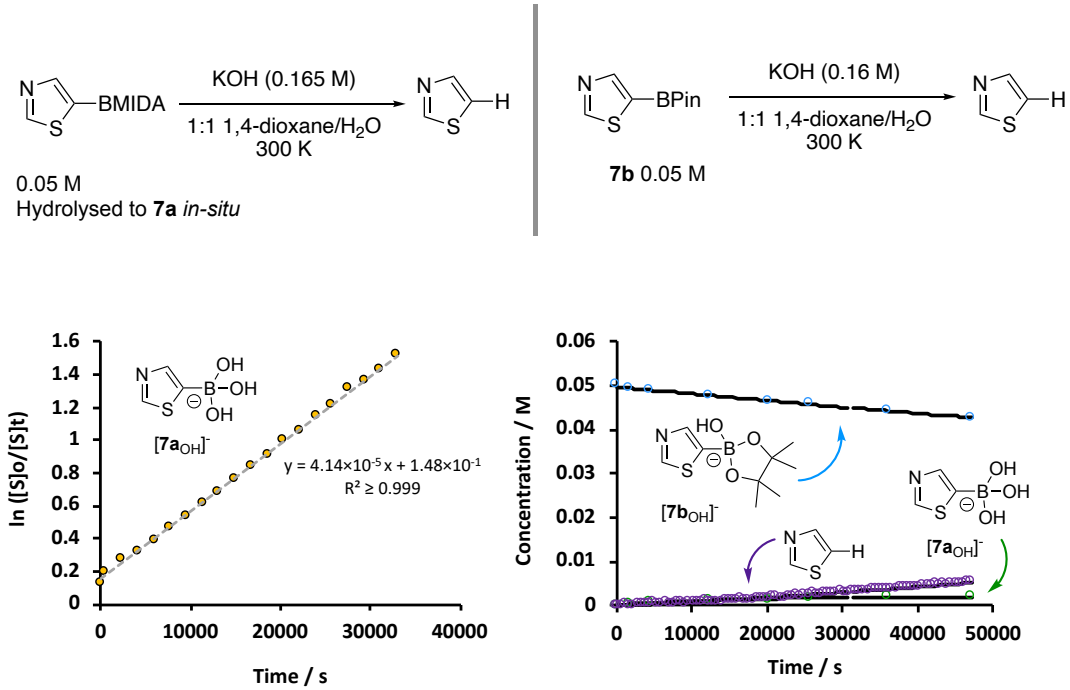

Reaction process	Rate constant (k)	Unit
[**7b**$_{OH}$]$^-$ > Thiazole	1.07 x 10^{-6}	1/s
[**7a**$_{OH}$]$^-$ > Thiazole	4.16 x 10^{-5}	1/s
[**7b**$_{OH}$]$^-$ > [**7a**$_{OH}$]$^-$ + PIN	2.20 x 10^{-6}	1/s
[**7a**$_{OH}$]$^-$ + PIN > [**7b**$_{OH}$]$^-$	6.95 x 10^{-4}	L/mol.s

Figure 55. Reaction set-up for protodeboronation of 5-thiazolyl MIDA ester (hydrolysed to **7a** *in-situ*) and **7b**. First order decay of [**7a**$_{OH}$]$^-$ (left) and temporal-concentration profile and kinetic simulation (right) for protodeboronation and hydrolysis of [**7b**$_{OH}$]$^-$ at pH > 13. *In-situ* reaction monitoring by ^{1}H NMR spectroscopy.

1-Methyl-1*H*-pyrazolyl-5-boronic acid, 8a

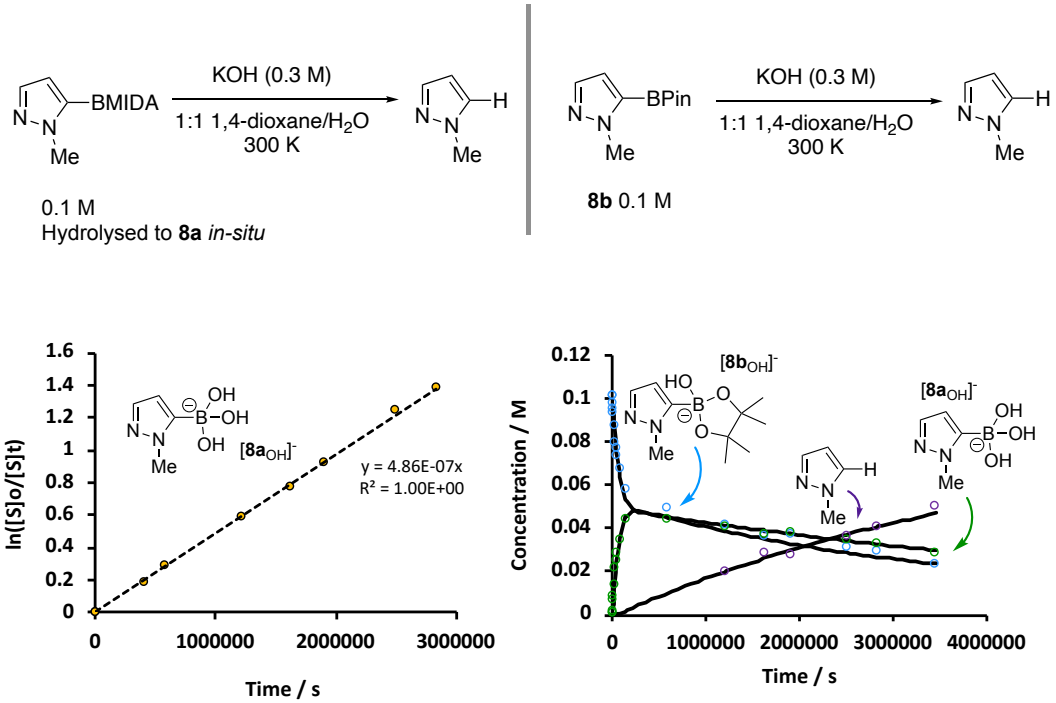

Reaction process	Rate constant (*k*)	Unit
$[\mathbf{8b}_{OH}]^-$ > 1-Methylpyrazole	1.27×10^{-8}	1/s
$[\mathbf{8a}_{OH}]^-$ > 1-Methylpyrazole	3.80×10^{-7}	1/s
$[\mathbf{8b}_{OH}]^-$ > $[\mathbf{8a}_{OH}]^-$ + PIN	6.64×10^{-6}	1/s
$[\mathbf{8a}_{OH}]^-$ + PIN > $[\mathbf{8b}_{OH}]^-$	1.21×10^{-4}	L/mol.s

Figure 56. Reaction set-up (left) for protodeboronation of 1-Me-1*H*-5-pyrazolyl MIDA ester (hydrolysed to **8a** *in-situ*) and **8b** (right). First order decay of $[\mathbf{8a}_{OH}]^-$ (left) and temporal-concentration profile and kinetic simulation (right) for protodeboronation and hydrolysis of $[\mathbf{8b}_{OH}]^-$. Reaction profile for the base-catalysed protodeboronation of $[\mathbf{8b}_{OH}]^-$ from the interleaving of two overlapping data sets from *in-situ* monitoring by ^{1}H NMR spectroscopy.

3,5-Dimethylisoxazolyl boronic acid, 9a

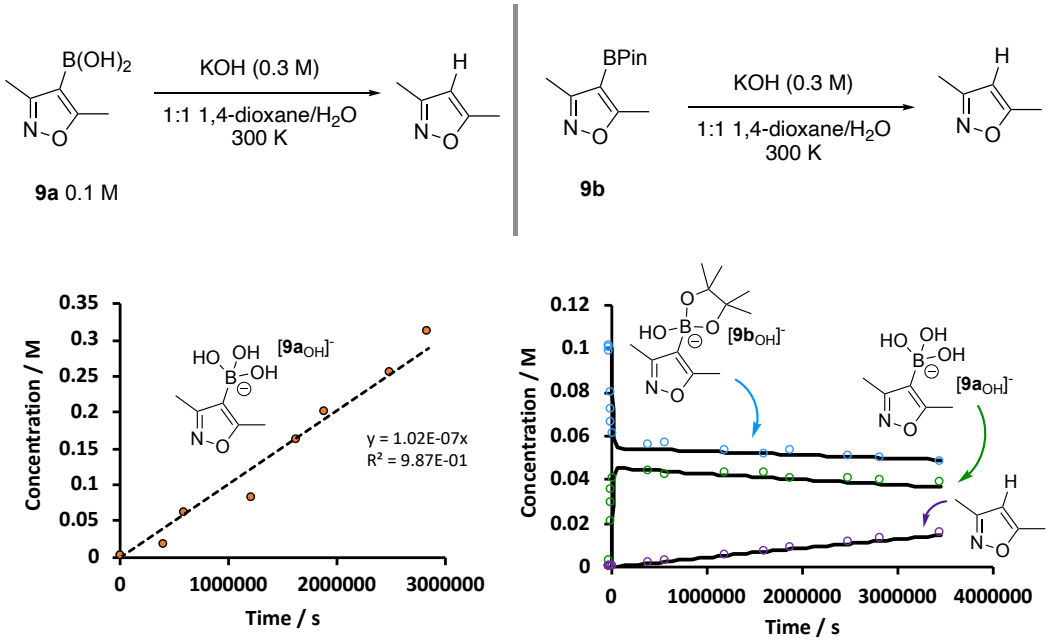

Reaction process	Rate constant (*k*)	Unit
$[\mathbf{9b}_{OH}]^-$ > 3,5-Dimethylisoxazole	1.35 x 10^{-9}	1/s
$[\mathbf{9a}_{OH}]^-$ > 3,5-Dimethylisoxazole	1.02 x 10^{-7}	1/s
$[\mathbf{9b}_{OH}]^-$ > $[\mathbf{9a}_{OH}]^-$ + PIN	2.42 x 10^{-5}	1/s
$[\mathbf{9a}_{OH}]^-$ + PIN > $[\mathbf{9b}_{OH}]^-$	6.37 x 10^{-4}	L/mol.s

Figure 57. Reaction set-up for protodeboronation of **9a** (left) and **9b** (right) at pH > 13. First order decay for the protodeboronation of $[\mathbf{9a}_{OH}]^-$ (left). *In-situ* reaction monitoring by ^{1}H NMR spectroscopy and line deconvolution tool in MestReNova used to process overlapping methyl peaks for the starting material and product. Reaction profile and kinetic simulation (right) for the base-catalysed protodeboronation of $[\mathbf{9b}_{OH}]^-$ from the interleaving of two overlapping data sets. *In-situ* reaction monitoring both by ^{11}B and ^{1}H NMR spectroscopy and line deconvolution tool in MestReNova used to process overlapping peaks.

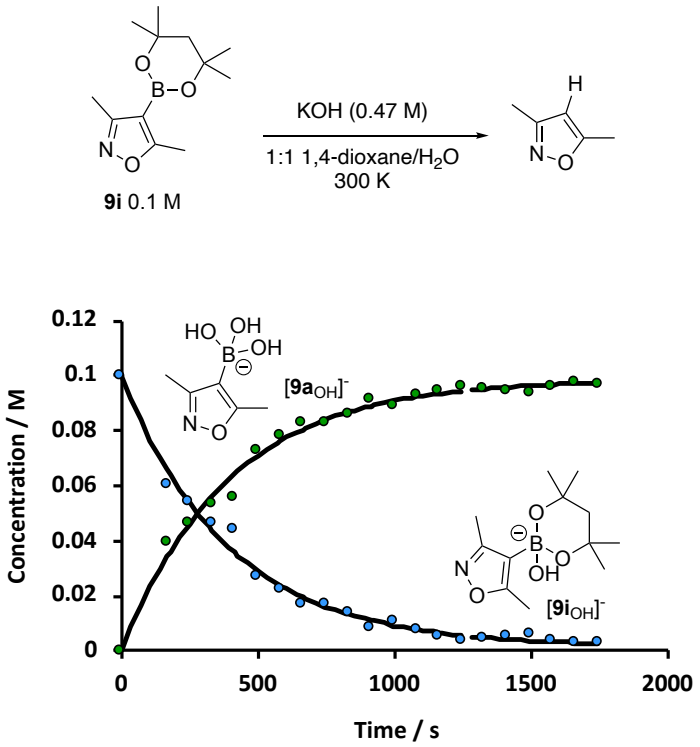

Reaction process	Rate constant (*k*)	Unit
$[\mathbf{9i}_{OH}]^-$ > $[\mathbf{9a}_{OH}]^-$ + 2,4-Dimethyl-2,4-pentanediol	2.50 x 10^{-3}	1/s
$[\mathbf{9a}_{OH}]^-$ + 2,4-Dimethyl-2,4-pentanediol > $[\mathbf{9i}_{OH}]^-$	4.16 x 10^{-4}	L/mol.s

Figure 58. Reaction conditions, profile and kinetic simulation for the hydrolysis of $[\mathbf{9i}_{OH}]^-$ at pH >13. *In-situ* reaction monitoring by ^{1}H NMR spectroscopy and line deconvolution tool in MestReNova used to process overlapping methyl peaks for $[\mathbf{9i}_{OH}]^-$ and $[\mathbf{9a}_{OH}]^-$.

2-Pyridyl boronic acid, 10a

*Protodeboronation of **10a** at neutral pH.*

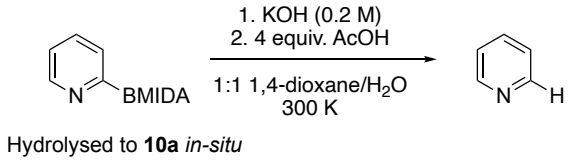

Hydrolysed to **10a** *in-situ*

An 8 M solution of KOH in H_2O was prepared in a 10 mL volumetric flask. In a 5 mL volumetric flask was prepared a solution of 1:1 1,4-dioxane/water and 1 mmol KOH. This solution was transferred to a round-bottomed flask and allowed to stir at 27 °C. To the flask was added 2-pyridyl boronic acid MIDA ester (0.05 M) and allowed to stir for approximately 5 seconds prior to the addition of 4 equivalents acetic acid buffer in order to maintain a pH 6.2-6.9. The reaction was monitored *in-situ* by ^{1}H NMR spectroscopy.

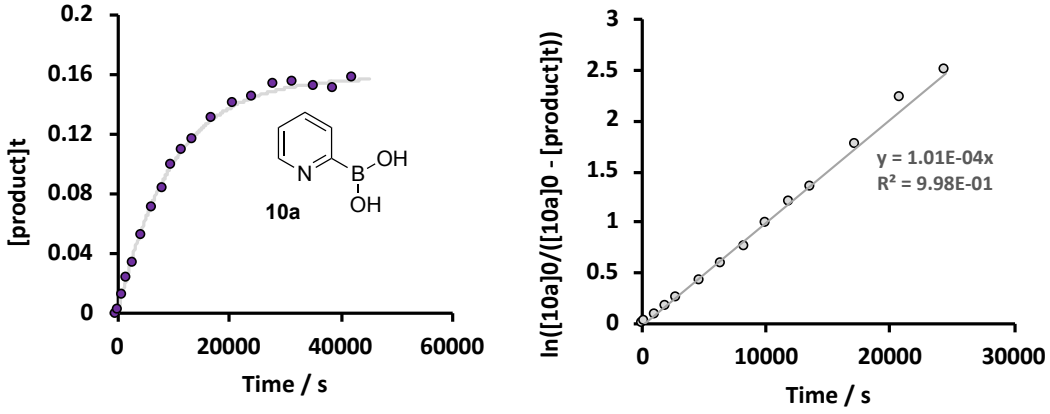

Figure 59. Reaction conditions and profile for the protodeboronation of 2-pyridyl MIDA ester (hydrolysed *in-situ* to **10a**) at neutral pH for product evolution (left; fit: $[\text{product}]_t = ([\mathbf{10a}]_0 - [\text{product}]_t)) \exp(-k_{BAt}))$ and reaction profile for the protodeboronation of **10a** at neutral pH for protodeboronation product (right; fit: $\ln([\mathbf{10a}]_0/([\mathbf{10a}]_0 - [\text{product}]_t)) = k_{BAt}$).

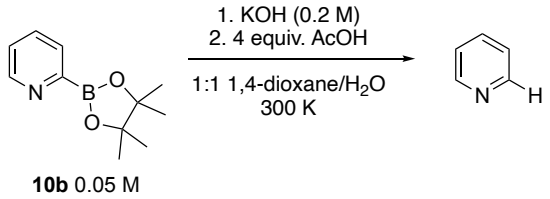

In a 5 mL volumetric flask was prepared a solution of 1:1 1,4-dioxane/water and 1 mmol KOH. This solution was transferred to a round-bottomed flask and allowed to stir at 27 °C. To the flask was added **10b** (0.05 M) and 4 equivalents acetic acid buffer in order to maintain a pH 6.2-6.9. The reaction was monitored *in-situ* by ^{1}H NMR spectroscopy.

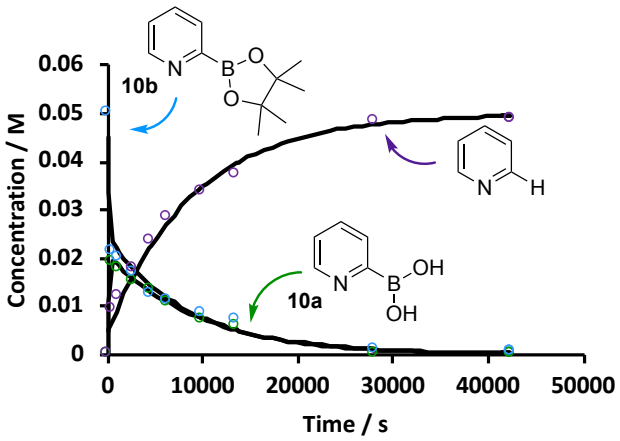

Reaction process	Rate constant (*k*)	Unit
[**10b**$_{OH}$]$^{-}$ > Pyridine	1.38 x 10^{-4}	1/s
[**10a**$_{OH}$]$^{-}$ > Pyridine	8.10 x 10^{-5}	1/s
[**10b**$_{OH}$]$^{-}$ > [**10a**$_{OH}$]$^{-}$ + PIN	3.00 x 10^{-3}	1/s
[**10a**$_{OH}$]$^{-}$ + PIN > [**10b**$_{OH}$]$^{-}$	1.76 x 10^{-1}	L/mol.s

Figure 60. Reaction conditions, profile and kinetic simulation for the protodeboronation of 10b at neutral pH. *In-situ* reaction monitoring by ^{1}H NMR spectroscopy.

*Protodeboronation of 2-pyridyl boronic acid **10a** at high pH.*

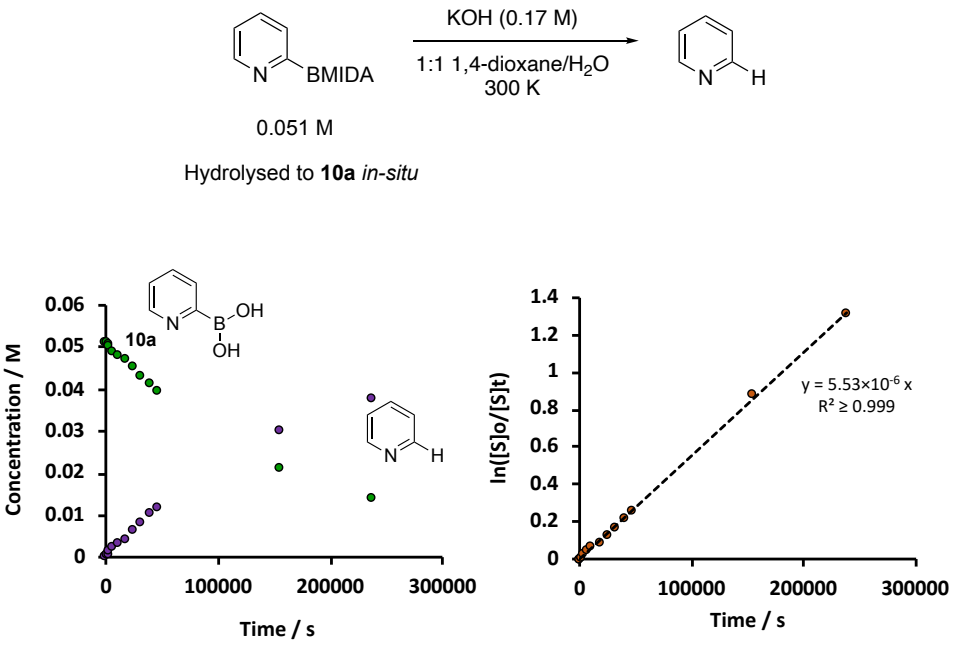

Figure 61. Reaction conditions, profile and first order decay of [**10a**$_{OH}$]$^-$ at pH > 13. *In-situ* reaction monitoring by ^{1}H NMR spectroscopy.

References

1. Thomas, S. E., *Organic Synthesis : The Roles of Boron and Silicon (Oxford Chemistry Primers)*. Oxford University Press, 1991.
2. Hall, D. G., In *Boronic Acids: Preparation and Applications in Organic Synthesis, Medicine and Materials (Volumes 1 and 2),* 2nd ed.; Hall, D. G.; Wiley VCH: Weinheim, Germany, 2011, pp 1-133.
3. Lennox, A. J.; Lloyd-Jones, G. C., Selection of boron reagents for Suzuki-Miyaura coupling. *Chem. Soc. Rev.* **2014,** *43*, 412-43.
4. Clayden, J.; Greeves, N.; Warren, S., *Organic Chemistry,* 2nd ed.; Oxford University Press, 2012.
5. Sivaev, I. B.; Bregadze, V. I., Lewis acidity of boron compounds. *Coord. Chem. Rev.* **2014,** *270-271*, 75-88.
6. Zeebe, R. E.; Sanyal, A.; Ortiz, J. D.; Wolf-Gladrow, D. A., A theoretical study of the kinetics of the boric acid–borate equilibrium in seawater. *Mar. Chem.,* **2001,** *73*, 113-124.
7. Adamczyk-Woźniak, A.; Sporzyński, A., The influence of ortho-substituents on the properties of phenylboronic acids. *J. Organomet. Chem.* **2020,** *913*.
8. Cox, P. A.; Reid, M.; Leach, A. G.; Campbell, A. D.; King, E. J.; Lloyd-Jones, G. C., Base-Catalyzed Aryl-$B(OH)_2$ Protodeboronation Revisited: From Concerted Proton Transfer to Liberation of a Transient Aryl Anion. *J. Am. Chem. Soc.* **2017,** *139*, 13156-13165.
9. Zarzeczańska, D.; Adamczyk-Woźniak, A.; Kulpa, A.; Ossowski, T.; Sporzyński, A., Fluorinated Boronic Acids: Acidity and Hydrolytic Stability of Fluorinated Phenylboronic Acids. *Eur. J. Inorg. Chem.* **2017**, 4493-4498.
10. Thomas, A. A.; Zahrt, A. F.; Delaney, C. P.; Denmark, S. E., Elucidating the Role of the Boronic Esters in the Suzuki-Miyaura Reaction: Structural, Kinetic, and Computational Investigations. *J. Am. Chem. Soc.* **2018,** *140*, 4401-4416.
11. Bowie, R. A.; Musgrave, O. C., Organoboron Compounds. Part V. The Hydrolysis of Cyclic Phenylboronates, *J. Chem. Soc.* **1963**, 3945-3949.

12. Roy, C. D.; Brown, H. C., Stability of boronic esters – Structural effects on the relative rates of transesterification of 2-(phenyl)-1,3,2-dioxaborolane. *J. Organomet. Chem.* **2007,** *692*, 784-790.
13. Roy, C. D.; Brown, H. C., A Comparative Study of the Relative Stability of Representative Chiral and Achiral Boronic Esters Employing Transesterification. *Monatsh. Chem.* **2007,** *138*, 879-887.
14. Frederick, M. O.; Kjell, D. P., A synthesis of abemaciclib utilizing a Leuckart–Wallach reaction. *Tetrahedron Lett.* **2015,** *56*, 949-951.
15. Maes, B. U. W.; R'kyek, O.; Košmrlj, J.; Lemière, G. L. F.; Esmans, E.; Rozenski, J.; Dommisse, R. A.; Haemers, A., Suzuki reactions on chloropyridazinones: an easy approach towards arylated 3(2H)-pyridazinones. *Tetrahedron* **2001**, 1323-1330.
16. Miyaura, N.; Yamada, K.; Suzuki, A., A New Stereospecific Cross-Coupling by the Palladium-Catalyzed Reaction of 1-Alkenylboranes with 1-Alkenyl or 1-Alkynyl Halides. *Tetrahedron Lett.* **1979,** *20*, 3437 - 3440.
17. Miyaura, N.; Suzuki, A., Stereoselective Synthesis of Arylated (E)-Alkenes by the Reaction of Alk-1-enylboranes with Aryl Halides in the Presence of Palladium Catalyst *J.C.S. Chem. Comm.* **1979**, 866–867.
18. Pagett, A. B.; Lloyd-Jones, G. C., Suzuki-Miyaura Cross-Coupling. *Org. React.*, **2020**, *100,* 547-620.
19. Delaney, C. P.; Kassel, V. M.; Denmark, S. E., Potassium Trimethylsilanolate Enables Rapid, Homogeneous Suzuki−Miyaura Cross-Coupling of Boronic Esters. *ACS Catal.* **2020,** *10*, 73-80.
20. Gonzalez, J. A.; Ogba, O. M.; Morehouse, G. F.; Rosson, N.; Houk, K. N.; Leach, A. G.; Cheong, P. H.-Y; Burke, M. D.; Lloyd-Jones, G. C., MIDA boronates are hydrolysed fast and slow by two different mechanisms. *Nat. Chem.* **2016,** *8*, 1067-1075.
21. Cho, C. S.; Uemura, S., Palladium-catalyzed cross-coupling of aryl and alkenyl boronic acids with alkenes via oxidative addition of a carbon-boron bond to palladium(0). *J. Organomet. Chem.* **1994,** *465*, 85–92.

22. Chan, D. M. T.; Monaco, K. L.; Wang, R.-P.; Winters, M. P., New N- and O-Arylations with Phenylboronic Acids and Cupric Acetate. *Tetrahedron Lett.* **1998,** *39*, 2933-2936.
23. Evans, D. A.; Katz, J. L.; West, T. R., Synthesis of Diaryl Ethers through the Copper-Promoted Arylation of Phenols with Arylboronic Acids. An Expedient Synthesis of Thyroxine. *Tetrahedron Lett.* **1998,** *39*, 2937–2940.
24. Lam, P. Y. S.; Clark, C. G.; Saubern, S.; Adams, J.; Winters, M. P.; Chan, D. M. T.; Combs, A., New Aryl/Heteroaryl C-N Bond Cross-coupling Reactions via Arylboronic Acid/Cupric Acetate Arylation. *Tetrahedron Lett.* **1998,** *39*, 2941–2944.
25. Liebeskind, L. S.; Srogl, J., Thiol Ester-Boronic Acid Coupling. A Mechanistically Unprecedented and General Ketone Synthesis. *J. Am. Chem. Soc.* **2000,** *122*, 11260–11261.
26. Lee, A.-L., Enantioselective oxidative boron Heck reactions. *Org. Biomol. Chem.* **2016,** *14*, 5357-66.
27. Vantourout, J. C.; Law, R. P.; Isidro-Llobet, A.; Atkinson, S. J.; Watson, A. J., Chan-Evans-Lam Amination of Boronic Acid Pinacol (BPin) Esters: Overcoming the Aryl Amine Problem. *J. Org. Chem.* **2016,** *81*, 3942-3950.
28. Vantourout, J. C.; Miras, H. N.; Isidro-Llobet, A.; Sproules, S.; Watson, A. J., Spectroscopic Studies of the Chan-Lam Amination: A Mechanism-Inspired Solution to Boronic Ester Reactivity. *J. Am. Chem. Soc.* **2017,** *139*, 4769-4779.
29. Modha, S. G.; Mehta, V. P.; Van der Eycken, E. V., Transition metal-catalyzed C-C bond formation *via* C-S bond cleavage: an overview. *Chem. Soc. Rev.* **2013,** *42*, 5042-55.
30. Prokopcová, H.; Kappe, C. O., The Liebeskind-Srogl C-C Cross-Coupling Reaction. *Angew. Chem., Int. Ed. Engl.* **2009,** *48*, 2276-2286.
31. Petasis, N. A.; Zavialov, I. A., A New and Practical Synthesis of α-Amino Acids from Alkenyl Boronic Acids. *J. Am. Chem. Soc.* **1997,** *119*, 445-446.

32. Petasis, N. A.; Zavialov, I. A., Highly Stereocontrolled One-Step Synthesis of *anti*-β-Amino Alcohols from Organoboronic Acids, Amines, and α-Hydroxy Aldehydes. *J. Am. Chem. Soc.* **1998,** *120*, 11798-11799.
33. Jayaram, V.; Sridhar, T.; Sharma, G. V.; Berrée, F.; Carboni, B., Synthesis of 1-Amino-*1H*-Indenes via a Sequential Suzuki-Miyaura Coupling/Petasis Condensation Sequence. *J. Org. Chem.* **2017,** *82*, 1803-1811.
34. Otera, J., *Modern Carbonyl Chemistry*. Wiley-VCH: Weinheim, Germany, 2000.
35. Blais, J.; L'Honore, A.; Soulie, J.; Cadiot, P., Boronates allyliques, alleniques et propargyliques: Preparations et proprietes. *J. Organomet. Chem.* **1974,** *78*, 323-337.
36. Huo, H.-X.; Duvall, J. R.; Huang, M.-Y.; Hong, R., Catalytic asymmetric allylation of carbonyl compounds and imines with allylic boronates. *Org. Chem. Front.* **2014,** *1*, 303-320.
37. Sakai, M.; Ueda, M.; Miyaura, N., Rhodium-Catalyzed Addition of Organoboronic Acids to Aldehydes. *Angew. Chem., Int. Ed.* **1998,** *37*, 3279-3281.
38. Sakai, M.; Hayashi, H.; Miyaura, N., Rhodium-Catalyzed Conjugate Addition of Aryl- or 1-Alkenylboronic Acids to Enones. *Organometallics* **1997,** *16*, 4229-4231.
39. Adonin, N. Y.; Bardin, V. V., Polyfluorinated arylboranes as catalysts in organic synthesis. *Mendeleev Commun.* **2020,** *30*, 262-272.
40. Al-Zoubi, R. M.; Marion, O.; Hall, D. G., Direct and Waste-Free Amidations and Cycloadditions by Organocatalytic Activation of Carboxylic Acids at Room Temperature. *Angew. Chem., Int. Ed.* **2008,** *47*, 2876-2879.
41. Charville, H.; Jackson, D.; Hodges, G.; Whiting, A., The thermal and boron-catalysed direct amide formation reactions: mechanistically understudied yet important processes. *Chem. Commun.* **2010,** *46*, 1813-1823.

42. Ishihara, K.; Ohara, S.; Yamamoto, H., 3,4,5-Trifluorobenzeneboronic Acid as an Extremely Active Amidation Catalyst. *J. Org. Chem.* **1996,** *61*, 4196-4197.
43. Ishihara, K.; Ohara, S.; Yamamoto, H., Direct Polycondensation of Carboxylic Acids and Amines Catalyzed by 3,4,5-Trifluorophenylboronic Acid. *Macromolecules* **2000,** *33*, 3511-3513.
44. Ishihara, K.; Ohara, S.; Yamamoto, H., (3,4,5-Trifluorophenyl)Boronic Acid-Catalyzed Amide Formation from Carboxylic Acids and Amines: N-Benzyl-4-Phenylbutyramide. *Org. Synth.* **2002,** *79*, 176.
45. Sabatini, M. T.; Boulton, L. T.; Sheppard, T. D., Borate esters: Simple catalysts for the sustainable synthesis of complex amides. *Sci. Adv.* **2017,** *3*, e1701028.
46. Maki, T., Ishihara, K., Yamamoto, H.; Arylboronic Acid-Catalyzed Direct Condensation of Carboxylic Acids with Ureas. *Synlett* **2004**, 1355-1358.
47. Zheng, H.; Hall, D. G., Mild and efficient boronic acid catalysis of Diels–Alder cycloadditions to 2-alkynoic acids. *Tetrahedron Lett.* **2010,** *51*, 3561-3564.
48. Zheng, H.; Lejkowski, M.; Hall, D. G., Mild boronic acid catalyzed Nazarov cyclization of divinyl alcohols in tandem with Diels–Alder cycloaddition. *Tetrahedron Lett.* **2013,** *54*, 91-94.
49. Zheng, H.; McDonald, R.; Hall, D. G., Boronic Acid Catalysis for Mild and Selective [3+2] Dipolar Cycloadditions to Unsaturated Carboxylic Acids. *Chem. Eur. J.* **2010,** *16*, 5454-5460.
50. Bryan, M. C.; Dunn, P. J.; Entwistle, D.; Gallou, F.; Koenig, S. G.; Hayler, J. D.; Hickey, M. R.; Hughes, S.; Kopach, M. E.; Moine, G.; Richardson, P.; Roschangar, F.; Steven, A.; Weiberth, F. J., Key Green Chemistry research areas from a pharmaceutical manufacturers' perspective revisited. *Green Chem.* **2018,** *20*, 5082-5103.
51. Dimitrijević, E.; Taylor, M. S., Organoboron Acids and Their Derivatives as Catalysts for Organic Synthesis. *ACS Catal.* **2013,** *3*, 945-962.
52. Hall, D. G., Boronic acid catalysis. *Chem. Soc. Rev.* **2019,** *48*, 3475-3496.

53. Yan, J.; Springsteen, G.; Deeter, S.; Wang, B., The relationship among pKa, pH, and binding constants in the interactions between boronic acids and diols – it is not as simple as it appears. *Tetrahedron* **2004,** *60*, 11205-11209.
54. Springsteen, G.; Wang, B., A detailed examination of boronic acid-diol complexation. *Tetrahedron* **2002,** *58*, 5291-5300.
55. Lorand, J. P.; Edwards, J. O., Polyol Complexes and Structure of the Benzeneboronate Ion. *J. Org. Chem.* **1959,** *24*, 769-774.
56. Bull, S. D.; Davidson, M. G.; Van den Elsen, J. M. H.; Fossey, J. S.; Jenkins, A. T. A.; Jiang, Y.-B.; Kubo, Y.; Marken, F.; Sakurai, K.; Zhao, J.; James, T. D., Exploiting the Reversible Covalent Bonding of Boronic Acids: Recognition, Sensing, and Assembly. *Acc. Chem. Res.* **2012,** *46*, 312-326.
57. Wu, X.; Li, Z.; Chen, X.-X.; Fossey, J. S.; James, T. D.; Jiang, Y. B., Selective sensing of saccharides using simple boronic acids and their aggregates. *Chem. Soc. Rev.* **2013,** *42*, 8032-48.
58. Achilli, C.; Ciana, A.; Fagnoni, M.; Balduini, C.; Minetti, G., Susceptibility to hydrolysis of phenylboronic pinacol esters at physiological pH. *Open Chem.* **2013,** *11*, 137-139.
59. Bian, Z.; Liu, A.; Li, Y.; Fang, G.; Yao, Q.; Zhang, G.; Wu, Z., Boronic acid sensors with double recognition sites: a review. *Analyst* **2020,** *145*, 719-744.
60. Brooks, W. L. A.; Deng, C. C.; Sumerlin, B. S., Structure-Reactivity Relationships in Boronic Acid-Diol Complexation. *ACS Omega* **2018,** *3*, 17863-17870.
61. Hansen, J. S.; Christensen, J. B.; Petersen, J. F.; Hoeg-Jensen, T.; Norrild, J. C., Arylboronic acids: A diabetic eye on glucose sensing. *Sens. Actuators B Chem.* **2012,** *161*, 45-79.
62. Peters, J. A., Interactions between boric acid derivatives and saccharides in aqueous media: Structures and stabilities of resulting esters. *Coord. Chem. Rev.* **2014,** *268*, 1-22.

63. Sun, X.; Chapin, B. M.; Metola, P.; Collins, B.; Wang, B.; James, T. D.; Anslyn, E. V., The mechanisms of boronate ester formation and fluorescent turn-on in ortho-aminomethylphenylboronic acids. *Nat. Chem.* **2019,** *11*, 768-778.
64. Wu, X.; Chen, X.-X.; Jiang, Y. B., Recent advances in boronic acid-based optical chemosensors. *Analyst* **2017,** *142*, 1403-1414.
65. Collins, J.; Nadgorny, M.; Xiao, Z.; Connal, L. A., Doubly Dynamic Self-Healing Materials Based on Oxime Click Chemistry and Boronic Acids. *Macromol. Rapid. Commun.* **2017,** *38*, 1600760.
66. Vancoillie, G.; Hoogenboom, R., Responsive Boronic Acid-Decorated (Co)polymers: From Glucose Sensors to Autonomous Drug Delivery. *Sensors* **2016,** *16*, 1736.
67. Liu, Y.; Liu, Y.; Wang, Q.; Han, Y.; Tan, Y., Boronic ester-based self-healing hydrogels formed by using intermolecular B-N coordination. *Polymer* **2020,** *202,* 122624.
68. Commins, P.; Al-Handawi, M. B.; Karothu, D. P.; Raj, G.; Naumov, P., Efficiently self-healing boronic ester crystals. *Chem. Sci.* **2020,** *11*, 2606-2613.
69. Smithmyer, M. E.; Deng, C. C.; Cassel, S. E.; LeValley, P. J.; Sumerlin, B. S.; Kloxin, A. M., Self-Healing Boronic Acid-Based Hydrogels for 3D Co-cultures. *ACS Macro Lett.* **2018,** *7*, 1105-1110.
70. Wang, S.; Urban, M. W., Self-healing polymers. *Nat. Rev. Mater.* **2020,** *5*, 562-583.
71. Vancoillie, G.; Hoogenboom, R., Synthesis and polymerization of boronic acid containing monomers. *Polym. Chem.* **2016,** *7*, 5484-5495.
72. Brooks, W. L. A.; Vancoillie, G.; Kabb, C. P.; Hoogenboom, R.; Sumerlin, B. S., Triple Responsive Block cCpolymers Combining pH-Responsive, Thermoresponsive, and Glucose-Responsive Behaviors. *J. Polym. Sci. Part A: Polym. Chem.* **2017,** *55*, 2309-2317.
73. Yang, F.; Zhu, M.; Zhang, J.; Zhou, H., Synthesis of biologically active boron-containing compounds. *Med. Chem. Commun.* **2018,** *9*, 201-211.

74. Diaz, D. B.; Yudin, A. K., The versatility of boron in biological target engagement. *Nat. Chem.* **2017,** *9*, 731-742.
75. Fernandes, G. F. S.; Denny, W. A.; Dos Santos, J. L., Boron in drug design: Recent advances in the development of new therapeutic agents. *Eur. J. Med. Chem.* **2019,** *179*, 791-804.
76. Pizer, R. D.; Tihal, C. A., Mechanism of Boron Acid/Polyol Complex Formation. Comments on the Trigonal/Tetrahedral Interconversion on Boron. *Polyhedron* **1996,** *15*, 3411-3416.
77. Pizer, R., Boron acid complexation reactions with polyols and α-hydroxy carboxylic acids: Equilibria, reaction mechanisms, saccharide recognition. *Inorg. Chim. Acta* **2017,** *467*, 194-197.
78. Pizer, R.; Tihal, C., Equilibria and reaction mechanism of the complexation of methylboronic acid with polyols. *Inorg. Chem.* **2002,** *31*, 3243-3247.
79. Ito, H.; Kono, Y.; Machida, A.; Mitsumoto, Y.; Omori, K.; Nakamura, N.; Kondo, Y.; Ishihara, K., Kinetic study of the complex formation of boric and boronic acids with mono- and diprotonated ligands. *Inorg. Chim. Acta* **2003,** *344*, 28-36.
80. Miyamoto, C.; Suzuki, K.; Iwatsuki, S.; Inamo, M.; Takagi, H. D.; Ishihara, K., Kinetic Evidence for High Reactivity of 3-Nitrophenylboronic Acid Compared to Its Conjugate Boronate Ion in Reactions with Ethylene and Propylene Glycols. *Inorg. Chem. Commun.* **2008,** *47*, 1417-1419.
81. Suzuki, Y.; Kusuyama, D.; Sugaya, T.; Iwatsuki, S.; Inamo, M.; Takagi, H. D.; Ishihara, K., Reactivity of Boronic Acids toward Catechols in Aqueous Solution. *J. Org. Chem.* **2020,** *85*, 5255-5264.
82. Furikado, Y.; Nagahata, T.; Okamoto, T.; Sugaya, T.; Iwatsuki, S.; Inamo, M.; Takagi, H. D.; Odani, A.; Ishihara, K., Universal Reaction Mechanism of Boronic Acids with Diols in Aqueous Solution: Kinetics and the Basic Concept of a Conditional Formation Constant. *Chemistry* **2014,** *20*, 13194-202.

83. Bosch, L. I.; Fyles, T. M.; James, T. D., Binary and ternary phenylboronic acid complexes with saccharides and Lewis bases. *Tetrahedron* **2004,** *60*, 11175-11190.
84. Michaelis, A.; Becker, P., Ueber Monophenylborchlorid Und Einige Derivate Desselben. **1882,** *15*, 180-185.
85. Ainley, A. D.; Challenger, F., Studies of the boron-carbon linkage. Part I . The oxidation and nitration of phenylboric Acid. *J. Chem. Soc.* **1922**, 2171-2180.
86. Kuivila, H. G.; Reuwer, J. F.; Mangravite, J. A., Electrophilic Displacement Reactions. XVI. Metal Ion Catalysis in the Protodeboronation of Areneboronic Acids. *J. Am. Chem. Soc.* **1964,** *86*, 2666–2670.
87. Liu, C.; Li, X.; Wu, Y.; Qiu, J., Copper-catalyzed protodeboronation of arylboronic acids in aqueous media. *RSC Adv.* **2014,** *4*, 54307-54311.
88. Liu, C.; Li, X.; Wu, Y., Base-promoted silver-catalyzed protodeboronation of arylboronic acids and esters. *RSC Adv.* **2015,** *5*, 15354-15358.
89. Barker, G.; Webster, S.; Johnson, D. G.; Curley, R.; Andrews, M.; Young, P. C.; Macgregor, S. A.; Lee, A. L., Gold-Catalyzed Proto- and Deuterodeboronation. *J. Org. Chem.* **2015,** *80*, 9807-9816.
90. Shen, F.; Tyagarajan, S.; Perera, D.; Krska, S. W.; Maligres, P. E.; Smith, M. R., III; Maleczka, R. E., Jr., Bismuth Acetate as a Catalyst for the Sequential Protodeboronation of Di- and Triborylated Indoles. *Org. Lett.* **2016,** *18*, 1554-1557.
91. Molloy, J. J.; Law, R. P.; Fyfe, J. W.; Seath, C. P.; Hirst, D. J.; Watson, A. J. B., A modular synthesis of functionalised phenols enabled by controlled boron speciation. *Org. Biomol. Chem.* **2015,** *13*, 3093-3102.
92. Cammidge, A. N.; Crépy, K. V. L., Application of the Suzuki Reaction as the Key Step in the Synthesis of a Novel Atropisomeric Biphenyl Derivative for Use as a Liquid Crystal Dopant. *J. Org. Chem.* **2003,** *68*, 6832-6835.

93. Watanabe, T.; Miyaura, N.; Suzuki, A., Synthesis of Sterically Hindered Biaryls via the Palladium-Catalyzed Cross-Coupling Reaction of Arylboronic Acids or Their Esters with Haloarenes. *Synlett* **1992**, 207–210.
94. Bulfield, D.; Huber, S. M., Synthesis of Polyflourinated Biphenyls; Pushing the Boundaries of Suzuki-Miyaura Cross Coupling with Electron-Poor Substrates. *J. Org. Chem.* **2017,** *82*, 13188-13203.
95. Robbins, D. W.; Hartwig, J. F., A C-H Borylation Approach to Suzuki-Miyaura Coupling of Typically Unstable 2-Heteroaryl and Polyfluorophenyl Boronates. *Org. Lett.* **2012,** *16*, 4266–4269.
96. Yoshida, H.; Seki, M.; Kamio, S.; Tanaka, H.; Izumi, Y.; Li, J.; Osaka, I.; Abe, M.; Andoh, H.; Yajima, T.; Tani, T.; Tsuchimoto, T., Direct Suzuki–Miyaura Coupling with Naphthalene-1,8-diaminato (dan)-Substituted Organoborons. *ACS Catal.* **2019,** *10*, 346-351.
97. Mutoh, Y.; Yamamoto, K.; Saito, S., Suzuki–Miyaura Cross-Coupling of 1,8-Diaminonaphthalene (dan)-Protected Arylboronic Acids. *ACS Catal.* **2019,** *10*, 352-357.
98. Lennox, A. J. J.; Lloyd-Jones, G. C., The Slow-Release Strategy in Suzuki-Miyaura Coupling. *Isr. J. Chem.* **2010,** *50*, 664-674.
99. Chen, L.; Francis, H.; Carrow, B. P., An “On-Cycle” Precatalyst Enables Room-Temperature Polyfluoroarylation Using Sensitive Boronic Acids. *ACS Catal.* **2018,** *8*, 2989-2994.
100. Kinzel, T.; Zhang, Y.; Buchwald, S. L., A New Palladium Precatalyst Allows for the Fast Suzuki-Miyaura Coupling. *J. Am. Chem. Soc.* **2010,** *132*, 14073–14075.
101. Bream, R. N.; Clark, H.; Edney, D.; Harsanyi, A.; Hayler, J.; Ironmonger, A.; Mc Cleary, N.; Phillips, N.; Priestley, C.; Roberts, A.; Rushworth, P.; Szeto, P.; Webb, M. R.; Wheelhouse, K., Application of C–H Functionalization in the Development of a Concise and Convergent Route to the Phosphatidylinositol-3-kinase Delta Inhibitor Nemiralisib. *Org. Process Res. Dev.* **2021,** *25*, 529-540.

102. Masuda-Herrera, M. J.; Dobo, K. L.; Kenyon, M. O.; Kenny, J. D.; Galloway, S. M.; Escobar, P. A.; Reddy, M. V.; Jolly, R. A.; Trejo-Martin, A.; Brown, C.; McKeon, M.; Young, M.; Bruce, S.; Pant, K.; Dutta, A.; Kulkarni, R.; Bercu, J. P., *In Vivo* Mutagenicity Testing of Arylboronic Acids and Esters. *Environ. Mol. Mutagen* **2019,** *60*, 766-777.
103. Kuivila, H. G.; Joseph F. Reuwer, J.; Mangravite, J. A., Electrophilic Displacement Reactions XV. Kinetics and Mechanism of the Base-Catalysed Protodeboronation of Areneboronic Acids. *Can. J. Chem.* **1963,** *41*, 3081–3090.
104. Kuivila, H. G.; Nahabedian, K. V., Electrophilic Displacement Reactions, X. General Acid Catalysis in the Protodeboronation of Areneboronic Acids. *J. Am. Chem. Soc.* **1961,** *83*, 2159–2163.
105. Kuivila, H. G.; Nahabedian, K. V., Electrophilic Displacement Reactions. XL Solvent Isotope Effects in the Protodeboronation of Areneboronic Acids. *J. Am. Chem. Soc.* **1961,** *83*, 2164–2166.
106. Kuivila, H. G.; Nahabedian, K. V., Electrophilic Displacement Reactions. XII. Substituent Effects in the Protodeboronation of Areneboronic Acids. *J. Am. Chem. Soc.* **1961,** *83*, 2167–2174.
107. Frohn, H.-J.; Adonin, N. Y.; Bardin, V. V.; Starichenko, V. F., Base-catalysed Hydrodeboration of Polyfluorophenyl(dihydroxy)boranes. *Z. Anorg. Allg. Chem.* **2002,** *628*, 2834-2838.
108. Lozada, J.; Liu, Z.; Perrin, D. M., Base-promoted protodeboronation of 2,6-disubstituted arylboronic acids. *J. Org. Chem.* **2014,** *79*, 5365-5368.
109. Cox, P. A.; Leach, A. G.; Campbell, A. D.; Lloyd-Jones, G. C., Protodeboronation of Heteroaromatic, Vinyl, and Cyclopropyl Boronic Acids: pH-Rate Profiles, Autocatalysis, and Disproportionation. *J. Am. Chem. Soc.* **2016,** *138*, 9145-57.
110. Perrin, C. L.; Reyes-Rodríguez, G. J., Selectivity and isotope effects in hydronation of a naked aryl anion. *J. Am. Chem. Soc.* **2014,** *136*, 15263-15269.
111. Nieto-Sepulveda, E.; Bage, A. D.; Evans, L. A.; Hunt, T. A.; Leach, A. G.; Thomas, S. P.; Lloyd-Jones, G. C., Kinetics and Mechanism of the

Arase-Hoshi R_2BH-Catalyzed Alkyne Hydroboration: Alkenylboronate Generation via B-H/C-B Metathesis. *J. Am. Chem. Soc.* **2019,** *141*, 18600-18611.

112. West, T. H.; Walden, D. M.; Taylor, J. E.; Brueckner, A. C.; Johnston, R. C.; Cheong, P. H.; Lloyd-Jones, G. C.; Smith, A. D., Catalytic Enantioselective [2,3]-Rearrangements of Allylic Ammonium Ylides: A Mechanistic and Computational Study. *J. Am. Chem. Soc.* **2017,** *139*, 4366-4375.
113. Wei, R.; Hall, A. M. R.; Behrens, R.; Pritchard, M. S.; King, E. J.; Lloyd-Jones, G. C., Stopped-Flow ^{19}F NMR Spectroscopic Analysis of a Protodeboronation Proceeding at the Sub-Second Time-Scale. *Eur. J. Org. Chem.* **2021**, 2331-2342.
114. Calero, C. S.; Farwer, J.; Gardiner, E. J.; Hunter, C. A.; Mackey, M.; Scuderi, S.; Thompson, S.; Vinter, J. G., Footprinting Molecular Electrostatic Potential Surfaces for Calculation of Solvation Energies. *Phys. Chem. Chem. Phys.* **2013,** *15*, 18262-73.
115. Ben-Nairn, A.; Marcus, Y., Solvation Thermodynamics of Nonionic Solutes. *J. Chem. Phys.* **1984,** *81*, 2016-2027.
116. Page, M. I.; Jencks, W. P. Entropic Contributions to Rate Accelerations in Enzymatic and Intramolecular Reactions and the Chelate Effect. *Proc. Natl. Acad. Sci.* **1971,** *68*, 1678–1683.
117. Inglesby, P. A.; Agnew, L. R.; Carter, H. L.; Ring, O. T., Diethanolamine Boronic Esters: Development of a Simple and Standard Process for Boronic Ester Synthesis. *Org. Process Res. Dev.* **2020,** *24*, 1683-1689.
118. Armarego, W. L. F.; Perrin, D. D., *Purification of Laboratory Chemicals,* 4th ed.; Butterworth-Heinemann, 1996.
119. Chotana, G. A.; Rak, M. A.; Smith, M. R. Sterically Directed Functionalization of Aromatic C-H Bonds: Selective Borylation Ortho to Cyano Groups in Arenes and Heterocycles. *J. Am. Chem. Soc.* **2005**, *127*, 10539–10544.

120. Budiman, Y. P.; Lorenzen, S.; Liu, Z.; Radius, U.; Marder, T. B. Base-Free Pd-Catalyzed C−Cl Borylation of Fluorinated Aryl Chlorides. *Chem. Eur. J.* **2021**, *27*, 3869 – 3874.
121. Takaya, J.; Ito, S.; Nomoto, H.; Saito, N.; Kirai, N.; Iwasawa, N. Fluorine-Controlled C-H Borylation of Arenes Catalyzed by a PSiN-Pincer Platinum Complex. *Chem. Commun.* **2015**, *51*, 17662–17665.
122. Cho, J-Y.; Iverson, C. N.; Smith, M. R. Steric and Chelate Directing Effects in Aromatic Borylation. *J. Am. Chem. Soc.* **2000**, *122*, 12868-12869.
123. Primas, N.; Bouillon, A.; Lancelot, J. C.; El-Kashef, H.; Rault, S. Synthesis of 5-Arylthiazoles. Comparative Study between Suzuki Cross-Coupling Reaction and Direct Arylation. *Tetrahedron* **2009**, *65* (29–30), 5739–5746.
124. Tang, W.; Keshipeddy, S.; Zhang, Y.; Wei, X.; Savoie, J.; Patel, N. D.; Yee, N. K.; Senanayake, C. H. Efficient Monophosphorus Ligands for Palladium-Catalysed Miyaura Borylation. *Org. Lett.* **2011**, *13*, 1366-1369.
125. Adamczyk-Woźniak, A.; Jakubczyk, M.; Sporzyński, A.; Zukowska, G. Quantitative Determination of the Lewis Acidity of Phenylboronic Catechol Esters - Promising Anion Receptors for Polymer Electrolytes. *Inorg. Chem. Commun.* **2011**, *14*, 1753–1755.
126. Liu, K.; Li, N.; Ning, L.; Zhu, C.; Xie, J. Gold-Catalyzed Oxidative Biaryl Cross-Coupling of Organometallics. *Chem*. **2019**, *5*, 2718-2730.
127. Leowanawat, P.; Resmerita, A. M.; Moldoveanu, C.; Liu, C.; Zhang, N.; Wilson, D. A.; Hoang, L. M.; Rosen, B. M.; Percec, V. Zero-Valent Metals Accelerate the Neopentylglycolborylation of Aryl Halides Catalyzed by $NiCl_2$-Based Mixed-Ligand Systems. *J. Org. Chem.* **2010**, *75*, 7822–7828.
128. Hermans, P. H. Über die Konstitution der Borsäuren und einiger ihrer Derivate. *Z. Anorg. Allg. Chem*. **1925**, *42*, 83-110.
129. Johnston, C. P.; West, T. H.; Dooley, R. E.; Reid, M.; Jones, A. B.; King, E. J.; Leach, A. G.; Lloyd-Jones, G. C. Anion-Initiated

Trifluoromethylation by $TMSCF_3$: Deconvolution of the Siliconate-Carbanion Dichotomy by Stopped-flow NMR/IR. *J. Am. Chem. Soc.* **2018**, *140*, 11112–11124.

Chapter 6

Appendix

6.1 Boronate speciation

$$x_{\mathrm{BOH}} = \frac{1}{1 + 10^{(\mathrm{p}K_\mathrm{a} - \mathrm{pH})}} \quad (7)$$

$$x_{\mathrm{BOH}} = \frac{\mathrm{BOH}}{\mathrm{BOH} + \mathrm{B}}$$

$$x_{\mathrm{BOH}} = \frac{\frac{\mathrm{BOH}}{\mathrm{BOH}}}{\frac{\mathrm{BOH}}{\mathrm{BOH}} + \frac{\mathrm{B}}{\mathrm{BOH}}}$$

$$x_{\mathrm{BOH}} = \frac{1}{1 + \frac{\mathrm{B}}{\mathrm{BOH}}}$$

$$K_\mathrm{a} = \frac{[\mathrm{ArB(OH)(OR)_2}]^- [\mathrm{H_3O}]^+}{[\mathrm{ArB(OR)_2}]} \quad (2)$$

$$K_\mathrm{a} = \frac{\mathrm{BOH}}{\mathrm{B}} + \mathrm{H}^+$$

$$\mathrm{p}K_\mathrm{a} - \mathrm{pH} = -\log_{10} \frac{\mathrm{BOH}}{\mathrm{B}}$$

$$\mathrm{p}K_\mathrm{a} - \mathrm{pH} = \log_{10} \frac{\mathrm{B}}{\mathrm{BOH}}$$

$$10^{(\mathrm{p}K_\mathrm{a} - \mathrm{pH})} = \frac{\mathrm{B}}{\mathrm{BOH}}$$

6.2 NMR spectra of synthesised compounds

^{1}H (400 MHz); $CDCl_3$:

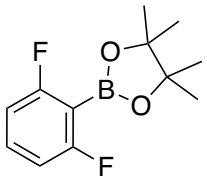

2b

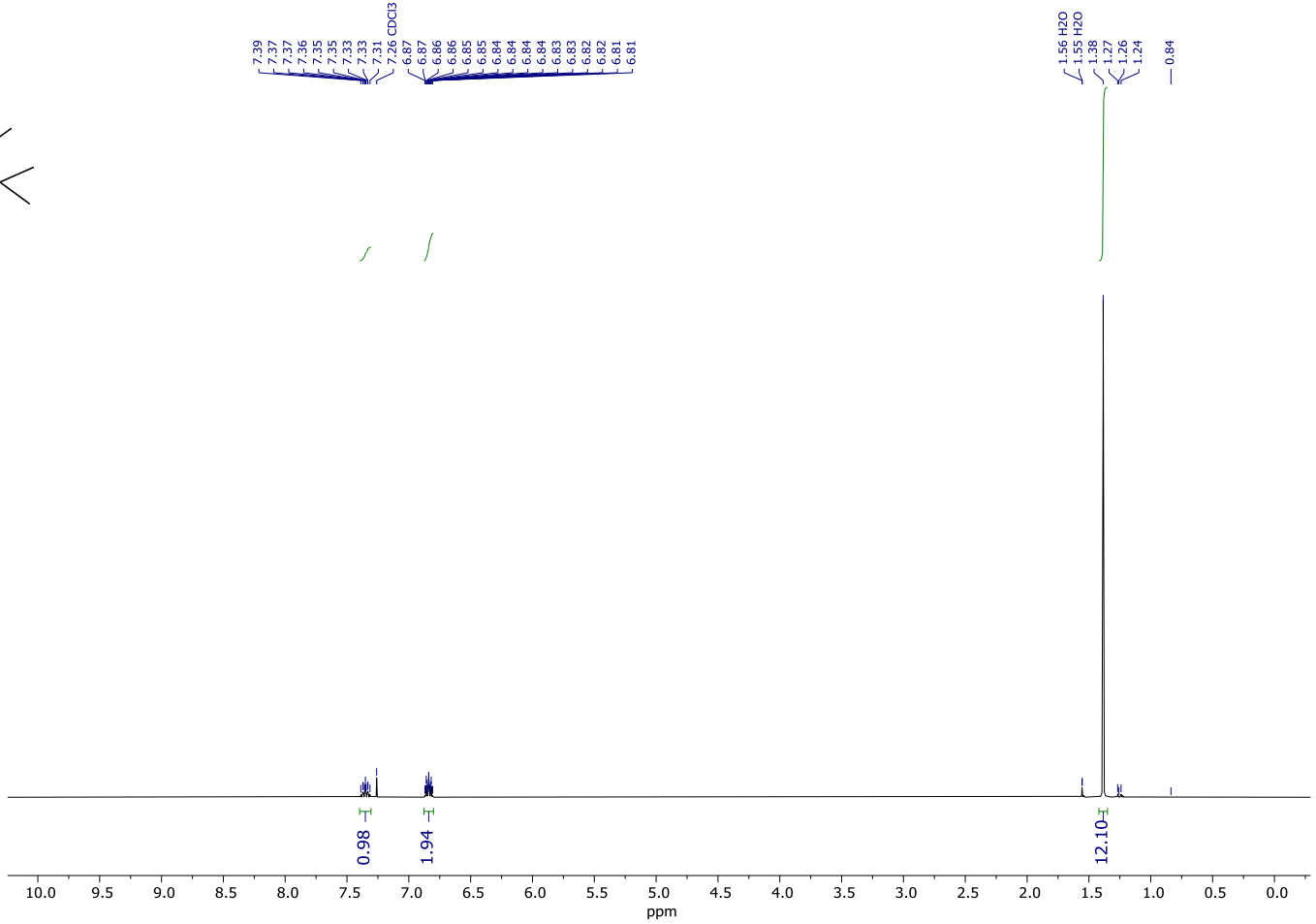

^{19}F (377 MHz); $CDCl_3$:

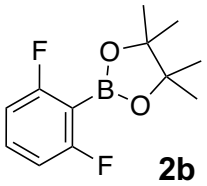

2b

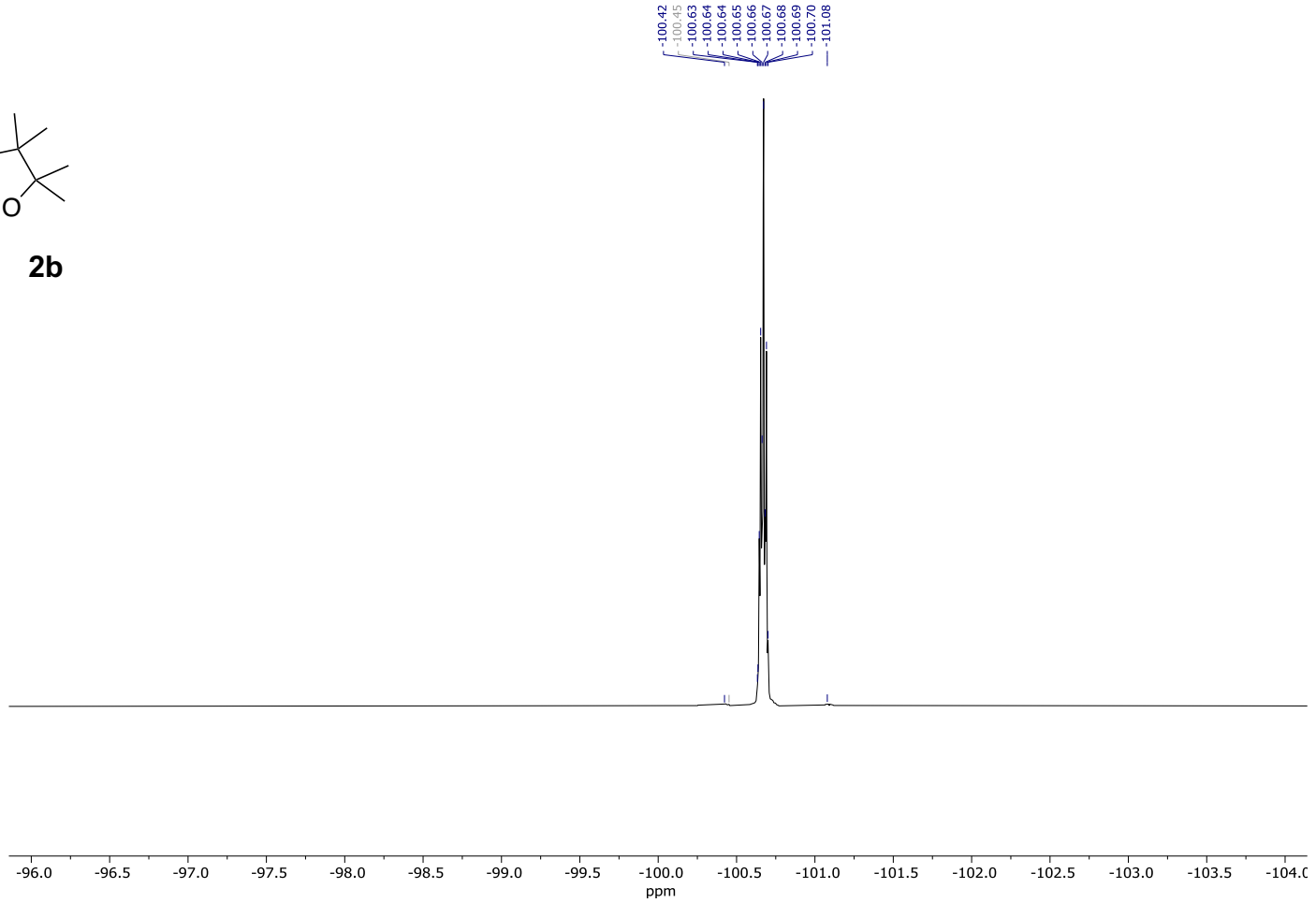

$^{13}C\{^{1}H\}$ (101 MHz); $CDCl_3$:

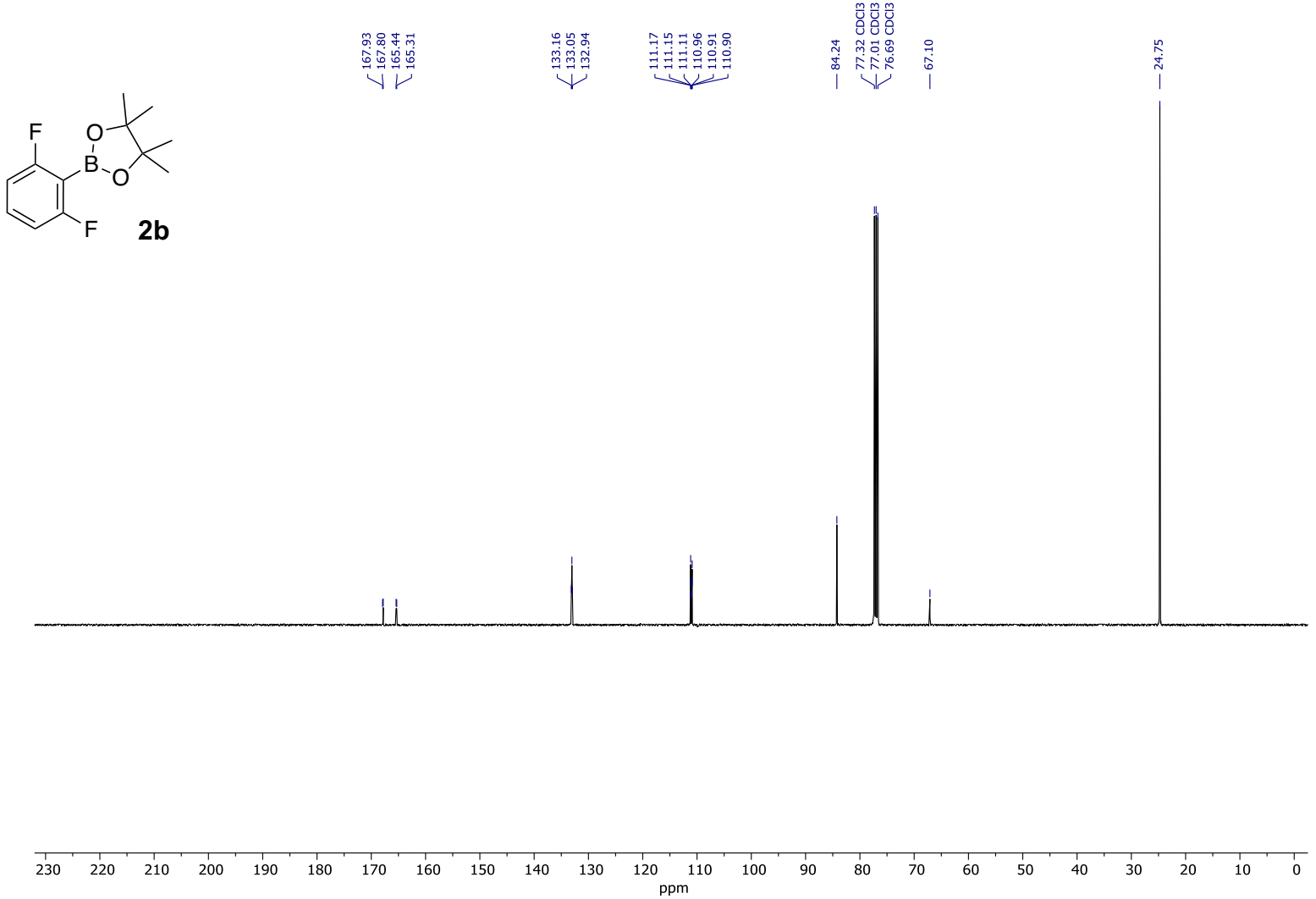

^{11}B (128 MHz); $CDCl_3$:
Trace decomposition to boric acid evident in NMR spectrum.

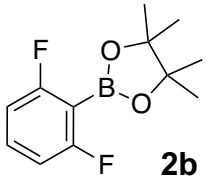

2b

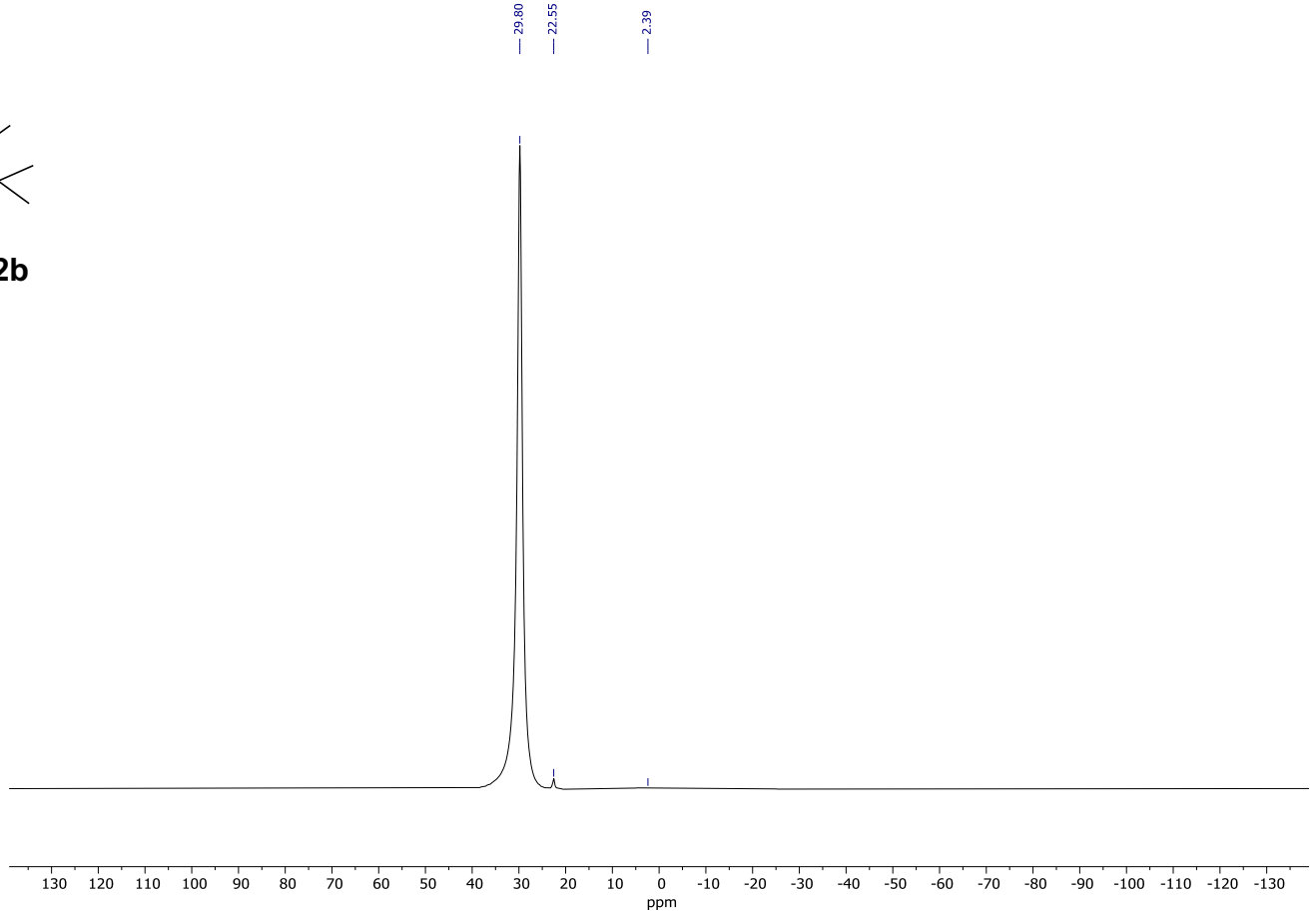

^{1}H (400 MHz); $CDCl_3$:

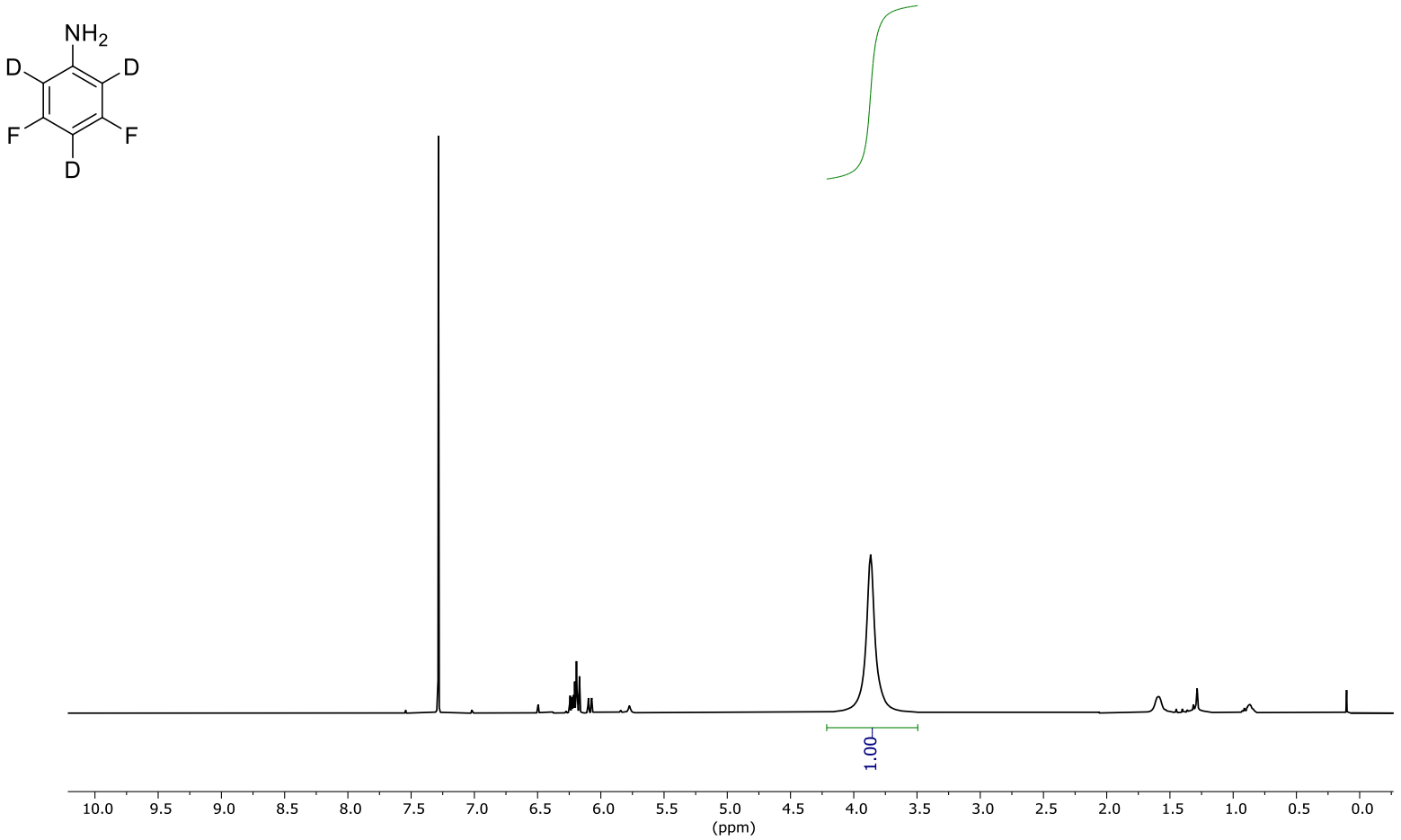

^{19}F (377 MHz); $CDCl_3$:

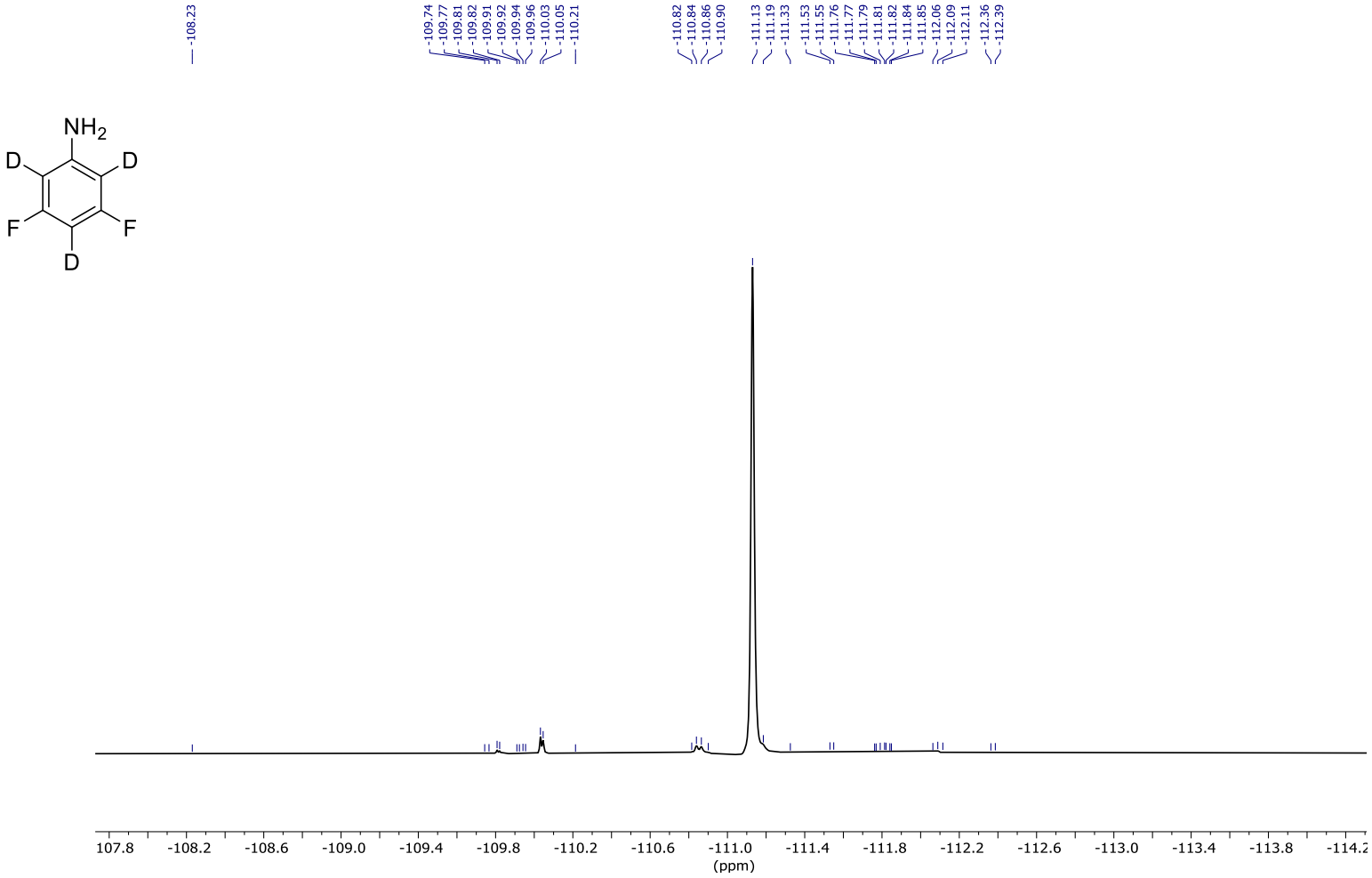

$^{13}C\{^{1}H\}$ (101 MHz); $CDCl_3$:

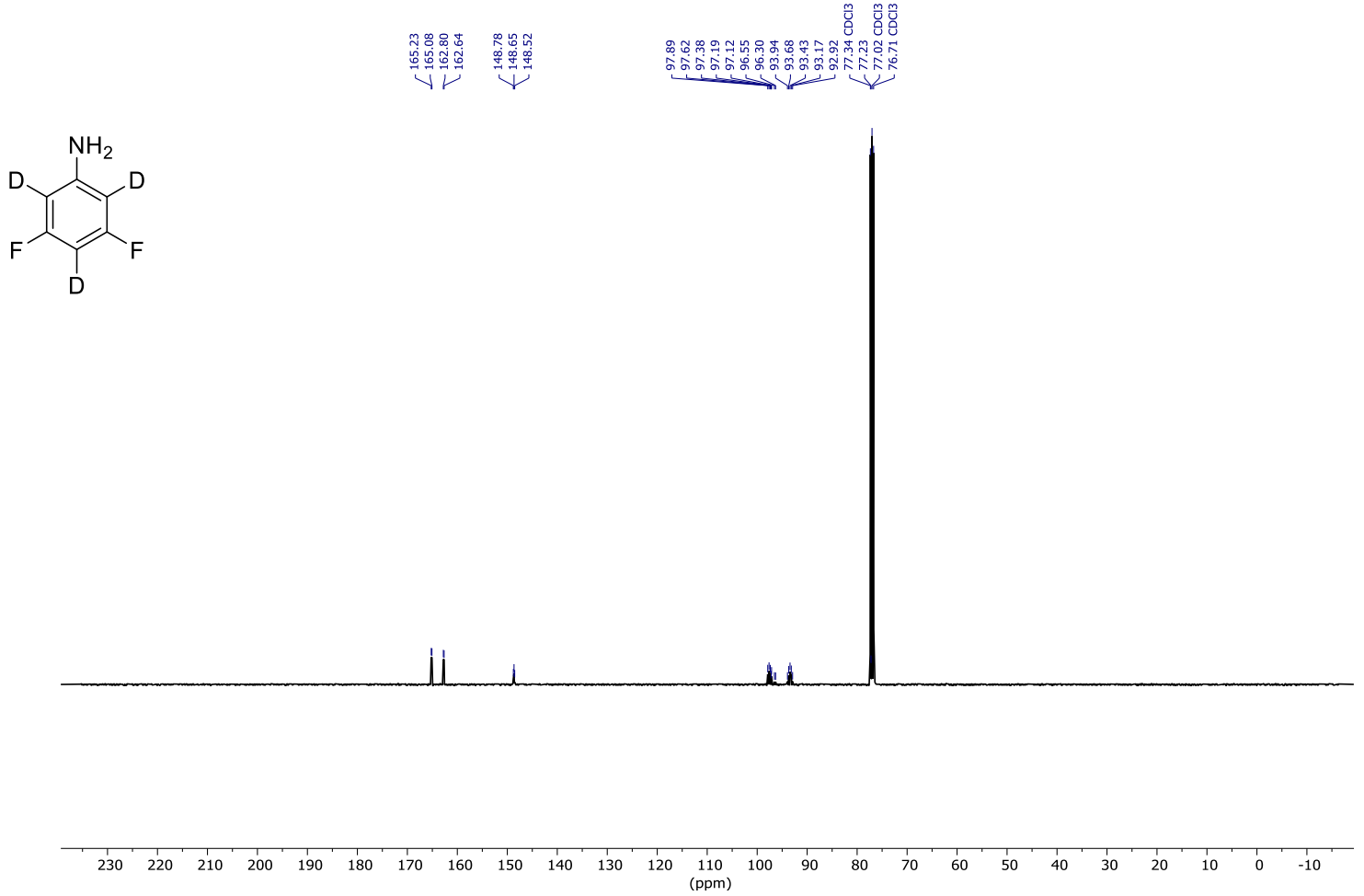

^{1}H (400 MHz); $CDCl_3$:

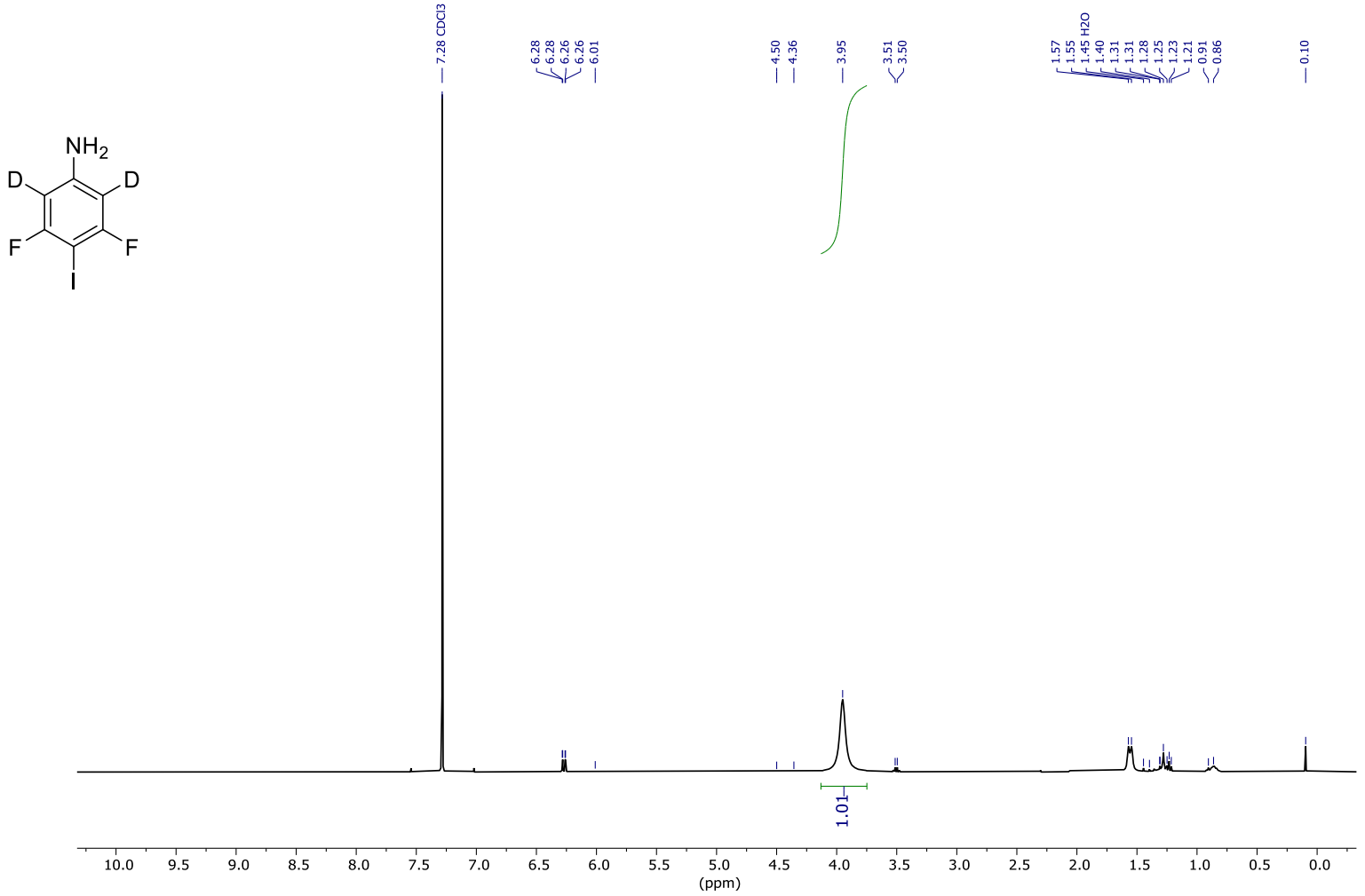

^{19}F (377 MHz); $CDCl_3$:

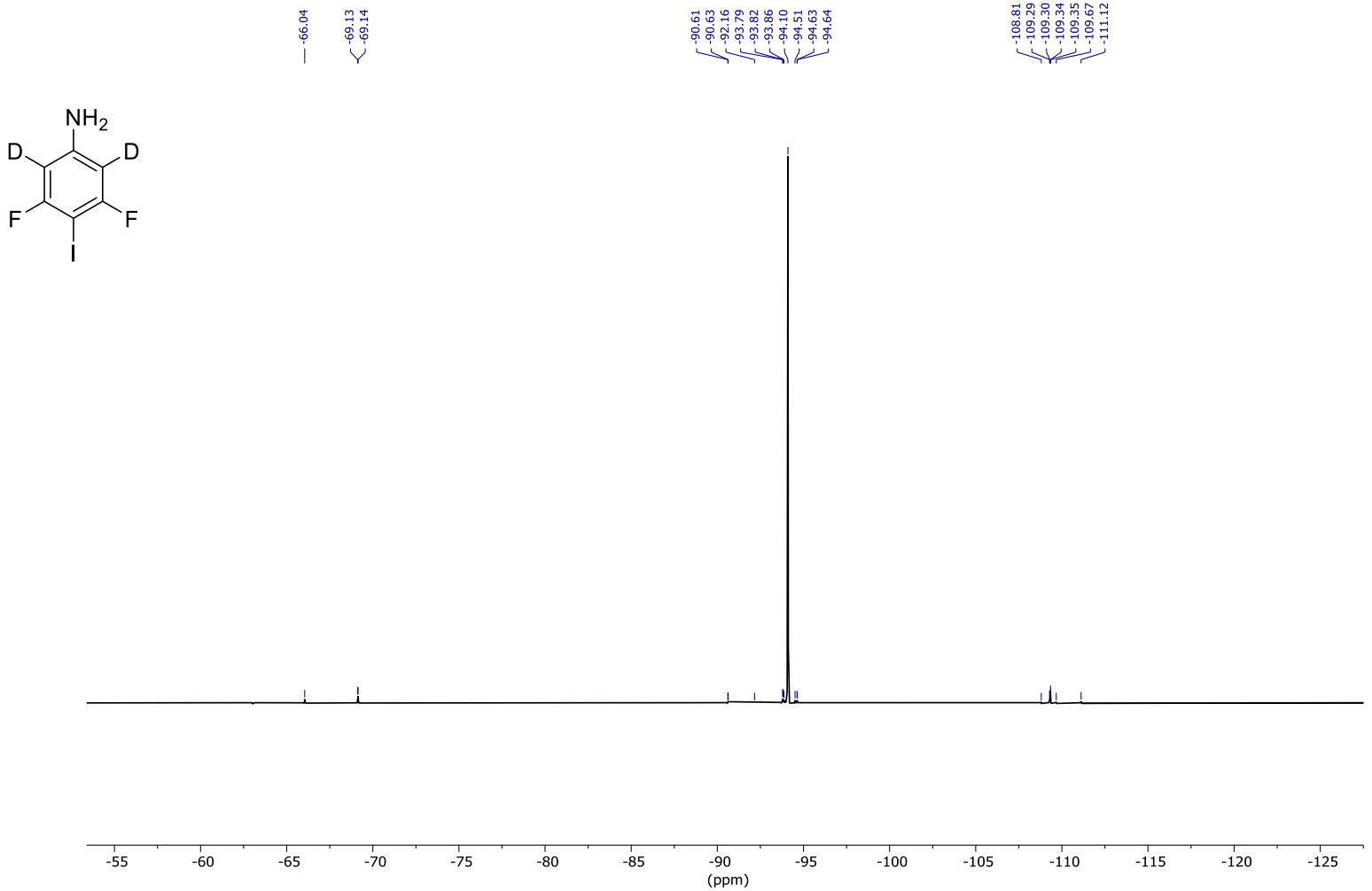

$^{13}C\{^{1}H\}$ (101 MHz); $CDCl_3$:

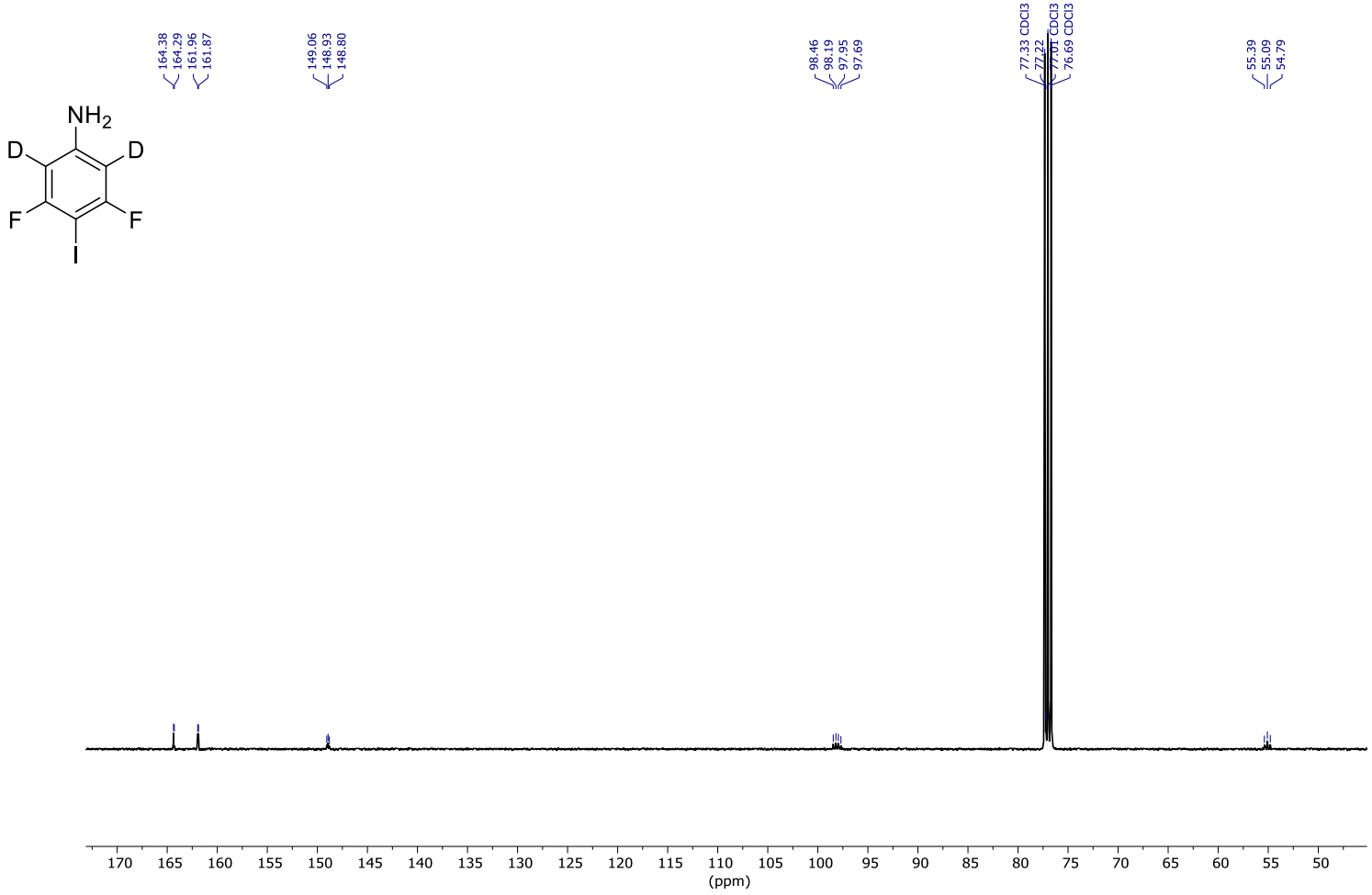

^{1}H (400 MHz); $CDCl_3$:

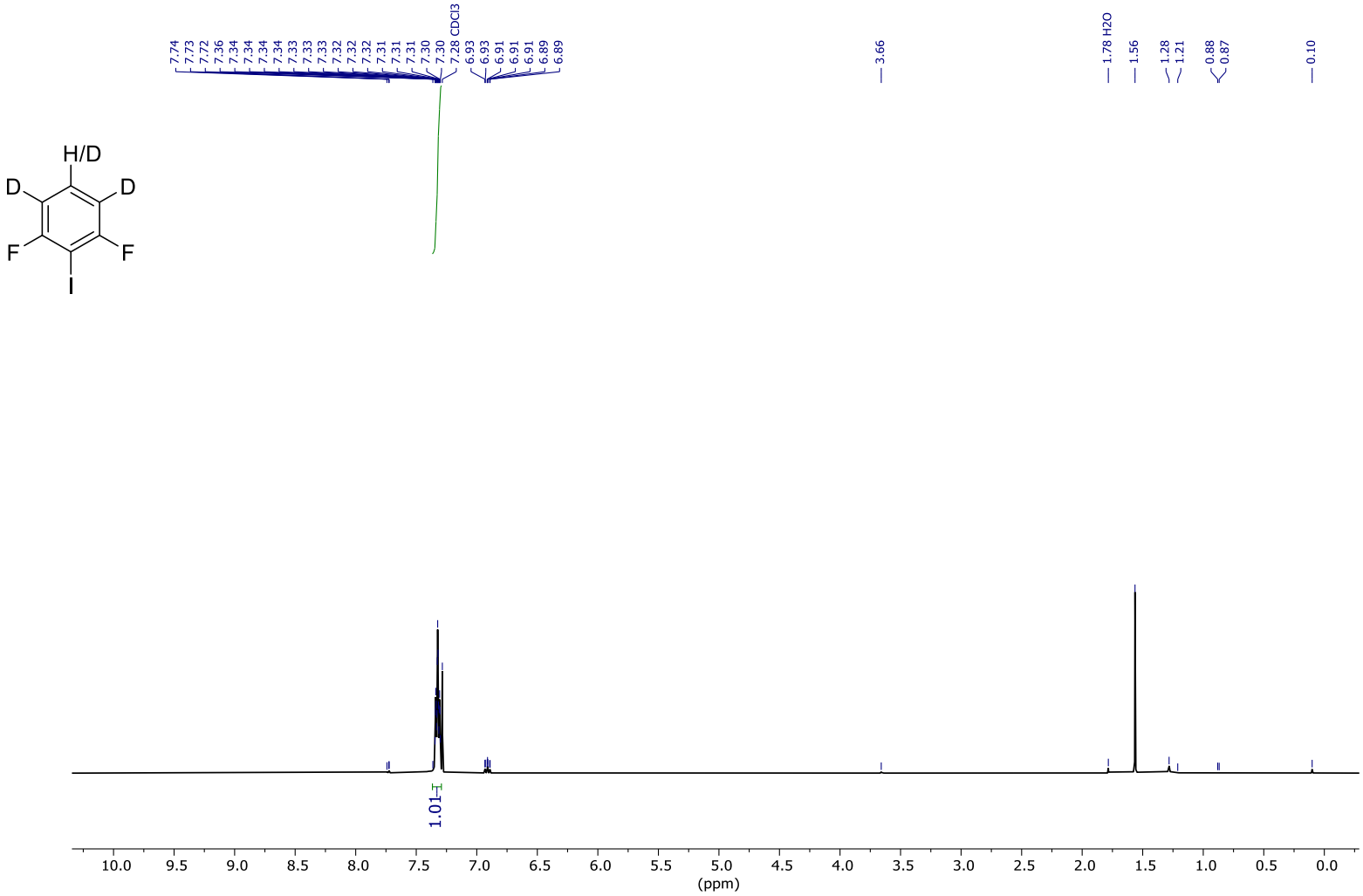

^{19}F (377 MHz); $CDCl_3$:

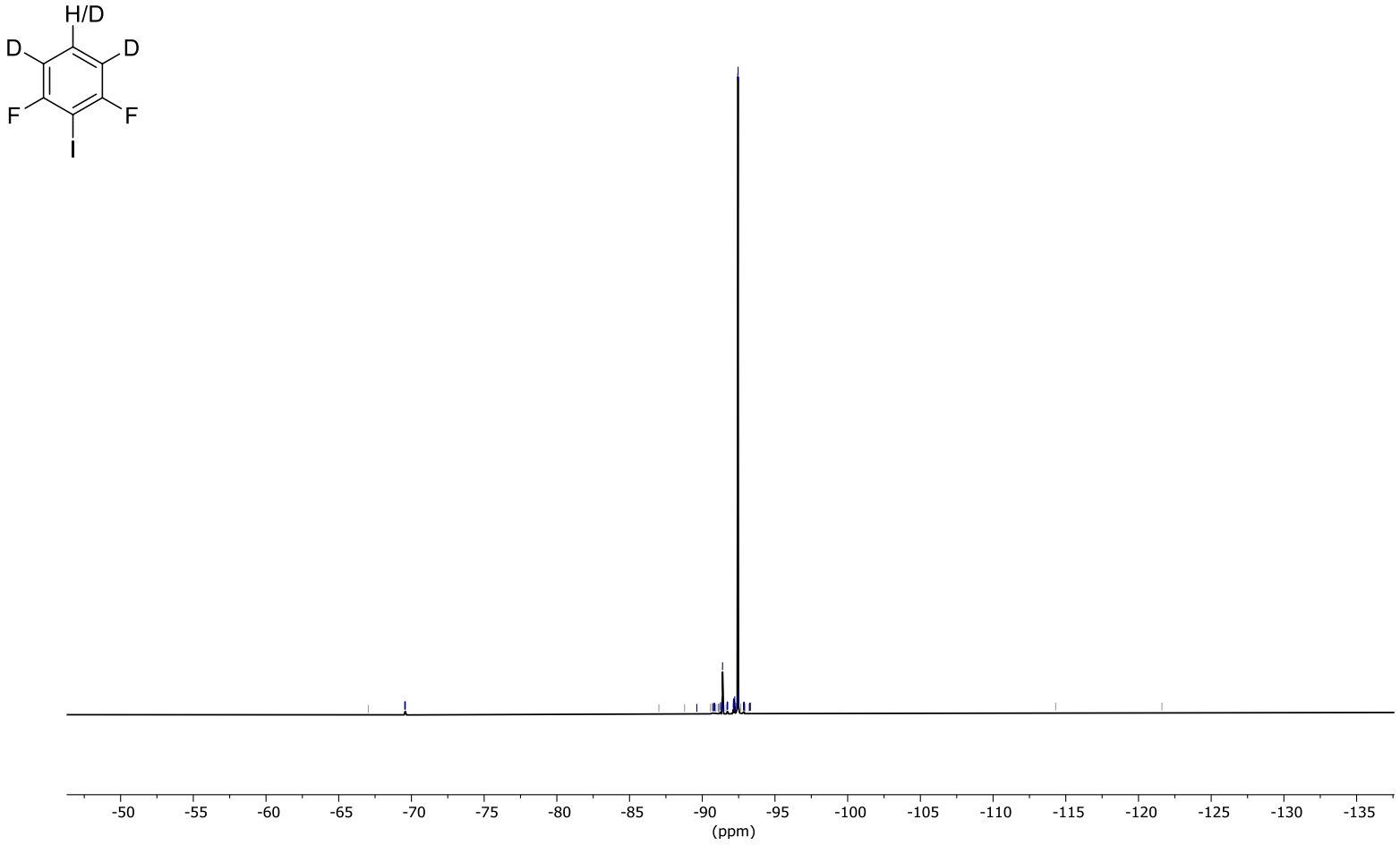

$^{13}C\{^{1}H\}$ (101 MHz); $CDCl_3$:

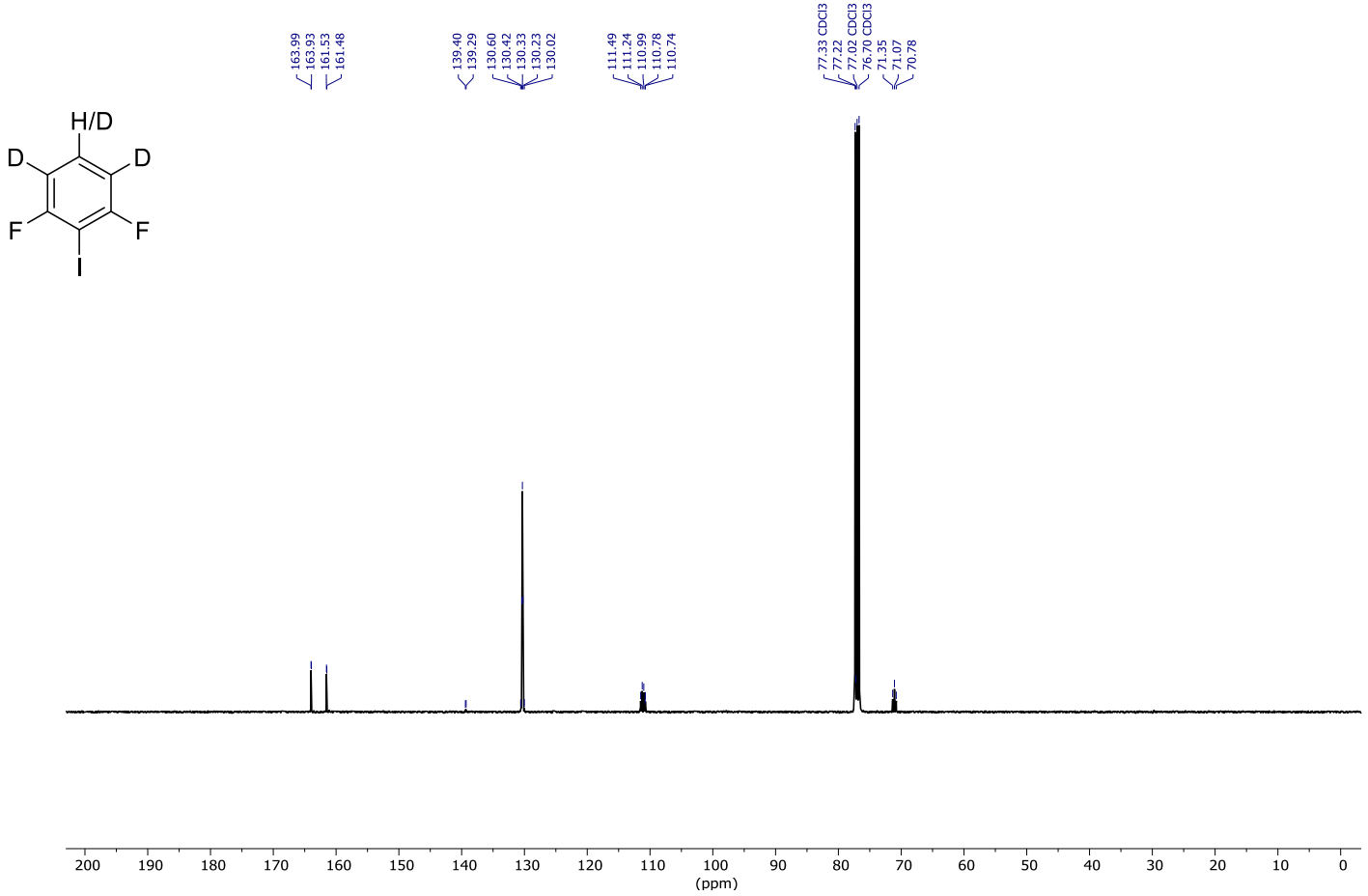

^{1}H (400 MHz); $CDCl_3$:

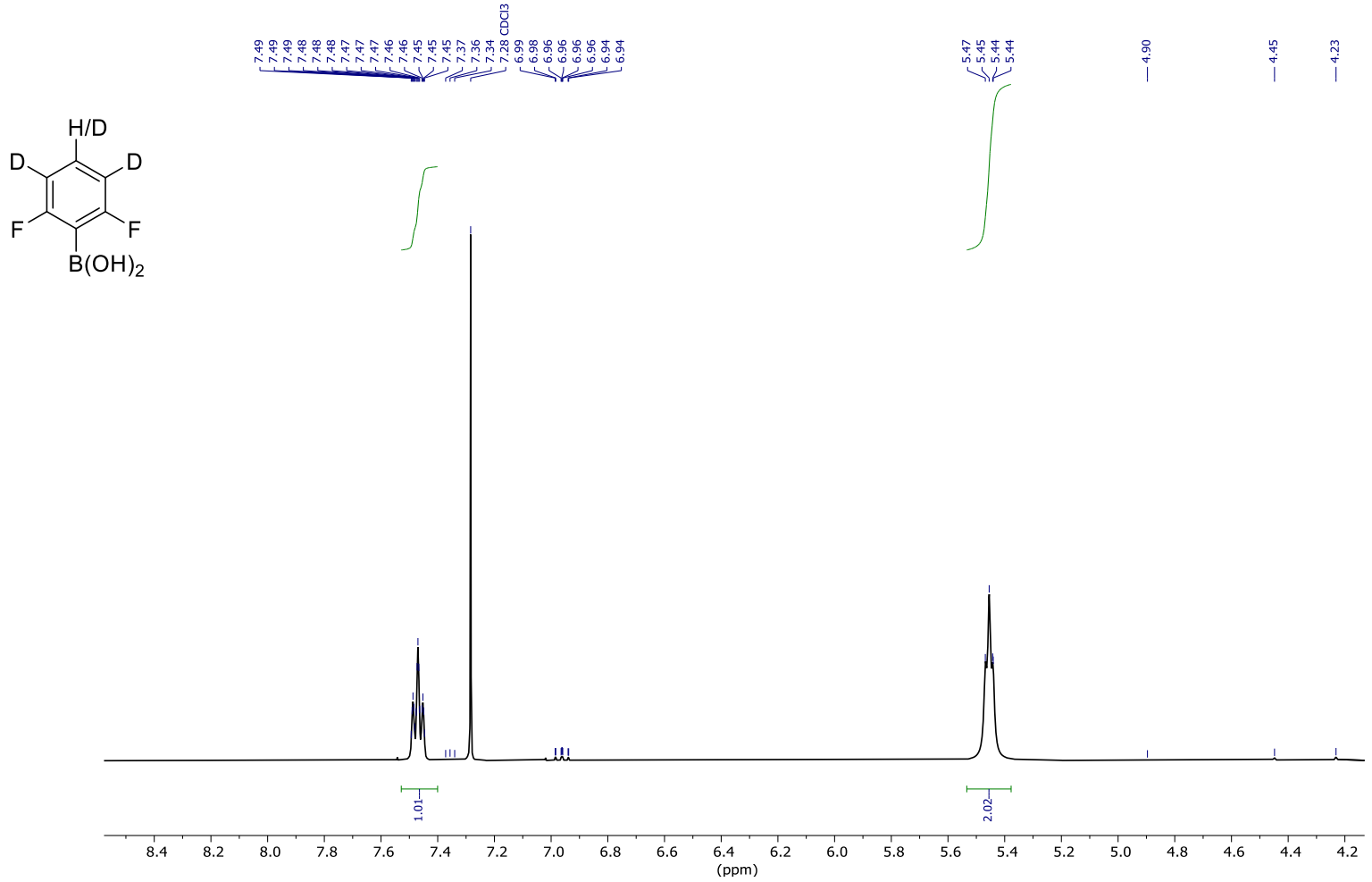

^{19}F (377 MHz); $CDCl_3$:

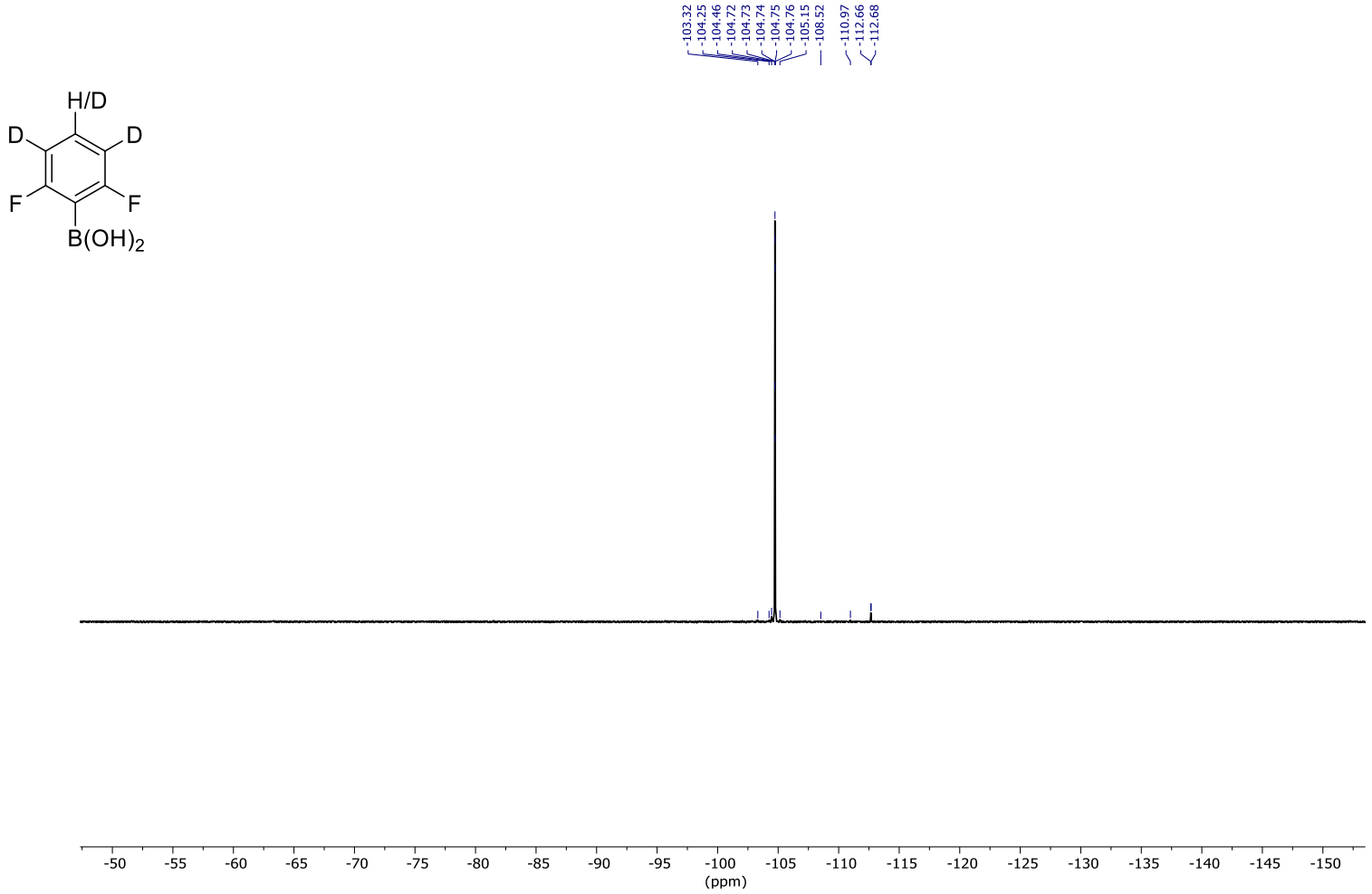

$^{13}C\{^{1}H\}$ (101 MHz); $CDCl_3$:

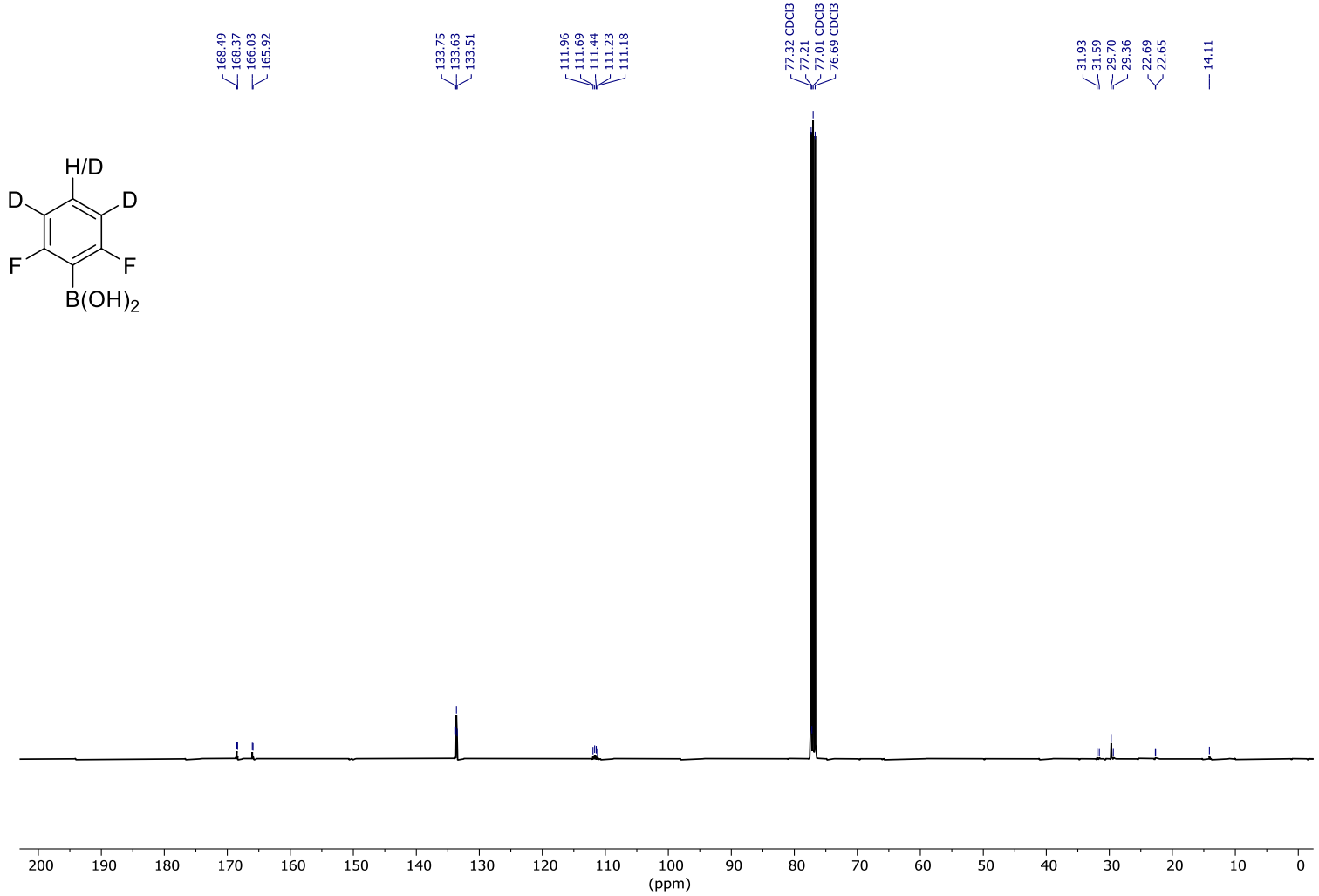

^{11}B (128 MHz); $CDCl_3$:

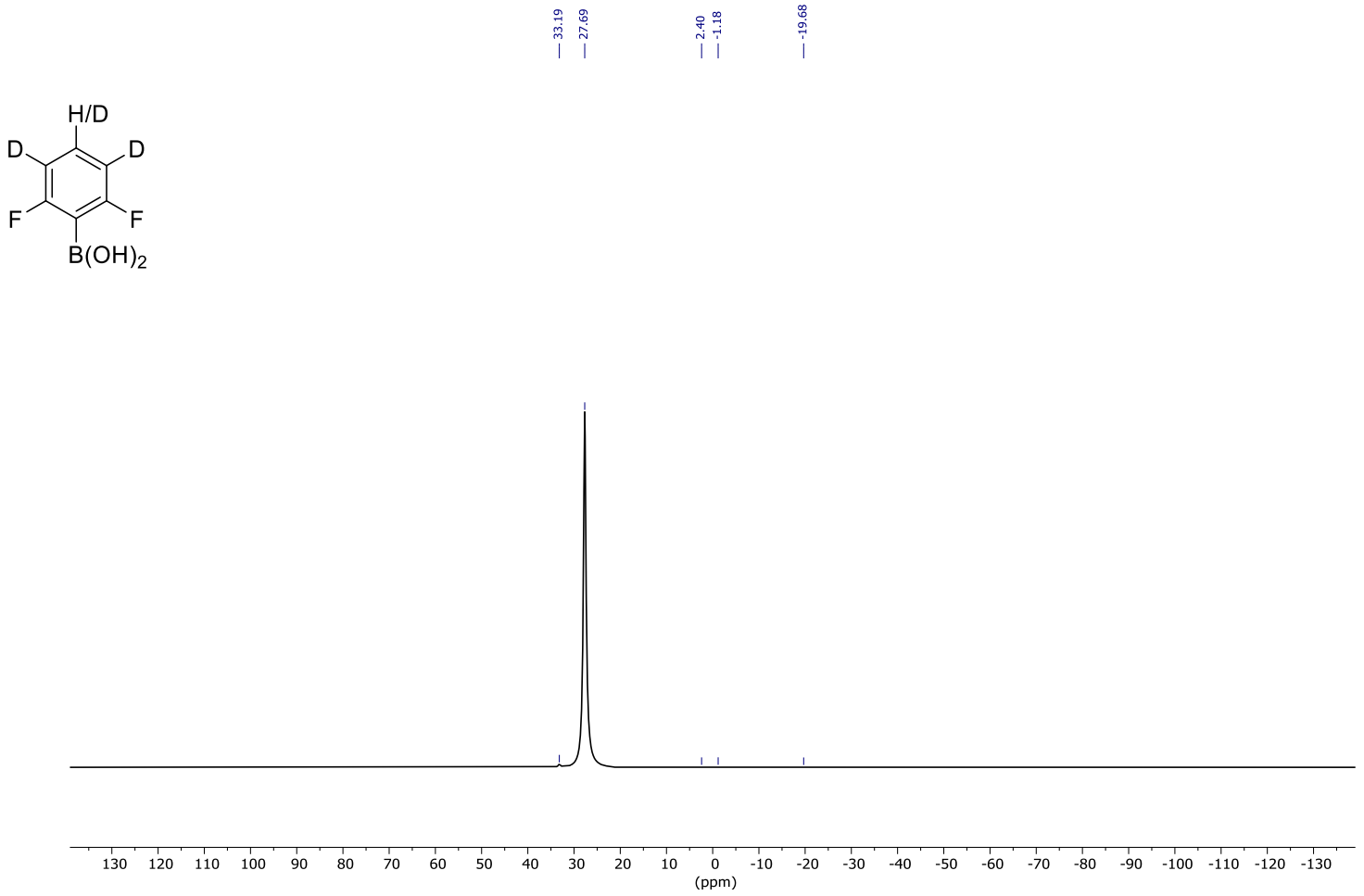

^{1}H (400 MHz); $CDCl_3$:

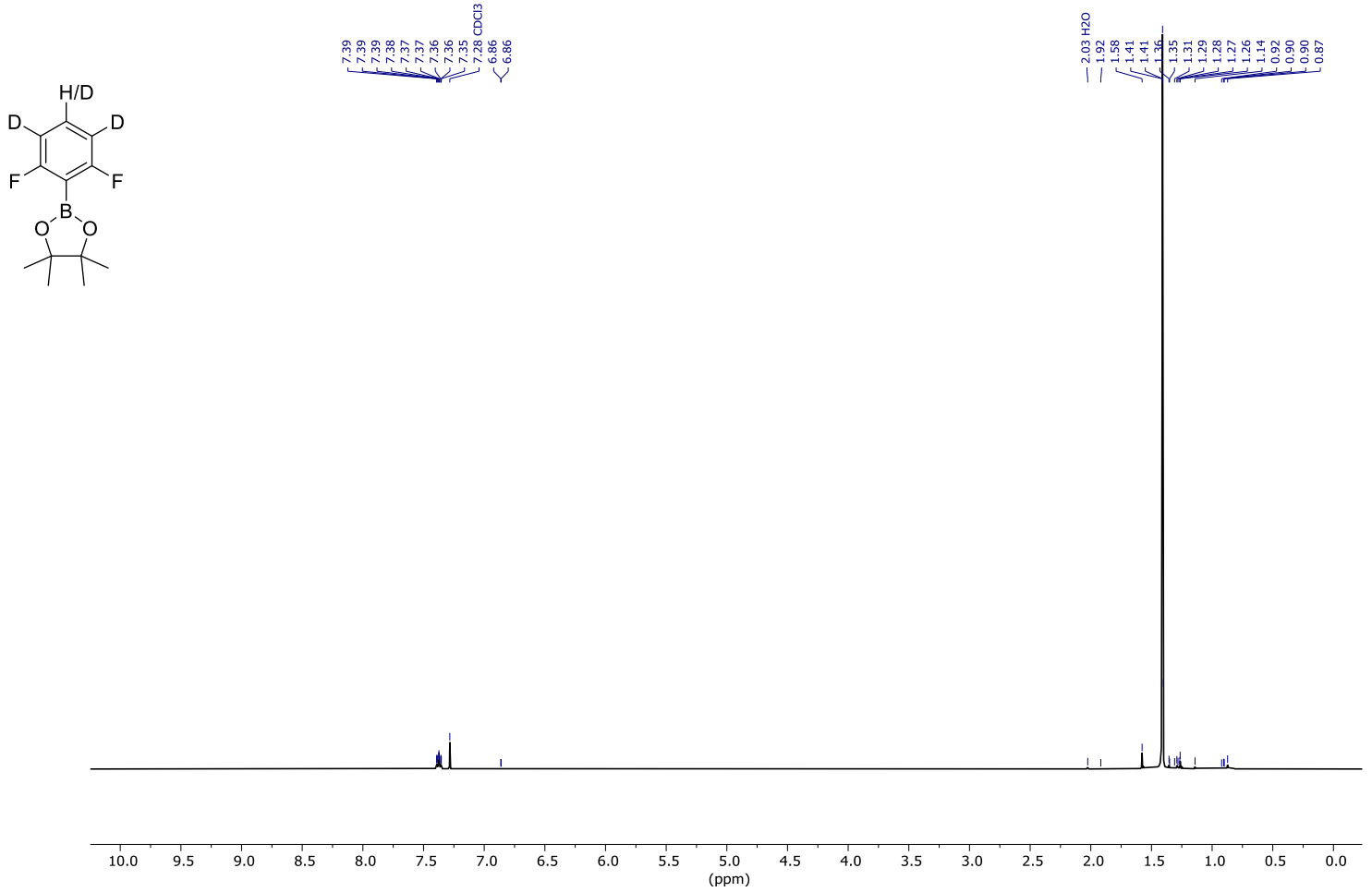

^{19}F (377 MHz); $CDCl_3$:

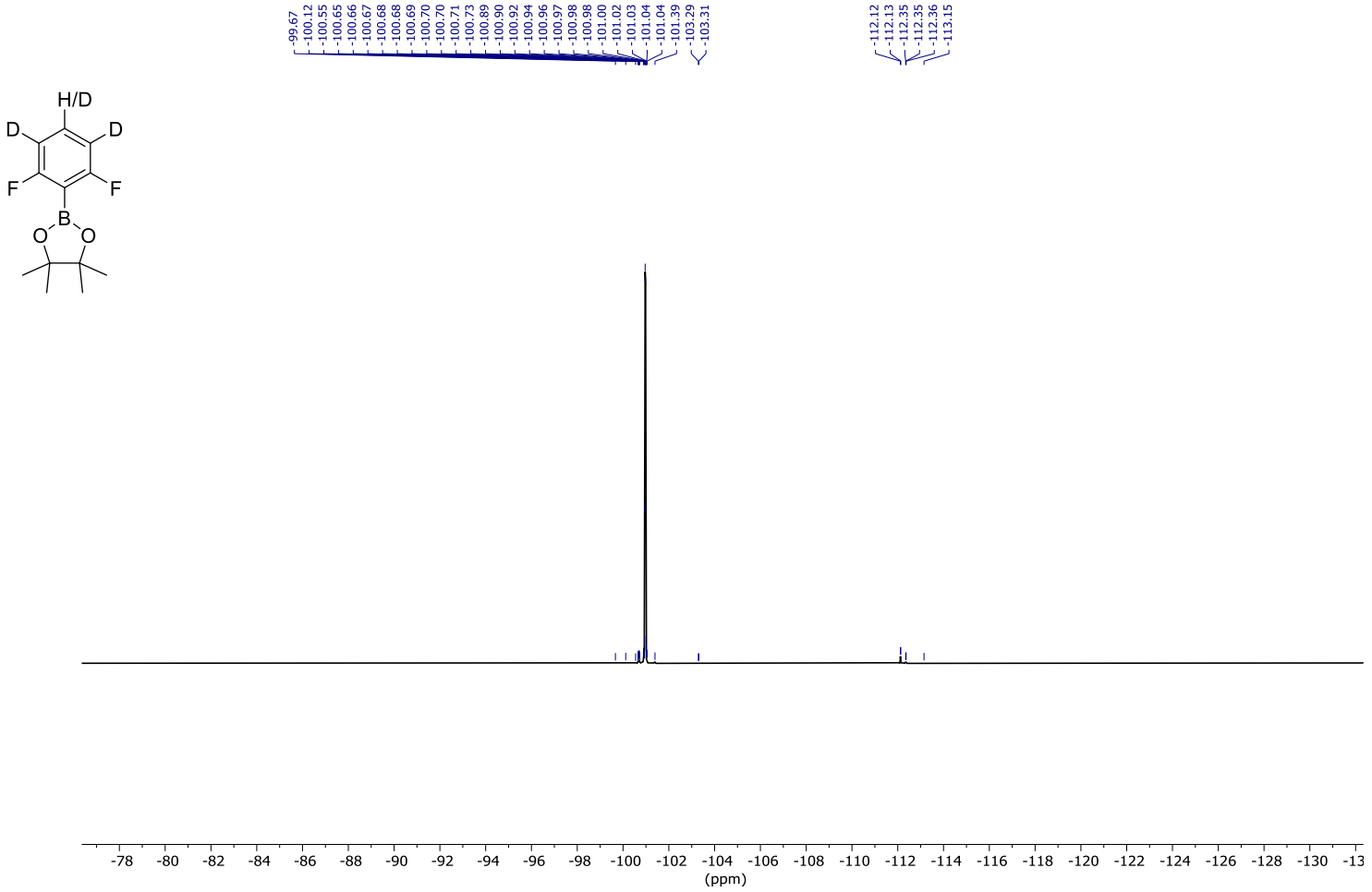

$^{13}C\{^{1}H\}$ (101 MHz); $CDCl_3$:

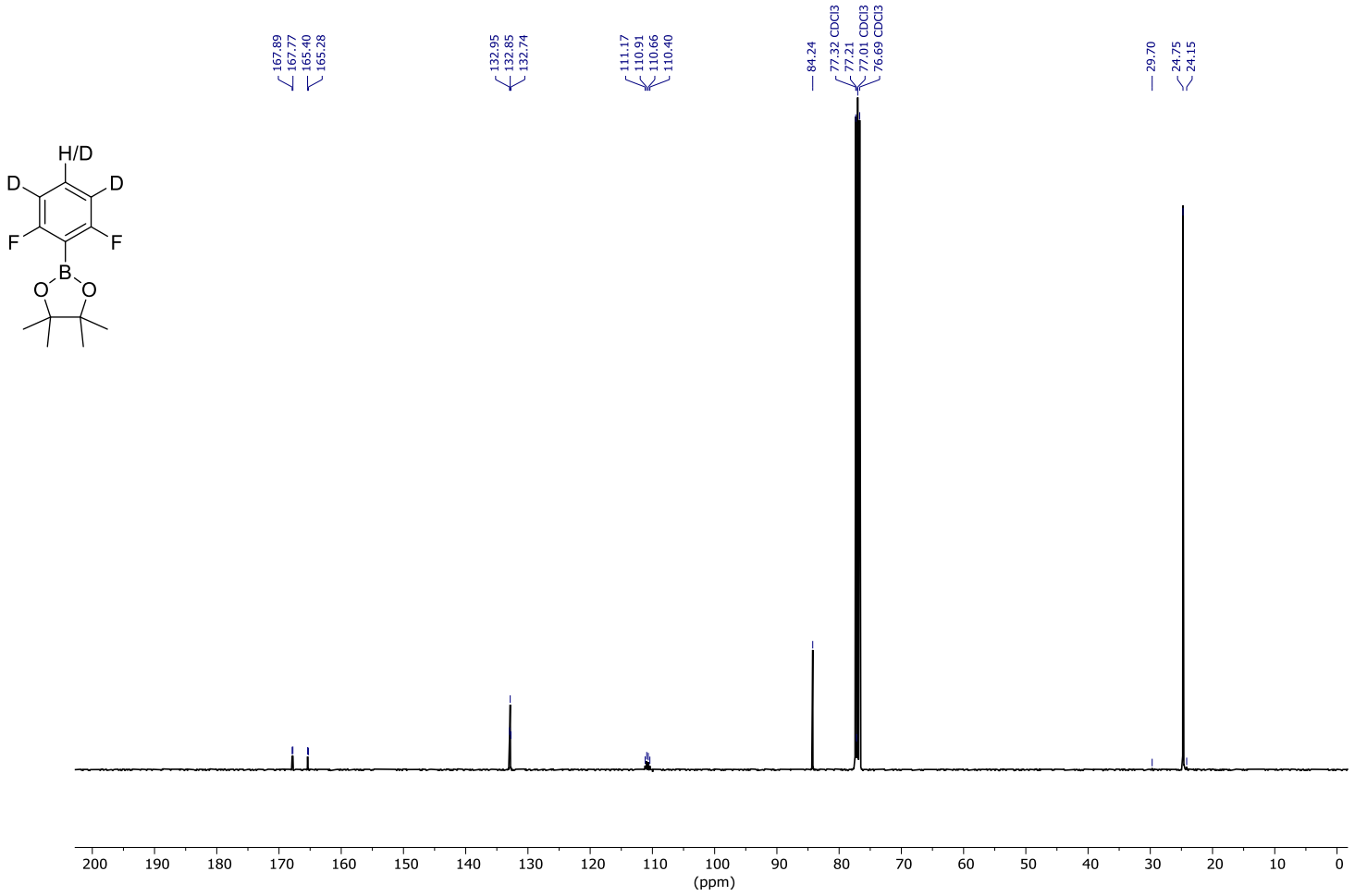

^{11}B (128 MHz); $CDCl_3$:

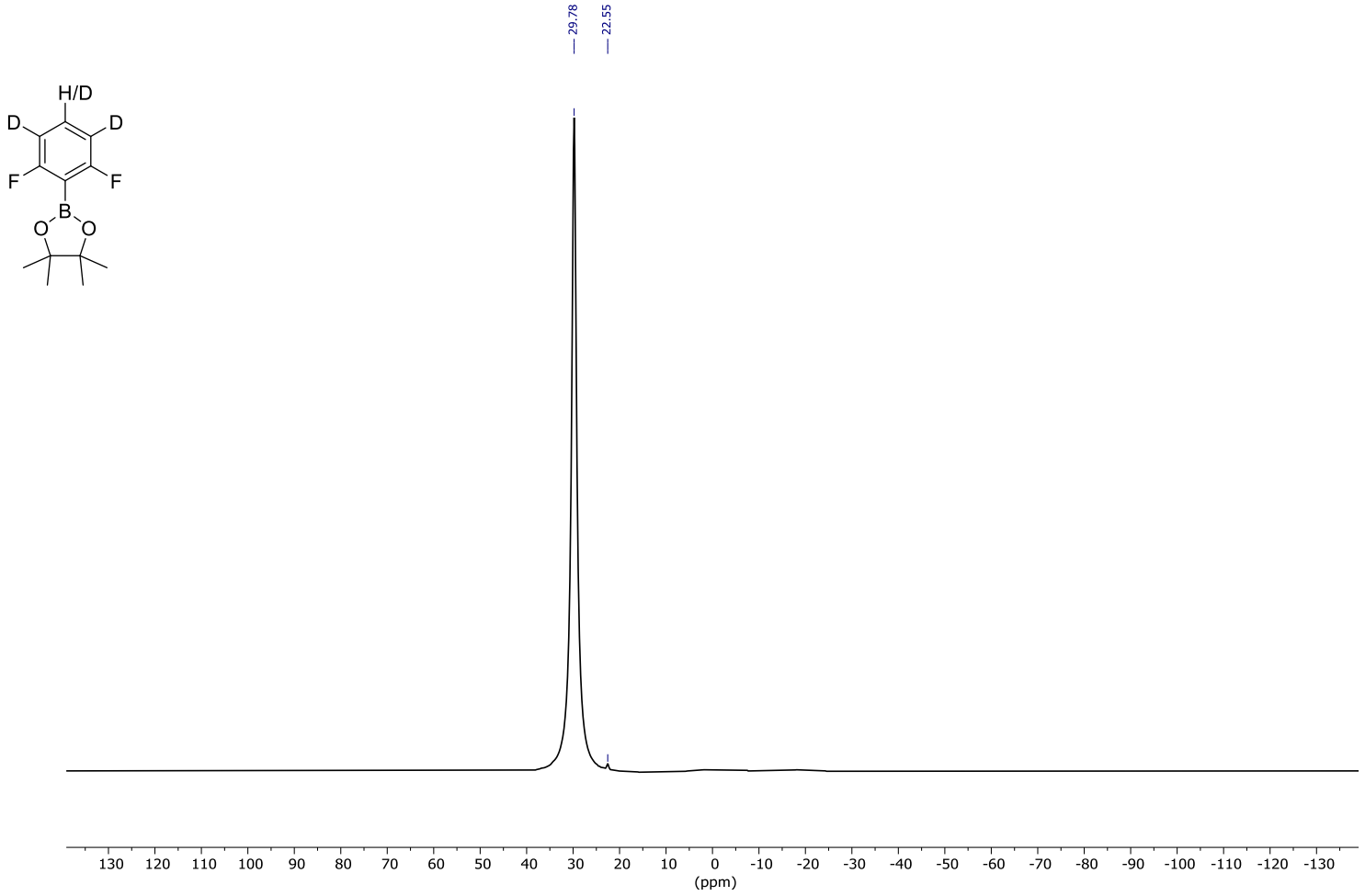

^{1}H (400 MHz); $CDCl_3$:

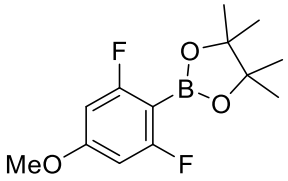

3b

^{19}F (377 MHz); $CDCl_3$:

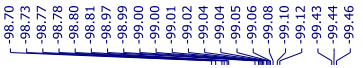

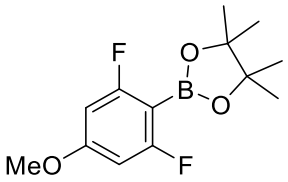

3b

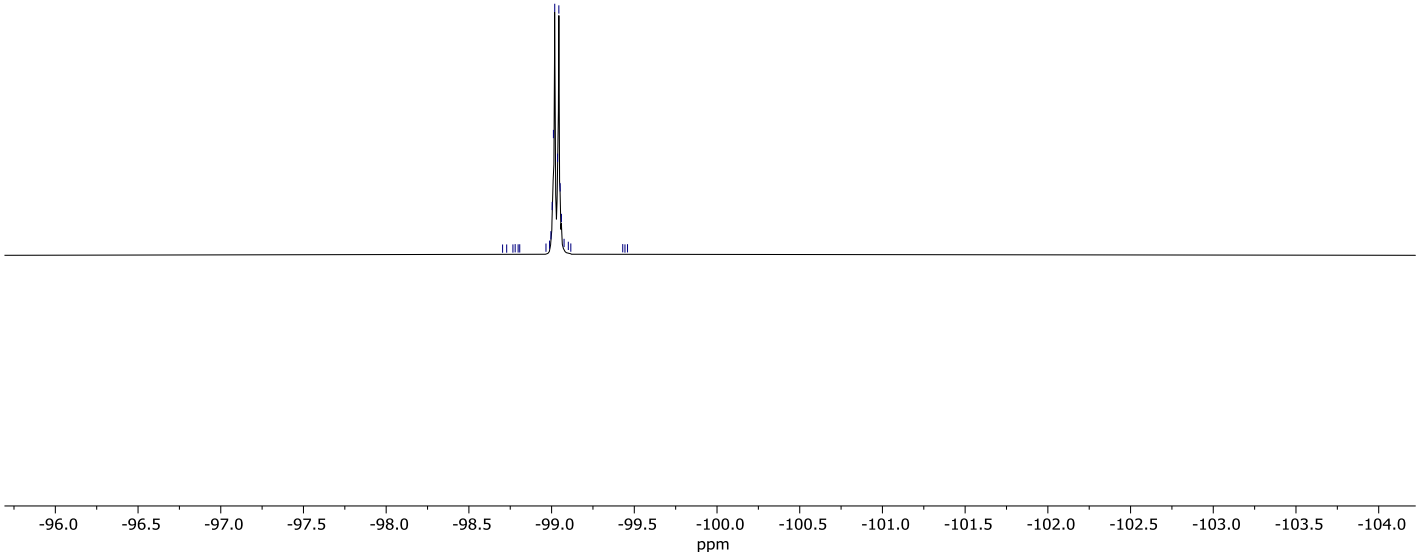

$^{13}C\{^{1}H\}$ (101 MHz); $CDCl_3$:

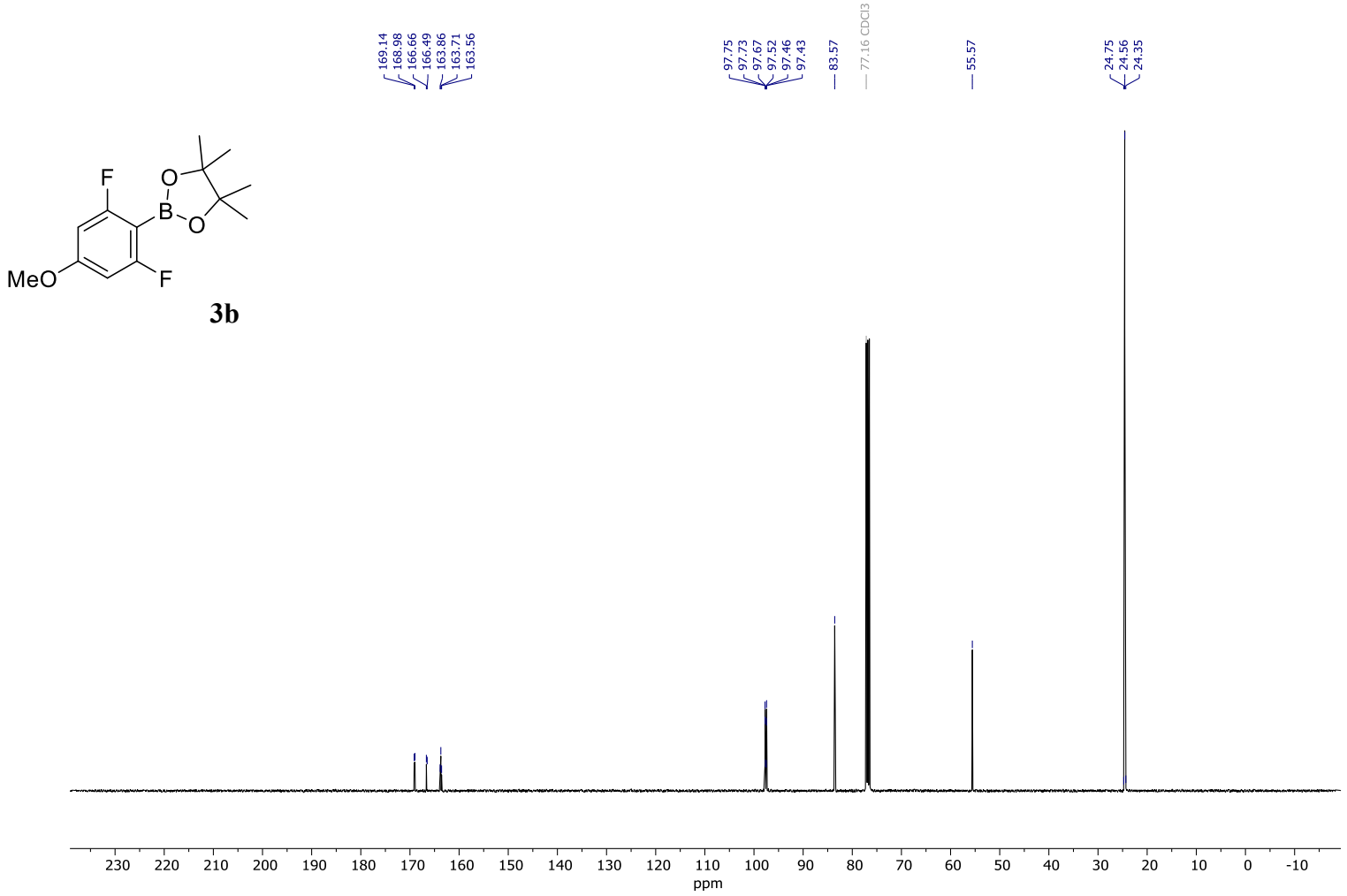

^{11}B (128 MHz); $CDCl_3$:

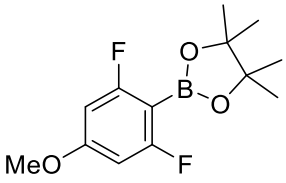

3b

^{1}H (400 MHz); $CDCl_3$:

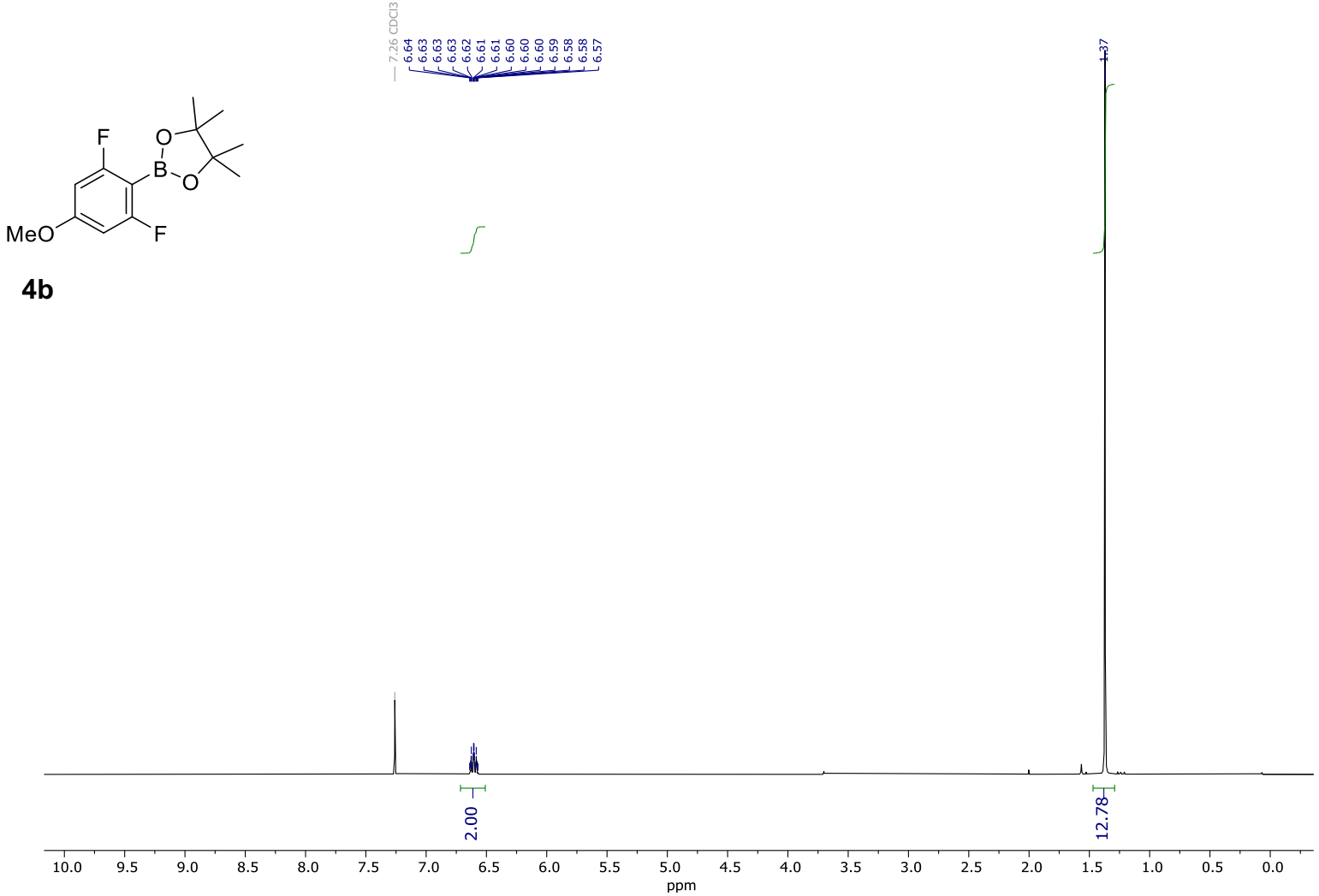

4b

^{19}F (377 MHz); $CDCl_3$:

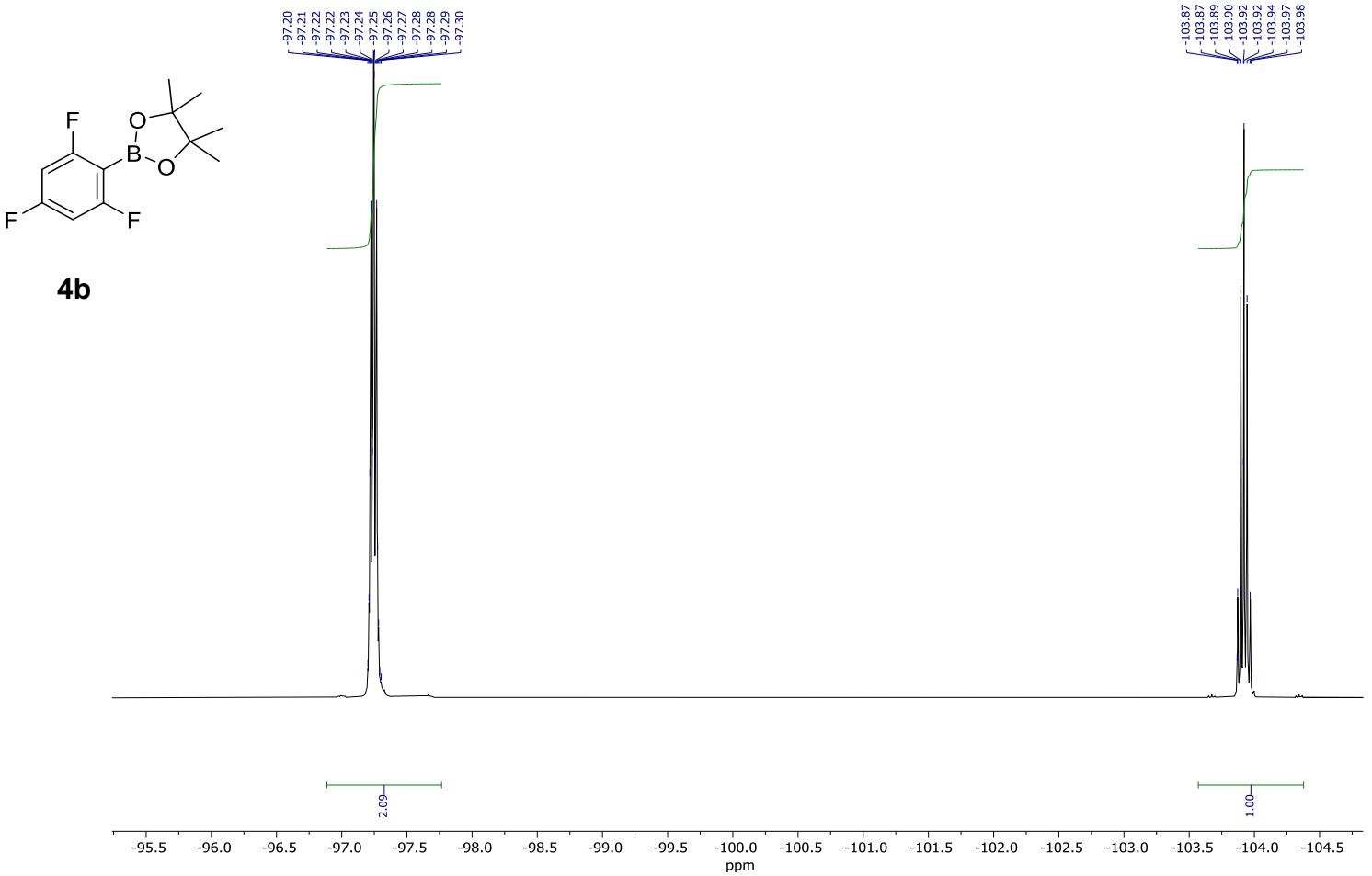

4b

$^{13}C\{^{1}H\}$ (101 MHz); $CDCl_3$:

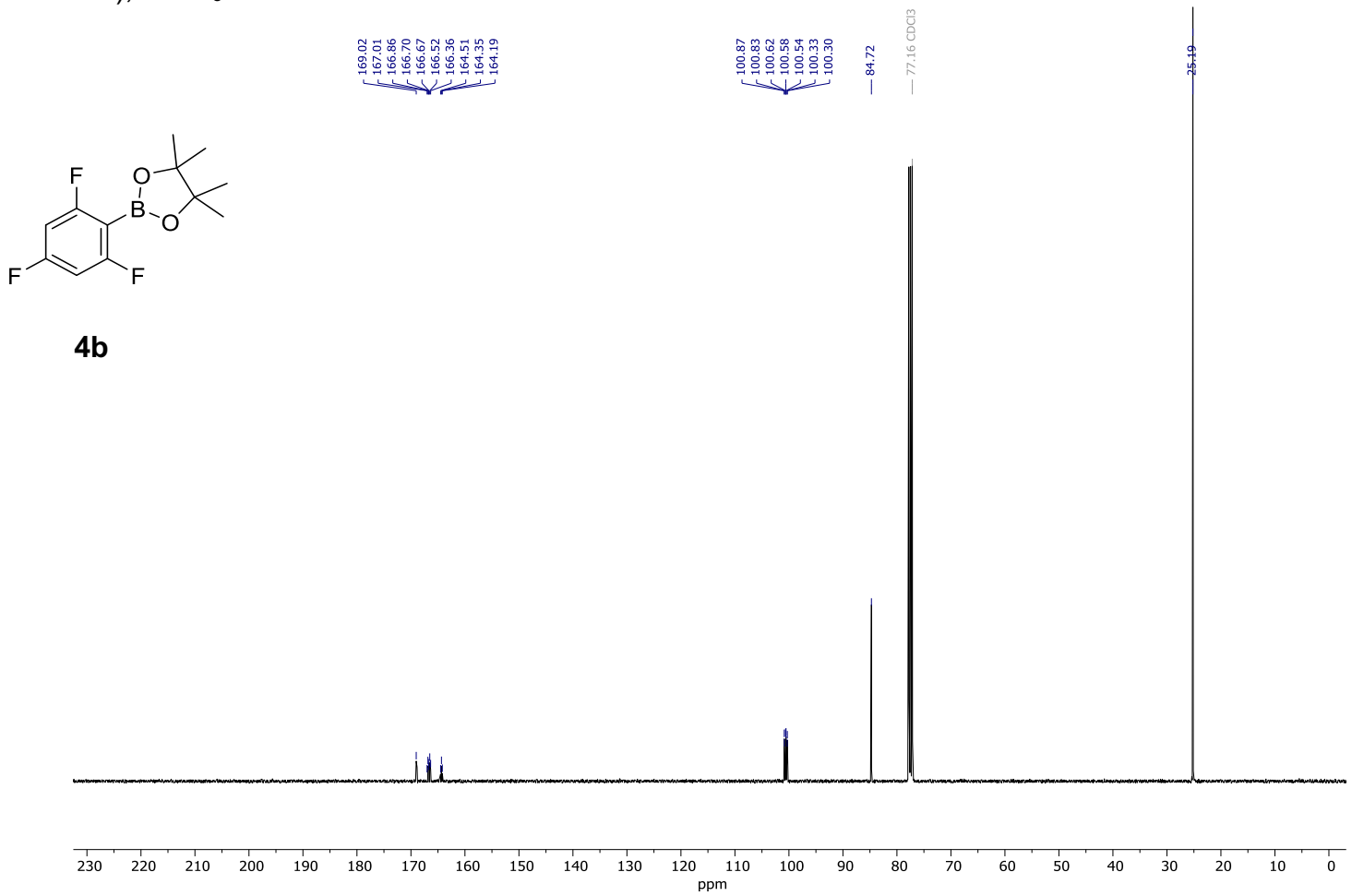

4b

^{11}B (128 MHz); $CDCl_3$:

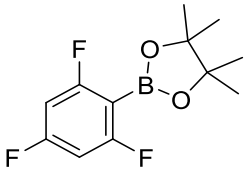

4b

^{1}H (400 MHz); $CDCl_3$:

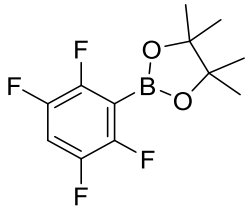

5b

^{19}F (377 MHz); $CDCl_3$:

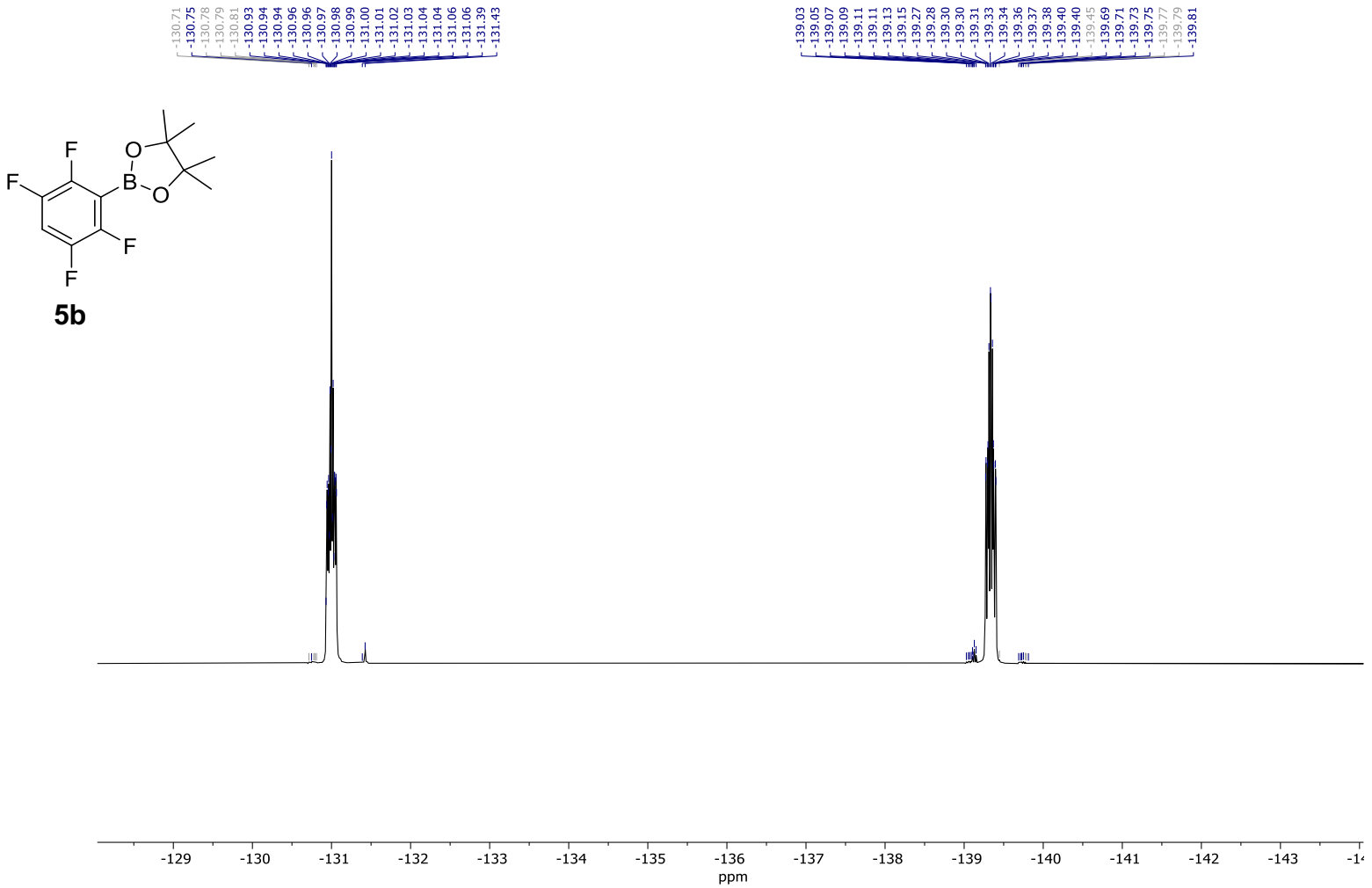

$^{13}C\{^{1}H\}$ (101 MHz); $CDCl_3$:

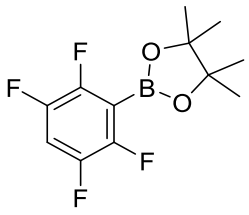

5b

^{11}B (128 MHz); $CDCl_3$:
Trace decomposition to boric acid evident in NMR spectrum.

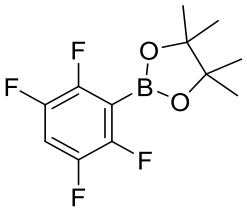

5b

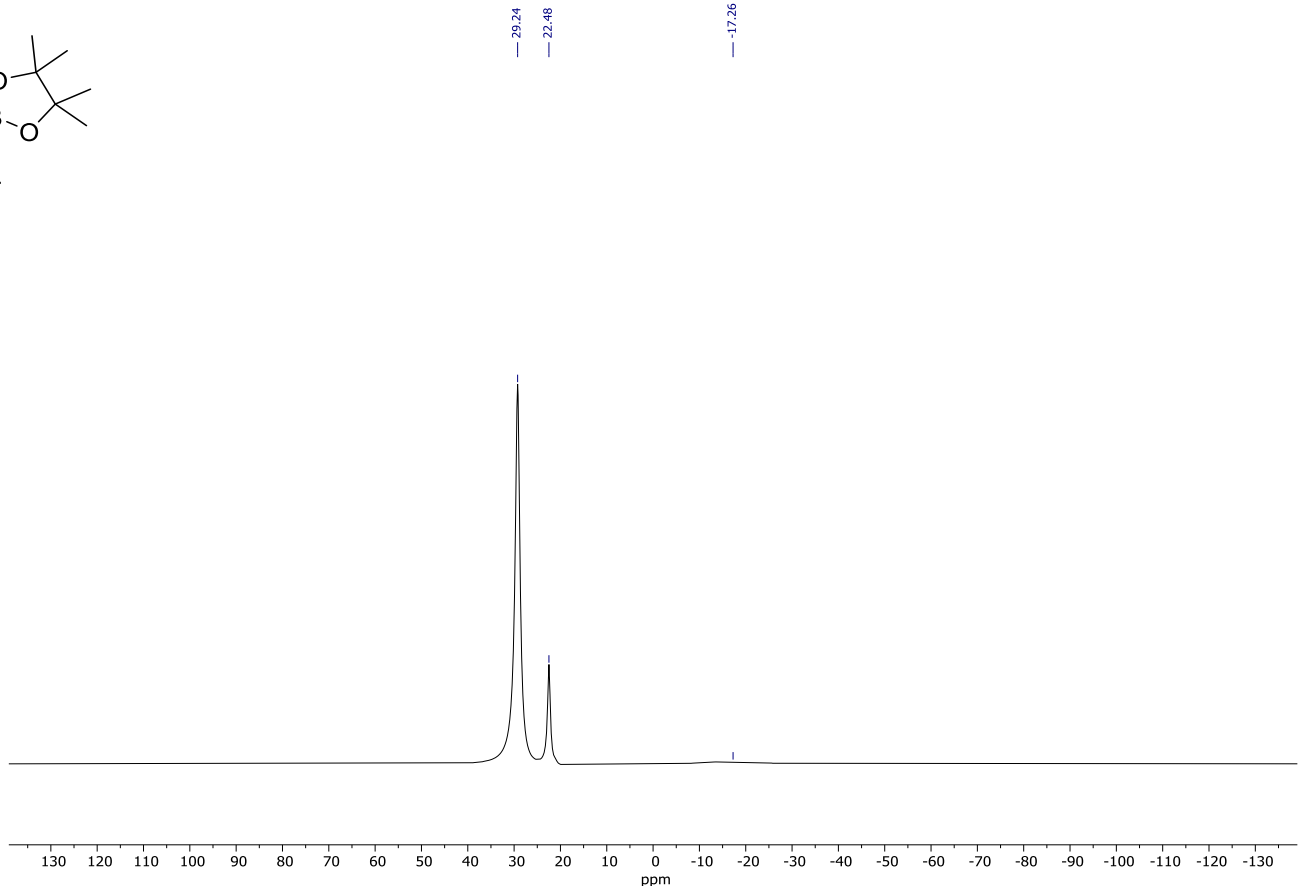

^{1}H (400 MHz); $CDCl_3$:

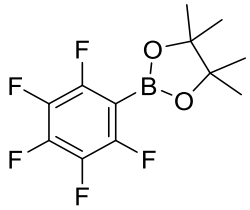

6b

^{19}F (377 MHz); $CDCl_3$:
Trace protodeboronation product (C_6F_5H) observed.

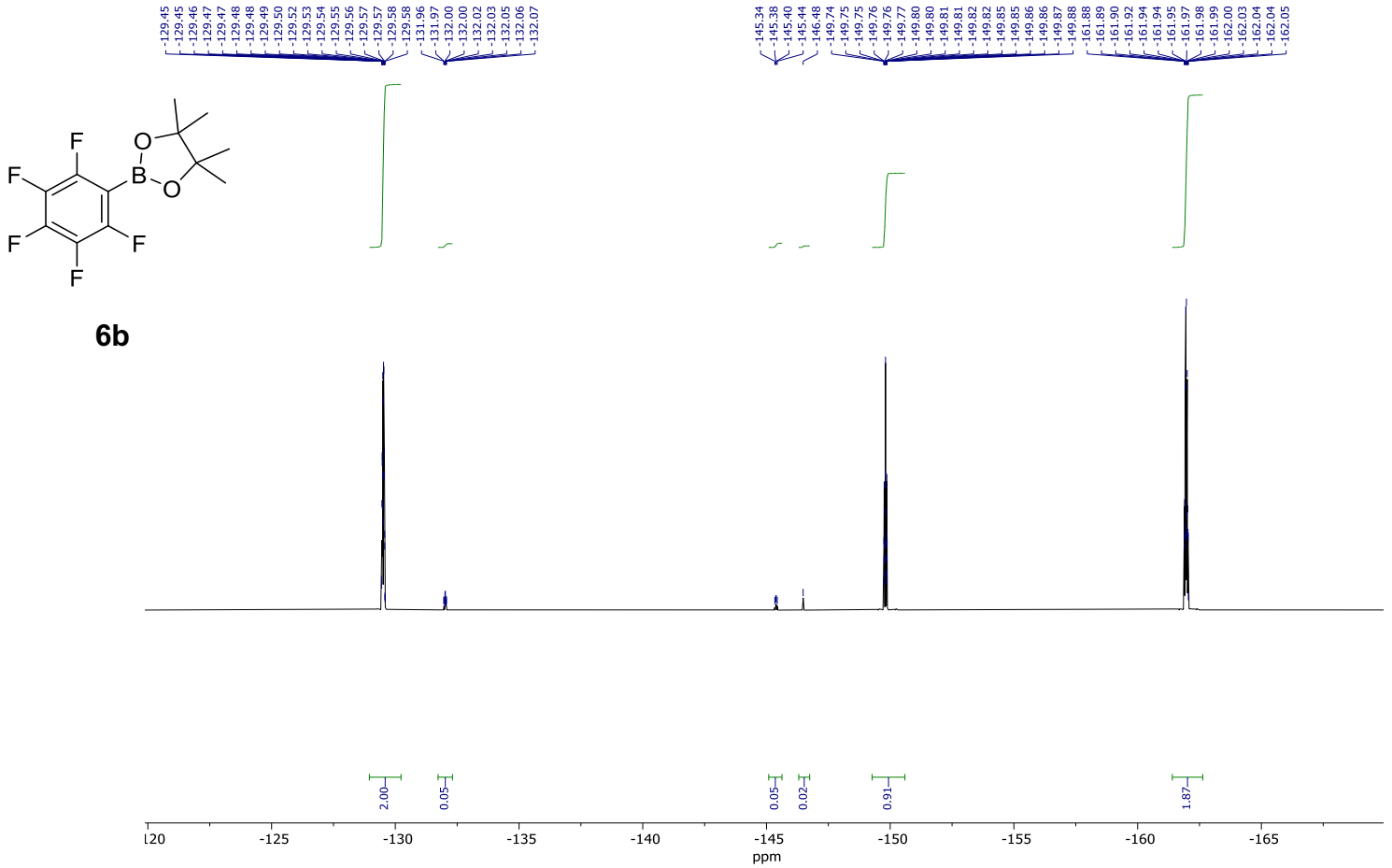

$^{13}C\{^{1}H\}$ (101 MHz); $CDCl_3$:

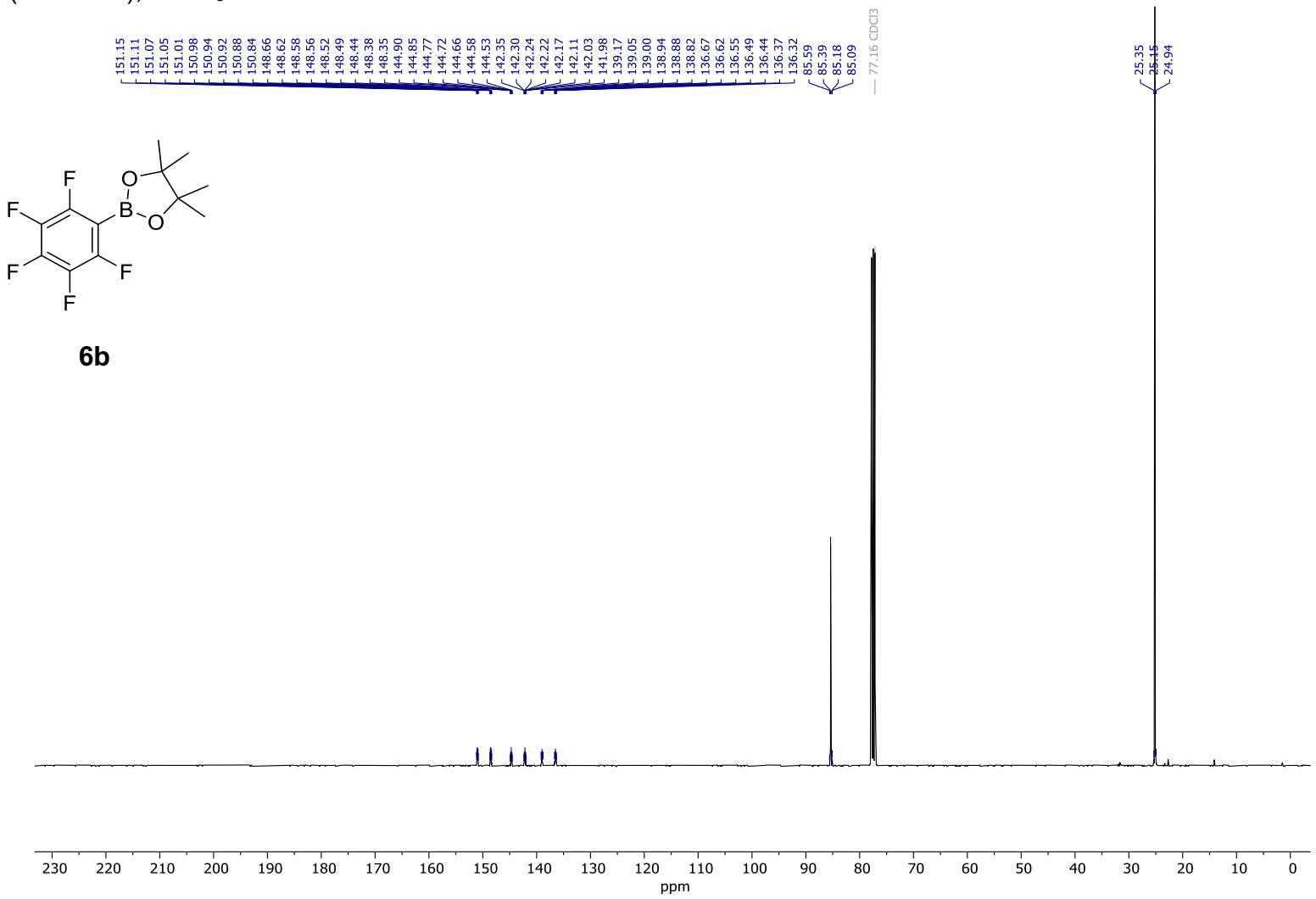

6b

^{11}B (128 MHz):

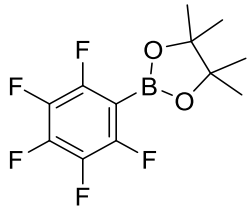

6b

^{1}H (400 MHz); $CDCl_3$:

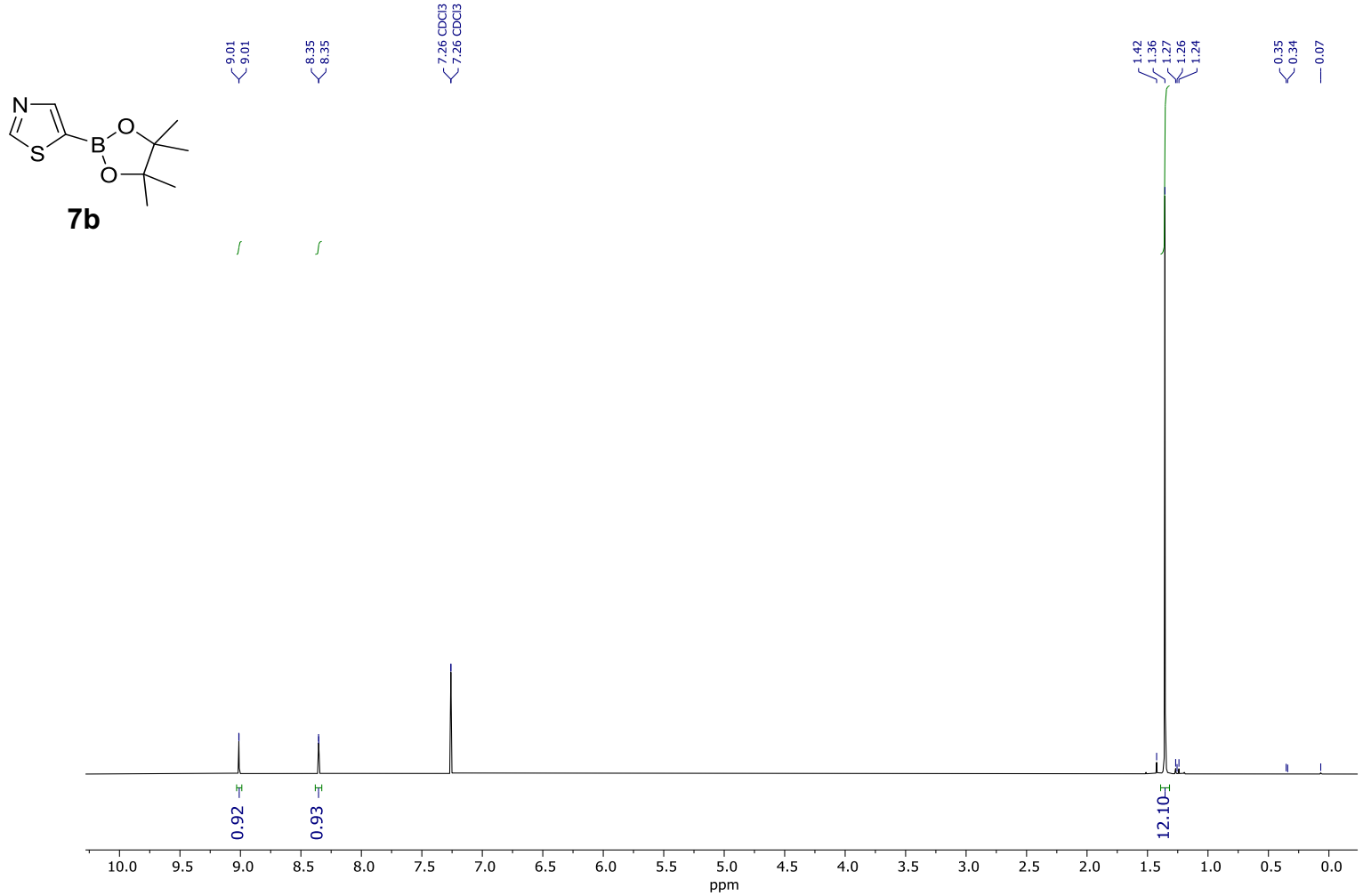

7b

$^{13}C\{^{1}H\}$ (101 MHz); $CDCl_3$:

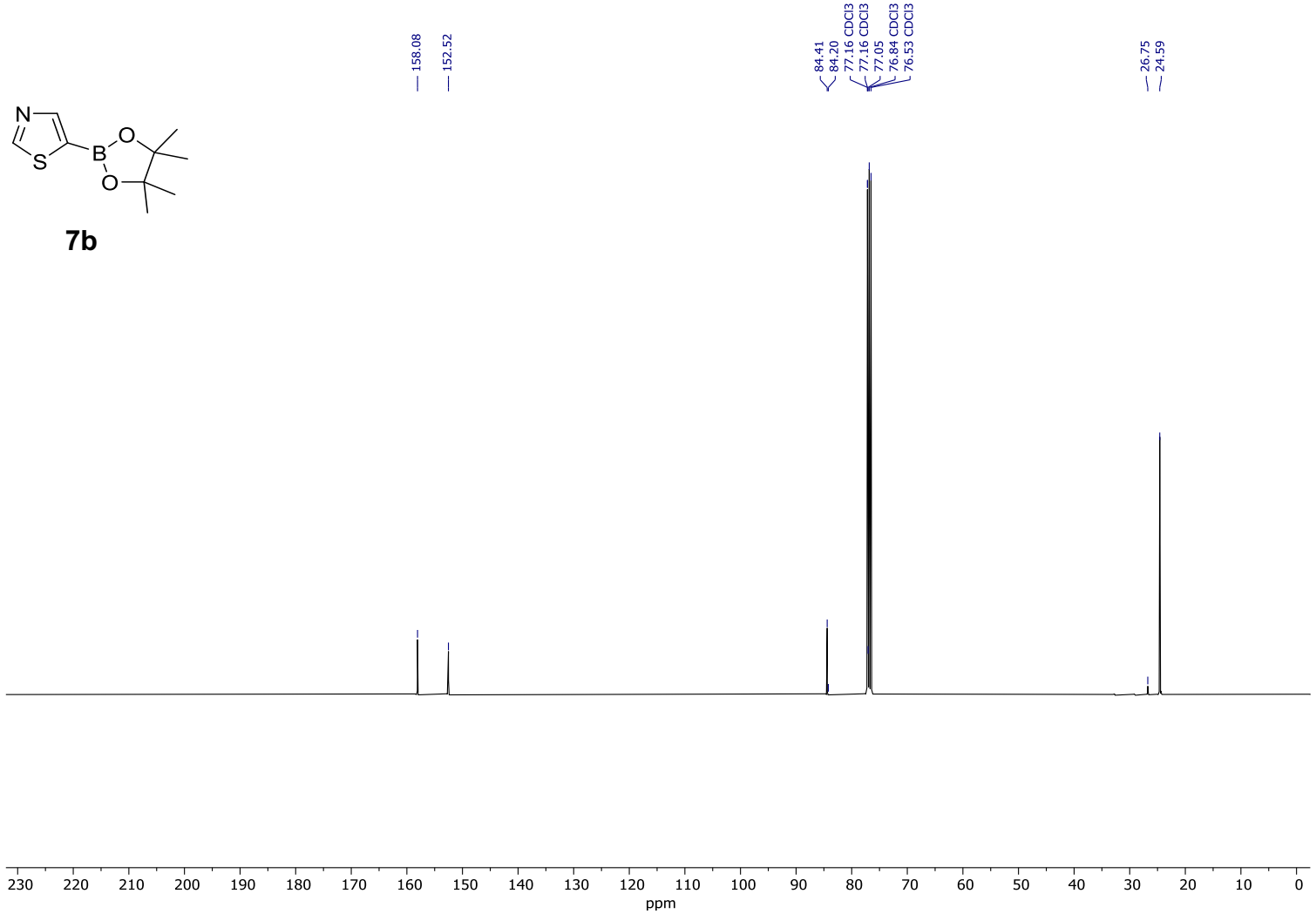

7b

^{11}B (128 MHz); $CDCl_3$:
Trace decomposition to boric acid evident in NMR spectrum.

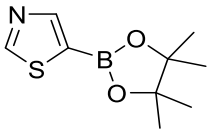

7b

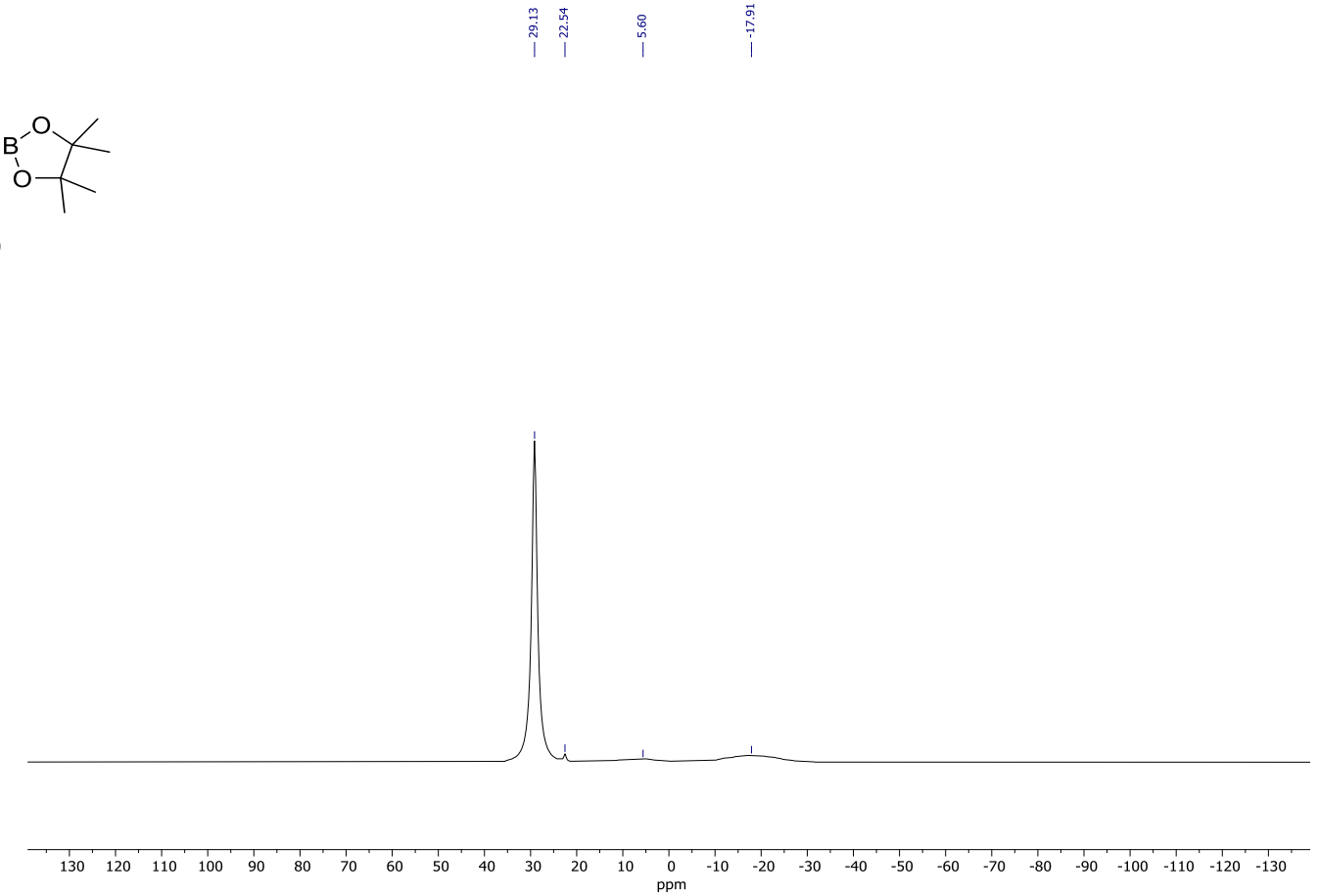

^{1}H (400 MHz); DMSO-d_6:

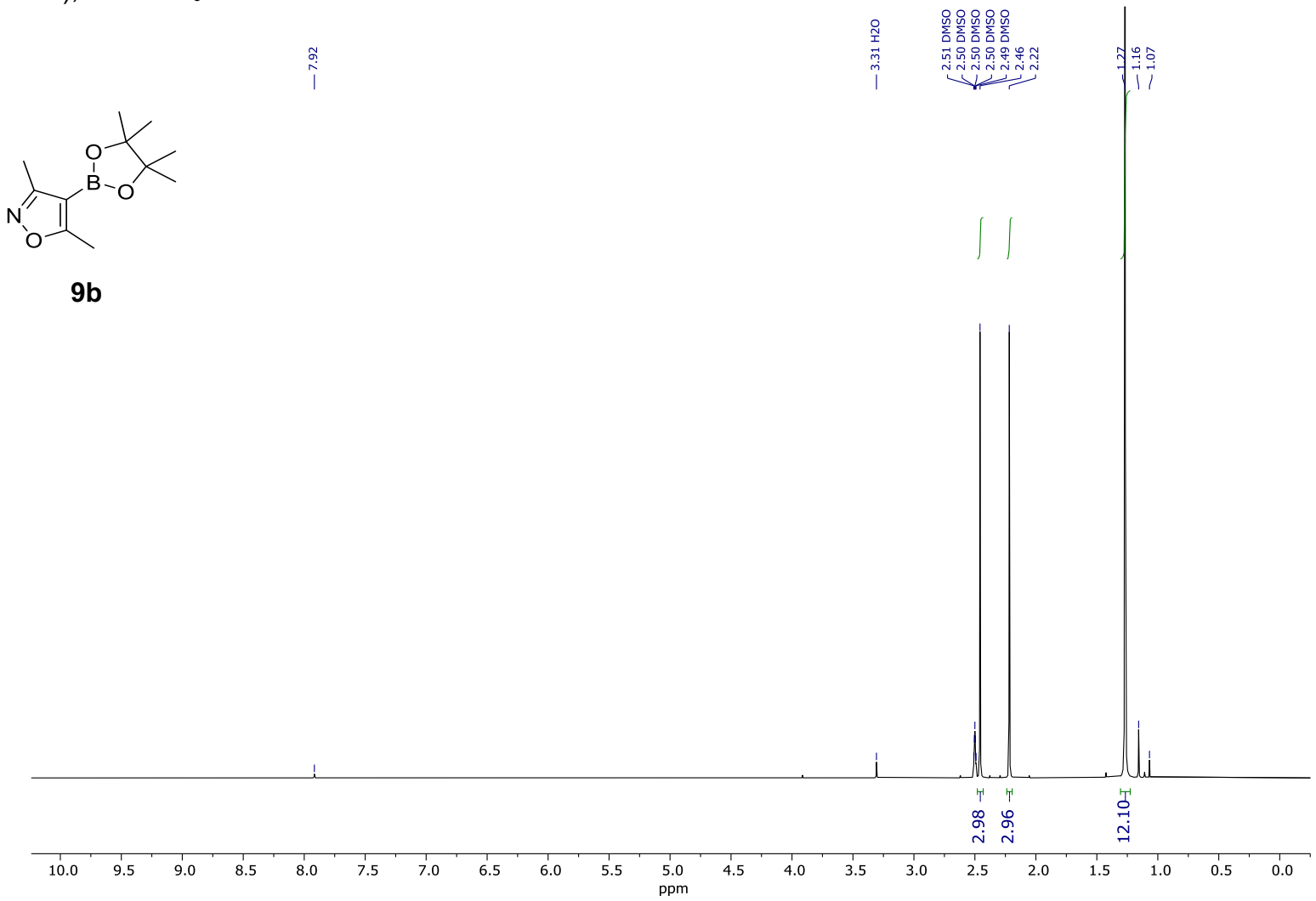

9b

$^{13}C\{^{1}H\}$ (101 MHz); DMSO-d_6:

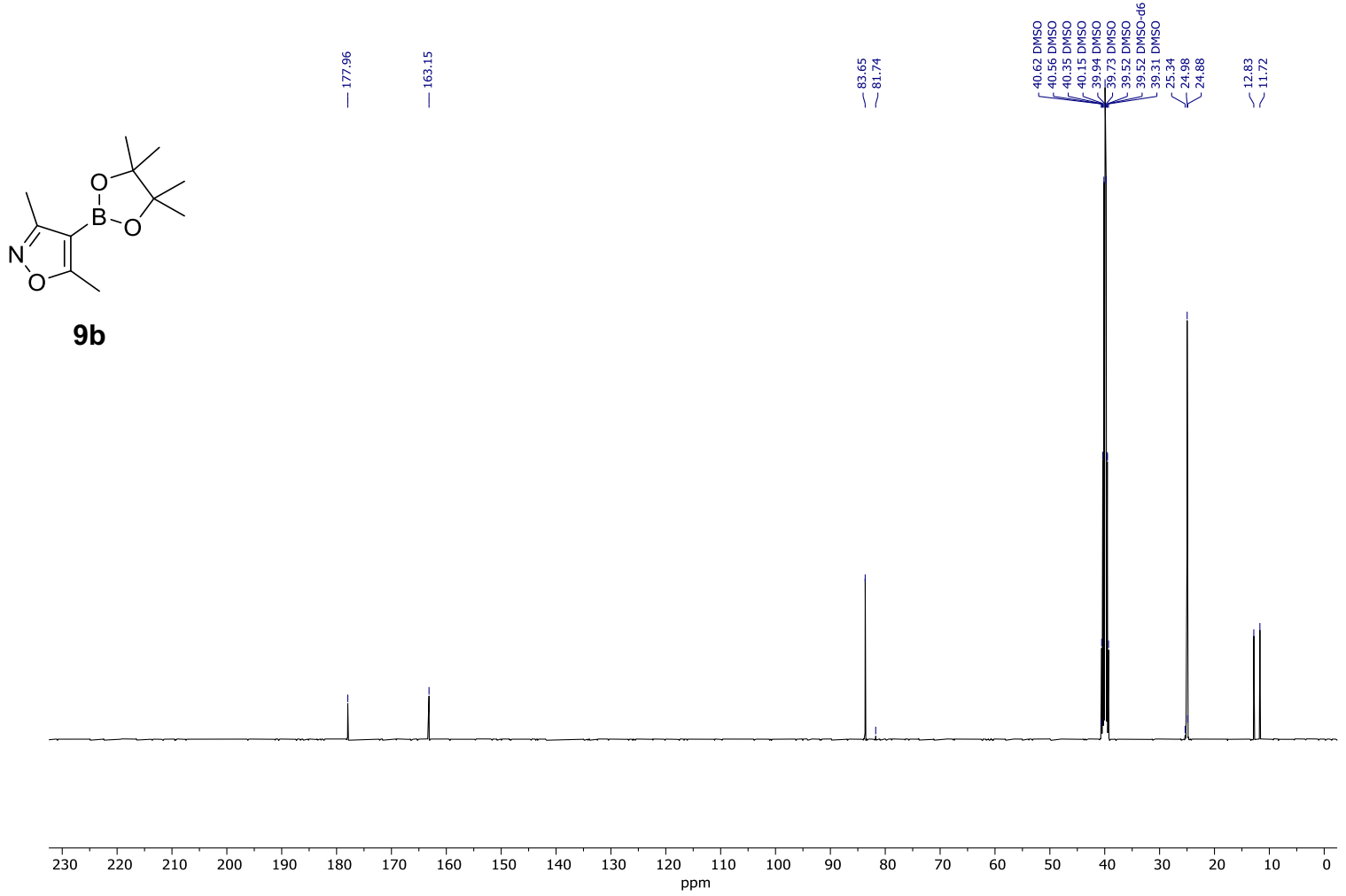

9b

^{11}B (128 MHz); DMSO-d_6:
Trace decomposition to boric acid evident in NMR spectrum.

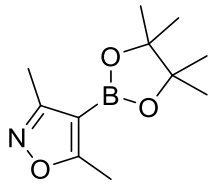

9b

[1]H (400 MHz); DMSO-*d*$_6$:

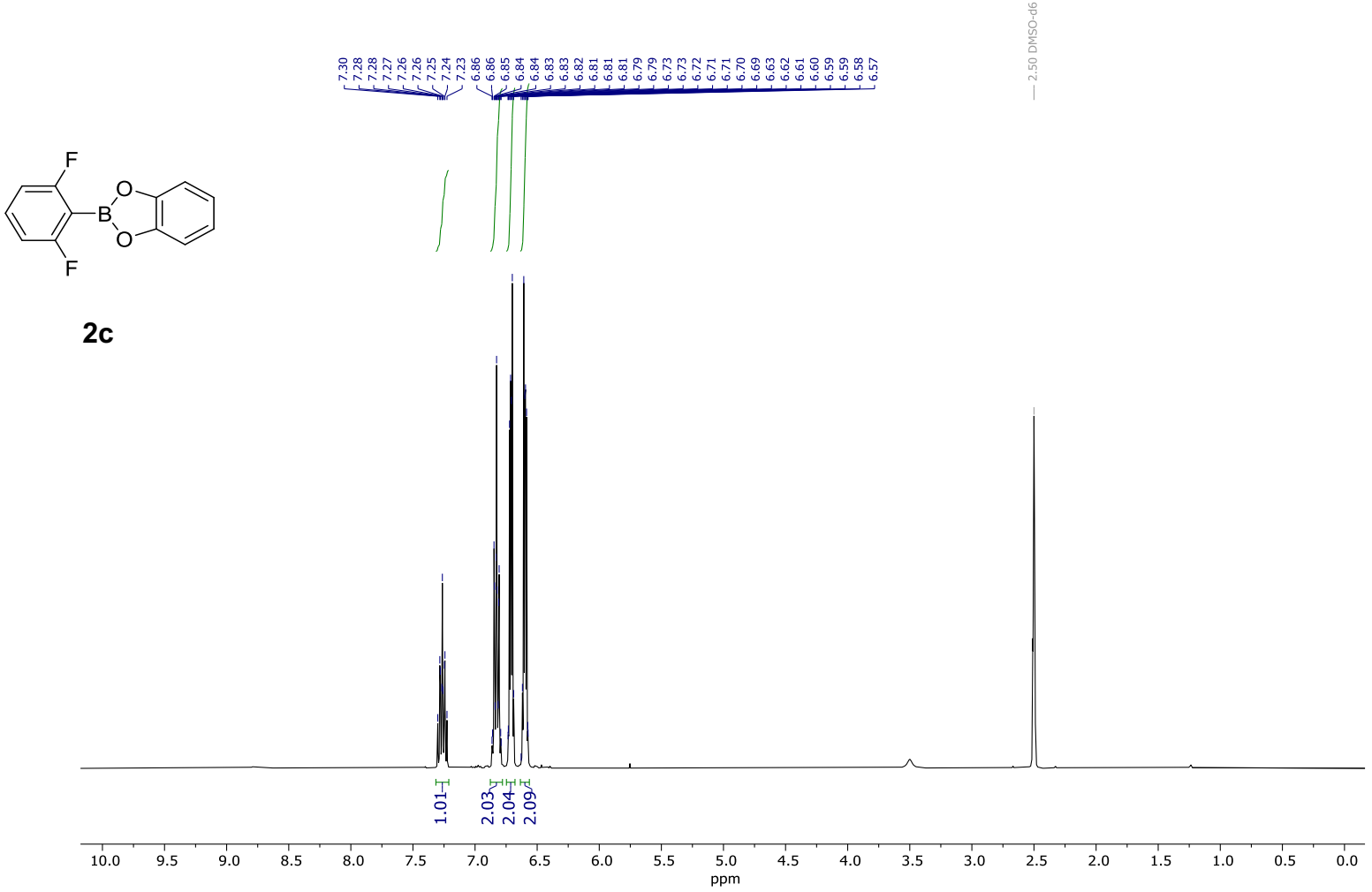

^{19}F (377 MHz); DMSO-d_6:

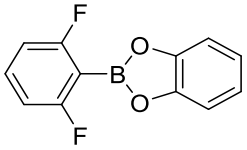

2c

$^{13}C\{^{1}H\}$ (101 MHz); DMSO-*d*$_6$:

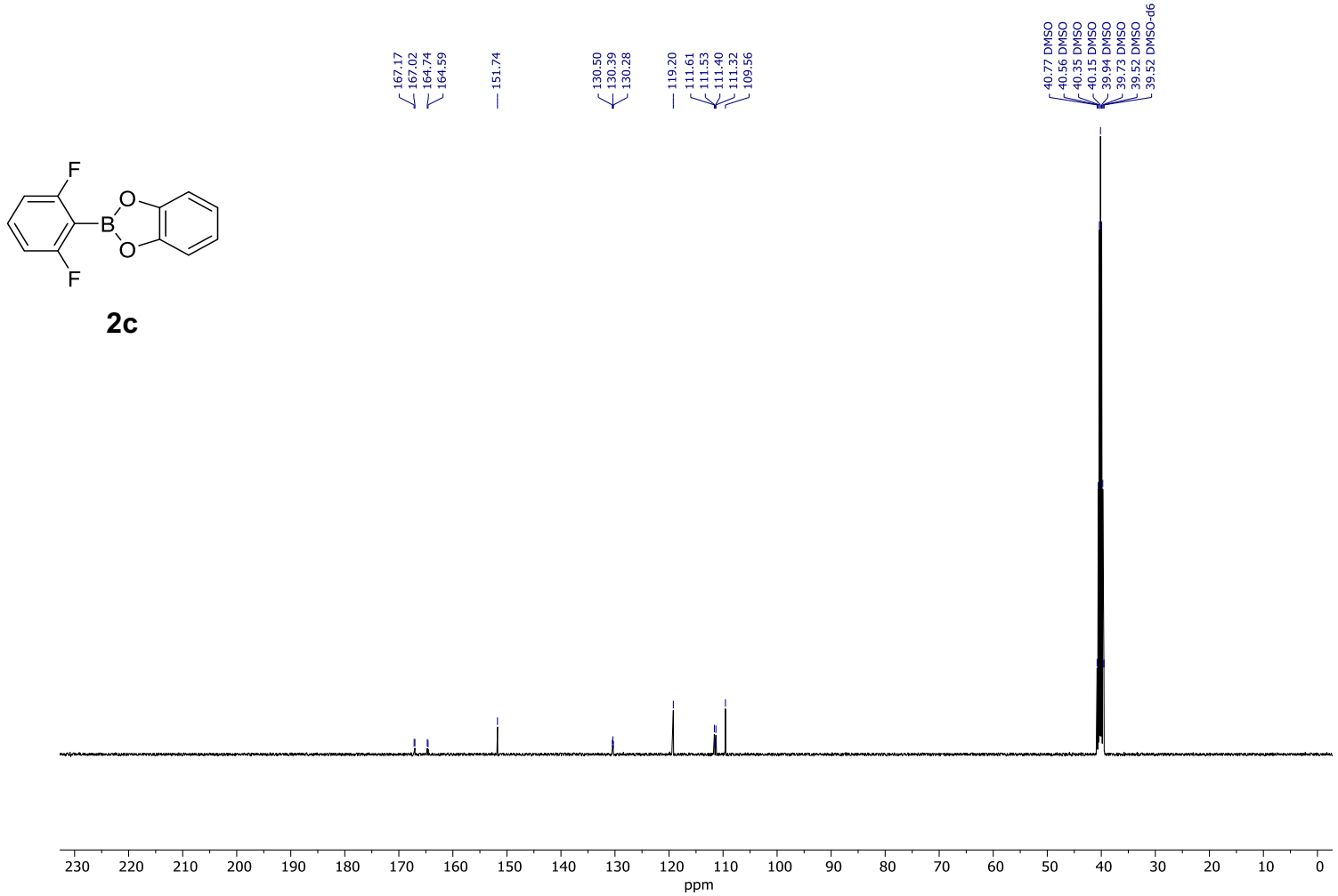

2c

^{11}B (128 MHz); DMSO-d_6:

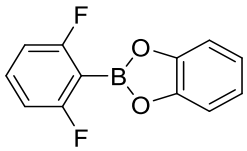

2c

^{1}H (400 MHz); $CDCl_3$:

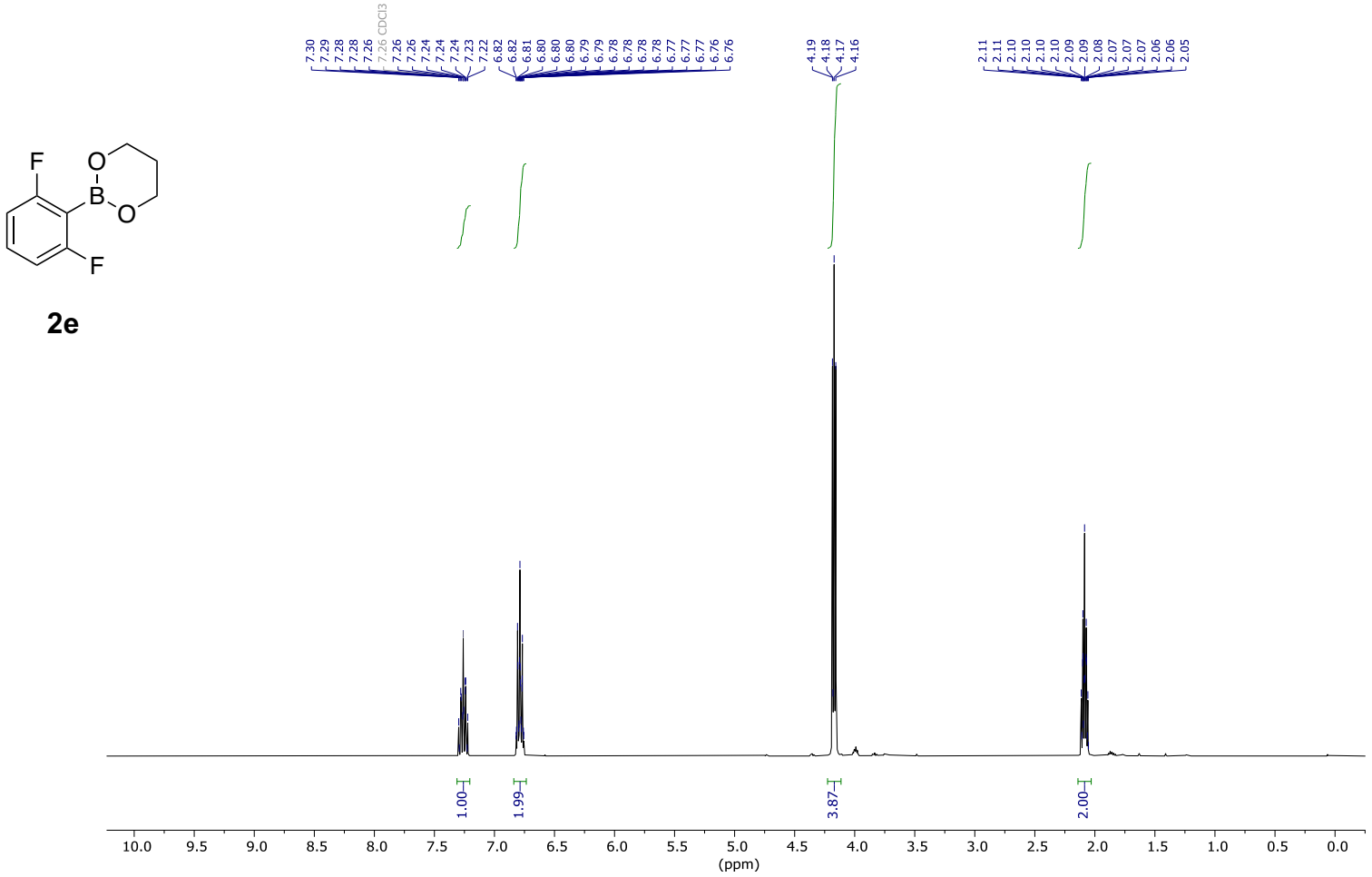

2e

^{19}F (377 MHz); $CDCl_3$:

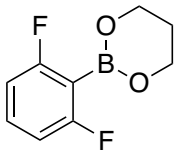

2e

$^{13}C\{^{1}H\}$ (101 MHz); $CDCl_3$:

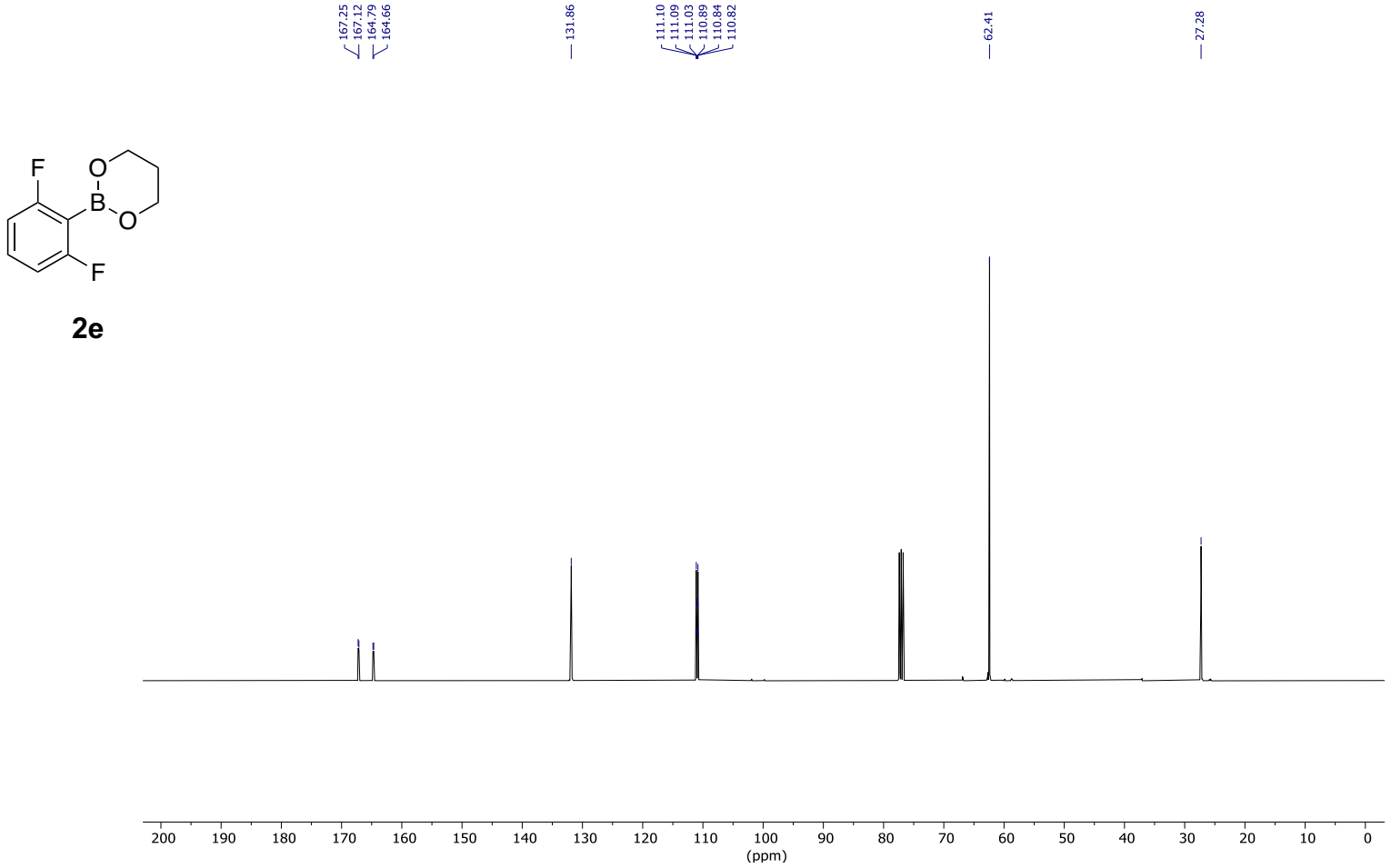

2e

^{11}B (128 MHz); $CDCl_3$:

Trace decomposition to boric acid evident in NMR spectrum.

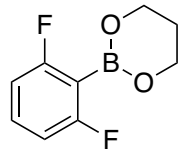

2e

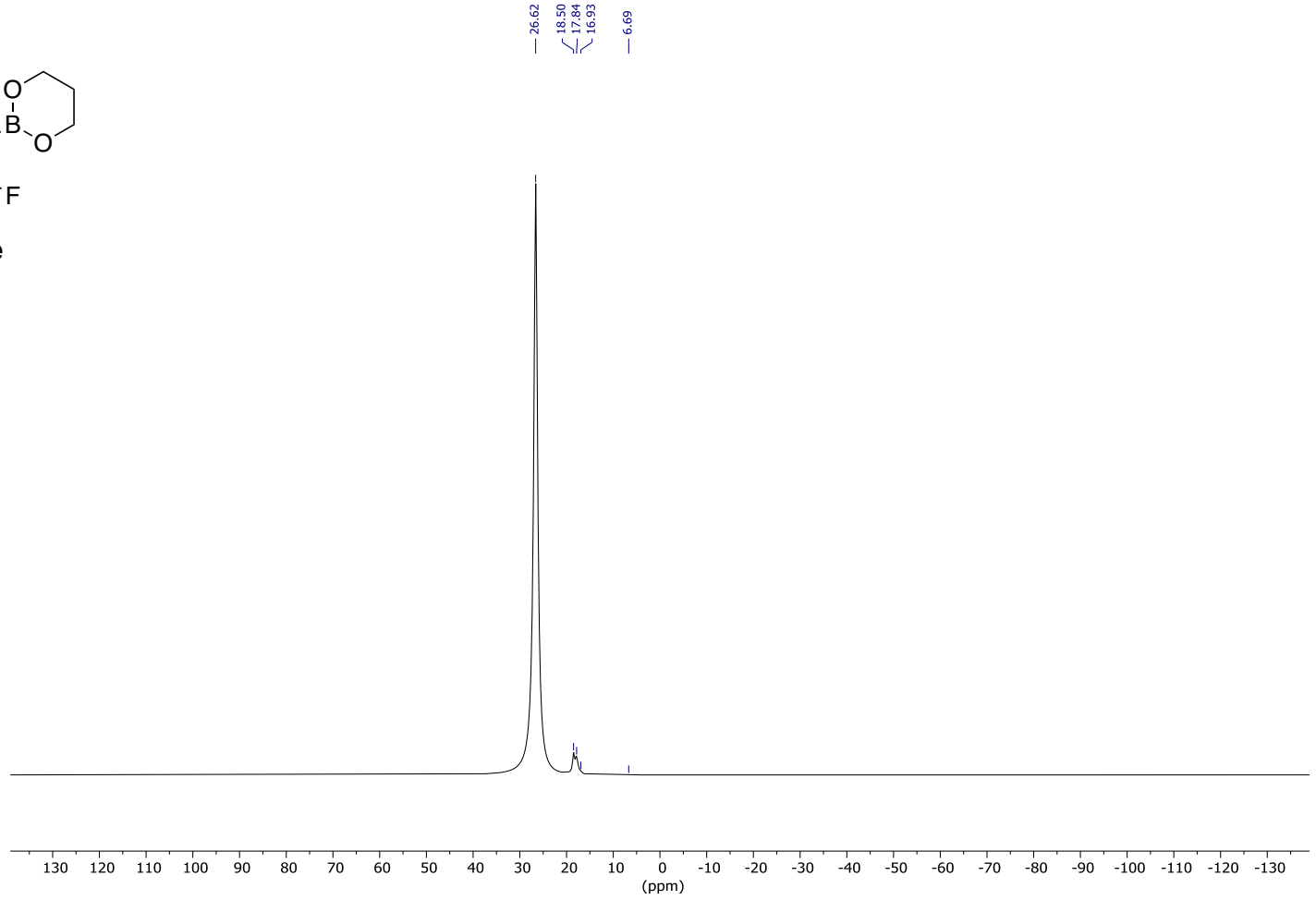

^{1}H (400 MHz); $CDCl_3$:

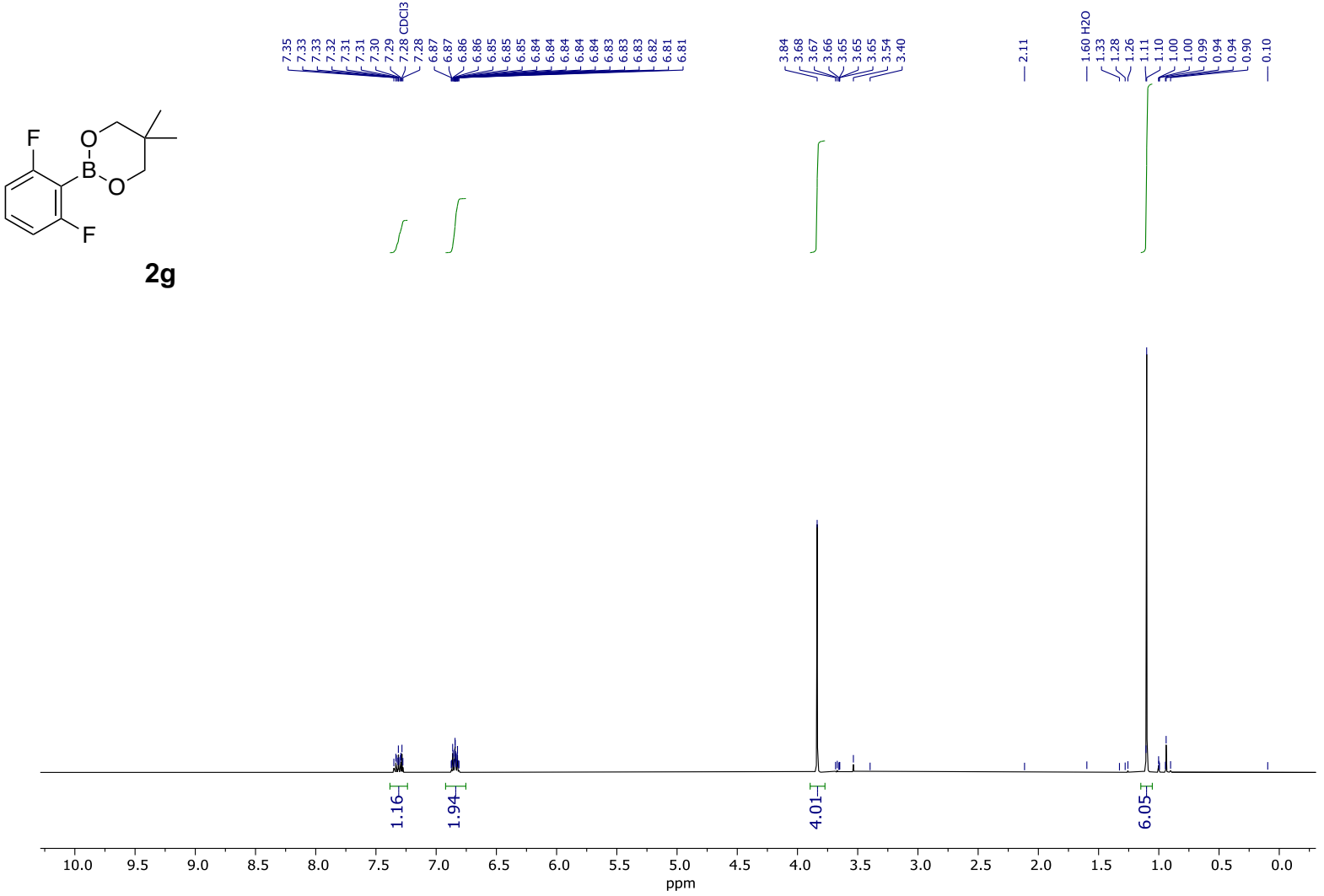

2g

^{19}F (377 MHz); $CDCl_3$:

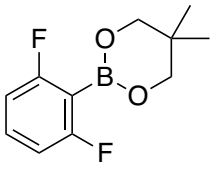

2g

$^{13}C\{^{1}H\}$ (101 MHz); $CDCl_3$:

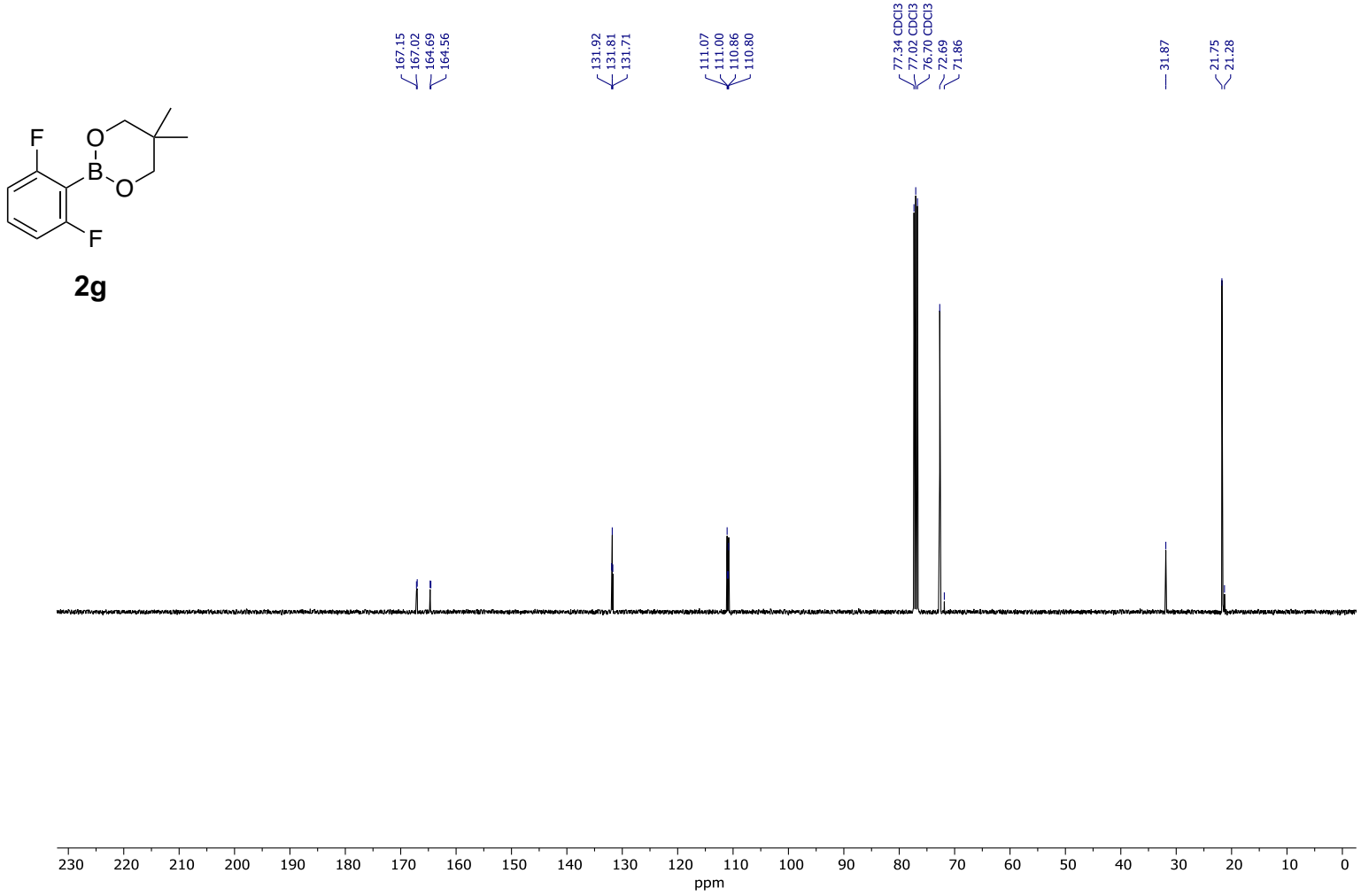

2g

^{11}B (128 MHz); $CDCl_3$:
Trace decomposition to boric acid evident in spectrum.

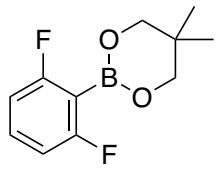

2g

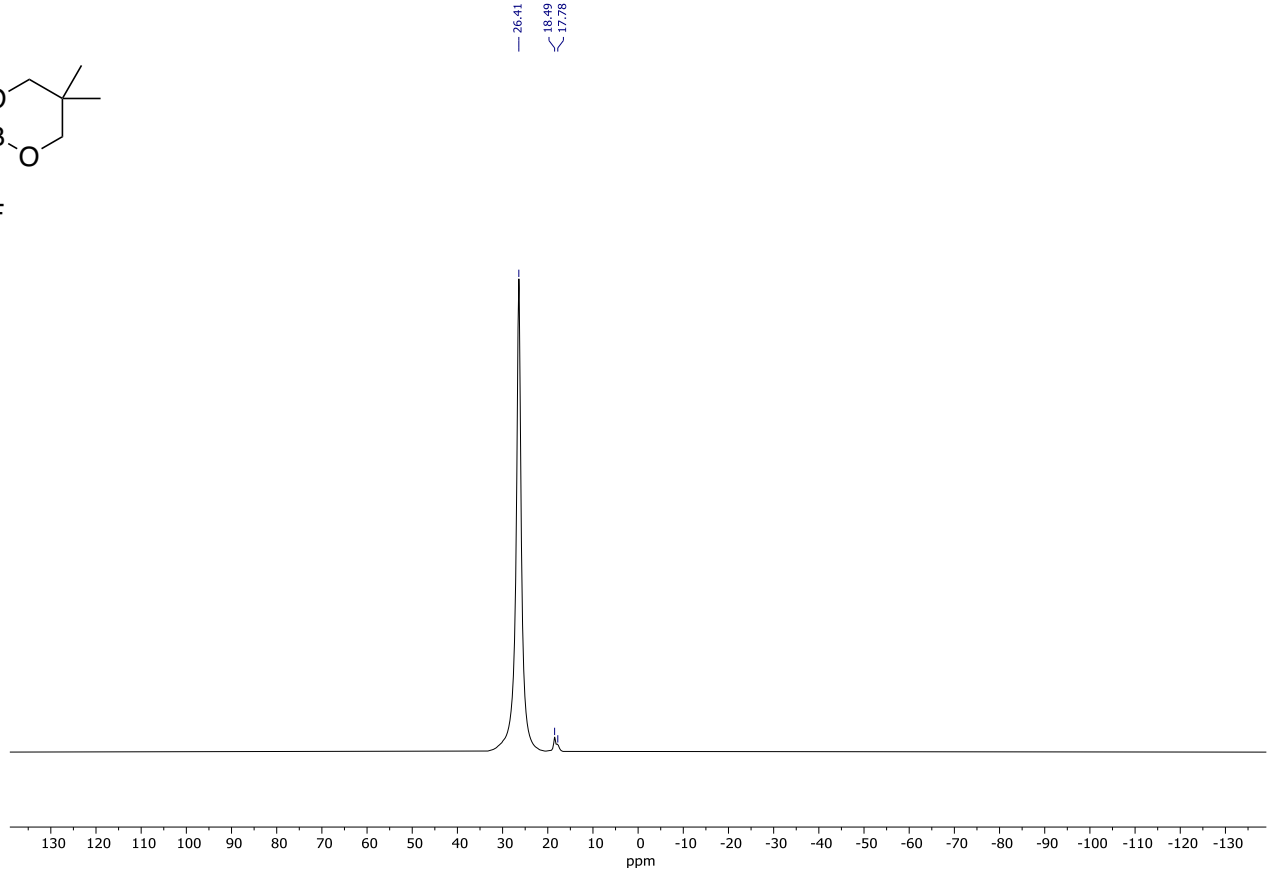

^{1}H (400 MHz); DMSO-d_6:

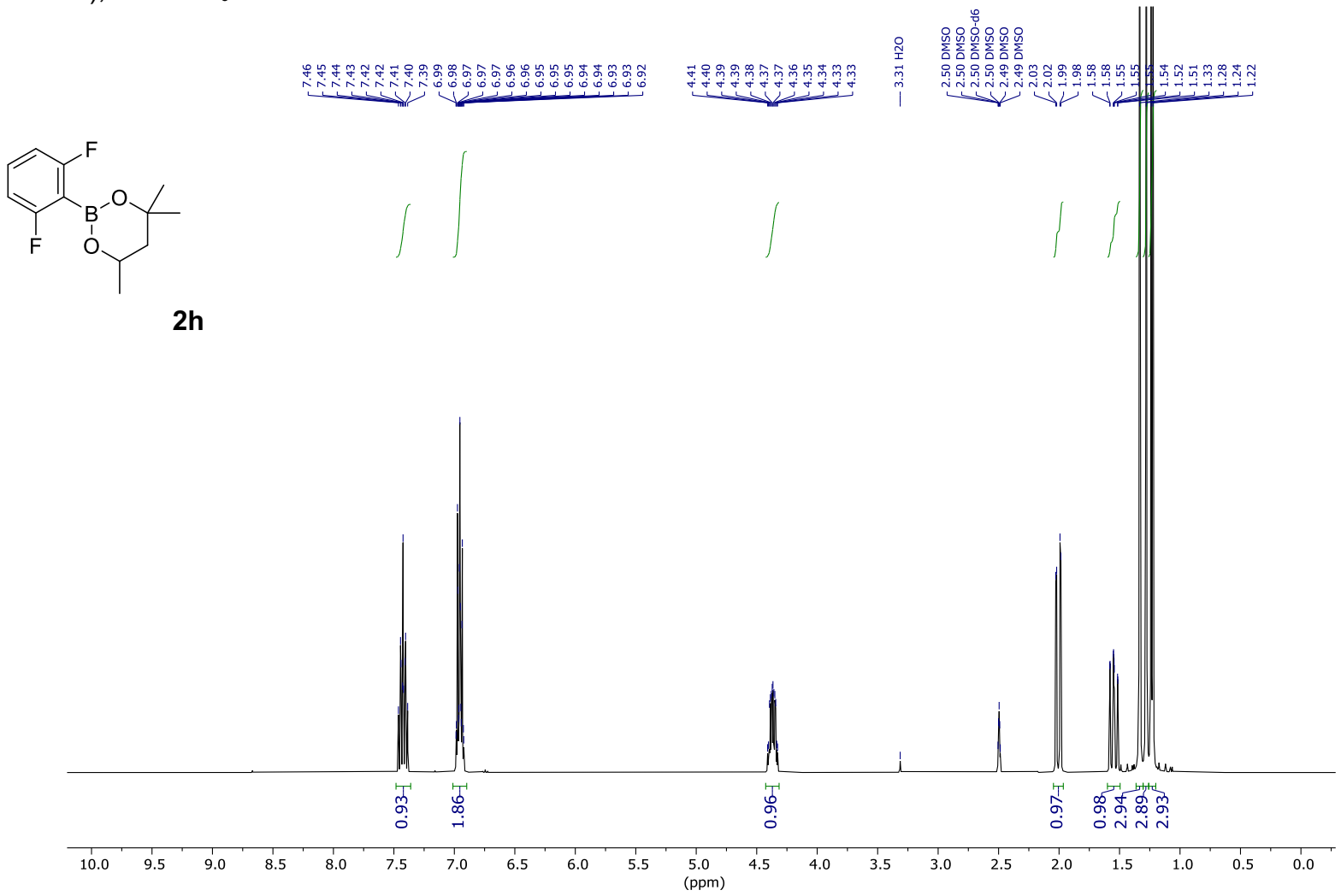

^{19}F (377 MHz); $CDCl_3$:

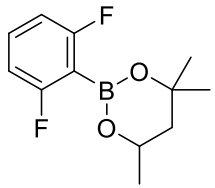

2h

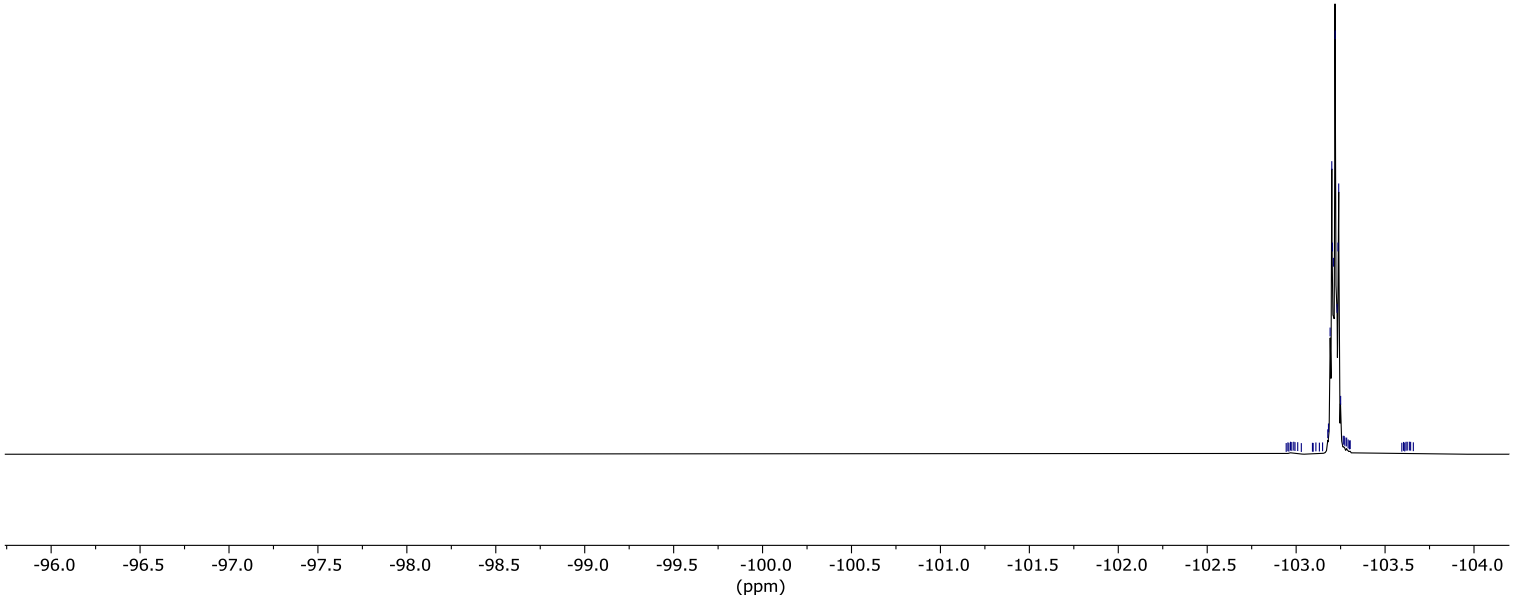

$^{13}C\{^{1}H\}$ (101 MHz); DMSO-*d_6*:

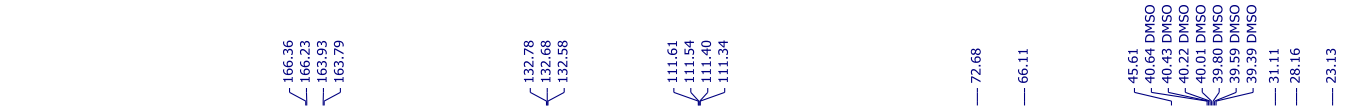

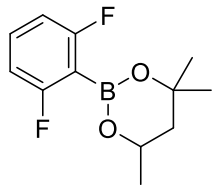

2h

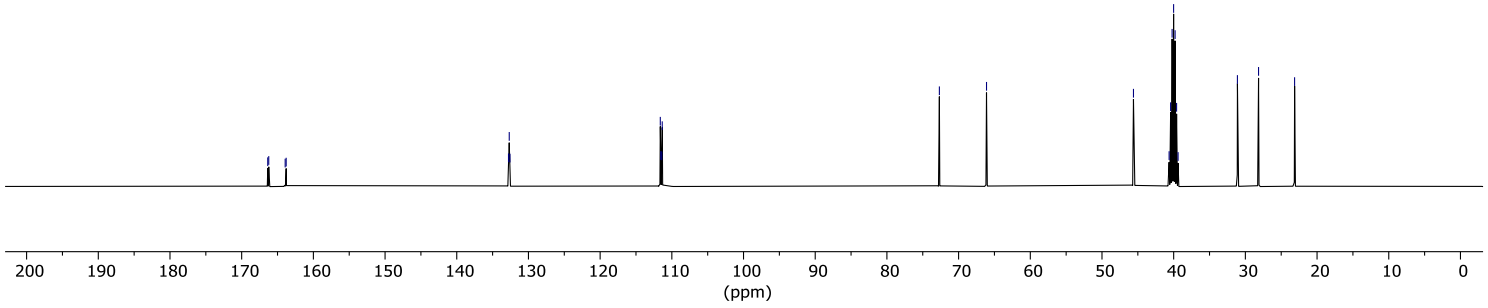

^{11}B (128 MHz); DMSO-d_6:

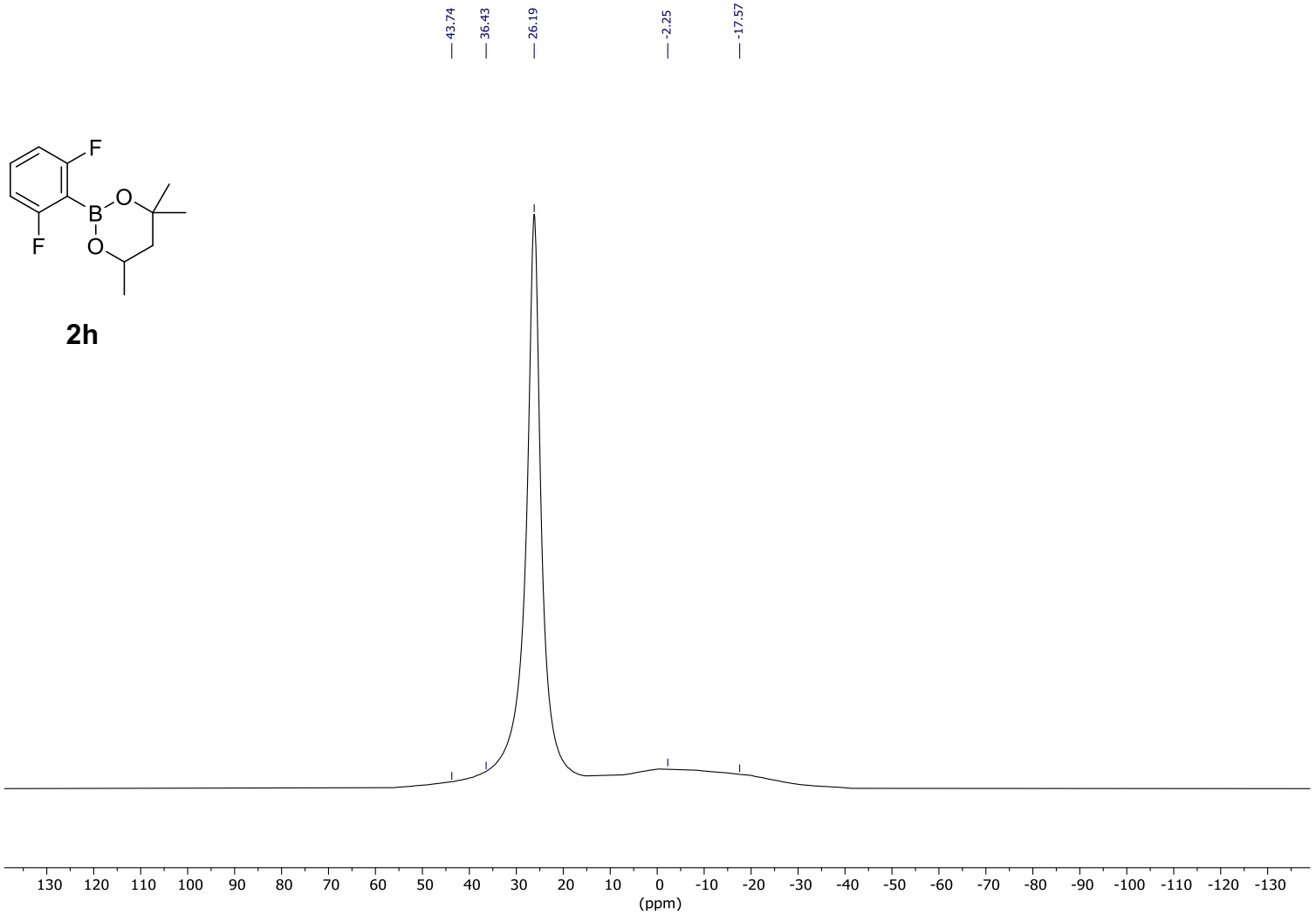

2h

^{1}H (400 MHz); DMSO-d_6:

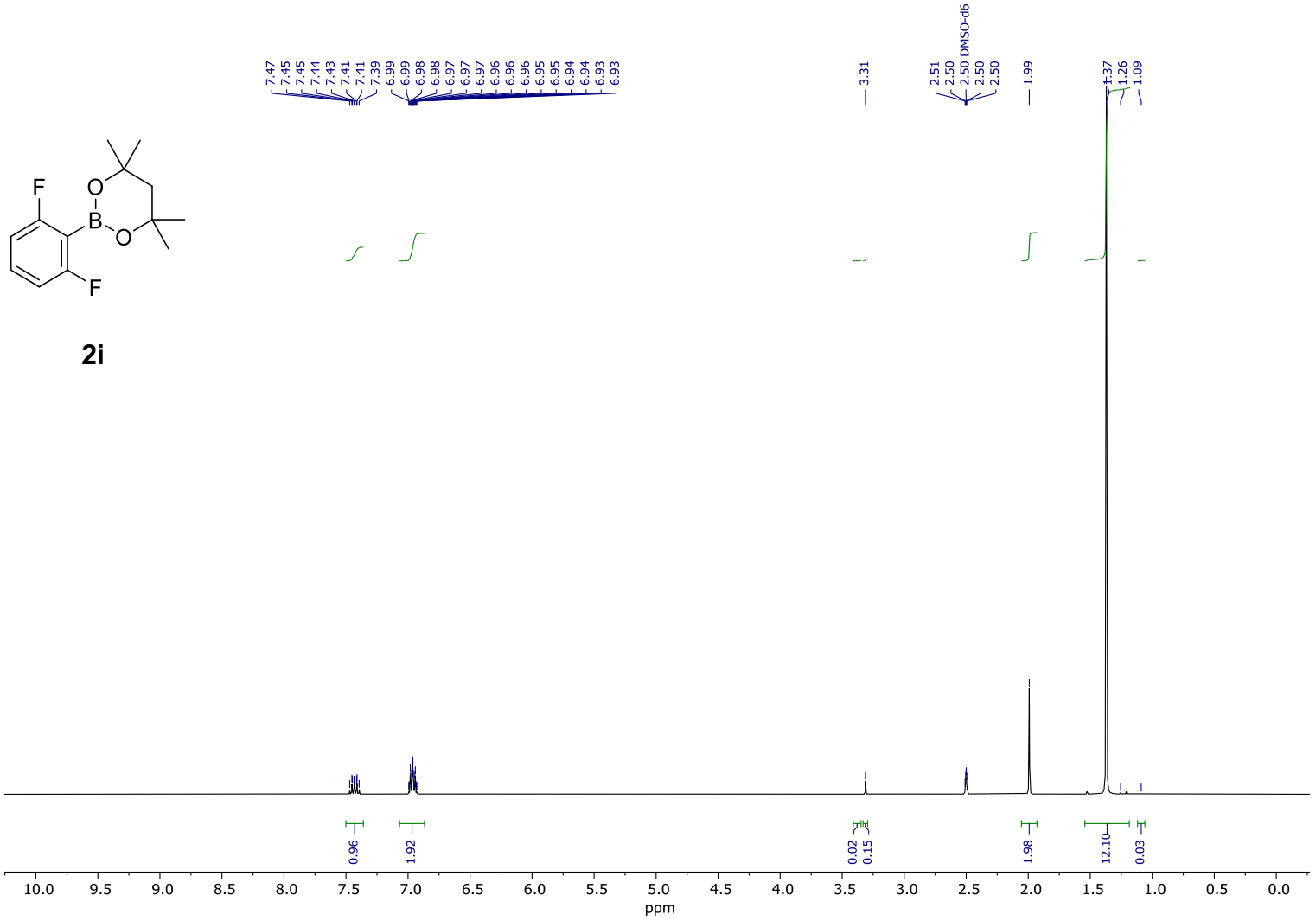

2i

^{19}F (377 MHz); DMSO-d_6:

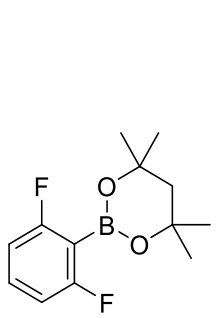

2i

$^{13}C\{^{1}H\}$ (101 MHz); DMSO-*d*$_6$:

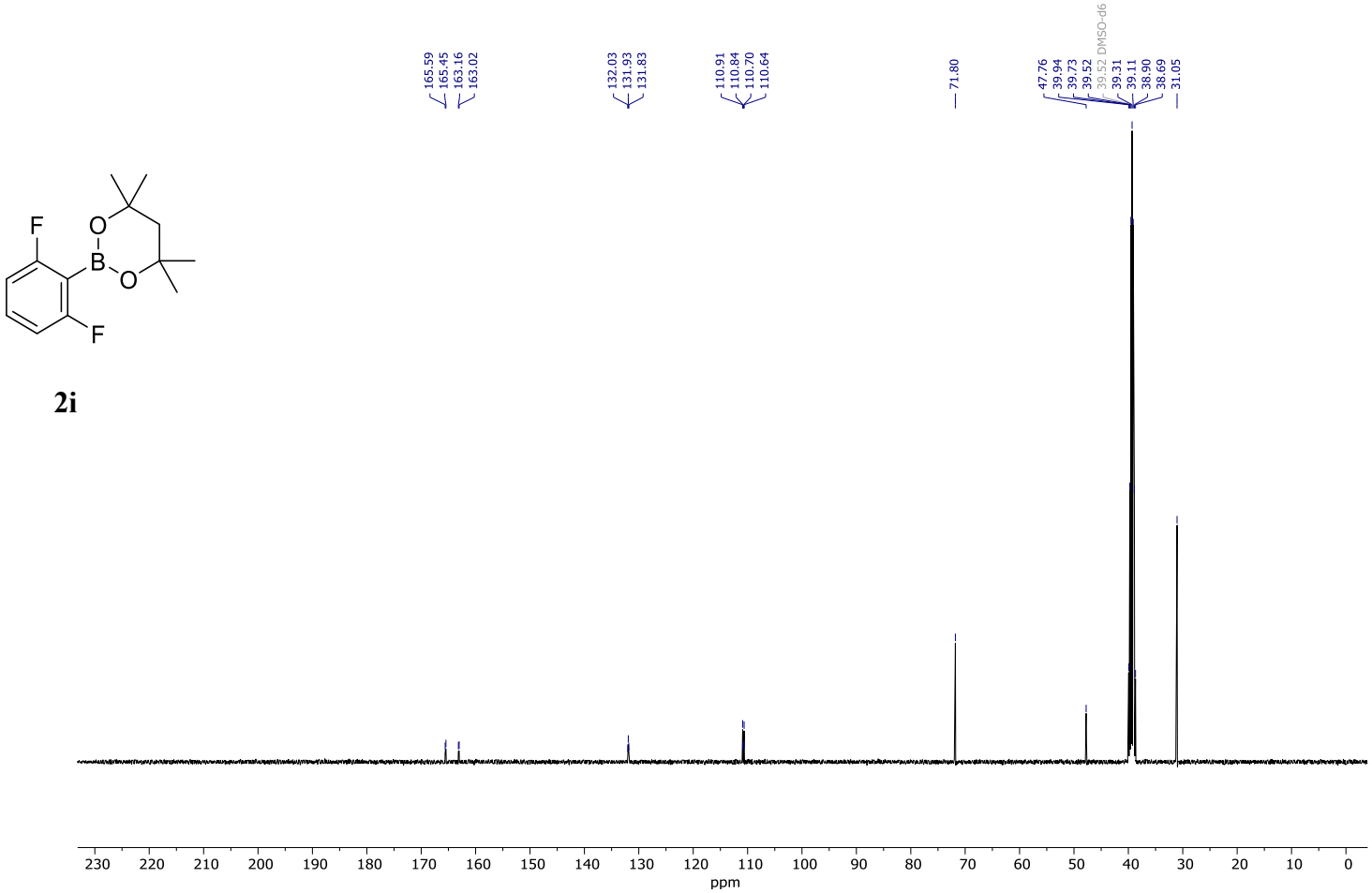

2i

^{11}B (128 MHz); DMSO-d_6:

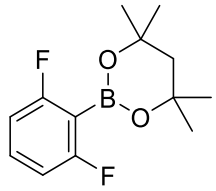

2i

^{1}H (400 MHz); $CDCl_3$:

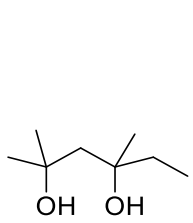

^{1}H (400 MHz); DMSO-d_6:

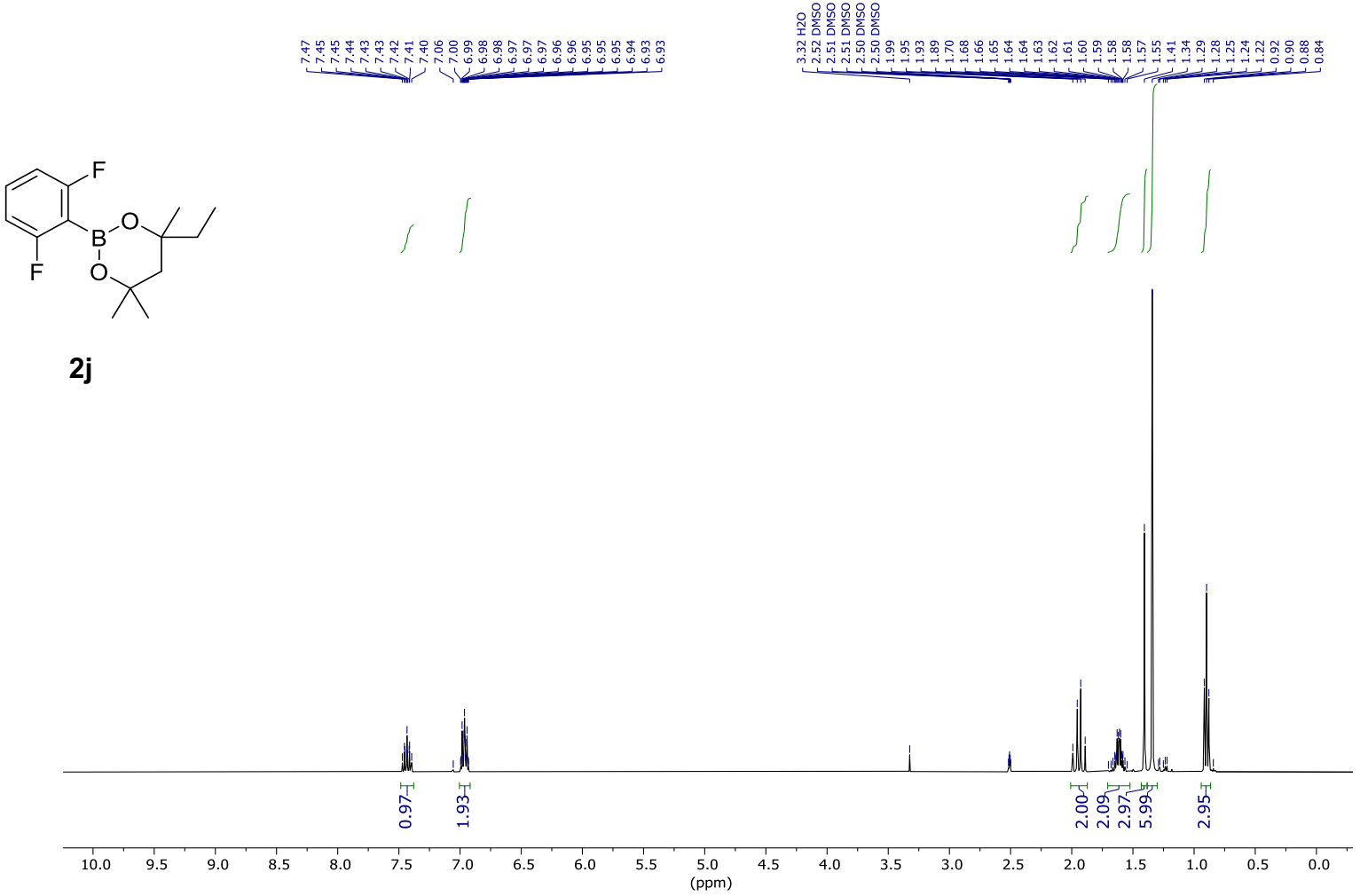

^{19}F (377 MHz); $CDCl_3$:

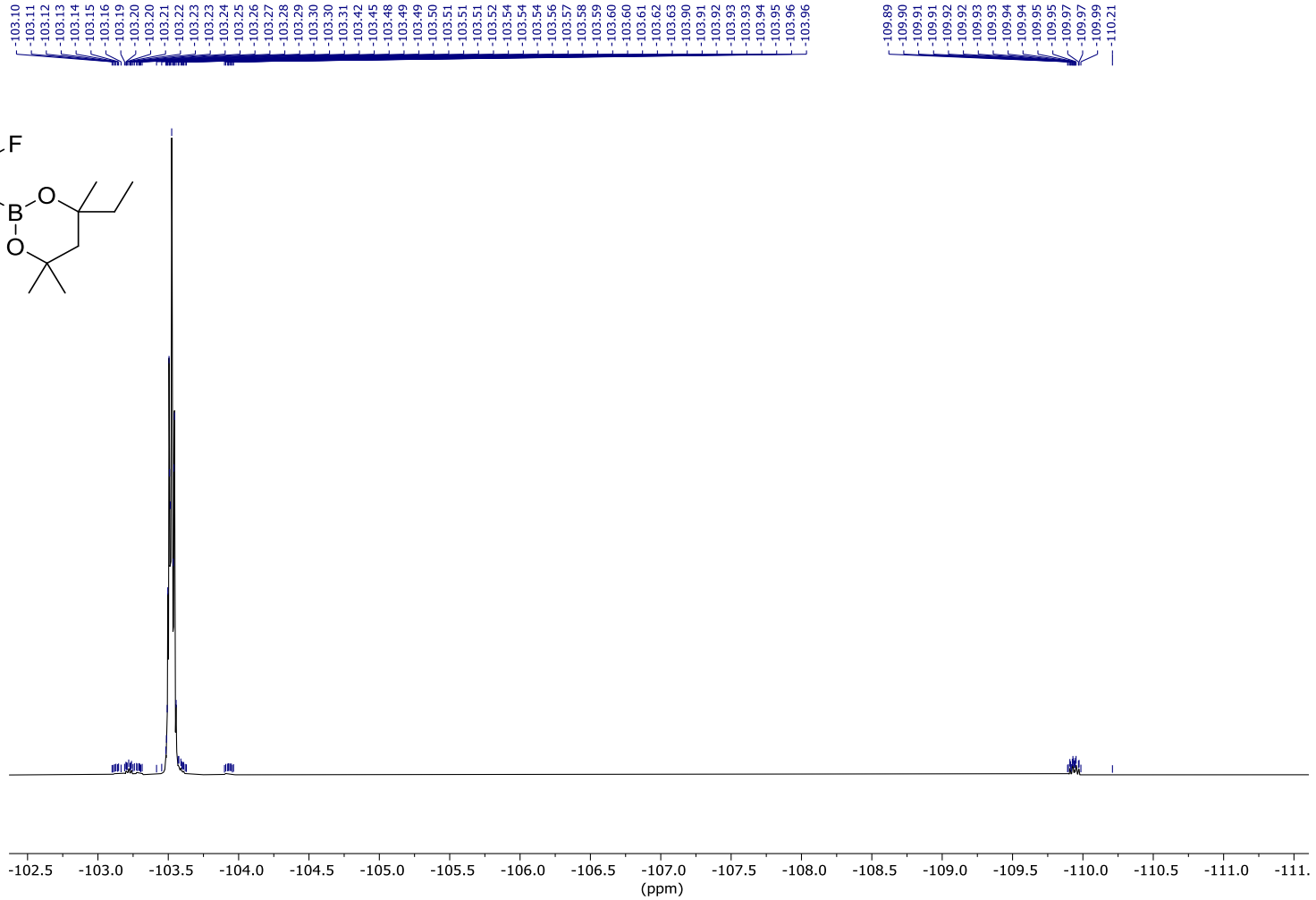

2j

$^{13}C\{^{1}H\}$ (101 MHz); DMSO-d_6:

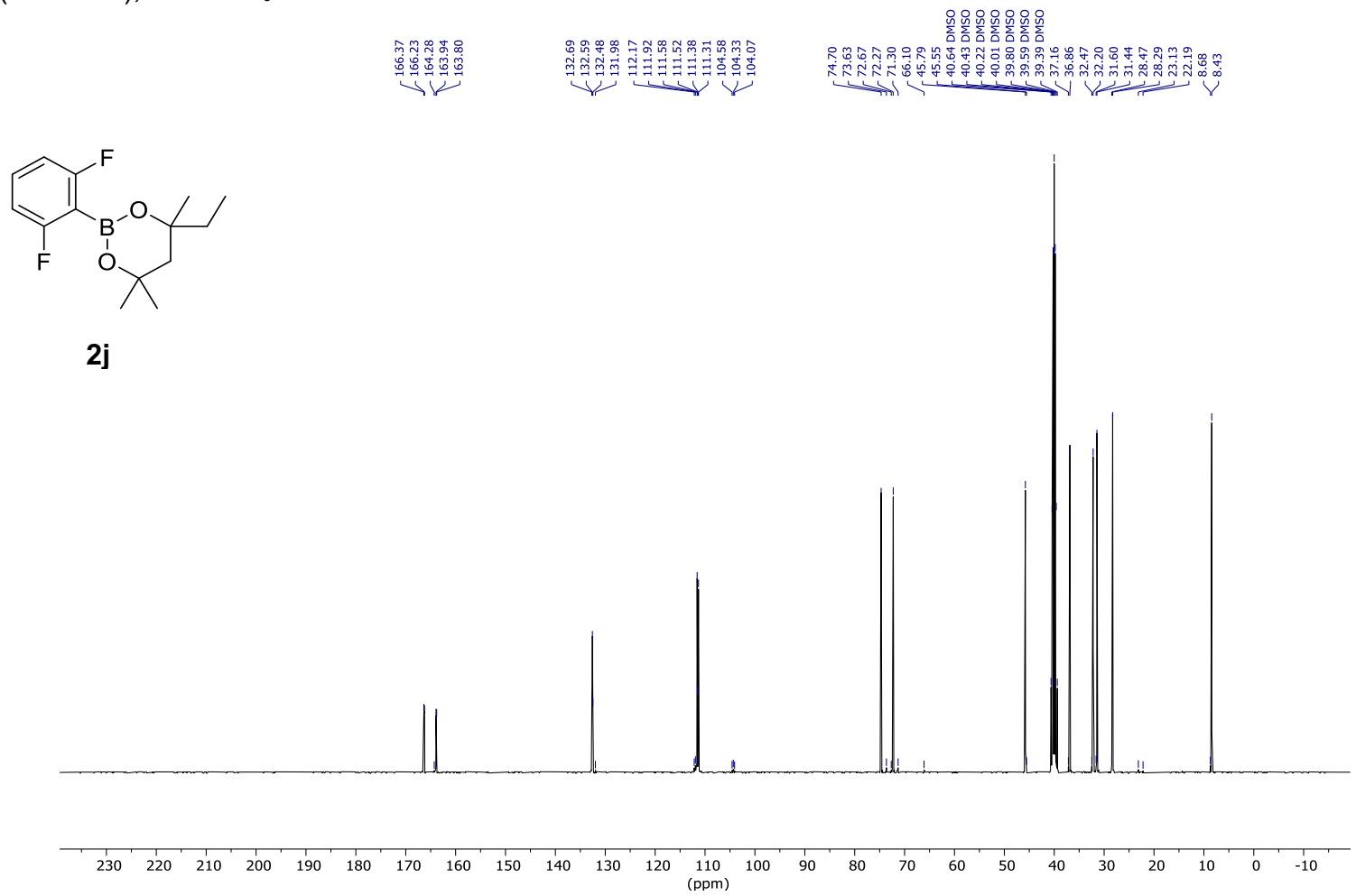

2j

^{11}B (128 MHz); DMSO-d_6:
Trace decomposition to boric acid evident in NMR spectrum.

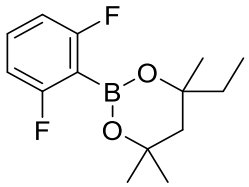

2j

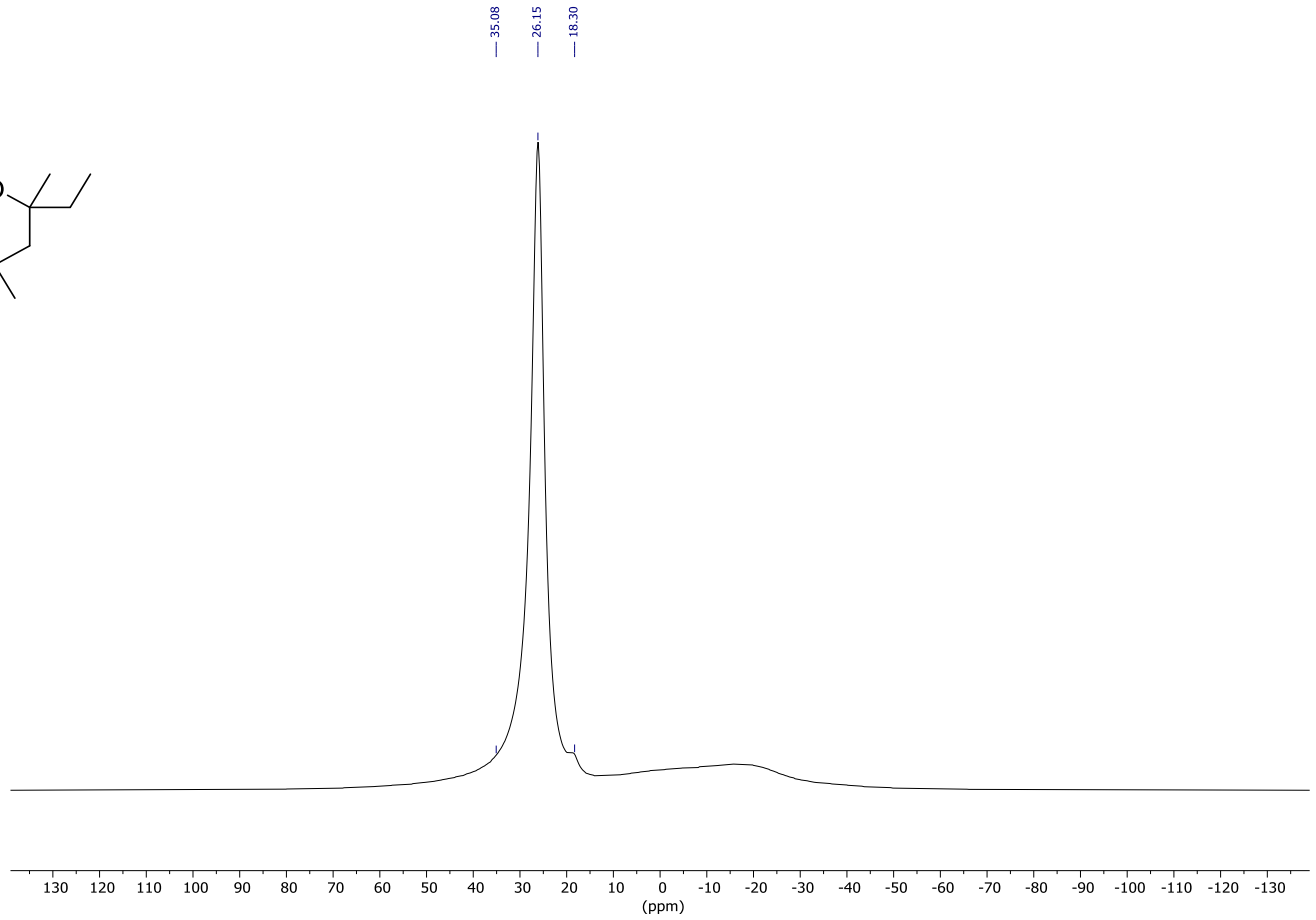

[1]H (400 MHz); DMSO-*d*$_6$:

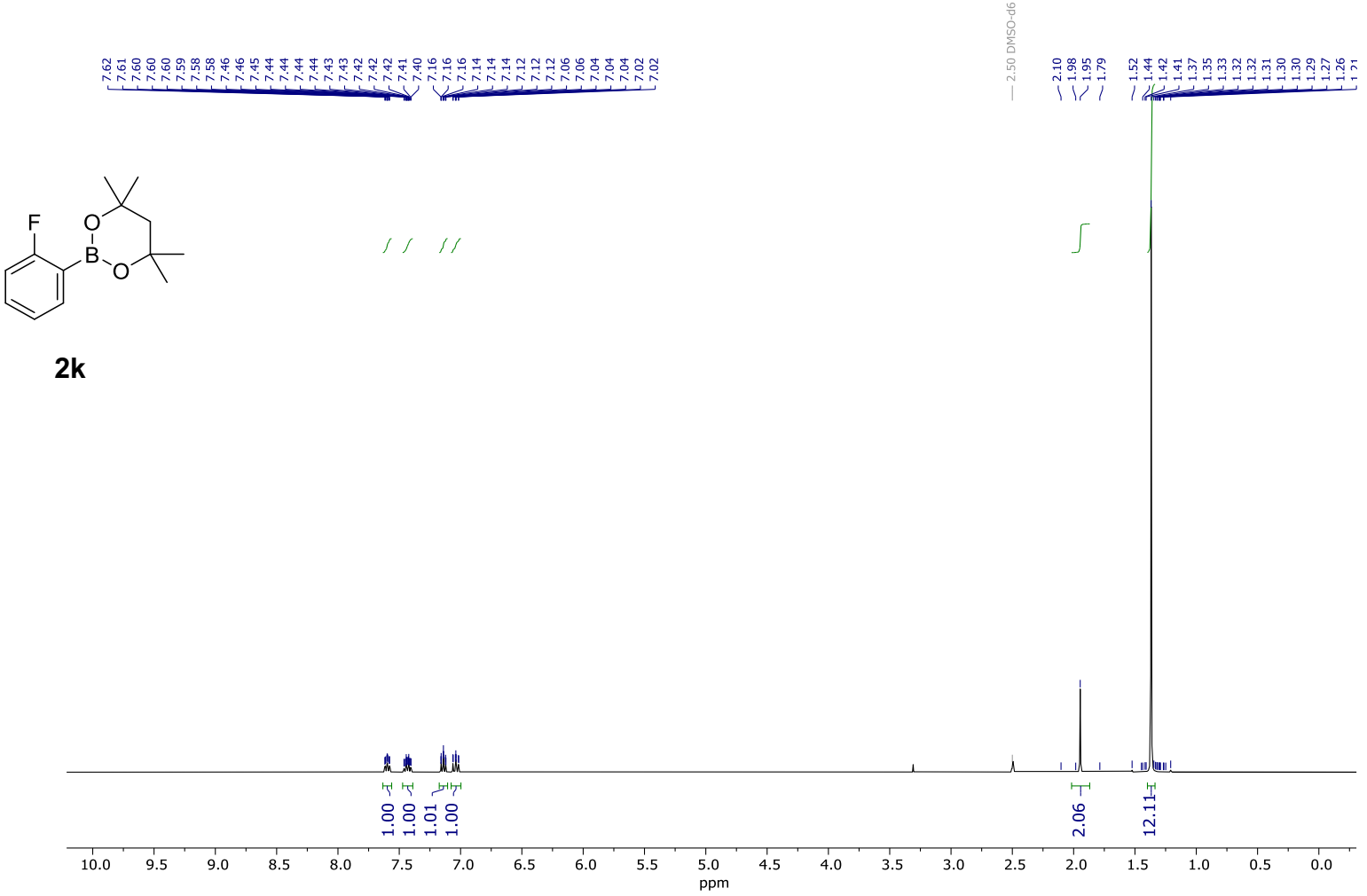

^{19}F (377 MHz); DMSO-d_6:

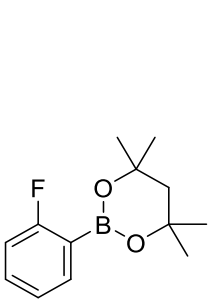

2k

$^{13}C\{^{1}H\}$ (101 MHz); DMSO-*d_6*:

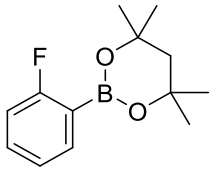

2k

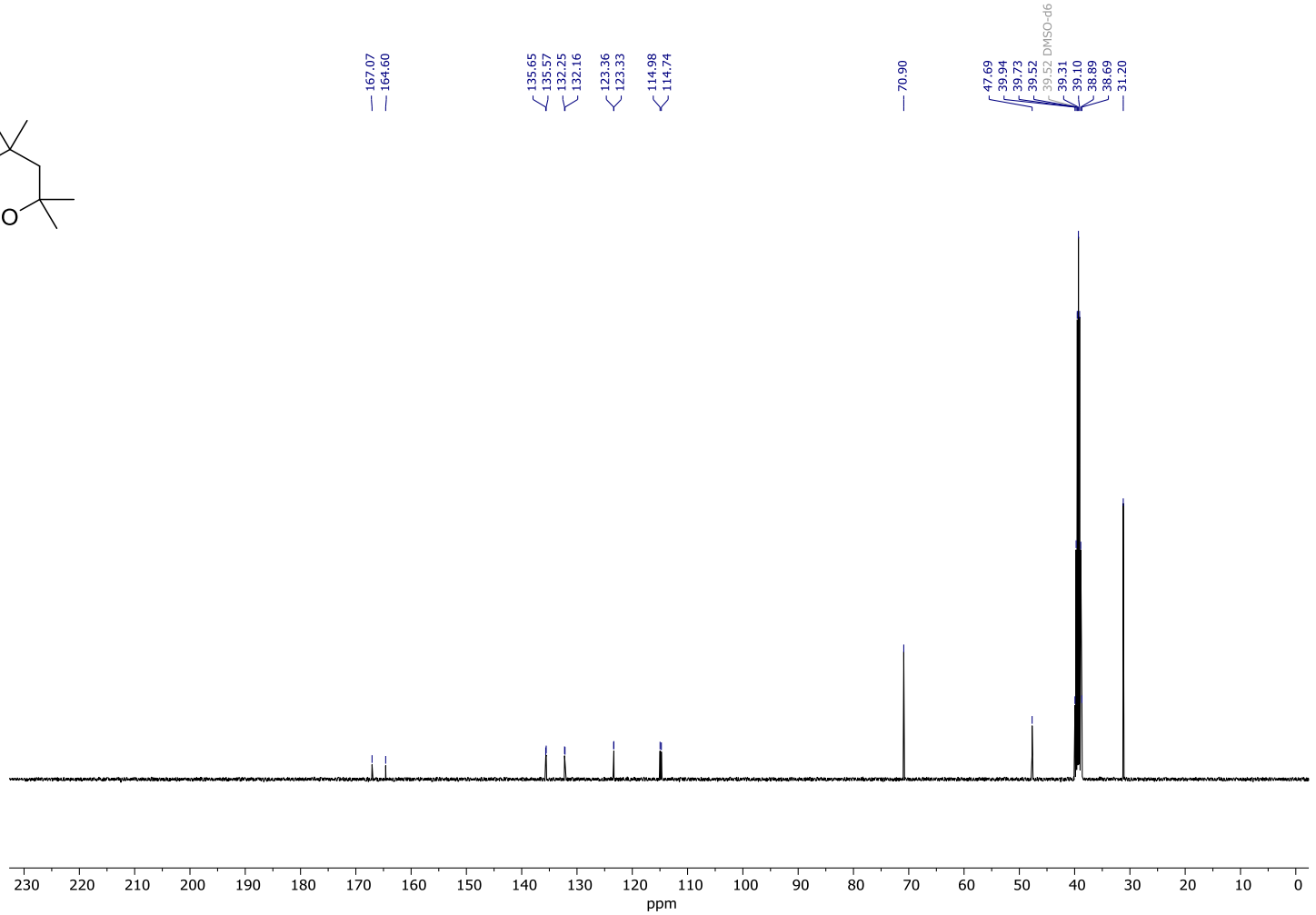

^{11}B (128 MHz); DMSO-*d*$_6$:

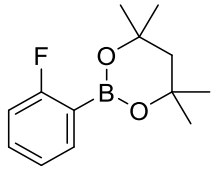

2k

^{1}H (400 MHz); DMSO-d_6:

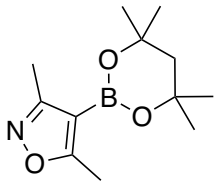

9i

$^{13}C\{^{1}H\}$ (101 MHz); DMSO-*d*$_6$:

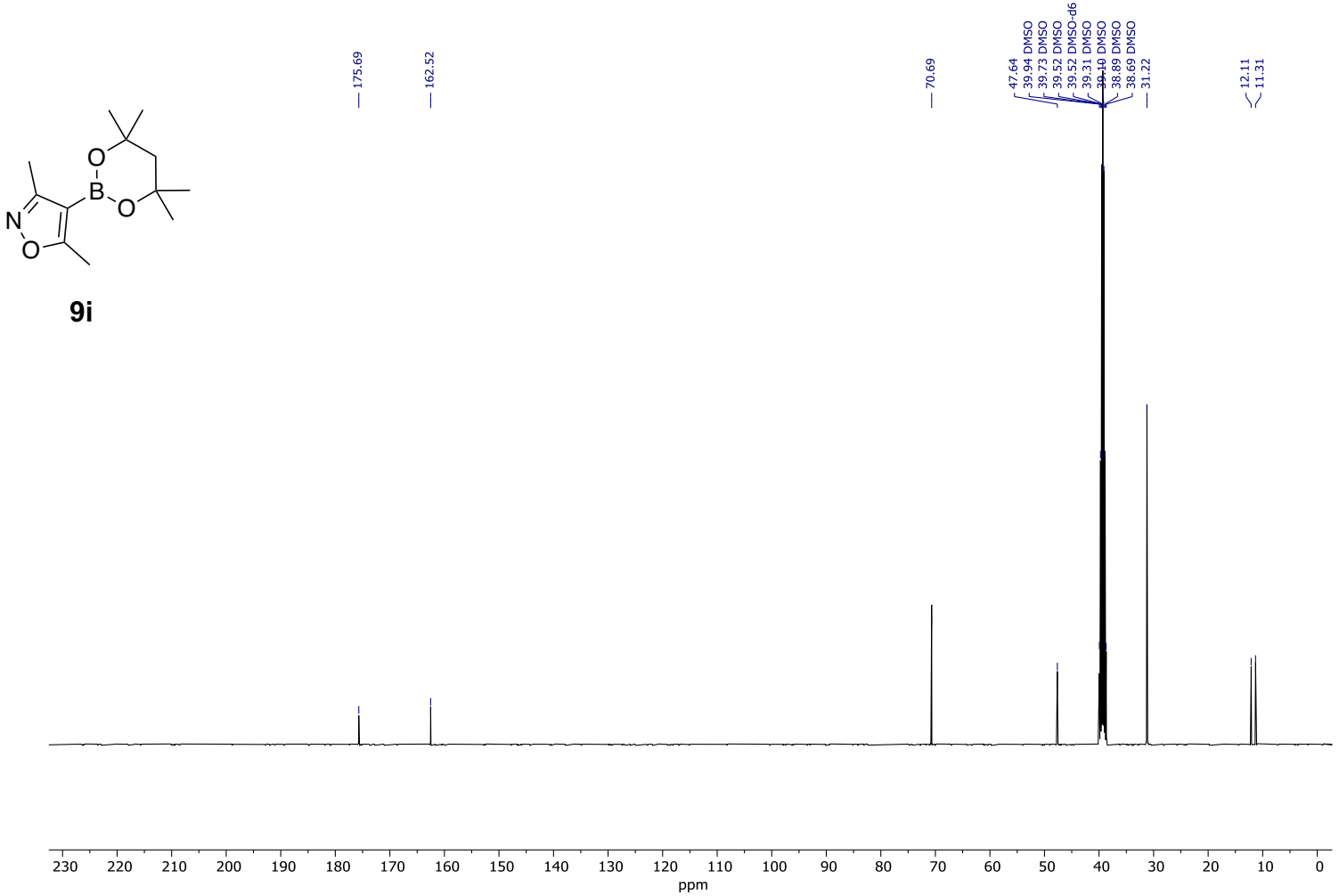

9i

^{11}B (128 MHz); DMSO-d_6:

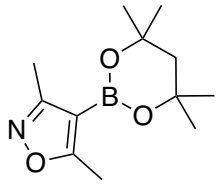

9i